THE ASTROPHYSICAL JOURNAL

An International Review of Spectroscopy and Astronomical Physics

FOUNDED IN 1895 BY GEORGE E. HALE AND JAMES E. KEELER

VOLUME 95

JANUARY–MAY 1942

THE UNIVERSITY OF CHICAGO PRESS
CHICAGO, ILLINOIS

THE CAMBRIDGE UNIVERSITY PRESS, LONDON

PUBLISHED JANUARY, MARCH, MAY, 1942

COMPOSED AND PRINTED BY THE UNIVERSITY OF CHICAGO PRESS
CHICAGO, ILLINOIS, U.S.A.

CONTENTS

NUMBER 1

NUMBER 2

NUMBER 3

VOLUME 95 NUMBER 1

THE ASTROPHYSICAL JOURNAL

AN INTERNATIONAL REVIEW OF SPECTROSCOPY AND ASTRONOMICAL PHYSICS

Founded in 1895 by GEORGE E. HALE *and* JAMES E. KEELER

Edited by

PAUL W. MERRILL
Mount Wilson Observatory of the Carnegie Institution of Washington

HARLOW SHAPLEY
Harvard College Observatory Cambridge, Massachusetts

OTTO STRUVE
Yerkes Observatory of the University of Chicago

JANUARY 1942

THE UNIVERSITY OF CHICAGO PRESS
CHICAGO, ILLINOIS, U.S.A.

January 1942 Vol. 95, No. 1

THE ASTROPHYSICAL JOURNAL

AN INTERNATIONAL REVIEW OF SPECTROSCOPY AND ASTRONOMICAL PHYSICS

The Astrophysical Journal is published bimonthly by the University of Chicago at the University of Chicago Press, 5750 Ellis Avenue, Chicago, Illinois, during July, September, November, January, March, and May. ¶The subscription price is $10.00 a year; the price of single copies is $2.00. Orders for service of less than a full year will be charged at the single-copy rate. ¶Postage is prepaid by the publishers on all orders from the United States and its possessions, Argentina, Bolivia, Brazil, Chile, Colombia, Costa Rica, Cuba, Dominican Republic, Ecuador, Guatemala, Haiti, Republic of Honduras, Mexico, Morocco (Spanish Zone), Nicaragua, Panama, Paraguay, Peru, Rio de Oro, El Salvador, Spain (including Balearic Islands, Canary Islands, and the Spanish Offices in Northern Africa; Andorra), Spanish Guinea, Uruguay, and Venezuela. ¶Postage is charged extra as follows: for Canada and Newfoundland, 42 cents on annual subscriptions (total $10.42); on single copies, 7 cents (total $2.07); for all other countries in the Postal Union, 96 cents on annual subscriptions (total $10.96), on single copies 16 cents (total $2.16). ¶Patrons are requested to make all remittances payable to The University of Chicago Press, in United States currency or its equivalent by postal or express money orders or bank drafts.

The following are authorized agents:

For the British Empire, except North America, India, and Australasia: The Cambridge University Press, Bentley House, 200 Euston Road, London, N.W. 1, England. Prices of yearly subscriptions and of single copies may be had on application.

For China: The Commercial Press, Ltd., 211 Honan Road, Shanghai.

Claims for missing numbers should be made within the month following the regular month of publication. The publishers expect to supply missing numbers free only when losses have been sustained in transit, and when the reserve stock will permit.

Business correspondence should be addressed to The University of Chicago Press, Chicago, Illinois.

Communications for the editors and manuscripts should be addressed to: Otto Struve, Editor of THE ASTROPHYSICAL JOURNAL, Yerkes Observatory, Williams Bay, Wisconsin.

Line drawings and photographs should be made by the author, and all marginal notes such as co-ordinates, wave lengths, etc., should be included in the cuts. It will not be possible to set up such material in type.

One copy of the corrected galley proof should be returned as soon as possible to the editor, Yerkes Observatory, Williams Bay, Wisconsin. Authors should take notice that the manuscript will not be sent to them with the proof.

The cable address is "Observatory, Williamsbay, Wisconsin."

The articles in this journal are indexed in the *International Index to Periodicals*, New York, N.Y.

Applications for permission to quote from this journal should be addressed to The University of Chicago Press, and will be freely granted.

Entered as second-class matter, July 31, 1940, at the Post-Office, at Chicago, Ill., under the act of March 3, 1879.
Acceptance for mailing at special rate of postage provided for in United States Postal Act of October 3, 1917, Section 1103, amended February 28, 1925.

[PRINTED IN U.S.A.]

THE ASTROPHYSICAL JOURNAL

AN INTERNATIONAL REVIEW OF SPECTROSCOPY AND ASTRONOMICAL PHYSICS

VOLUME 95 JANUARY 1942 NUMBER 1

THE CURVATURE OF PHOTOGRAPHIC PLATES

LEIGH PAGE

ABSTRACT

It is shown that the curvature of a photographic plate, owing to the contraction of the emulsion in drying, should be independent of the length or width of the plate and inversely proportional to the square of the thickness.

When the emulsion on a photographic plate dries, it tends to contract, curving the glass plate to which it adheres. Unless allowance is made for this curvature, errors may be introduced into the measurement of spectral lines or star images on the plate. Therefore it is important for the spectroscopist or astronomer to know how the curvature of such a plate depends upon its linear dimensions.

First, it is necessary to calculate the forces exerted on the surface of the plate by the film. We may consider the film to be attached to the plate at points a, b, c (Fig. 1) at regular intervals Δx in the unstrained state of the plate. Let $\Delta x' = \sigma \Delta x$, where $\sigma < 1$, be the length to which the section of the film between a and b would contract when the film dries, if the film were under no stress. If ξ is component displacement parallel to the X-axis of the surface of the plate when distorted by the contracted film, the actual separation of b from a when the film has dried is $(1 + [\partial\xi/\partial x])\Delta x$, and the elongation of this section of the film is

$$\left(1 + \frac{\partial \xi}{\partial x}\right) \Delta x - \Delta x' = \left(1 - \sigma + \frac{\partial \xi}{\partial x}\right) \Delta x .$$

Therefore the surface tension in the film per unit width is

$$t = u \left(1 - \sigma + \frac{\partial \xi}{\partial x}\right) \frac{\Delta x}{\Delta x'} = \frac{u}{\sigma}\left(1 - \sigma + \frac{\partial \xi}{\partial x}\right), \tag{1}$$

where u is the elastic constant of the dried film.

At a point of attachment not at the end of the film (such as b) there is, in addition to the surface tension t to the left, the surface tension

$$t' = \frac{u}{\sigma}\left(1 - \sigma + \frac{\partial \xi}{\partial x} + \frac{\partial^2 \xi}{\partial x^2} \Delta x\right) \tag{2}$$

to the right. Hence the film exerts a shear on the surface of the plate. Taking the Z-axis normal to the surface of the plate, we find this shear to be

$$X_z = T = \frac{t' - t}{\Delta x} = \frac{u}{\sigma} \frac{\partial^2 \xi}{\partial x^2} . \tag{3}$$

So, if we put

$$v \equiv \frac{u}{\sigma} (1 - \sigma) , \qquad w \equiv \frac{u}{\sigma} ,$$

and designate the length of the rectangular plate (dimension parallel to the X-axis) by $2k$ and the width (dimension parallel to the Y-axis) by $2l$, we have a force

$$F_x = \mp \left(v + w \frac{\partial \xi}{\partial x} \right) \tag{4}$$

per unit width at the ends $x = \pm k$ of the plate; a similar force

$$F_y = \mp \left(v + w \frac{\partial \eta}{\partial y} \right) \tag{5}$$

per unit length at the sides $y = \pm l$ of the plate, where η is the displacement parallel to the Y-axis; and the shears

$$X_z = T = w \frac{\partial^2 \xi}{\partial x^2} \tag{6}$$

and

$$Y_z = S = w \frac{\partial^2 \eta}{\partial y^2} \tag{7}$$

on the upper surface of the plate. In addition there is a normal tension on the upper surface of the plate due to its curvature, given by

$$Z_z = R = \frac{\partial}{\partial x} \left\{ \left(v + w \frac{\partial \xi}{\partial x} \right) \frac{\partial \zeta}{\partial x} \right\} + \frac{\partial}{\partial y} \left\{ \left(v + w \frac{\partial \eta}{\partial y} \right) \frac{\partial \zeta}{\partial y} \right\} , \tag{8}$$

where ζ is the displacement parallel to the Z-axis.

On account of the large magnitude of the elastic constants of glass as compared with those of the film, the strains $\partial \xi / \partial x$, $\partial \eta / \partial y$, $\partial \zeta / \partial x$, $\partial \zeta / \partial y$, and their derivatives must be very small compared with unity. Therefore, even though v is less than w, it would seem that all terms in equations (4), (5), (6), (7), and (8) involving the strains as factors are negligible as compared with the terms in v alone. This approximation simplifies the problem enormously. Proceeding on this basis, we find the solution obtainable with the

same displacements as those involved in the problem of bending of a rectangular plate by terminal couples.[1]

We place the origin at the center of the rectangular plate and orient the axes as in

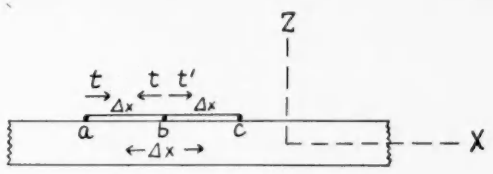

FIG. 1

Figure 1 and designate the thickness of the plate by $2h$. We use the usual notation for the stresses, that is,

$$\left.\begin{aligned} &P \equiv X_x\,, && Q \equiv Y_y\,, && R \equiv Z_z\,, \\ &U \equiv X_y = Y_x\,, && S \equiv Y_z = Z_y\,, && T \equiv Z_x = X_z\,. \end{aligned}\right\} \tag{9}$$

Then, employing St. Venant's principle, the boundary conditions are as follows:

$$x = \pm k\,; \quad \int_{-h}^{h} P dz = -v\,, \quad \int_{-h}^{h} Pz dz = -vh\,, \quad U = 0\,, \quad T = 0\,;$$

$$y = \pm l\,; \quad \int_{-h}^{h} Q dz = -v\,, \quad \int_{-h}^{h} Qz dz = -vh\,, \quad U = 0\,, \quad S = 0\,;$$

$$z = \pm h\,; \quad R = 0\,, \quad S = 0\,, \quad T = 0\,.$$

These boundary conditions can be satisfied by the displacements

$$\left.\begin{aligned} &\xi = Ax(z + b)\,, && \eta = Ay(z + b)\,, \\ &\zeta = -\tfrac{1}{2}A(x^2 + y^2) - \frac{\lambda}{\lambda + 2\mu} A(z + b)^2\,, \end{aligned}\right\} \tag{10}$$

which also satisfy the conditions for equilibrium in the interior of the plate. We have at once

$$U = \mu\left(\frac{\partial \eta}{\partial x} + \frac{\partial \xi}{\partial y}\right) = 0\,,$$

$$S = \mu\left(\frac{\partial \eta}{\partial z} + \frac{\partial \zeta}{\partial y}\right) = 0\,,$$

$$T = \mu\left(\frac{\partial \xi}{\partial z} + \frac{\partial \zeta}{\partial x}\right) = 0\,,$$

$$R = \lambda\left(\frac{\partial \xi}{\partial x} + \frac{\partial \eta}{\partial y} + \frac{\partial \zeta}{\partial z}\right) + 2\mu \frac{\partial \zeta}{\partial z} = 0\,,$$

[1] Love, *Mathematical Theory of Elasticity*, 3d ed., pp. 130 ff.

everywhere. In these formulae, μ is the rigidity and $\lambda = \kappa - \frac{2}{3}\mu$, where κ is the volume elasticity. The surviving stresses are

$$P = Q = \lambda\left(\frac{\partial\xi}{\partial x} + \frac{\partial\eta}{\partial y} + \frac{\partial\zeta}{\partial z}\right) + 2\mu\frac{\partial\xi}{\partial x} = \frac{2\mu(3\lambda + 2\mu)}{\lambda + 2\mu}A(z + b)\,. \tag{11}$$

The boundary conditions on P and Q give us

$$A = -\frac{3(\lambda + 2\mu)}{4\mu(3\lambda + 2\mu)}\frac{v}{h^2}\,, \tag{12}$$

and

$$b = \tfrac{1}{3}h\,. \tag{13}$$

Therefore, if we put

$$\gamma \equiv \frac{3\kappa(\lambda + 2\mu)}{4\mu(3\lambda + 2\mu)} = \frac{\kappa + \frac{4}{3}\mu}{4\mu}\,,$$

the displacements are

$$\left.\begin{aligned} \xi &= -\frac{\gamma v}{\kappa h^2}x(z + \tfrac{1}{3}h)\,, \qquad \eta = -\frac{\gamma v}{\kappa h^2}y(z + \tfrac{1}{3}h)\,, \\ \zeta &= \frac{\gamma v}{2\kappa h^2}(x^2 + y^2) + \frac{(2\gamma - 1)v}{2\kappa h^2}(z + \tfrac{1}{3}h)^2\,. \end{aligned}\right\} \tag{14}$$

The curvature of the plate,

$$\frac{\partial^2\zeta}{\partial x^2} = \frac{\gamma v}{\kappa h^2}\,, \tag{15}$$

is independent of the length or width and inversely proportional to the square of the thickness.

The dilatation is

$$\frac{\partial\xi}{\partial x} + \frac{\partial\eta}{\partial y} + \frac{\partial\zeta}{\partial z} = -\frac{v}{\kappa h^2}(z + \tfrac{1}{3}h)\,, \tag{16}$$

showing that the plate is compressed above the plane $z = -\frac{1}{3}h$ and stretched below this plane. The total decrease in volume is $\frac{2}{3}v/\kappa$ per unit area of the surface.

The author is indebted to his colleague, Professor Frank Schlesinger, for drawing his attention to this problem.

SLOANE PHYSICS LABORATORY
YALE UNIVERSITY
June 28, 1941

THE ROTATION OF THE SPIRAL NEBULA MESSIER 33*

N. U. MAYALL AND L. H. ALLER[1]

ABSTRACT

The investigation is based on radial velocity observations of 25 bright-line condensations well distributed over the spiral (Pl. I), and upon several long exposures that record the spectrum of the unresolved nebulosity of the nuclear region. As preliminary steps in the derivation of the relation between rotational velocity and nuclear distance, the *velocity of the system* is found to be -167 ± 5 km/sec from three different groups of the data; also, the *inclination to the line of sight* of the principal plane of the spiral is found to be 33° from long-exposure direct photographs on $6\frac{1}{2} \times 8\frac{1}{2}$-inch plates taken with the Crossley reflector. By using these results, together with the assumption of simple circular motion in the plane, rotational velocities of low precision (the linear dispersion of the spectra is 304 A/mm at λ 3950) are first obtained for the individual condensations (Fig. 1) and then combined to give a first approximation to the *rotational-velocity-curve* (Fig. 2). The latter may be briefly described as follows: the *main body* of the spiral, some 18′ in radius, appears to rotate almost like a solid body (rotational velocity increases fairly uniformly with distance), while the *outer parts*, represented by a zone having least and greatest radii of 18′ and 30′, respectively, appear to rotate like a *planetary system* (rotational velocity decreases with distance). The transition between these two types of motion occurs in the general vicinity of 16′ (1000 parsecs) from the center, at which distance the rotational velocity attains a *maximum* of approximately 120 km/sec. The observations define fairly well the character of the motion out to the extreme limits of the spiral (30′, or nearly 2000 parsecs) shown on the photographs. Comparison of the results for these most distant regions of M 33 with similar ones for the solar neighborhood of the Galaxy strengthens the current hypothesis that *the sun is located at a considerable distance from the main body of our own stellar system.*

I. INTRODUCTION

The investigation of the rotational motions of the spiral nebulae is of value in at least two respects. In the first place, a knowledge of such motions is fundamental in the study of the dynamics of stellar systems. In the second, a comparative study of the rotational motions of spirals and of the Galaxy may contribute something toward the solution of certain problems of galactic rotation, such as, for example, the determination of the distribution and total mass of the Galaxy, the orbital velocity of the sun, and the position of the solar neighborhood relative to the main body of our stellar system.

The best means available at present for the measurement of nebular rotational velocities is the spectroscope. Unfortunately, its use is attended with many difficulties, owing to the extreme faintness of spirals and their component parts; and the measurements accordingly lack precision. Nevertheless, the application of the spectroscopic method gives a general idea of the character of the motions, especially when, as in the present instance, the velocity measures extend to the outermost parts of a spiral.

A good deal of the earlier work in this field is represented by the pioneer observations of V. M. Slipher[2] and of F. G. Pease,[3] together with the more recent work of M. L. Humason[4] and of H. W. Babcock.[5] In most of these investigations the rotational velocities were measured only in the immediate vicinity of the nucleus; the measures stopped at distances far short of the full size of the nebula. A notable exception in this respect is Babcock's study of the Andromeda nebula, in which the rotational velocities are traced to the farthest extensions recognizable on long-exposure photographs.

* *Contributions from the Lick Observatory, University of California*, Ser. II, No. 1.

[1] Society of Fellows, Harvard University.

[2] *Lowell Obs. Bull.*, **2**, 65, 1914; *Pop. Astr.*, **23**, 21, 1915; **25**, 36, 1917; **29**, 272, 1921.

[3] *Proc. Nat. Acad. Sci.*, **2**, 517, 1916; **4**, 21, 1918; *Pub., A.S.P.*, **28**, 191, 1916.

[4] *Ann. Rept. of the Director of Mt. W. Obs., 1936–1937*, p. 31; *1938–39*, p. 27.

[5] *Lick Obs. Bull.*, **19**, 41, 1939 (No. 498).

In the belief that velocity measures which describe the rotational motion of a spiral as a whole are likely to be of more value in general studies of the dymanics of stellar systems, the present investigation has been undertaken as a natural sequel to that of Babcock for M 31. In order to separate the observations from their interpretation, this paper is limited to a presentation of the observational material. The theoretical discussion of the data is made the subject of a paper by Wyse and Mayall, entitled "Distribution of Mass in the Spiral Nebulae Messier 31 and Messier 33" (see p. 24 of this issue).

The particular spiral selected for study is M 33, often termed the "spiral nebula in Triangulum."[6] It was chosen for two reasons. First, it is the nearest late-type spiral, and its distance, 220,000 parsecs, is accurately known from Hubble's observations of Cepheid variables.[7] Consequently, the constituent parts are sufficiently bright, and the angular size is sufficiently large, to allow of spectroscopic investigation with a telescope of moderate light-gathering power and of medium focal length. Second, no late-type spiral has hitherto been studied for rotation by the spectroscopic method, despite the significant fact that late-type spirals occur more frequently than others.

M 33 is typically "Sc" in Hubble's system of classification.[8] Its principal characteristic, besides irregular spiral structure, is a high degree of resolution into stars, groups or clusters of stars, and numerous nebulous condensations. The three brightest of the latter —NGC 604, observed by Slipher[9] and by Pease,[10] and NGC 588 and 595, observed by Hubble[11]—have long been known to possess bright-line spectra. In each spectrum the intensity of $H\beta$ is much greater than that of N_2. On the basis of this criterion, the validity of which has been established by a comparative study of the galactic nebulae,[12] Hubble has inferred that these three condensations in M 33 are similar to the diffuse galactic nebulae.

The occurrence in spirals of condensations that exhibit a bright-line spectrum is a phenomenon of much importance in at least two respects. In the first place, it points to a relationship between nebular contents and nebular type. The relationship, suggested by recent work on the spectra and colors of nebulae, is in the sense that emission patches are common in the Sc or late-type spirals and are seen rarely, if at all, in the Sa or early-type spirals. In the second place, the presence of bright-line objects in spirals is of the greatest value for spectroscopic investigations of internal motions, that is to say, for the measurement of rotational velocities. Owing to the apparent faintness of most condensations (few are brighter than the twelfth photographic magnitude), it is necessary to employ spectrographs with low dispersion, of the order of 250–500 A/mm. Under these conditions an emission spectrum can be measured more accurately for radial velocity than can an absorption spectrum. This circumstance suggested the possibility that M 33 might be a suitable object for rotational study, provided that a sufficiently large number of emission patches could be identified, and that the principal plane of the spiral was not too greatly inclined from the line of sight. These two conditions are, accordingly, considered first of all.

II. INCLINATION OF THE PRINCIPAL PLANE OF M 33

A casual glance at published photographs of M 33 is likely to convey the impression that the principal plane of the spiral is nearly at right angles to the line of sight. How-

[6] The position of the nucleus, NGC 598, for 1900 is $\alpha = 1^h28^m.2$, $\delta = +30°9'$.

[7] *Ap. J.*, **63**, 83, 1926; *Mt. W. Contr.*, No. 310; also *The Realm of the Nebulae*, p. 143, Yale University Press, 1936.

[8] *Ap. J.*, **64**, 321, 1926; *Mt. W. Contr.*, No. 324.

[9] *Pop. Astr.*, **23**, 23, 1915; *Proc. Amer. Phil. Soc.*, **56**, 406, 1917.

[10] *Pub. A.S.P.*, **27**, 239, 1915.

[11] *Ap. J.*, **63**, 236, 1926; *Mt. W. Contr.*, No. 310.

[12] *Ap. J.*, **66**, 217, 397, 1922; *Mt. W. Contr.*, Nos. 241 and 250.

PLATE I*a*

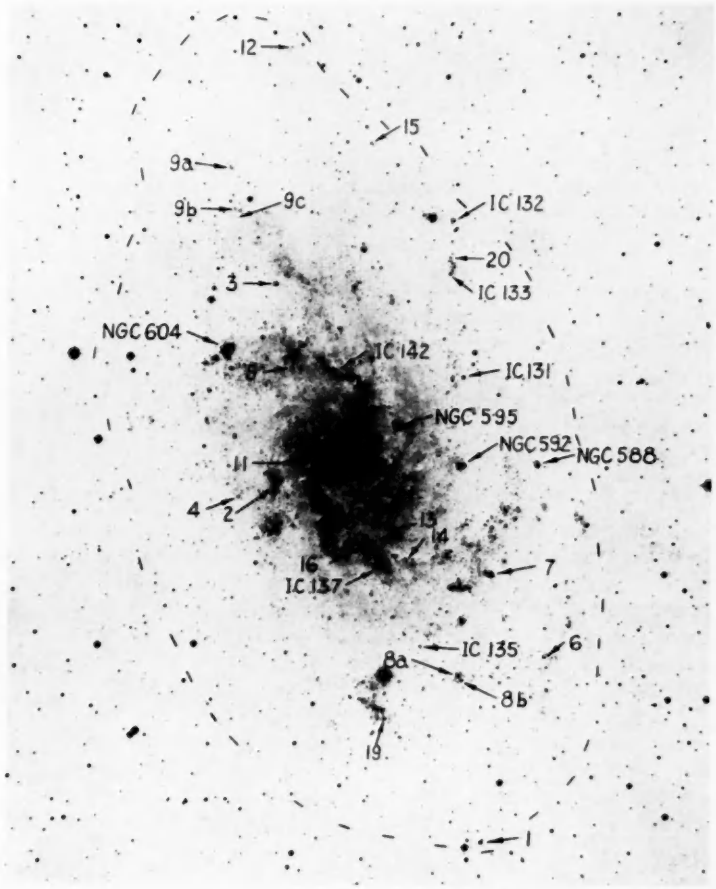

MESSIER 33

The dashed line outlines the limits of the spiral, while the arrows mark 31 condensations whose spectra have been obtained.

PLATE I*b*

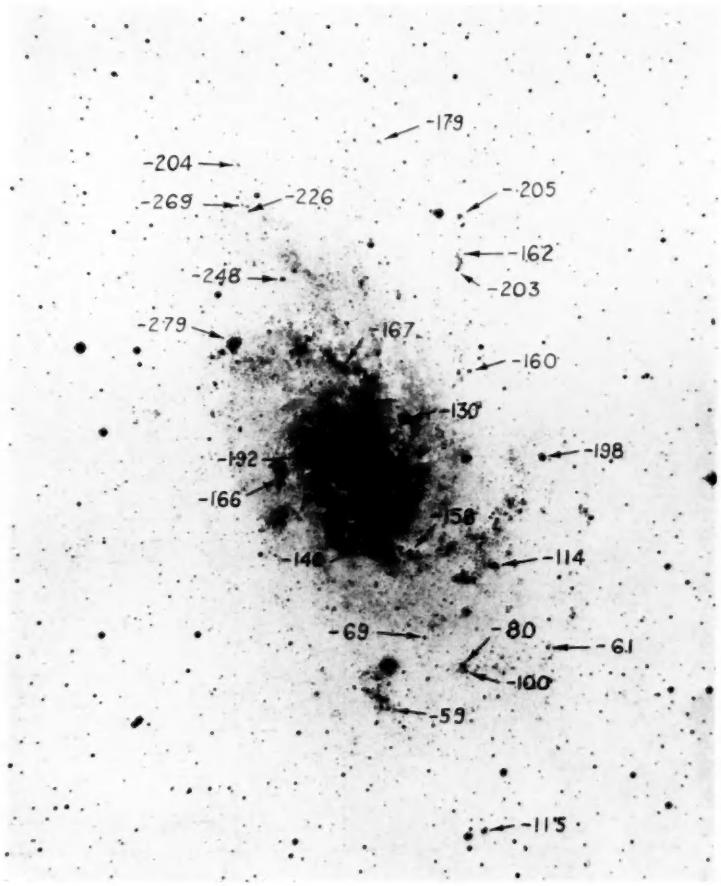

Observed Radial Velocities of 25 Emission Condensations in M 33

ever, as a result of some experimental direct photography with the 36-inch Crossley reflector, in which a plate larger than usual was used,[13] it became evident that the spiral extends over an approximately elliptical area whose major and minor axes are 62′ and 34′, respectively, with the major axis lying in position angle 20°. These dimensions are rather well defined on 3-hour exposures made on the fastest available plates, and they represent the limits to which the faintest stars (about the twentieth photographic magnitude) in the spiral can be traced with reasonable confidence.[14] If it is assumed that the outline of the spiral in its own plane is circular, it follows from the above dimensions that M 33 is tipped only 33° from the line of sight.[15] Accordingly, rotational velocities in the principal plane are decreased, in projection, by a factor of $1-\cos 33°$, or only 16 per cent, and hence their measurement by the spectroscopic method is not precluded by an unfavorable inclination of the spiral.

III. CONDENSATIONS OBSERVED IN M 33

The direct photographs of M 33 referred to in the preceding section were closely examined for condensations that seemed likely to be emission patches. The survey immediately showed that the spiral contains a considerable number of such objects, and that some restrictive rule would have to be employed in selecting those to be observed. The most natural thing to do was to observe them in the order of their brightness. As the work progressed, it became necessary to make exceptions to this rule, in order to extend the observations to the limits of the system, and to obtain a satisfactory distribution of objects along the major and minor axes.

Plate I*a* shows the outline of the spiral, with arrows marking 31 condensations whose spectra are available for discussion. Of these objects, 25 exhibit one or more bright lines in their spectra, while 6 show only a continuous spectrum.[16] There are undoubtedly many more emission knots in M 33. In several cases very faint condensations, indistinguishable from stars, happened to fall on the slit when it was placed on a brighter patch, and their spectra are characterized by a single bright line, λ 3727 [*O* II]. Since there are innumerable such condensations shown on the photographs, and since most of those observed spectroscopically show bright lines, it seems safe to conclude that emission lines are of very general occurrence in this system. This is not altogether unexpected, in view of a recent report from this observatory on the spectra of some 80 extragalactic nebulae.[17]

All the spectroscopic observations were made with a specially designed nebular spectrograph[18] mounted at the primary focus of the Crossley reflector. The exposures range from 1 to 18 hours, the most frequent exposure being one full night in length, although toward the end of the program, when the brighter objects had been observed, the average exposure was of two nights' duration. In a number of instances the maximum slit-

[13] J. H. Moore, N. U. Mayall, and J. F. Chappell, *Astronomical Photographs Taken at the Lick Observatory*.

[14] Through the courtesy of Dr. Hubble one of the best negatives of M 33 in the Mount Wilson Observatory files was made available for comparison with the Crossley plates. The negative is an 8×10 Seed 30 plate, exposed 6½ hours on August 4–5, 1921, by J. C. Duncan, with the 100-inch reflector stopped to 84 inches. Essentially the same limiting outline for the spiral was obtained from this 100-inch plate as from the Crossley plates.

[15] This angle agrees closely with that obtained from microphotometer tracings by Miss Patterson (*Harvard Bull.*, No. 914, p. 9, December, 1940), who found the inclination to the plane of the sky to be 60°. She also located the major axis in position angle 20°.

[16] All six of these continuous spectra are so narrow as to show few or no absorption lines. On this account, the spectral types are difficult, if not impossible, to estimate. In most cases the distribution of intensity in the spectra suggests an early-type classification. Further discussion of these continuous spectra does not appear warranted.

[17] *Lick Obs. Bull.*, **19**, 33, 1939 (No. 497).

[18] *Pub. A.S.P.*, **48**, 14, 1936.

length, 6′.2 was used, and in this way it was often possible to record simultaneously the spectra of several objects.

Plate II illustrates the general appearance of several of the spectra. The most conspicuous line—the one farthest to the left in all of the spectra—is λ 3727 of [*O* II]. The group of three lines to the far right on some of the plates is composed of (left to right) $H\beta$, N_2, and N_1. Lines lying between are Balmer lines, the only exception being, in a

TABLE 1

IDENTIFICATION AND POSITIONS OF CONDENSATIONS IN M 33

Object (1)	x (2)	y (3)	θ (4)	sec θ (5)	R (6)	Spectrum (7)
Anon. 12	+29′.0	− 5′.7	19°.0	1.06	30′.8	Continuous
9*a*	+22.4	+ 1.4	6.7	1.01	22.6	
15	+20.6	− 8.9	38.2	1.27	26.2	Only λ 3727
9*b*	+19.4	+ 2.0	10.5	1.02	19.7	
9*c*	+19.0	+ 2.1	11.3	1.02	19.4	Only λ 3727
3	+13.4	+ 1.0	7.7	1.01	13.5	
IC 132	+13.4	−12.9	60.5	2.03	27.1	
Anon. 20	+11.0	−11.9	63.5	2.22	24.3	Only λ 3727
IC 133	+10.0	−11.6	64.8	2.35	23.4	
NGC 604	+10.0	+ 5.8	46.7	1.46	14.6	
Anon. 5	+ 7.2	+ 1.8	24.6	1.10	7.9	Continuous
IC 142	+ 5.8	− 1.1	19.1	1.06	6.1	
131	+ 2.4	− 9.9	82.5	.....	18.3	
NGC 595	+ 0.5	− 4.1	86.2	.....	7.5	
Anon. 11	0.0	+ 2.6	90.0	.....	4.7	
2	− 0.4	+ 5.8	87.8	.....	10.6	
4	− 0.4	+ 8.6	88.6	.....	15.7	Continuous
18	− 2.9	0.0	0.0	1.00	2.9	Only λ 3727
NGC 592	− 3.6	− 7.6	75.5	.....	14.4	Continuous*
588	− 5.5	−12.8	76.8	.....	24.0	
Anon. 13	− 6.5	− 1.3	20.3	1.07	6.9	Continuous
16	− 6.8	+ 0.6	9.2	1.01	6.9	
IC 137	− 8.6	+ 0.5	6.0	1.01	8.6	Continuous
Anon. 14	− 8.8	− 1.5	17.1	1.05	9.2	
7	−11.8	− 7.0	47.3	1.47	17.4	
IC 135	−15.0	− 0.4	2.7	1.00	15.0	
Anon. 8*a*	−18.0	− 2.4	13.7	1.03	18.5	
8*b*	−18.5	− 2.5	14.0	1.03	19.1	
6	−18.8	− 8.7	40.3	1.31	24.6	Only λ 3727†
19	−19.3	+ 3.8	19.7	1.06	20.5	
1	−29.8	0.0	0.0	1.00	29.8	

* Hubble has reported (*Ap. J.*, **63**, 260, n. 2, 1926) no trace of diffuse nebulosity around this object. The spectrum shows no bright lines, not even a faint λ 3727.

† This appears to be a foreground star superposed on a small and faint patch of nebulosity.

few cases, a line at λ 3869, which is the violetward component of the [*Ne* III] pair. The redward component, λ 3968, is blended with $H\epsilon$.

Table 1 gives data relating to the positions and identifications of the objects marked on Plate I. Column 1 of the table contains, in so far as possible, the catalogue numbers of the condensations observed;[19] in cases for which no such identification is available, arbitrary numbers are assigned. Columns 2 and 3 list the rectangular co-ordinates, x and

[19] Two of the identifications made by means of Dreyer's *First Index Catalogue* (*Memoirs of the Royal Astronomical Society* [London], **51**, 185, 1895), namely, IC 135 and 137, are uncertain because of the inadequacy of the summary description and the inaccuracy of position. The objects listed as IC 134, 136, 139, and 140 could not be found. NGC 603 appears to be a small group of three faint stars.

PLATE II

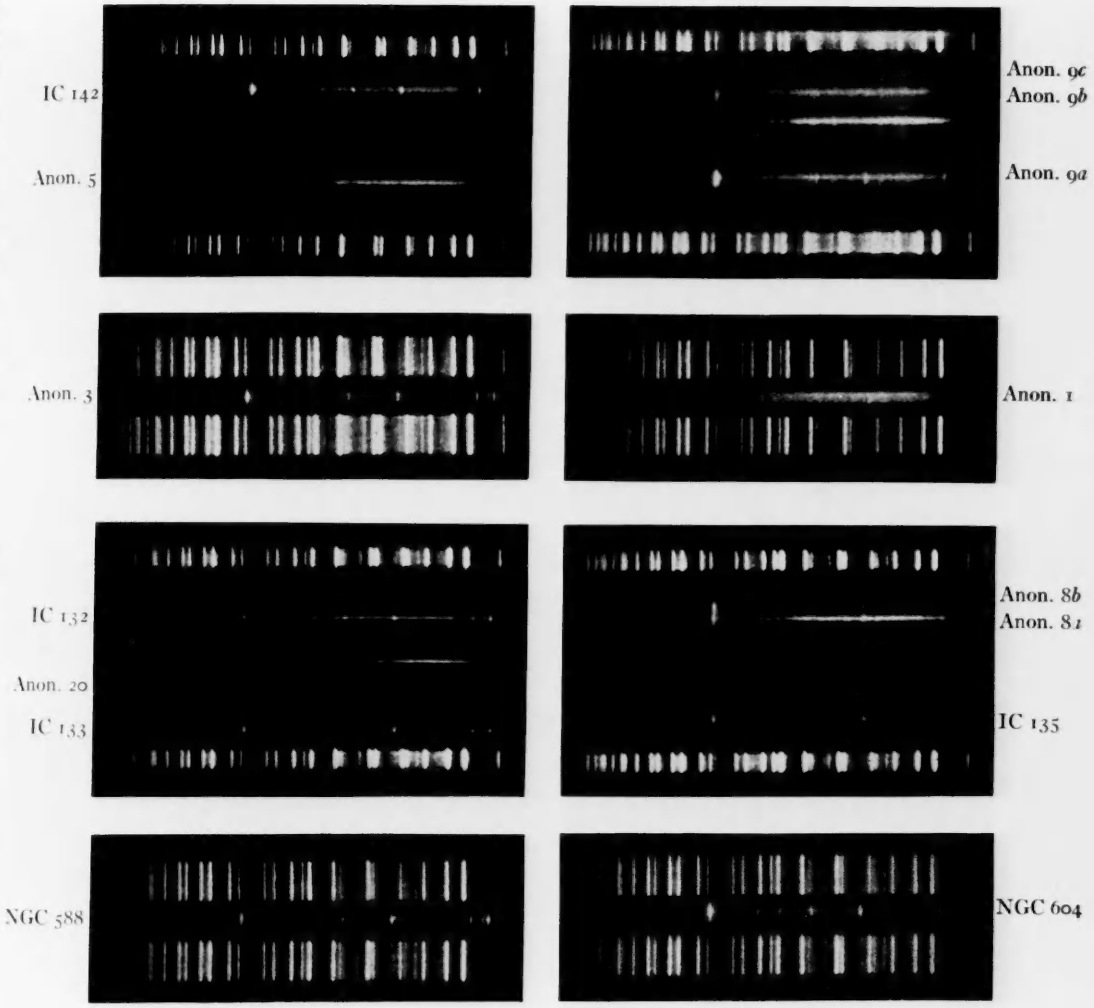

TYPICAL SPECTRA OF EMISSION CONDENSATIONS IN M 33

The scale of enlargement is 11× the original negatives, on which the linear dispersion at λ 3950 is 304 A/mm

y; the reference frame is centered on the nucleus, with axes corresponding to those of the apparent elliptical outline of the spiral. The major axis is taken to lie in position angle 20°; positive x is in the same direction north-following the nucleus, while positive y is in position angle 110° south-following the nucleus. The next three columns give certain data which, calculated from the rectangular co-ordinates and the angle of inclination, and hence referred to the plane of the spiral,[20] are used later for the derivation of the relation between rotational velocity and nuclear distance. Column 4 lists for each object the angle, in the plane of the spiral, between the major axis and the radius vector from the nucleus to the object. This angle, hereafter referred to as the azimuth angle θ, is found from the obvious relation $\tan \theta = (y \csc i)/x$, where i is the angle of inclination with respect to the line of sight (33°), as indicated in a preceding paragraph. Column 5 is self-explanatory, while column 6 contains for each object the nuclear distance, R, obtained from the simple formula $R = \sqrt{x^2 + (y \csc i)^2}$. Lastly, column 7 notes those condensations which show either a continuous spectrum or only one bright line: λ 3727.

IV. RADIAL VELOCITIES OF THE EMISSION-LINE CONDENSATIONS

As soon as the first few spectra had been measured for radial velocity, it became clear that the rotational velocities in M 33 are rather small, being, on the average, only a few times the probable error of a velocity. Hence, in order to improve the accuracy of the measures, a considerable number of duplicate plates has been obtained, and, furthermore, almost every plate has been measured twice by each observer. All this material is collected in Tables 2*a* and 2*b*, which are arranged in a manner designed to facilitate the discussion of the accuracy of the data in Section V.

Column 1 of Table 2*a* requires no comment, but for Table 2*b* a few remarks are necessary. In order to ascertain whether there are any anomalies in the rotational velocity in the immediate vicinity of the nucleus, such as those found by Babcock[21] for the Andromeda nebula, the long slit was placed on the minor axis with the nucleus central, and then on the major axis, first, with the nucleus at one end of the slit, second, with it central, and third, with it at the other end. In all cases the image of the nebula was held steady on the slit, and, as the exposures were purposely made long enough to record the spectrum of the faint, unresolved nebulosity, the spectrum of the nucleus itself was, naturally, "burned out." To obtain the spectrum of the nucleus alone, two plates of shorter exposure, each of 6 hours, were obtained; and, since the nucleus is semistellar, it was allowed to drift along the slit by an amount (about 0.′5) large enough to give a satisfactorily wide spectrum. These spectra of the nucleus and its immediate surroundings are separately discussed in Section VI (*b*).

Columns 2 and 3 of Tables 2*a* and 2*b* are self-explanatory, although, to complete the record, it may be stated that three different kinds of fast emulsions were used. These were: Imperial "1200," Imperial "Eclipse Soft" H & D 850, and Agfa "Spectral Blau Ultra Rapid." It may be of interest to note the rather lengthy average exposure: 9.1 hours. Columns 4 and 5, labeled "Set I," and columns 7 and 8, labeled "Set II," contain the first and second measured velocities, V_1 and V_2, for each plate; they have been corrected only for the orbital motion of the earth. Set I represents measures by Mayall; Set II, by Aller. The measures are given in detail to indicate the uncertainties inherent in small-scale spectra; differences between the first and the second measures of each plate are given in column 6 for Set I and in column 9 for Set II. These differences are used, in Section V (*a*), to calculate the probable error of measurement for each observer. Col-

[20] This calculation contains the implicit assumption that all the objects lie in the plane of the spiral, and it may be justified by analogy with the galactic diffuse nebulae, which are known to lie close to the galactic plane.

[21] *Op. cit.*, p. 48.

TABLE 2*a*

RADIAL VELOCITIES OF BRIGHT-LINE CONDENSATIONS IN M 33

Object in M 33	Date (PST)	Exp. Time	Set I			Set II			Mean V	Wt. w
			V_1	V_2	Δ	V_1	V_2	Δ		
(1)	(2)	(3)	(4)	(5)	(6)	(7)	(8)	(9)	(10)	(11)
Anon. 9*a*	1939 Sept. 8, 9	15^h45^m	−184	−176	8	−206	−194	12	−186	1.0
9*a*	39 Oct. 8, 9	18 20	220	235	15	234	179	55	221	1.0
15	39 Nov. 7, 9, 10	16 15	187	210	23	133	171	38	184	0.3
15	40 Oct. 26, 27, 29	16 00	157	186	29	.....	.....	....	172	0.3
9*b*	39 Sept. 8, 9	15 45	310	300	10	370	328	42	318	1.0
9*b*	39 Oct. 8, 9	18 20	198	204	6	244	282	38	220	1.0
9*c*	39 Sept. 8, 9	15 45	222	222	0	328	241	87	241	0.3
9*c*	39 Oct. 8, 9	18 20	185	166	19	311	272	39	211	0.3
3	38 Aug. 27	5 00	284	253	31	281	271	10	270	1.0
3	39 Oct. 15	5 30	238	215	23	234	211	23	225	1.0
IC 132	38 Aug. 30	7 00	269	271	2	290	285	5	275	1.0
132	39 Oct. 19, 20	9 43	150	138	12	75	67	8	122	1.0
132	40 Sept. 7, 8	10 00	217	204	13	218	246	28	217	1.0
Anon. 20	39 Oct. 19, 20	9 43	142	127	15	104	114	10	126	0.3
20	40 Sept. 7, 8	10 00	195	206	11	192	202	10	199	0.3
IC 133	39 Oct. 19, 20	9 43	102	93	9	166	162	4	118	1.0
133	40 Sept. 7, 8	10 00	302	266	36	282	313	31	288	1.0
NGC 604	38 Aug. 24	4 24	281	281	0	241	284	43	275	1.0
604	39 Jan. 21	1 00	305	290	15	332	264	68	298	1.0
604	39 Sept. 4	0 15	248	243	5	221	228	7	239	1.0
604	39 Sept. 7	1 00	303	302	1	308	309	1	304	1.0
IC 142	39 Oct. 14	9 00	161	168	7	170	180	10	167	1.0
131	38 Aug. 28	4 50	179	214	35	190	197	7	195	1.0
131	39 Oct. 18	5 40	140	134	6	99	98	1	125	1.0
NGC 595	38 Sept. 1	5 35	169	181	12	198	179	19	179	1.0
595	39 Sept. 15	3 50	87	82	5	99	50	49	81	1.0
Anon. 11	38 Sept. 22, 23	15 45	204	162	42	207	217	10	192	1.0
2	38 Sept. 2, 3	7 50	158	175	17	136	162	26	161	1.0
2	39 Oct. 16	5 30	174	155	19	206	175	31	172	1.0
18	39 Oct. 11, 12	15 00	117	66	51	42	27	15	75	0.3
NGC 588	38 Aug. 31	5 45	178	197	19	210	178	32	190	1.0
588	39 Aug. 21	4 50	212	194	18	211	221	10	207	1.0
Anon. 16	39 Sept. 17	6 55	125	158	33	134	137	3	140	1.0
14	39 Nov. 6	10 00	128	176	48	163	181	18	158	1.0
7	38 Oct. 20	8 40	85	84	1	100	140	40	95	1.0
7	40 Sept. 9, 10	7 25	127	156	29	.....	.....	....	142	0.7
IC 135	39 Nov. 4, 5	12 30	56	59	3	106	85	21	69	1.0
Anon. 8*a*	38 Nov. 20	9 00	89	58	31	50	86	36	72	1.0
8*a*	39 Nov. 4, 5	12 30	98	115	17	38 *	53 *	15	88	1.0
8*b*	39 Nov. 4, 5	12 30	87	113	26	.....	.....	....	100	0.7
6	38 Oct. 19	9 00	55	65	10	26	103	77	61	0.3
19	40 Oct. 30, 31	13 00	56	61	5	.....	.....	....	58	0.7
19	40 Nov. 23, 24	11 30	63	56	7	.....	.....	....	60	0.7
1	38 Nov. 17, 18	13 00	109	140	31	130	157	27	130	1.0
1	39 Sept. 15, 16	16 46	− 96	− 90	6	−130	−103	27	−100	1.0

* 8*a* and 8*b* measured as one object.

umn 10 contains the mean velocity, V, for each plate, deduced as described in Section V (*a*). Lastly, column 11 gives the weight, w, for each mean plate velocity, V. These weights are assigned on the following basis: a plate for which there are two measures by each observer, $w = 1.0$; one for which the measures are missing in Set II,[22] $w = 0.7$; and one for which only λ 3727 was measured, $w = 0.3$. The latter assignment depends upon the circumstance that, when more than one line is measured per plate, λ 3727, because of its favorable position and good intensity in the spectra, contributes, on the average, nearly one-third of the total weight from all the lines.

At this point it is appropriate to describe the manner in which the velocities V_1 and V_2 were obtained. The number of bright lines measured per plate ranged from one (λ 3727) to ten (λ 3727, $H\eta$, 3869, $H\zeta$, 3968+$H\epsilon$, $H\delta$, $H\gamma$, $H\beta$, N_2, and N_1). The scatter in the velocities from individual lines on a single plate is large, sometimes amounting to as much as 250 km/sec. The range of intensity between the lines is also considerable: from an emission so faint as to be hardly distinguishable, to a radiation so strong as to appear "burned out." The linear dispersion ranges from 240 A/mm for λ 3727 to 688 A/mm for N_1. In order to take account of all these factors in deriving a velocity for a plate, the shifts for each line have been given weights, which, in the judgment of each observer, seemed most likely to represent the reliability of the measures. Hence the individual velocities, V_1 and V_2, are, in a sense, weighted means.

TABLE 2*b*

RADIAL VELOCITIES OF THE NUCLEUS (NGC 598) AND NUCLEAR REGION OF M 33

Object in M 33	Date (PST)	Exp. Time	Set I			Set II			Mean V	Wt. w
			V_1	V_2	Δ	V_1	V_2	Δ		
(1)	(2)	(3)	(4)	(5)	(6)	(7)	(8)	(9)	(10)	(11)
6′.2 nf to nucleus	1939 Oct. 10, 11	14^h00^m	−190	−189	1	− 89	−156	67	−170	1.0
3′.1 nf to 3′.1 sp	40 Oct. 3, 4	18 00	183	180	3	.....	.....	....	182	0.7
Nucleus drifted	38 Aug. 23	6 00	166	161	5	164	152	12	162	1.0
Nucleus drifted	38 Aug. 25	6 00	185	164	21	200	195	5	181	1.0
3′.1 np to 3′.1 sf*	38 Sept. 22, 23	15 45	186	141	45	127	81	46	146	1.0
Nucleus to 6′.2 sp	39 Oct. 11, 12	15 00	−182	−162	20	−149	−161	12	−167	1.0

* Slit along minor axis; in all other cases, along the major axis.

V. ACCURACY OF THE RADIAL VELOCITIES

This question may be examined by comparing (*a*) the repeated measures of a single plate, which will give an estimate for the error of measurement, and (*b*) the measures of duplicate plates, which will lead to an estimate for the error of a single plate of unit weight.

a) Since there are available two sets of measures, it is possible to derive an error of measurement for each set, to calculate their relative weights, and to combine the two sets. Before this is done, however, it is desirable to know whether any large systematic difference exists between the two sets. From the values of V_1 and V_2 for Set I and Set II given in Tables 2*a* and 2*b* it is found that the systematic difference, in the sense Set I *minus* Set II, amounts to +1.6 and +4.5 km/sec, for the first and second measures in each set, respectively. Since the mean difference, +3.0 km/sec, is so small, it may be concluded that no systematic correction need be applied to one set in order to reduce it to

[22] The lack of a few measures in Set II is due to the fact that Aller left the Lick Observatory before all the plates were obtained.

the other. The probable error of measurement for each set may be obtained from the formula

$$\pm 0.6745\sqrt{\frac{\Sigma v^2}{N-n}} = \pm 0.6745\sqrt{\frac{\Sigma\Delta^2}{2n}},$$

where $v = \pm\frac{1}{2}\Delta$, $\Sigma v^2 = 2\Sigma(\Delta/2)^2$, n is the number of plates, and $N = 2n$ is the number of observations. If ϵ_{I} and ϵ_{II} are these errors for Set I and Set II, respectively, then the values of Δ given in columns 6 and 9 of Tables *2a* and *2b* lead to the following probable errors:

$$\epsilon_{\text{I}} = \pm 10.2 \text{ km/sec}, \qquad \epsilon_{\text{II}} = \pm 15.9 \text{ km/sec}.$$

Since the relative weights are inversely proportional to the squares of the probable errors, it is evident that

$$w_{\text{I}} = 0.7, \qquad w_{\text{II}} = 0.3.$$

By using these values of the relative weights, the two sets of measures may be combined and a single velocity deduced for each plate. If V_{I} and V_{II} are the means of V_1 and V_2 for Set I and Set II, respectively, then the combined velocity, V, may be calculated from the relation

$$V = 0.7V_{\text{I}} + 0.3V_{\text{II}}.$$

The values of V obtained in this manner are listed in column 10 of Tables *2a* and *2b*. The error of measurement associated with V, if termed ϵ_m, is given by the formula

$$\epsilon_m^2 = \left(\frac{\partial V}{\partial V_{\text{I}}}\right)^2 \epsilon_{\text{I}}^2 + \left(\frac{\partial V}{\partial V_{\text{II}}}\right)^2 \epsilon_{\text{II}}^2 = (0.7)^2\,(10.3)^2 + (0.3)^2\,(15.9)^2,$$

or

$$\epsilon_m = \pm 8.6 \text{ km/sec}.$$

b) An examination of the data in column 10 shows that there are 16 objects with duplicate plates, one (IC 132) with 3 plates, and one (NGC 604) with 4 plates. Thus there is available a total of 39 plates of 18 objects for a determination of the probable error of a plate of unit weight. Let this quantity be denoted by ϵ_{p+m} to indicate the fact that it is composed of two parts—one, ϵ_p, inherent in the plate, the other, ϵ_m, due to measurement. Then, to take account of the different weights of the plates, it is evident that

$$\epsilon_{p+m} = \pm 0.6745\sqrt{\frac{\Sigma wv^2}{N-n}} = \pm 0.6745\sqrt{\frac{47734}{39-18}},$$

$$= \pm 32.1 \text{ km/sec}.$$

This is a rather large probable error for a single plate; hence, the advantage of taking the mean of two plates, thereby reducing the error to $\pm 32.1/\sqrt{2} = \pm 22.7$ km/sec, is readily apparent. Since a probable error of 23 km/sec corresponds to a displacement, at λ 3950, of precisely 1 μ, this result indicates the microscopic size of the velocity shifts measured in the spectra.

Since the probable error of a plate of unit weight is found to be much larger than the error of measurement, it is clear that the principal source of uncertainty in a derived radial velocity resides in the plate itself. The actual value of this plate error for the present data is given by the relation

$$\epsilon_p^2 = \epsilon_{p+m}^2 - \epsilon_m^2 = (32.1)^2 - (8.6)^2,$$

PLATE III

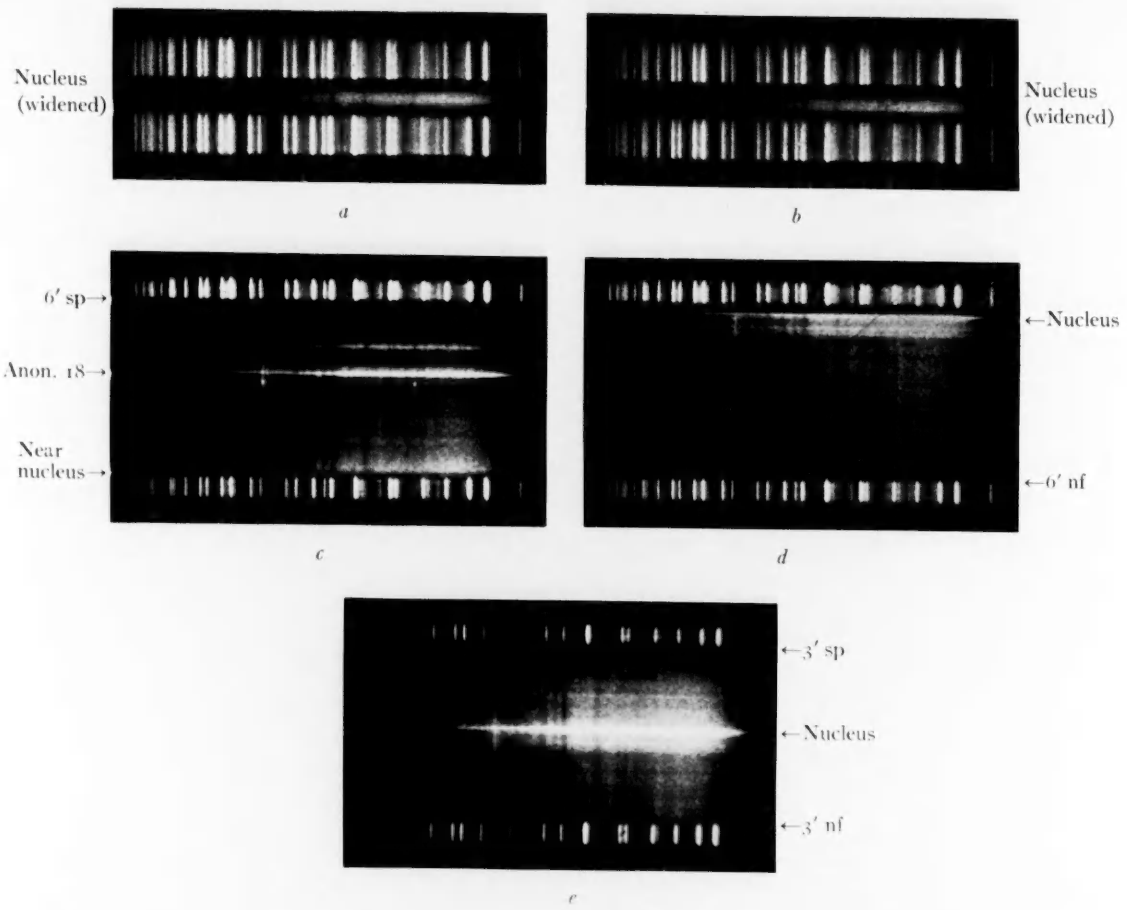

SPECTRA OF THE NUCLEUS AND NUCLEAR REGION OF M 33

a and *b* are two 6-hour exposures of the nucleus, which was drifted along the slit about 0′.5. *c*, *d*, and *e* are exposures of 15, 14, and 18 hours, respectively, with the slit held steady on the major axis (p.a. = 20°). Enlargement, 11×.

or

$$\epsilon_p = \pm 30.9 \text{ km/sec}.$$

The result, that the plate error is nearly four times the error of measurement, emphasizes the importance of obtaining several plates per object rather than making repeated measures of a single plate. Unfortunately, when a plate has to be exposed as long as one or two nights, the meeting of this condition consumes a great deal of time. The result is that the measurement of rotational motions in spirals, under present circumstances, proceeds very slowly.

VI. SYSTEMIC RADIAL VELOCITY OF M 33

The first step in determining the rotational velocities of the emission knots observed in M 33 is to obtain a value for the velocity of the spiral as a whole; this quantity will be referred to hereafter as the "systemic" velocity. In its evaluation it will be expedient to discuss separately the spectra and velocities found for (*a*) the nucleus, (*b*) the nuclear region, and (*c*) those condensations on or near the minor axis.

a) *Nucleus.*—The two plates of this object, reproduced in Plate III (*a* and *b*), yield a mean velocity of −172 km/sec and a spectral type of A7. Although the spectrum is primarily an absorption spectrum, it is probable that λ 3727 is present, for measures of a very faint emission feature give a velocity in substantial agreement with that found from the absorption lines.[23] These values for the nuclear velocity and spectral type do not agree very well with earlier Mount Wilson determinations, which are: −70 km/sec and Fo by Adams and Pease,[24] −330 km/sec and Fo by Humason,[25] and −320 km/sec and F5 quoted by Hubble.[26] However, Mr. M. L. Humason, of the Mount Wilson Observatory, kindly informs us, in a private communication, that these early measures may be discarded, since he has recently obtained plates of the nuclear spectrum, with higher dispersion, that are much superior in quality to the earlier ones. His unpublished results for the mean of two plates are: −189 km/sec and A7, which agree quite satisfactorily with the −172 km/sec and A7 mentioned above.

On the basis of all the available material, it would appear that the most probable value of the nuclear velocity lies in the neighborhood of −180 km/sec; but since it is not possible to examine the question of a systematic difference between the two sets of data, the figure −172 km/sec will be used in this paper in order to preserve the homogeneity of the material.

The evaluation of the nuclear velocity has been considered in detail, for the reason that it is important to investigate the degree of accordance that may exist between it and the systemic velocity. On purely dynamical grounds it is difficult to imagine how the two velocities could be appreciably different. In the next two parts of this section, (*b*) and (*c*), evidence is adduced which indicates rather definitely that the nuclear and systemic velocities probably are equal to within the errors of observation.

[23] Seyfert (*Ap. J.*, **91**, 538, 1940; *McDonald Contr.*, No. 20) has suggested that the difference of 0.25 mag. between his determination of the color (red index) of the nucleus and that by Stebbins and Whitford (*Ap. J.*, **86**, 255, 1937; *Mt. W. Contr.*, No. 577) "is probably accounted for by the presence of emission lines in the spectrum of the nucleus of M 33," as reported by the present writers (*Pub. A.S.P.*, **51**, 112, 1939). It is to be noted that only one bright line, λ 3727, was reported, and this in the nuclear region, not in the nucleus itself, so that it is perhaps questionable whether Seyfert's explanation is altogether adequate.

[24] *Pub. A.S.P.*, **28**, 34, 1916.

[25] *Pub. Lick Obs.*, **18**, 218, 1932 (J. H. Moore's *General Catalogue of Radial Velocities*). Owing to a typographical error, the estimate of type is connected with Slipher's determination of the velocity of NGC 604 from bright lines.

[26] *The Realm of the Nebulae*, p. 141. These figures represent a slight revision of the measures given in Moore's *General Catalogue*.

b) *Nuclear region.*—The spectral characteristics of the unresolved nebulosity out to a distance of some 6′ each side of the nucleus, along the major axis (p.a. = 20°), are also shown in Plate III (*c*, *d*, and *e*). As mentioned in Section IV, the region was surveyed by taking three exposures with the nucleus held steady on the south-preceding end, in the middle, and on the north-following end of the slit. All three spectra, as may be seen in the reproduction, appear very similar, and the estimates of spectral type from the three plates fall in the narrow range F9 to G0. A plate taken with the slit placed on the minor axis, nucleus central, has previously been reproduced,[27] and from it the spectral type was estimated as G0.[28] Therefore, the present data, which have the desirable property of homogeneity, indicate a significant difference in the character of the absorption-line spectrum of the nucleus and its near-by environs, amounting to almost one and a half spectral classes.

Another spectral characteristic of the nuclear region meriting comment is the bright line λ 3727 of [*O* II]. On all four plates of the nuclear region, this emission may be seen in good strength out to approximately 1′ from the nucleus. At that distance its intensity suddenly decreases so much that thereafter it is difficult, except on one plate (that labeled [*c*] in Pl. III), to follow the line across the remaining width of the spectrum. Since there is a more or less corresponding variation in the strength of the continuous spectrum, it is possible that the bright line in question actually is present at distances greater than 1′ or 1½′ from the nucleus, but that the circumstances of observation were such as to fail to reveal it except on one plate. The presence of λ 3727 in considerable strength, in a small region of unresolved nebulosity immediately surrounding the nucleus, makes it probable that the faint emission feature measured in the spectrum of the nucleus itself is due to unavoidable superposition of both sources of light simultaneously on the slit. So far as can be determined from the data, there is no appreciable variation in the spectral type of the absorption lines within the observed range of 6′ each side of the nucleus.

The radial velocity measures of the three major-axis plates and the one minor-axis plate of the nuclear region yield quite consistent results, as may be seen from the values of *V* given in column 10 of Table 2*b*. The range in velocity is from −146 to −182 km/sec. The tabulated values, however, represent the means for each plate of a number of measures made at 1′ or 2′ intervals from the nucleus. The reason for making these additional measures was to find out whether or not there are small rotational velocities in the nuclear region of M 33, similar to those found by Babcock in M 31. Although, with one exception (slit along the major axis, nucleus central), each spectrum was measured twice by each observer, there is no definite evidence of any velocity variation from 1′ to 6′ from the nucleus. The scatter in the measures is so considerable that it is not possible to detect the slight inclination of the lines to be expected from the mean rotational velocities, shown below in Figure 2, where, according to the smooth curve, the maximum rotational velocity difference from the nucleus to a distance of 6′ would amount to only 20 km/sec in the plane of the spiral. In view of these measures, it seems justifiable to average all the velocity measures for each plate of the nuclear region. When this is done, there results a weighted mean value for the systemic velocity, from the four plates described, of −166 km/sec. This figure may be compared with that found above for the nucleus itself, namely, −172 km/sec. Hence, the present observations furnish support for the assumption that there is little, if any, relative line-of-sight motion between the nucleus of M 33 and the unresolved nebulosity in which it is imbedded.

c) *Condensations on or near the minor axis.*—Obviously, radial velocities for objects so situated in the spiral that their rotational motions are nearly across the line of sight may also be used to estimate the systemic velocity. It must be assumed in this case, of course, that the motions along the radius vector from the nucleus to the object are so small as to be negligible. To what degree this assumption is valid for the objects ob-

[27] *Pub. A.S.P.*, **51**, 112, 1939, Pl. XV.

[28] *Lick Obs. Bull.*, **19**, 36, 1939 (No. 497).

served in M 33 cannot be estimated from the approximate data at hand; but, in the light of current theories of stellar dynamics, it seems a permissible one to make, especially in a first approximation. Accordingly, a third check on the systemic velocity may be obtained by calculating the weighted mean velocity for those condensations in Table 1 for which no value of sec θ is given, namely, IC 131, NGC 595, Anon. 11, Anon. 2, and NGC 588 (Anon. 4 and NGC 592 are omitted because their spectra are continuous). The result is a mean velocity of -167 km/sec.

Thus, three different groups of data yield values for the systemic velocity of M 33 as follows: nucleus, -172; nuclear region, -166; and minor-axis condensations, -167. All three ways of estimating the same quantity agree so closely that it appears justifiable to form the weighted mean of all the material. Table 3 summarizes the foregoing results and leads to the final value of the systemic velocity, V_s, and its probable error, ϵ_s.

TABLE 3

SYSTEMIC RADIAL VELOCITY OF M 33

Object or Region	Mean Observed Velocity*	Total Assigned Weight	Region
NGC 598	-172 km/sec	2.0	Nucleus
6′.2 nf to nucleus	-170	1.0	Nuclear region
3′.1 nf to 3′.1 sp	-182	0.7	
3′.1 np to 3′.1 sf	-146	1.0	
Nucleus to 6′.2 sp	-167	1.0	
IC 131	-160	2.0	Condensations on or near minor axis
NGC 595	-130	2.0	
Anon. 11	-192	1.0	
2	-166	2.0	
NGC 588	-198	2.0	

* The velocity is a mean of two plates when the weight is 2.0.

Systemic velocity, $-167 \pm 5 = V_s \pm \epsilon_s$

VII. ROTATIONAL VELOCITIES OF 20 BRIGHT-LINE CONDENSATIONS IN M 33

At this point it is necessary to introduce a fundamental assumption, which seems to be unavoidable. This assumption is that all the bright-line objects observed for radial velocity move in circular orbits around the nucleus and in the principal plane of the spiral. The justification for this hypothesis of simple circular motion comes mainly from theoretical investigations of dynamics of stellar systems and from studies of the rotational motions of stars in the Galaxy.[29] Moreover, unless the departures from circular motion are fairly large in M 33, they will be masked by the rather large errors of observation; and, in a first crude attempt to find out something about the general character of the motion, it appears permissible to use the simplest possible method to derive the rotational velocities. Under the assumption mentioned, the rotational velocity V_R is found from the obvious relation

$$V_R = (V_o - V_s) \sec \theta \sec i \, .$$

In this equation, θ is the azimuth angle and i the inclination angle—quantities previously defined and evaluated. V_o is the observed velocity for each object, obtained by forming the weighted mean velocity from the several plates, according to the appropriate values of the plate velocity, V, and its weight, w, as listed in columns 10 and 11 of Table 2*a*.

[29] Cf., in this connection, J. H. Oort, *Ap. J.*, **91**, 277, 1940; *M.N.*, **99**, 374, 1939.

Furthermore, if ϵ_0 is the probable error of V_0, and ϵ_s that of V_s, then the probable error of a rotational velocity, ϵ_R, is easily seen to be given by the formula

$$\epsilon_R^2 = (\epsilon_0^2 + \epsilon_s^2) \sec^2 \theta \sec^2 i ,$$

in which the effect of an error in the inclination is neglected.

Application of the above two equations to the data already described leads to the quantities in Table 4. The objects in column 1 are arranged according to their nuclear

TABLE 4

ROTATIONAL VELOCITIES OF 20 BRIGHT-LINE CONDENSATIONS IN M 33

Object (1)	R (2)	V_0 (3)	ϵ_0 (4)	w_0 (5)	V_R (6)	ϵ_R (7)	w_R (8)
		km/sec	km/sec		km/sec	km/sec	
Anon. 1	29'.8 sp	−115	±23	2.0	+ 62	± 28	2.0
6	24.6 sp	61	60	0.3	+165	94	0.2
19	20.5 sp	59	28	1.4	+136	36	1.2
8*b*	19.1 sp	100	39	0.7	+ 82	48	0.7
8*a*	18.5 sp	80	23	2.0	+107	29	1.9
7	17.4 sp	114	25	1.7	+ 93	45	0.8
IC 135	15.0 sp	69	33	1.0	+117	40	1.0
Anon. 14	9.2 sp	158	33	1.0	+ 11	42	0.9
16	6.9 sp	140	33	1.0	+ 32	40	1.0
18	2.9 sp	75	60	0.3	+110	72	0.3
IC 142	6.1 nf	167	33	1.0	0	42	0.9
Anon. 3	13.5 nf	248	23	2.0	− 98	28	2.0
NGC 604	14.6 nf	279	16	4.0	−195	29	1.9
Anon. 9*c*	19.4 nf	226	42	0.6	− 71	51	0.6
9*b*	19.7 nf	269	23	2.0	−124	29	2.0
9*a*	22.6 nf	204	23	2.0	− 44	28	2.0
IC 133	23.4 nf	203	23	2.0	−101	66	0.4
Anon. 20	24.3 nf	162	42	0.6	+ 13	112	0.1
15	26.2 nf	179	42	0.6	− 18	64	0.4
IC 132	27.1 nf	−205	±19	3.0	− 92	± 47	0.7

distances, R, in column 2; the upper half of the table contains those south-preceding the nucleus, the lower half, those north-following. Columns 3, 4, and 5 contain, respectively, the observed velocity, V_0, its probable error, ϵ_0, and its weight, w_0. The values given for ϵ_0 are found from the relation

$$\epsilon_0 = \frac{\pm 32.1}{\sqrt{w_0}} ,$$

in which, as already stated, 32.1 is the probable error of a plate of unit weight, while w_0 is, of course, the sum of the weights of all plates of the same object. In order to indicate, as directly as possible, the principal observational result, before the rotational velocities are deduced, the mean observed velocities for the 25 emission condensations listed in Tables 3 and 4 are shown in Plate I*b*. Columns 6, 7, and 8 list, respectively, the rotational velocity, V_R; its probable error, ϵ_R; and its weight, w_R. The values of V_R and ϵ_R were obtained as indicated in the preceding paragraph, while the weights w_R were calculated from the relation $w_R = 1600/\epsilon_R^2$, in which the factor of proportionality obviously is the square of the probable error for a rotational velocity having unit weight, i.e., $\epsilon_R = 40$ km/sec for $w_R = 1.0$.

To indicate the run of rotational velocity with distance from the nucleus, the values of V_R in Table 4 are plotted against the nuclear distance, R, in Figure 1. Also, to show the uncertainties inherent in the data, the probable errors ϵ_R are shown as vertical lines extending equal distances above and below the points corresponding to the appropriate values of V_R. The figure plainly shows two features of the rotational motion that are worthy of mention. First, the apparent direction of rotation seems well established, for all objects south-preceding the nucleus indicate velocities of recession with respect to the nucleus, while all objects but one (Anon. 20) north-following the nucleus show relative velocities of approach. The actual direction of rotation—in particular, that with respect to the curvature of the spiral arms—is, in this spiral, quite indeterminate. Second, it is

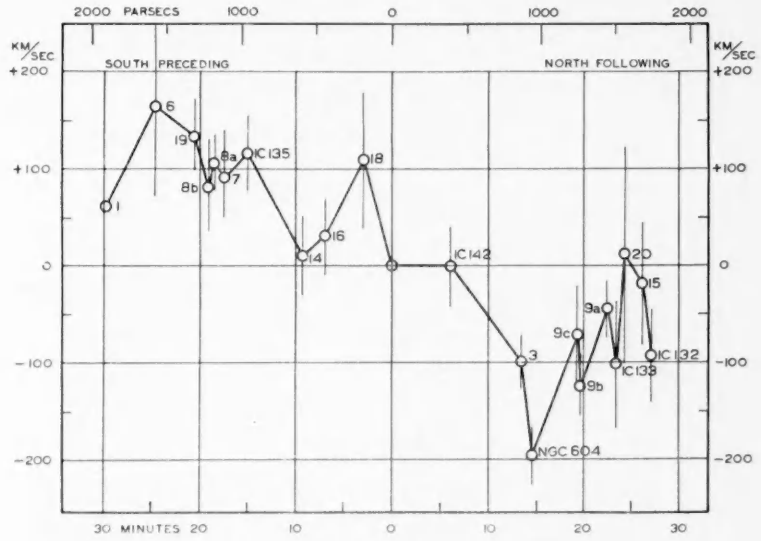

FIG. 1.—Rotational velocities of 20 emission condensations in M 33

clear that the errors of the rotational velocities are not sufficiently small to allow of any but the most general conclusions regarding the nature of the rotation. It is manifestly impossible to decide, for example, whether or not the relation between rotational velocity and nuclear distance is symmetrical about the nucleus. To a first approximation, it appears to be so, and this property of the motion will therefore be assumed in an attempt to define, as far as practicable, the character of the relation between V_R and R.

With so large a scatter in the rotational velocities, it is desirable to try to minimize the effect of the errors of observation on the relation between V_R and R. This may be attempted in one of several ways—for example, by taking the weighted means of several values of V_R corresponding to several consecutive values of R. In other words, overlapping or running weighted means for three objects at a time may be formed, and this procedure was tried for the data in Table 3. However, the resulting "rotational curve" displayed curious irregularities close to, and distant from, the nucleus that were directly traceable to several of the objects (Anon. 18, 6, and 20) whose velocities are those most inaccurately determined. Furthermore, this way of smoothing the data disclosed that one object, NGC 604, tended to distort the curve in the region of maximum rotational velocity. The disturbance was in the sense that inclusion of this one object raised the curve by an amount equal to 50 km/sec over a distance of nearly 10′ in R. Finally, the practice of taking running means, while perhaps permissible in this case where large errors and gentle

slopes are involved, introduces systematic errors in the shape of a derived curve. For these reasons, the curve resulting from smoothing the velocities in the manner stated was discarded. Nevertheless, the process proved useful in pointing out NGC 604 as an object having an anomalous velocity. Since NGC 604 is by far the largest and brightest condensation in M 33, it is, perhaps, reasonable to regard it more as a satellite system than a component part of the main spiral. If this were the case, its velocity may be appreciably different in direction and amount from that to be expected on the basis of simple circular motion about the nucleus of M 33.[30]

Another way in which the general run of the rotational velocities with nuclear distance may be more definitely established is to take weighted means of V_R for different

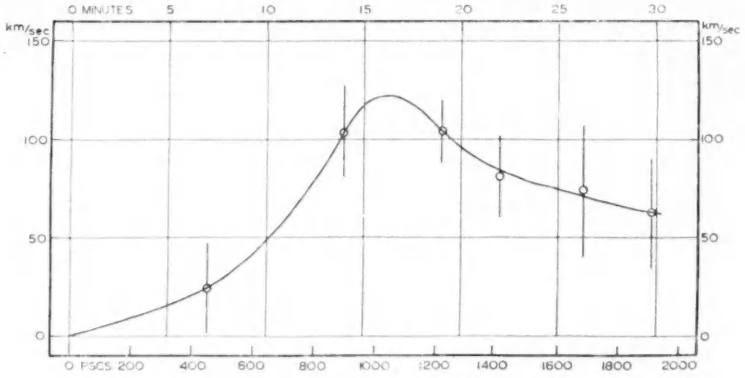

FIG. 2.—Mean rotational velocities in M 33

intervals of R, and several trials of this method have led to a form of the relation between V_R and R that appears to be the most satisfactory one deducible from observations of such low precision. The data, as finally combined into group means, or normal places, are tabulated herewith and are shown in Figure 2.

MEAN ROTATIONAL VELOCITIES IN M 33

Bright-Line Objects in M 33	Interval in R	$\bar{R}$	$\bar{V}_R$	ϵ Km/Sec	Wt.
IC 142; Anon. 14, 16, 18	0′–12′	7′.0	24	±23	3.1
IC 135; Anon. 3	12–16	14.0	104	23	3.0
Anon. 7, 8*a*, 8*b*, 9*b*, 9*c*	16–20	18.9	104	16	6.0
IC 133; Anon. 9*a*, 19	20–24	22.0	81	21	3.6
IC 132; Anon. 6, 15, 20	24–28	26.3	74	34	1.4
Anon. 1	28–32	29.8	62	28	2.0

The grouping shown in the accompanying table, which omits NGC 604 for the reason previously stated, is for intervals between multiples of 4′ in R, except for the region from the nucleus to $R = 12'$. Since in this interval there are only four objects, one of which (Anon. 18) has a large probable error, it has appeared best to take the weighted mean of them all. In any case, the manner in which the group means is taken is arbitrary, and the particular method adopted here represents an effort to form normal places from

[30] An analogous situation may exist between the Andromeda nebula (M 31) and its close companion, NGC 221 (M 32). Cf. Hubble, *The Realm of the Nebulae*, p. 141.

those objects whose low-weight velocities display a large but rather symmetrical scatter about the mean (Anon. 6 and 20), as well as to guide the final mean relation through individual velocities having relatively high weight (Anon. 1).

The principal result of this investigation is graphically exhibited in Figure 2, in which the group means tabulated above are plotted together with their probable errors, ϵ. The points are connected with a smooth curve, which is drawn with the realization that it indicates, in only the most general way, the relation between rotational velocity and nuclear distance. In judging the value of the result, it must not be forgotten that departures from the fundamental assumption of simple circular motion will, of course, change the positions of the mean points on the velocity axis and will also increase the dispersion about each mean. It is difficult, if not impossible, to estimate the magnitude of these noncircular components; but, by analogy with the known peculiar motions of the galactic diffuse nebulae, it may be presumed that they are, in general, fairly small, of the order of 10 km/sec.[31] In any event, it may be supposed that the peculiar motions of the bright-line objects in M 33 are not so large as that indicated for NGC 604, that is to say, of the order of 50 km/sec.

VIII. DISCUSSION OF RESULTS AND COMPARISON OF M 33 WITH OTHER SYSTEMS

Although, as stated at the beginning of this paper, the theoretical discussion of the data is made the subject of another article, there are, nevertheless, a few points in connection with the observations that may appropriately be considered at this time.

The rotation of M 33 may conveniently be described by supposing the spiral to be divided into two parts, corresponding to two regions in which the character of the motion is significantly different. These two regions are: (1) the "main body" of the spiral, some 18′ in radius; (2) the "outer parts," represented by a zone having least and greatest radii of 18′ and 30′, respectively. Briefly stated, the rotation of the main body appears to be of the "solid-body" type, since the more or less uniform increase of the rotational velocity with distance from the center indicates an approach to constant angular velocity, while for the outer parts the rotation appears to be of the "planetary" type, since the rotational velocities decrease with distance from the center.

While the results given here for M 33 may possess some interest and value considered only by themselves, possibly their significance would become plainer if they could be compared with similar results for other spirals. However, an attempt to make such a comparison at the present time meets with two difficulties. In the first place, M 33 is an average spiral in respect to its more important characteristics, such as luminosity and diameter, while the other systems for which rotations are available, are, with one probable exception, giants. Whether the internal motions in giant and average spirals are comparable in respect to their rotations is, on dynamical grounds, open to question, for the larger and more massive systems would be expected to rotate more slowly than average systems. In the second place, the rotation measures that have heretofore been published for other spirals, with the exception of the Andromeda nebula, have not yet been published in sufficient detail; nor do they extend far enough throughout the spirals to allow of a fair comparison with those reported here for M 33. In order to bring out more plainly these difficulties and to indicate in which directions further rotational measures appear to be especially desirable, the following paragraphs and tables summarize the principal results for the few nebulae whose rotations have been investigated in some detail.

There are currently available detailed results for five systems: the Andromeda nebula (M 31), Messier 33, and NGC 4594, 4111, and 3115. The following table gives the more

[31] This figure is based on the result found by Campbell and Moore (*Pub. Lick Obs.*, **13**, 182, 1918) that "the average radial velocity of the 5 extended irregular nebulae with reference to the stellar system is 11 km/sec." The five nebulae are: Orion, η Carinae, Trifid, M 8, and the Horseshoe.

important physical characteristics of these systems, as collected from the various sources noted below.

Nebula (1)	Type (2)	Distance (Parsecs) (3)	Luminosity (Pg. Mag.) (4)	Diameter (Parsecs) (5)
M 33	Sc	2.2×10^5	−14.9	4,000
M 31	Sb	2.1×10^5	17.5	12,000
4594	Sa	1.9×10^6	18.5	3,900
4111	Sa	1.6×10^6	14.5	1,600
3115	E7	1.5×10^6	−16.2	1,700

The distance, luminosity, and diameter given in columns 3, 4, and 5, respectively, for M 31 and for M 33, are taken from Hubble's book, *The Realm of the Nebulae*, page 126. The distances listed for 4594 and 4111 are calculated from their observed velocities,[32] corrected for galactic rotation,[33] using the velocity-distance relation.[34] The distance quoted for 3115 is an estimate by Oort,[35] who gives reasons for believing that the distance obtained from the velocity-distance relation, 8.6×10^5 parsecs, probably is too small, although he qualifies his estimate with the remark that "the true distance may well differ from it by a factor as large as 2 in either direction." The absolute magnitudes for the same three objects are based on the tabulated distances and on Shapley and Ames's apparent total magnitudes,[36] corrected for zero point by −0.08 mag., as suggested by Stebbins and Whitford's photoelectric work on nebular magnitudes;[37] they are also corrected by -0.25 (csc $b-1$) for galactic absorption, as suggested by Hubble's counts of extragalactic nebulae.[38] The red-shift correction to the apparent magnitudes may be neglected for these near-by systems.

Thus, in respect to their luminosity and size, it appears that M 31, NGC 4594, and NGC 3115 are giants, while M 33 and NGC 4111 are average systems. If the observed rotational velocities are now used to calculate the periods of rotation,[39] and the latter, in turn, are used to estimate the masses,[40] then it likewise seems to be true that there exists a similar division of this group of nebulae in respect to their masses. The results of such a calculation are given in the table herewith, which also includes the current estimates of the mass of the Galaxy and of the period of rotation for the solar neighborhood. In order not to make misleading comparisons and to represent the observations properly, it seems advisable to list the periods for three regions: the nuclear region, the

[32] These are: for 4594, +1180 km/sec, Pease (*Proc. Nat. Acad. Sci.*, **2**, 517, 1916; *Mt. W. Comm.*, No. 32); for 4111, +810 km/sec, Humason (*Ann. Rept. of the Director of Mt. W. Obs., 1936–1937*, p. 31).

[33] The solar galactic rotation term is taken as $+275\cos(l-55^\circ)\cos b$, where l and b are galactic coordinates.

[34] The velocity-distance factor employed here is 525 km/sec/10^6 parsecs (Hubble, *Ap. J.*, **84**, 292, 1936; *Mt. W. Contr.*, No. 549).

[35] *Op. cit.*, p. 295.

[36] *Harvard Ann.*, **88**, No. 2, 1932.

[37] *Ap. J.*, **86**, 264, 1937; *Mt. W. Contr.*, No. 577.

[38] *Ap. J.*, **84**, 273, 1936; *Mt. W. Contr.*, No. 549.

[39] If V_R is the rotational velocity in km/sec, R the nuclear distance in seconds of arc, and d the distance to the spiral in parsecs, then P, the period of rotation in years, is given by the formula $P = 29.7\times d\times R/V_R$.

[40] The mass in units of the sun, $M_\odot$, may be found from the relation

$$M_\odot = 1.13\times10^{-3}\times d\times R\times V_R^2 = 3.81\times10^{-5}\times P\times V_R^3 .$$

main body, and the outer parts; this is done in columns 3, 4, and 5 upon the basis of the sources noted below.

Nebula	Type	Period in Years			Mass in Suns
		Nuclear Region	Main Body	Outer Parts	
(1)	(2)	(3)	(4)	(5)	(6)
Galaxy	(Sc)	.....	.....	2.2×10^{8}	1 to 2×10^{11}
M 33	Sc	.....	5.9×10^{7}	0.6 to 2.0×10^{8}	1.7×10^{9}
M 31	Sb	1.1×10^{7}	9.2×10^{7}	.....	9.5×10^{10}
4594	Sa	.....	2.0×10^{7}	.....	2.8×10^{10}
4111	Sa	1.4×10^{6}	.....	.....	.....
3115	E7	.....	4.5×10^{6}	.....	1.5×10^{10}

The periods given in columns 4 and 5 for M 33 are derived from the mean observed rotational velocities shown in Figure 2 of this paper; for M 31 the periods are those deduced by Babcock;[41] for 4594 it is computed from Pease's rotation measures;[42] for 4111 and 3115 they are obtained from Humason's results.[43] The masses given in column 6 for M 33 and M 31 are those deduced in the following paper, while for 4594 and 3115 they have been calculated, as indicated in the preceding paragraph, from the periods. For the Galaxy, M 31, M 33, 4594, and, in lesser degree, for 3115, the masses tabulated may suggest the correct order of magnitude of the total mass, since the rotational measures in these systems extend to distances fairly large compared with the size of the systems. In the case of 4111, however, Humason has published his results in detail only for the central lens; for the rest of the nebula, out to at least 50″, he finds that "the rotation decreases with increasing distance in a manner which suggests the operation of an inverse quadratic law." Until the measures for these outer parts are published in detail, it does not appear worth while to try to estimate the total mass for 4111.

The foregoing table shows rather definitely that the Galaxy, M 31, 4594, and probably 3115 are giant systems in respect to their masses. Furthermore, M 33, with the lowest mass but with other characteristics that are average, presumably is also of average mass. On the same grounds, 4111 may be assumed to be of average mass. Hence, in this group of six nebulae there probably are four giant and two average stellar systems. One of the latter is M 33, and, therefore, its rotational characteristics are strictly comparable only with the other, NGC 4111, for which, at present, detailed rotation measures are available only for the nuclear region. This circumstance suggests that further comparison of these two average spirals—at least for the present—is unprofitable.

A comparison of the rotation of the main body of M 33 with the rotations of the corresponding parts of M 31, 4594, and 3115 probably means little, for the reason already stated, namely, that M 33 is an average spiral, while the other three are giants. There seems to be no serious objection, however, to comparing the rotational properties of the principal parts of these giants; and, if this is done, there is a suggestion that the period of rotation increases with advancing nebular type, for the above table yields the sequence of periods in years, 4.5×10^{6}, 2.0×10^{7}, and 9.2×10^{7}, corresponding to E7, Sa, and Sb, respectively. The correlation has already been noted by Hubble, who has described, as follows, a similar result based upon Humason's rotation measures: "From E7 to

[41] *Op. cit.*, p. 48.

[42] *Proc. Nat. Acad. Sci.*, **2**, 520, 1916.

[43] *Ann. Rept. of the Director of Mt. W. Obs., 1936–1937*, p. 31.

the end of the sequence, the periods of rotation, *as indicated by the table*, seem to increase steadily and rapidly—from about 3 million years to 200 million years."[44] The table referred to presented results for the six systems NGC 3115 (E7), 2685 (So), 4111 (Sa), 4594 (Sa), M 31 (Sb), and the Galaxy (Sc). The number of objects in this group is reduced to four, however, if the correlation of the periods of rotation is made for only the main bodies of these spirals; as mentioned above, the available data lead to periods for 4111 and for the Galaxy that refer to the nuclear and outer regions, respectively. The detailed measures for 2685 have not yet been published.

It is an interesting question whether the period of rotation for the principal part of the Galaxy, presumably a giant Sc, is still longer than any of the above periods, and also whether the periods for the earlier-type elliptical nebulae increase from E7 to E0, as might be expected purely from their decreasing ellipticity. If further observations should demonstrate that a minimum rotation period, or a maximum spin, occurs in the vicinity of E7 to Sa—a stage in the sequence termed "So" by Hubble—then the rotation measures would yield a datum of much significance for the study of the dynamics of nebulae, for it is just at this stage in the system of classification that spiral structure becomes recognizable.

As for the rotation of the outer part of M 33, it appears that this, likewise, stands by itself, to an even higher degree than for the other parts of the spiral. Rotation measures for the corresponding region in other spirals are not yet available, for the very good reason that such measures are extremely difficult to obtain. Even in the case of the Andromeda nebula, in which the measures extend to 100′ from the center, it is doubtful whether the outermost parts have been reached, for the rotational velocity is observed to be still increasing. The photoelectric measures of surface brightness in the vicinity of this object made by Stebbins and Whitford[45] and the distribution of the globular clusters discovered by Hubble[46] are additional evidence that M 31 extends considerably beyond the point where the rotation measures stop.[47]

There is one point in connection with the rotation of the outer parts of M 33 that may well be emphasized, because of its bearing on the estimation of the sun's relative position in the Galaxy. In the solar neighborhood it is now definitely established that the rotational velocity decreases with the distance from the center and that the rate of decrease, according to an authoritative estimate,[48] is 0.005 km/sec/parsec. In the outer parts of M 33, at a nuclear distance of 1600 parsecs, the rotational velocity also decreases, approximately 0.030 km/sec/parsec. Since the sun is of the order of 8000 parsecs from the galactic center, the comparison of these figures strongly suggests the hypothesis that the solar neighborhood lies far out from the main body of the Galaxy. This idea is, of course, by no means new; for example, Lindblad has expressed it, on the basis of more general dynamical considerations.[49] However, the present observations may be regarded as furnishing a bit of direct observational evidence in support of the hypothesis mentioned.

The comparison of the outer parts of M 33 and of the Galaxy given in the preceding paragraph suggests that it may also be of interest to calculate Oort's rotational constant A for several points in the outer regions in M 33. For this purpose it is convenient, in

[44] Reported in an unpublished paper read at the dedication of the McDonald Observatory, May 7, 1939.

[45] *Proc. Nat. Acad. Sci.*, **20**, 93, 1934; *Mt. W. Comm.*, No. 113.

[46] *Ap. J.*, **76**, 44, 1932; *Mt. W. Contr.*, No. 452.

[47] After this was written, R. C. Williams and W. A. Hiltner (*Michigan Univ. Obs. Pub.*, **8**, 103, 1941) published a paper on the "Dimensions and Shape of the Andromeda Nebula." By using a new type of highly sensitive microphotometer of their own design, which traces directly the isophotal contours from photographs, they found that "the apparent diameter of the Andromeda nebula along the major axis must be *at least* 400′, or 6°.7." The linear diameter, therefore, is not less than 25,000 parsecs, or 80,000 light-years.

[48] Oort, *M.N.*, **99**, 375, 1939.

[49] *Festskrift Tillägnad Östen Bergstrand*, p. 30, 1938.

order to use the data presented in Figure 2, to transform the usual expression for A, which involves the central force K, into a form which includes only the rotational velocity V_R and the distance R. From the relation, $V_R^2 = KR$ it follows that

$$A = \frac{1}{2}\left(\frac{V_R}{R} - \frac{dV_R}{dR}\right).$$

From the smooth curve drawn through the mean points plotted in Figure 2, it is easy to determine graphically values of dV_R/dR, which lead to the following approximate values of A:

R	20	25	30 minutes of arc
R	1280	1600	1920 parsecs
V_R	98	74	62 km/sec
dV_R/dR	−0.091	−0.051	−0.029 km/sec/parsec
A	+0.084	+0.048	+0.030 km/sec/parsec

According to Oort,[50] a provisional value of $A = +0.018$ km/sec/parsec may be adopted for the region surrounding the sun in the Galaxy. Hence, even at a nuclear distance of 1900 parsecs in M 33, a region has not yet been reached wherein the rotational motion is comparable with that existing in the solar neighborhood. The rather marked variation of A with nuclear distance in the outer parts of M 33 is also a point of difference worth noting; and, if the variation indicated above is maintained beyond where the observations end, a rough extrapolation suggests that A would decrease to +0.018 km/sec/parsec at a nuclear distance of approximately 2200 parsecs. This distance is nearly twice the radius of the main body of M 33, and, if an analogy with the Galaxy may again be drawn, then the diameter of the main part of the Galaxy may be inferred to be of the order of 8000 parsecs. Since this inference is justifiable only to the degree that the unknown distributions of mass in the two systems are similar, its speculative character is obvious.

The foregoing review of the rotational motions observed in spirals appears to shed more light on what is needed in the way of further observations than it does on the nature and significance of the rotational motions measured up to now. From the point of view of correlating these motions with the progressive structural changes that are so well arranged by means of the system of classification, it would seem that rotational measures are highly desirable for, first, a representative collection of nebulae of all types.[51] Second, in order to insure a valid comparison between the different types of objects, it would be advantageous if the nebulae selected for observation had nearly the same physical properties, such as luminosity, size, and mass. Third, in order to make an adequate comparison of the homologous parts of nebulae of different types, it is important that the rotation measures extend from the nucleus to the outermost parts. Since the meeting of any one of these conditions presents an observational problem of the first magnitude, it is probable that considerable time will be required before a well-rounded body of factual knowledge is acquired in the field of nebular rotations.

LICK OBSERVATORY
MOUNT HAMILTON, CALIFORNIA
March 1941

[50] *M.N.*, **99**, 374, 1939.

[51] It is a curious fact that no rotation measures for the barred spirals have yet been published.

DISTRIBUTION OF MASS IN THE SPIRAL NEBULAE MESSIER 31 AND MESSIER 33*

A. B. WYSE AND N. U. MAYALL

ABSTRACT

The relation between density distribution in a plane, circularly symmetrical disk, and the central force exerted upon points in its plane is investigated. For a disk in which the surface density can be expressed as a polynomial of the fifth degree in the distance from the center, it is possible to determine the force-curve in the plane, for interior and exterior points, by means of equations (8), (11), and (16), with the aid of Tables 1 and 2. The determination consists of the simultaneous solution of five linear equations. The curve of force can be converted into a curve of rotational velocity if simple circular motion is assumed. Conversely, it is possible to find the density distribution corresponding to a given force-curve.

The observed rotational-velocity-curves of M 31 and M 33 are found to be adequately represented by thin-disk models. The solutions indicate a wide distribution of mass throughout both systems with but little tendency toward central concentration. The average *projected density* in the main body of M 31 is of the order of 10^3 ⊙/psc²; and of M 33, 5×10^2 ⊙/psc². With reasonable assumptions of the thickness of the two nebulae, the mean *space density*, averaged perpendicularly to the principal plane, is approximately 2 ⊙/psc³ in the main bodies of both objects. In the outer parts of M 33 the space density is probably between 0.0 and 0.3 ⊙/psc³, which is comparable with the density of matter in the solar neighborhood of the Galaxy. The total mass of M 31 is found to be 9.5×10^{10} ⊙; and of M 33, 1.7×10^9 ⊙.

The constants of galactic rotation, in Oort's formulation of the problem, are re-examined with regard to the information they may yield concerning the distribution of mass. It is concluded that the high central concentration of matter, commonly quoted for the Galaxy, is not a necessary consequence of the observational data.

I. INTRODUCTION

Recent investigations of the rotation of the spirals in Andromeda (M 31)[1] and in Triangulum (M 33)[2] give information that can be utilized in finding the distribution of matter in these objects. The relation between the rotational-velocity-curve and the density distribution, as well as other parameters, has been discussed by Lindblad,[3] Babcock,[1] Holmberg,[4] Oort,[5] and others. In the present paper such a relation is derived for a thin-disk model, and the results are applied to the radial-velocity observations of rotation for M 31 and M 33. It is assumed, in the simple model under consideration, first, that the nebula is an infinitesimally thin disk; second, that it possesses circular symmetry, i.e., that the surface density is a function of the distance from the center but is independent of the angle; and, third, that the individual parts of the disk are revolving in circular orbits about the center, in the plane of the disk.

The principal reason for studying the model described above is the relative simplicity of the mathematical treatment. In addition, there are several grounds for the belief that the thin-disk model is capable of yielding useful information about the dynamics of the majority of extragalactic nebulae. In the first place, nebulae that show a well-defined spiral structure are relatively thin—so thin in comparison with their diameters that only a small error is introduced by the assumption that the mass is concentrated in a plane. In the second place, there is good basis for the supposition that the irregularities in density suggested by the spiral arms are not nearly so great as might be inferred from an in-

* *Contributions from the Lick Observatory, University of California*, Ser. II, No. 2.

[1] H. W. Babcock, *Lick Obs. Bull.*, **19**, 41, 1939 (No. 498).

[2] Mayall and Aller, *Ap. J.*, **95**, 5, 1942.

[3] *Zs. f. Ap.*, **15**, 124, 1938.

[4] *M.N.*, **99**, 650, 1939.

[5] *Ap. J.*, **91**, 273, 1940.

spection of a photograph.[6] Moreover, the apparent darkness of the spaces between the spiral arms may in some cases be accentuated by dark material, the presence of which would tend to smooth out the irregularities in density that might be inferred from the distribution of luminosity. The simple thin-disk model is not considered an extremely close approximation to any actual stellar system, but merely a fair approximation to the intermediate- and late-type spirals, which occur more frequently than the other classes of nebulae.[7]

It may be emphasized in the beginning that the density distributions deduced here for M 31 and M 33 are not unique. Even under the assumptions stated above, the derived density distribution is in some respects rather sensitive to errors in the observed rotation-curve. Furthermore, since plausible arguments might be advanced in support of various alternative models, some of which might include the hypothesis of noncircular motion of the component parts of the system, it is conceivable that a different formulation of the problem might indicate density distributions differing considerably from those derived here. The chief merit of the present method is that it makes use of but a few simple assumptions, which lead to an interpretation of the observed rotational velocities in terms of reasonable distributions of mass.

II. OUTLINE OF THE METHOD

The central force exerted by a plane, circular, homogeneous disk upon unit mass at any point in the plane can be expressed as a simple function of Legendre's complete elliptic integrals of the first and second kinds. The modulus of the integrals depends upon the radius of the disk and the distance of the attracted point from the center. In order to calculate the central force of a nonhomogeneous plane circular disk (i.e., of a disk in which the surface density is a function only of the distance from the center), we consider the disk to be composed of an infinite number of concentric, homogeneous, plane, circular disks, of different radii, each of infinitesimal density, and each exerting an element of central force upon a given unit mass. It is only necessary, then, to integrate the element of force over all the elemental disks in order to obtain the total central force. The integration is relatively easy if the density can be expressed as a series in ascending powers of the distance from the center. The fact is that the first few terms of such a series are capable of representing a great variety of assumed laws of density distribution. We have found it both convenient and satisfactory to terminate the series after the fifth-degree term.

The integrations that are required in order to calculate the central force exerted by the model at certain predetermined points, both inside and outside the disk, have been performed; the numerical results are presented in the main body of the paper. If a hypothetical density distribution is assumed, the central force at any distance can be calculated by means of the tabulated numerical coefficients; and the central force can then be converted into rotational velocity as a function of the distance from the center, to give a result that may be compared with the observed rotational-velocity-curve. Conversely, the order of the calculation may be reversed by converting the observed rotational-velocity-curve for a given nebula into a force-curve and then solving directly for the density distribution. The last two sections of the paper consist of applications of the method to the spiral nebulae, M 31 and M 33.

III. DERIVATION OF THE FORMULAE AND TABLES

Several reasons for treating the late-type spirals as thin disks have already been stated, but it will be useful to examine some of them a little more closely before restricting the

[6] Cf. Seyfert, *Ap. J.*, **91**, 539, 1940. The prominence of the spiral arms is due in large measure to an optical illusion, which is well illustrated in an investigation of the coronal streamers by O'Brien, Stewart, and Aronson, *Ap. J.*, **89**, 37–39, Pl. VI, 1939.

[7] Hubble, *The Realm of the Nebulae*, p. 55, 1936.

mathematical problem to two dimensions. It is natural to approach the relation between the density distribution of a body and its attractive force by way of the potential function, which is defined as

$$V = \int_B \frac{dm}{\Delta}, \tag{1}$$

where Δ is the distance between the attracted particle and any element of mass, dm, and where the integration is to be performed over the entire attracting body, B. The attractive central force, F_c, for a point situated at a distance ρ from the center of mass is given by the expression,

$$F_c = \frac{\partial V}{\partial \rho} = \frac{\partial}{\partial \rho} \int_B \frac{dm}{\Delta}. \tag{2}$$

It might be supposed that Poisson's equation, when expressed in polar or cylindrical co-ordinates, could be used to advantage to determine the density σ; e.g.,

$$\frac{\partial^2 V}{\partial \rho^2} + \frac{1}{\rho}\frac{\partial V}{\partial \rho} + \frac{\partial^2 V}{\partial z^2} = 0 \qquad \text{for exterior points,}$$

$$= -4\pi\sigma \qquad \text{for interior points,}$$

provided that $\partial^2 V/\partial\theta^2 = 0$. The difficulty in attempting to make use of this expression in our problem is that we have no means of evaluating $\partial^2 V/\partial z^2$. Consequently, the most practicable method that we have found of relating the density and the attractive force is to employ equation (2). Since the observational data provide numerical values for F_c, the problem is to solve the integral equation (2) for the unknown density distribution, which is implicitly contained in dm.

In order to express the limits of integration, it is necessary to choose some particular model; and, in any physical problem, the selection is guided by the form of the object. For the extragalactic nebulae, two models come naturally to mind: an ellipsoid of revolution, and a thin disk. The ellipsoidal model we have dismissed, principally for two reasons: (1) unless the equidensity surfaces are assumed to be ellipsoids similar to the ellipsoid of figure, the mathematical development becomes very complex; and (2) if the nebula under consideration is too thick to permit the application of the plane-disk model, then the degree of opacity of the nebula assumes a considerable importance, as is evident from Holmberg's[4] investigation. For these reasons, as well as for others mentioned in the Introduction, we have preferred to utilize the thin-disk model.

It can be readily shown[8] that the potential of a plane, circular, homogeneous disk of radius r and density σ, upon an interior point of unit mass in its plane, at distance ρ from the center, is

$$V = 4r\mathfrak{E}\sigma, \tag{3}$$

where $\mathfrak{E}$ is Legendre's complete elliptic integral of the second kind, with $k = \rho/r$ as the modulus. Similarly, the potential for an exterior point in the plane, at distance ρ from the center, is

$$V = 4r\left[\frac{1}{k}(\mathfrak{E} - \mathfrak{K}) + k\mathfrak{K}\right]\sigma, \tag{4}$$

[8] The proof of this theorem is relatively easy if the attracted point is taken as the origin of co-ordinates.

where $\mathcal{K}$ and $\mathcal{E}$ are Legendre's complete elliptic integrals of the first and second kinds, respectively, with $k = r/\rho$ as the modulus.

By taking the partial derivatives of equations (3) and (4) with respect to ρ, we find that the central forces are

$$F_c = \frac{\partial V}{\partial \rho} = -\frac{4}{k}(\mathcal{K} - \mathcal{E})\sigma\,, \qquad \text{for an interior point} \qquad \left(k = \frac{\rho}{r}\right), \quad (5)$$

$$F_c = \frac{\partial V}{\partial \rho} = -4(\mathcal{K} - \mathcal{E})\sigma\,, \qquad \text{for an exterior point} \qquad \left(k = \frac{r}{\rho}\right). \quad (6)$$

The minus sign, of course, simply indicates that the force is directed toward the center. Henceforward the force will be considered positive when directed toward the center, and the minus sign will be dropped. The force for a homogeneous disk of unit density and unit radius is shown by the solid line in Figure 6 (p. 33), where the quantity $F_c/4$ is plotted as ordinate against the distance from the center as abscissa. The attractive force at the edge of the disk is infinite. This property, which may not be well known, is, in fact, a general characteristic of bodies of fewer than three dimensions, regardless of shape. In the case of a uniform circular disk, the property is evident from equations (5) and (6) above, because when $k = 1$, $\mathcal{K} = \infty$, and $\mathcal{E} = 1$.

Equations (3) to (6) apply only to homogeneous disks. If the disk to be analyzed is not homogeneous but has a density that varies with the distance from the center, we may consider the disk to be composed of an infinite number of concentric, elemental disks of different radii, each of density $d\sigma$. The element of central force exerted by any one of these elemental disks is, from equations (5) and (6),

$$dF_c = +\frac{4}{k}(\mathcal{K} - \mathcal{E})d\sigma\,, \qquad \text{for an interior point} \qquad \left(k = \frac{\rho}{r}\right), \quad (5')$$

$$dF_c = +4(\mathcal{K} - \mathcal{E})d\sigma\,, \qquad \text{for an exterior point} \qquad \left(k = \frac{r}{\rho}\right). \quad (6')$$

The total force upon an interior point of unit mass at distance ρ from the center is, then, the integral of the above expressions, with appropriate limits:

$$F_c = +\frac{4}{k}(\mathcal{K} - \mathcal{E})\sigma_R + 4\int_{\sigma_R}^{\sigma_\rho} \frac{1}{k}(\mathcal{K} - \mathcal{E})d\sigma + 4\int_{\sigma_\rho}^{\sigma_0}(\mathcal{K} - \mathcal{E})d\sigma\,, \qquad (7)$$

where σ_R = density at edge of disk, where $r = R$; σ_ρ = density at the attracted point, where $r = \rho$; and σ_0 = density at center of disk, where $r = 0$. In equation (7) the first term of the right-hand side is the force exerted by a homogeneous disk of radius R and density σ_R. The second term on the right-hand side is the sum of the attractions of all the elemental disks having radii larger than ρ, the distance of the attracted point; while the third term is the sum of the attractions of all the elemental disks having radii smaller than ρ. Equation (7) is the general expression for the force of a circularly symmetrical thin disk upon an interior point in its plane; its applicability includes disks in which the edge density, σ_R, is finite. It is readily seen, however, that the application of the thin-disk model to the nebulae restricts the discussion to that class of disks in which $\sigma_R = 0$. For the density in the plane, σ, in so far as the nebulae are concerned, is interpreted as the amount of matter contained in a column of unit cross-sectional area, perpendicular to the principal plane of the nebula. And it is to be expected that, under the force of grav-

ity alone, such a projected density will display no discontinuities, even at the edge. For example, if the space density of an oblate spheroid is projected upon the equatorial plane, the projected density goes to zero at the edge. The foregoing remarks are equivalent to the assumption that a three-dimensional figure of equilibrium, having the general character of a nebula, will not contain any corners. We assume therefore that, so far as our present problem is concerned, $\sigma_R = 0$ and that the first term of the right-hand side of equation (7) vanishes.

Equation (7) would be ready to use if σ were expressed as a function of r, and therefore of k and ρ. Of the various possible forms for expressing σ as a function of r, we select the power series because of its flexibility and its mathematical simplicity. Let us assume that the density at any point in the disk, at distance r from the center, can be represented by the expression

$$\sigma = A + B\left(\frac{r}{R}\right) + C\left(\frac{r}{R}\right)^2 + D\left(\frac{r}{R}\right)^3 + E\left(\frac{r}{R}\right)^4 + F\left(\frac{r}{R}\right)^5, \tag{8}$$

where R is the radius of the disk, and $A, B, \ldots, F$ are suitable constants. For the assumed case that $\sigma_R = 0$, we have, by substituting $r = R$ in equation (8),

$$\sigma_R = A + B + C + D + E + F = 0;$$

this relation is used later in the numerical work. Differentiation of (8) gives

$$d\sigma = \left[B + 2C\left(\frac{r}{R}\right) + 3D\left(\frac{r}{R}\right)^2 + 4E\left(\frac{r}{R}\right)^3 + 5F\left(\frac{r}{R}\right)^4\right]\frac{dr}{R}. \tag{9}$$

When we substitute (9) in (7), taking account of the limits for the new variable, we get,

$$\left.\begin{aligned} F_c = &+ 4\int_R^\rho \frac{1}{k}(\mathcal{K} - \mathcal{E})\left[B + 2C\left(\frac{r}{R}\right) + 3D\left(\frac{r}{R}\right)^2 + 4E\left(\frac{r}{R}\right)^3 + 5F\left(\frac{r}{R}\right)^4\right]\frac{dr}{R} \\ &+ 4\int_\rho^0 (\mathcal{K} - \mathcal{E})\left[B + 2C\left(\frac{r}{R}\right) + 3D\left(\frac{r}{R}\right)^2 + 4E\left(\frac{r}{R}\right)^3 + 5F\left(\frac{r}{R}\right)^4\right]\frac{dr}{R}. \end{aligned}\right\} \tag{10}$$

Let $\rho/R = a$. In the first term of the right-hand side, $k = \rho/r$, wherefore

$$dk = -\frac{\rho}{r^2}dr = -\frac{k^2}{a}\cdot\frac{dr}{R}; \qquad \text{or} \qquad \frac{dr}{R} = -\frac{a\,dk}{k^2}.$$

In the second term of the right-hand side, $k = r/\rho$, whence it follows that

$$dk = \frac{dr}{\rho} = \frac{1}{a}\cdot\frac{dr}{R}; \qquad \text{or} \qquad \frac{dr}{R} = a\,dk.$$

The above substitutions permit equation (10) to be written in the form

$$-\frac{F_c}{4} = B\cdot M(a) + C\cdot N(a) + D\cdot O(a) + E\cdot P(a) + F\cdot Q(a), \tag{11}$$

where

$$\left.\begin{aligned}
M(a) &= a\int_a^1 \frac{1}{k^3}(\mathcal{K}-\mathcal{E})dk + a\int_0^1 (\mathcal{K}-\mathcal{E})dk,\\
N(a) &= 2a^2\int_a^1 \frac{1}{k^4}(\mathcal{K}-\mathcal{E})dk + 2a^2\int_0^1 k(\mathcal{K}-\mathcal{E})dk,\\
O(a) &= 3a^3\int_a^1 \frac{1}{k^5}(\mathcal{K}-\mathcal{E})dk + 3a^3\int_0^1 k^2(\mathcal{K}-\mathcal{E})dk,\\
P(a) &= 4a^4\int_a^1 \frac{1}{k^6}(\mathcal{K}-\mathcal{E})dk + 4a^4\int_0^1 k^3(\mathcal{K}-\mathcal{E})dk,\\
Q(a) &= 5a^5\int_a^1 \frac{1}{k^7}(\mathcal{K}-\mathcal{E})dk + 5a^5\int_0^1 k^4(\mathcal{K}-\mathcal{E})dk,
\end{aligned}\right\}$$

and where the modulus of $\mathcal{K}$ and $\mathcal{E}$ is k. (12)

Written in its complete form,

$$\left.\begin{aligned}
M(a) = a\int_a^1 dk\int_0^{\pi/2} \frac{d\theta}{k^3\sqrt{1-k^2\sin^2\theta}} - a\int_a^1 dk\int_0^{\pi/2} \frac{1}{k^3}\sqrt{1-k^2\sin^2\theta}\,d\theta\\
+ a\int_0^1 dk\int_0^{\pi/2} \frac{d\theta}{\sqrt{1-k^2\sin^2\theta}} - a\int_0^1 dk\int_0^{\pi/2} \sqrt{1-k^2\sin^2\theta}\,d\theta,
\end{aligned}\right\} \quad (13)$$

and similarly for $N(a)$, $O(a)$, $P(a)$, and $Q(a)$.

Equations (12) were reduced, after a considerable amount of labor, to equations (14). Further details are given in the Addendum.

$$\left.\begin{aligned}
M(a) &= \frac{1}{2}\left[\left(\frac{1}{a} - a\right)\mathcal{K} + \left(-\frac{1}{a}\right)\mathcal{E}\right.\\
&\qquad \left. + \frac{1}{2}\pi a \log_e \frac{1+\sqrt{1-a^2}}{a} + a\int_0^{\pi/2} \frac{\theta\cot\theta\,d\theta}{\sqrt{1-a^2\sin^2\theta}}\right];\\
N(a) &= \frac{1}{3}\left[\left(\frac{1}{a} - a\right)\mathcal{K} + \left(-\frac{1}{a} + 2a\right)\mathcal{E}\right];\\
O(a) &= \frac{1}{16}\left[\left(4\cdot\frac{1}{a} - a - 3a^3\right)\mathcal{K} + \left(-4\cdot\frac{1}{a} + 3a\right)\mathcal{E}\right.\\
&\qquad \left. + \frac{3}{2}\pi a^3 \log_e \frac{1+\sqrt{1-a^2}}{a} + 3a^3\int_0^{\pi/2} \frac{\theta\cot\theta\,d\theta}{\sqrt{1-a^2\sin^2\theta}}\right];\\
P(a) &= \frac{1}{45}\left[\left(9\cdot\frac{1}{a} - a - 8a^3\right)\mathcal{K} + \left(-9\cdot\frac{1}{a} + 4a + 16a^3\right)\mathcal{E}\right];\\
Q(a) &= \frac{1}{384}\left[\left(64\cdot\frac{1}{a} - 4a - 15a^3 - 45a^5\right)\mathcal{K} + \left(-64\cdot\frac{1}{a} + 20a + 45a^3\right)\mathcal{E}\right.\\
&\qquad \left. + \frac{45}{2}\pi a^5 \log_e \frac{1+\sqrt{1-a^2}}{a} + 45a^5\int_0^{\pi/2} \frac{\theta\cot\theta\,d\theta}{\sqrt{1-a^2\sin^2\theta}}\right].
\end{aligned}\right\} \quad (14)$$

The integral appearing in $M(a)$, $O(a)$, and $Q(a)$ in equations (14) can be expressed in the form

$$\left.\begin{aligned}\int_0^{\pi/2} \frac{\theta \cot \theta \, d\theta}{\sqrt{1 - a^2 \sin^2 \theta}} = \mathfrak{S}\left(\frac{\pi}{2}, a\right) + \frac{\pi}{2}\left[\log_e \left(\frac{4}{1 + \sqrt{1 - a^2}}\right) - 1\right. \\ \left. + \sum_{n=1}^{\infty} \left(\frac{1 \cdot 3 \cdot 5 \cdot \ldots \cdot (2n-1)}{2 \cdot 4 \cdot 6 \cdot \ldots \cdot 2n}\right)^2 \frac{a^{2n}}{2n(2n-1)}\right].\end{aligned}\right\} \quad (15)$$

The numerical values of the functions $M(a), \ldots, Q(a)$ have been calculated from equations (14), for suitable values of a, and are given in Table 1. Equation (15) was

TABLE 1

COEFFICIENTS FOR INTERIOR POINTS

a	$M(a)$	$N(a)$	$O(a)$	$P(a)$	$Q(a)$
0.00.....	0.000 000	0.000 000	0.000 000	0.000 000	0.000 000
0.05.....	.152 429	.078 467	0.059 270	0.052 508	0.049 181
0.10.....	.250 306	.156 490	0.120 110	0.105 891	0.098 935
0.15.....	.327 413	.233 622	0.183 255	0.161 000	0.149 893
0.20.....	.390 836	.309 407	0.249 048	0.218 626	0.202 764
0.30.....	.488 414	.455 024	0.388 685	0.344 138	0.317 438
0.40.....	.556 362	.589 266	0.537 178	0.486 420	0.449 627
0.50.....	.600 194	.707 442	0.689 528	0.646 259	0.605 285
0.60.....	.622 188	.803 799	0.837 191	0.819 431	0.786 914
0.70.....	.622 469	.870 658	0.966 765	0.993 740	0.988 674
0.80.....	.598 718	.896 406	1.056 628	1.143 057	1.186 751
0.90.....	.543 543	.859 079	1.066 319	1.210 724	1.314 476
0.95.....	.497 264	.800 152	1.012 205	1.171 750	1.297 028
1.00.....	0.415 966	0.666 667	0.842 961	0.977 778	1.086 418

utilized to evaluate the integral in equations (14), for all cases except $a = 0.95$, where the integral was found by Simpson's rule. The errors in the tabulated quantities are believed to be not more than one or two units in the sixth decimal place. In practice it will sometimes be advisable to round them off to five, or even to four, decimals. The functions $M(a)$, etc., it will be remembered, occur as coefficients in an expression (eq. [11]), which permits the calculation of the force exerted by a disk upon an interior point in its plane, situated at the fractional distance a from the center. For any assumed density distribution, i.e., with the quantitites A, B, C, D, E, and F of equation (8) known, it is now possible to compute from equation (11) the force for all interior points in the disk.[9]

The next step is to set down the analytic expression for the force at exterior points. It may frequently happen that emission nebulosities occur at such great distances from the center of a spiral nebula as to be in the region where the density is zero according to equation (8). If the rotational velocities of such "exterior points" are determined, it is desirable to compare them with the calculated force. Returning to equations (6) and (6′) and following an argument similar to that used in deriving equation (11), we find

[9] For the case where $a = 0$, i.e., where the attracted point is at the center, it has been shown (W. D. MacMillan, *Theoretical Mechanics*, pp. 153–155, 1930) that "the attraction of a uniform disk upon its center does not have a definite sense." The theorem does not apply, however, to a system of discrete particles, and there appears to be ample justification, for our purpose, of accepting the force as equal to zero at the center of the disk.

that the total force exerted by the disk upon an exterior point in its plane, at distance ρ from the center (letting $\beta = R/\rho \leq 1$), is given by the expression

$$-\frac{F_c}{4} = +B \cdot m(\beta) + C \cdot n(\beta) + D \cdot o(\beta) + E \cdot p(\beta) + F \cdot q(\beta), \quad (16)$$

where

$$\left.\begin{aligned} m(\beta) &= \frac{1}{\beta}\int_0^\beta (\mathcal{K} - \mathcal{E})dk, \\ n(\beta) &= \frac{2}{\beta^2}\int_0^\beta k\,(\mathcal{K} - \mathcal{E})dk, \\ o(\beta) &= \frac{3}{\beta^3}\int_0^\beta k^2(\mathcal{K} - \mathcal{E})dk, \\ p(\beta) &= \frac{4}{\beta^4}\int_0^\beta k^3(\mathcal{K} - \mathcal{E})dk, \\ q(\beta) &= \frac{5}{\beta^5}\int_0^\beta k^4(\mathcal{K} - \mathcal{E})dk, \end{aligned}\right\} \quad \begin{matrix}\text{and where} \\ \text{the modulus} \\ \text{of } \mathcal{K} \text{ and } \mathcal{E} \\ \text{is } k.\end{matrix} \quad (17)$$

No method of simplifying the integrals in equations (17) has been found. They are, however, fairly easy to evaluate by Simpson's rule, especially with the aid of a table of complete elliptic integrals[10] that was published after most of the present work had been completed. The quantities $m(\beta), \ldots, q(\beta)$, determined in this way, are given to five decimals in Table 2.

TABLE 2

COEFFICIENTS FOR EXTERIOR POINTS

β	$m(\beta)$	$n(\beta)$	$o(\beta)$	$p(\beta)$	$q(\beta)$
1.0	0.415 97	0.666 67	0.842 96	0.977 78	1.086 42
0.9	.279 62	.434 40	.535 23	.607 18	0.661 62
0.8	.203 01	.311 70	.380 55	.428 53	0.464 09
0.7	.146 80	.223 73	.271 64	.304 54	0.328 64
0.6	.103 44	.156 84	.189 70	.212 05	0.228 30
0.5	.069 61	.105 16	.126 84	.141 50	0.152 12
0.4	.043 51	.065 56	.078 92	.087 93	0.094 45
0.3	.024 06	.036 18	.043 51	.048 46	0.052 08
0.2	.010 57	.015 87	.019 11	.021 36	0.023 11
0.1	.002 62	.003 94	.004 92	.005 91	0.006 98
0.0	0.000 00	0.000 00	0.000 00	0.000 00	0.000 00

With the aid of the numerical coefficients listed in Tables 1 and 2 we are now in a position to determine, by means of equations (11) and (16), the complete force-curve, for points in the plane, corresponding to any assumed density distribution; or, conversely, to determine the density distribution required to produce a given force-curve.

The "observed" force-curve can be derived very simply from the observational data if circular motion in the plane is assumed. The observed radial velocities for various points in the nebula are corrected, first, for the velocity of the system; second, for any departures of the observed points from the major axis of the nebula; and, third, for the inclination of the principal plane of the nebula to the line of sight. The result is a curve

[10] Alan Fletcher, *London, Edinburgh and Dublin Phil. Mag. and J. Sci.*, **30**, 516, 1940.

giving the rotational velocity as a function of the distance from the center. The central force, F_c, is related to the rotational velocity, V, by the expression,[11]

$$V^2 = F_c \cdot \rho , \tag{18}$$

where ρ is the distance from the center to the attracted point; ρ must be measured in minutes of arc if the subsequent formulae are to be applicable. Equation (18) provides for the transformation of the "observed" curve of rotational velocity into an "observed" curve of force, which is then ready to be analyzed to find the density distribution.

The method of analysis outlined above permits the determination of the density distribution, which, since it is assumed that $A + B + C + D + E + F = 0$, satisfies the observed force-curve at five points and which automatically passes through the origin (i.e., the force at the center of the disk is zero). If it were desired to obtain the best possible fit over the whole force-curve, equations (11) and (16) could be used in their differential form, and a least-squares solution could be made. It is doubtful, however, whether the degree of observational accuracy at present attainable is sufficient to justify such refinements. It should be noted that the force-curve for many models is sensitive to the assumed value of R, the radius of the nebula; and that, if a least-squares solution were attempted, the correction to R should be included as one of the unknown quantities.

IV. TOTAL MASS OF THE NEBULA

With an assumed value for the distance of the nebula the total mass can be found. It is necessary to introduce an appropriate factor, however, because the Gaussian constant of attraction has not been included in the foregoing formulae. It is assumed in the calculations that the rotational velocity has been given in kilometers per second, and the distance ρ from the center in minutes of arc. The density σ, which results from the use of equations (8), (11), and (16), is in terms of an arbitrary unit and can be converted into solar masses per square minute of arc in the plane of the nebula by multiplication by the factor $0.0678d$, where d is the distance to the nebula in parsecs. The total mass in solar units is found by summing the density over the whole nebula:

$$M_\odot = 0.0678d \cdot 2\pi \int^R r\sigma dr . \tag{19}$$

Making use of equation (8) in the integration, we get

$$M_\odot = 0.426R^2d\left(\frac{A}{2} + \frac{B}{3} + \frac{C}{4} + \frac{D}{5} + \frac{E}{6} + \frac{F}{7}\right), \tag{20}$$

where R is the radius of the nebula in minutes of arc, d is the distance in parsecs, and A, B, etc., are the numerical values that result from the solution. If it is desired to find the density in solar masses per square parsec, the densities from the solution can be converted into this unit by multiplication by the factor $8.01 \times 10^5/d$.

V. CERTAIN APPLICATIONS OF THE METHOD

Before commencing an analysis of any actual nebula, it will be useful to examine the forces exerted by certain types of nonhomogeneous disks. Disks have been assumed with a variety of density distributions, and the corresponding forces in the plane have been determined in the manner outlined above. Typical models are exemplified in Figures 1–6, inclusive, where the densities and central forces, $F_c/4$ (in arbitrary units that are mutually consistent in eqs. [8], [11], and [16])are plotted as ordinates against distances from the center as abscissae.

[11] Cf. F. R. Moulton, *An Introduction to Celestial Mechanics*, pp. 80–81, 1928.

The assumed density distributions, which approximate to the analytic expressions given beneath each of the figures, are represented by six-term (or fewer) polynomials of

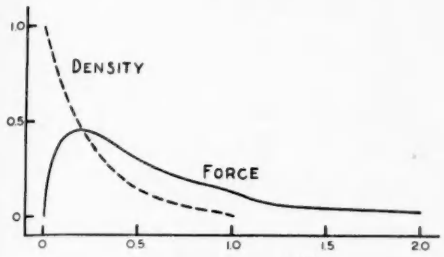

FIG. 1.—$\sigma \sim e^{-4(r/R)}$

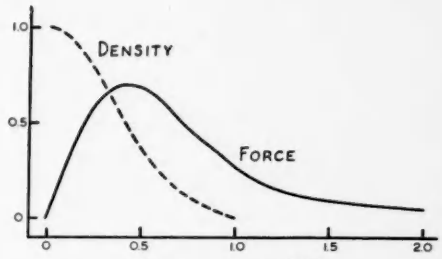

FIG. 2.—$\sigma \sim e^{-4(r/R)^2}$

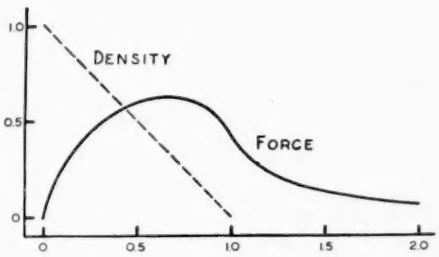

FIG. 3.—$\sigma = 1 - (r/R)$

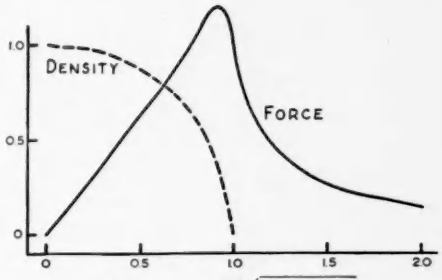

FIG. 4.—$\sigma \sim \sqrt{1 - (r/R)^2}$

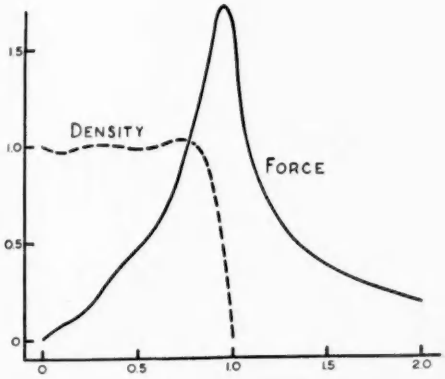

FIG. 5.—$\sigma \sim 1$

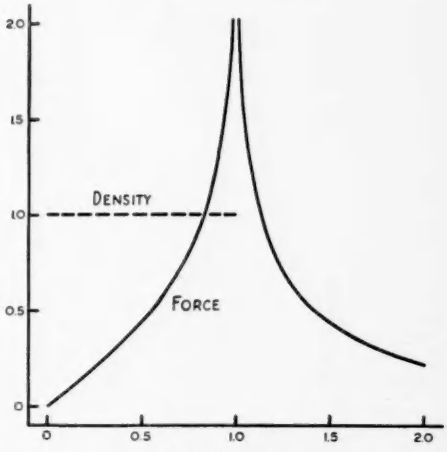

FIG. 6.—$\sigma = 1$

FIGS. 1–6.—Examples illustrating the relation between density distribution and central force for points in the plane of circularly symmetrical thin disks. Abscissae are distances from the center with the radius of the disk as unit. Ordinates are in arbitrary units, which are mutually consistent for the density and the force.

ascending powers of r/R, as detailed below. In Figures 1, 2, and 5 the departures of the assumed density distributions from those given by the approximate expressions are due to the condition that the edge density shall be zero—a condition that has been imposed in

order that the force at the edge shall remain finite, as discussed earlier. The assumed density distributions are as follows:

FIG. 1: $\sigma \sim e^{-4(r/R)}$: $\sigma = 1.0 - 3.97500\left(\frac{r}{R}\right) + 7.66042\left(\frac{r}{R}\right)^2 - 8.89636\left(\frac{r}{R}\right)^3 + 6.02084\left(\frac{r}{R}\right)^4 - 1.80990\left(\frac{r}{R}\right)^5$

FIG. 2: $\sigma \sim e^{-4(r/R)^2}$: $\sigma = 1.0 + 0.17105\left(\frac{r}{R}\right) - 5.87265\left(\frac{r}{R}\right)^2 + 6.93605\left(\frac{r}{R}\right)^3 - 1.46627\left(\frac{r}{R}\right)^4 - 0.76818\left(\frac{r}{R}\right)^5$

FIG. 3: $\sigma = 1 - \left(\frac{r}{R}\right)$

FIG. 4: $\sigma \sim 1 - \left(\frac{r}{R}\right)^2$: $\sigma = 1.0 - 0.2530\left(\frac{r}{R}\right) + 2.1460\left(\frac{r}{R}\right)^2 - 9.3284\left(\frac{r}{R}\right)^3 + 13.3833\left(\frac{r}{R}\right)^4 - 6.9479\left(\frac{r}{R}\right)^5$

FIG. 5: $\sigma \sim 1$: $\sigma = 1.0 - 1.0\left(\frac{r}{R}\right) + 10.41667\left(\frac{r}{R}\right)^2 - 36.45833\left(\frac{r}{R}\right)^3 + 52.08333\left(\frac{r}{R}\right)^4 - 26.04167\left(\frac{r}{R}\right)^5$

FIG. 6: $\sigma = 1$

The above expressions, of course, define σ only in the region, $0 \leq (r/R) \leq 1$. For $(r/R) > 1$, $\sigma = 0$ by definition.

The curves suggest the variety of density distributions that may be represented by the six-constant formula. The forces for the first five figures were calculated by means of equations (11) and (16); that for Figure 6 was found from equations (5) and (6). A comparison of Figures 5 and 6 discloses the fact that a very close fit can be obtained between the two force-curves, except near $r/R = 1$, by making slight adjustments in the horizontal and vertical co-ordinates.

The force-curve given in Figure 4 is particularly illuminating. It was actually the first one to be determined by means of the present method, and it was calculated for the purpose of testing the correctness of the values of $M(\alpha), \ldots, Q(\alpha)$, which were used in its determination. The expression for the potential of a homogeneous, oblate spheroid can be reduced,[12] for the limiting case of an infinitely thin spheroid, to the potential for a plane disk in which the density varies proportionally to the thickness of a spheroid; that is to say, for a plane disk in which the density is given by the relation

$$\sigma = \text{constant} \times \sqrt{1 - \left(\frac{r}{R}\right)^2}.$$

Thus the attractive force for such a disk can be calculated by a method that is independent of the method described here. We have determined the constants for a sixth-degree equation in r/R, which fits the expression

$$\sigma = \sqrt{1 - \left(\frac{r}{R}\right)^2}$$

[12] Cf. MacMillan, *Theoretical Mechanics*, p. 176, 1930.

at the following six points: r/R = 0.0, 0.2, 0.4, 0.6, 0.8, and 1.0. It is well known that a disk with strictly "spheroidal" density distribution exerts, upon interior points, forces that are proportional to the distances of the points from the center. In comparison, we see from Figure 4 that for the disk with approximately "spheroidal" density distribution, the force increases almost linearly from $\rho = 0$ to about $\rho = 0.9R$. A more detailed comparison, for both interior and exterior points, shows that qualitatively the differences are just what would be expected from the slight departures of the six-constant density formula from that of a true spheroid. Thus the check on the numerical coefficients, $M(a)$, $N(a)$, etc., is completely satisfactory.

VI. APPLICATION TO THE ANDROMEDA NEBULA (M 31)

We now proceed to a discussion of the spiral nebula in Andromeda (M 31). The rotation-curve, as determined by H. W. Babcock,[1] shows two especially striking features: first, the decline to zero of the speed of rotation, at a distance of about 9′ from the center; and, second, the increase of rotational velocity from that point out to the astonishing distance of 1½°—half a degree beyond the spiral structure that is shown on most photographs. The high velocity at so great a distance suggests, as Babcock points out, "that a very great proportion of the mass of the nebula must lie in the outer regions."

Babcock's smoothed curve of rotational velocity, given in his paper as Figure 4, was made the basis of the present analysis. It was converted into a force-curve by means of equation (18). With an assumed value of the radius a provisional solution of equation (11) for six points[13] of the curve yielded constants that failed to reproduce the force-curve; evidently a six-constant formula is incapable of representing Babcock's rotational-curve.

Next it was assumed that the nebula, heretofore treated as a single disk, might be supposed to consist of two concentric disks—a small one corresponding to the nuclear region, and a large one corresponding to the main body of the system. It might be objected that the thin-disk model for the nuclear region departs too far from the apparent shape of the central part of the nebula and that, therefore, some other model, such as a spheroid, should be employed. While it is true that a spheroid might be slightly preferable, it may be emphasized that the velocities near the nucleus are too uncertain to permit a clear differentiation between the two models. Furthermore, even if the spheroid were used, some density distribution would have to be assumed. In so far as the results are concerned, the only significant error introduced by applying the thin-disk formulae to a spheroid is that the total mass obtained thereby is too small. The error is not very large for the central mass, however, and, as will be seen later, its effect on the total mass of the system is negligible.

Of the two concentric disks mentioned above, it was proposed that the small one would have a size and density distribution that would account almost entirely for the force-curve between $\rho = 0$ and $\rho = 9'$; the large one would be such as to produce the residual forces after the deduction of the forces of the small disk from the "observed" force-curve. This artifice proved satisfactory. Since the density distribution for the small disk is uncertain within rather wide limits, as already noted, we found it convenient to choose a model from those shown in Figures 1–5. The model selected was the one in which the density decreases linearly from a maximum value at the center to zero at a distance of 4′.15. The force-curve for such a disk, which is equivalent to that of Figure 3 with a suitable adjustment of the co-ordinates, was calculated and deducted from the "observed" force-curve. For the large disk the radius R was assumed to be 100′; the choice was guided in part by the disturbing experience, in some preliminary calculations, of finding regions of negative density when too large a value of R was employed. A simul-

[13] The points selected were at nuclear distances of 0′, 3′, 9′, 32′, 69′.2, and 96′.5.

taneous solution of five equations of the form (11), corresponding to $a = 0.1$, 0.2, 0.4, 0.7, and 0.95, yielded the following constants for the large disk:

$$A = +\ 122.655 \qquad D = +38777.597$$
$$B = +\ 4697.613 \qquad E = -30865.827$$
$$C = -21602.998 \qquad F = +\ 8870.960$$

The constants employed for the small disk are as follows:

$$A = +\ 1493.0 \qquad B = -\ 1493.0$$

Substitution of the constants in equation (8) gives the density distribution for the large and small disks separately. The surface density of the nebula in its plane is the sum of the densities for the two disks and is plotted in Figure 8, in solar masses per square parsec (see p. 37). The rotational-velocity-curve, which would be produced by a disk with the density depicted in Figure 8, is shown in Figure 7. The filled circles in Figure 7 have been read from Babcock's smoothed curve of rotational velocities, and the open circles are Babcock's rotational velocities for the four gaseous nebulae that he observed near the major axis. The agreement between the observed and calculated rotational velocities is close. While it could be slightly improved, we feel that such refinements are unnecessary in view of the uncertainties of the observational curve and the extreme simplicity of the model. It need scarcely be mentioned that the computed decrease in velocity beyond a distance of 95′ from the center is a direct result of the assumed radius of the nebula; for this reason, the part of the velocity-curve for $R > 100'$, which clearly is an extrapolation beyond the observations, is shown in Figure 7 as a dashed line. If the true radius is larger than 100′ and if radial velocity observations become available for greater distances, then the constants can be adjusted accordingly.

A comparison between Figures 7 and 8 shows the existence of a minimum in the density 4′ from the center, corresponding to the observed minimum in the velocity-curve 9′ from the center. The location of the density minimum is uncertain, for fairly obvious reasons; but its existence somewhere in the vicinity of the velocity minimum is necessary in order to account for the latter. For, if the rotational velocity is small, the force must be small; and if the force is small, for a point well removed from the center, then it follows that, somewhere beyond the attracted point, there must be a maximum in the density to produce an outward force that will counterbalance the inward force exerted by the rest of the system. This condition is realized in the present case by the presence of a density maximum about 17′ from the center.

It should be mentioned that the balancing of inward and outward forces, discussed in the previous paragraph, is, in a sense, a direct result of the use of a thin-disk model. It is well known that the force, upon an interior point, exerted by a spheroid in which the equidensity surfaces are concentric and similar (i.e., Ratio of axes = Constant), increases monotonically from the center outward. Therefore, with the latter model it would be impossible, on the assumption of circular motion, to reproduce the minimum in Babcock's rotational-velocity-curve. If, however, we were to employ a spheroidal model in which the density distribution along the equatorial axis differs suitably from that along the polar axis—and there is no evidence at hand against such a hypothesis—then it should be possible to find a density distribution in which the inward and outward forces would be equal at any desired point, just as in the case of a thin disk.

It is interesting to compare the distribution in density, as shown in Figure 8, with the distribution in luminosity, as observed by Redman and Shirley.[14] The ratio of mass to luminosity shows a marked variation with distance from the center, as has already been

[14] *M.N.*, **97**, 416, 1937.

pointed out by Babcock. A similar variation is probably present in the E7 nebula NGC 3115, which has been investigated by Oort.[5] The ratio of mass density to light density for M 31 is given in column 4 of Table 3. The ratios were derived from the mass densities

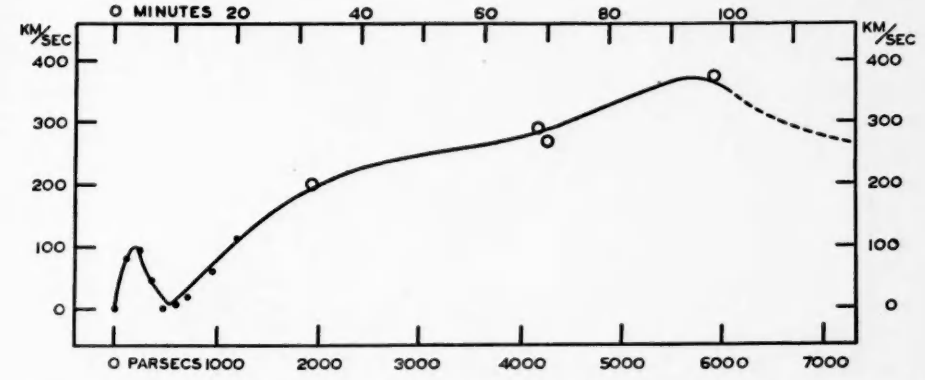

FIG. 7.—Calculated rotational-velocity-curve for M 31 (two-disk model). The dots and circles represent observations.

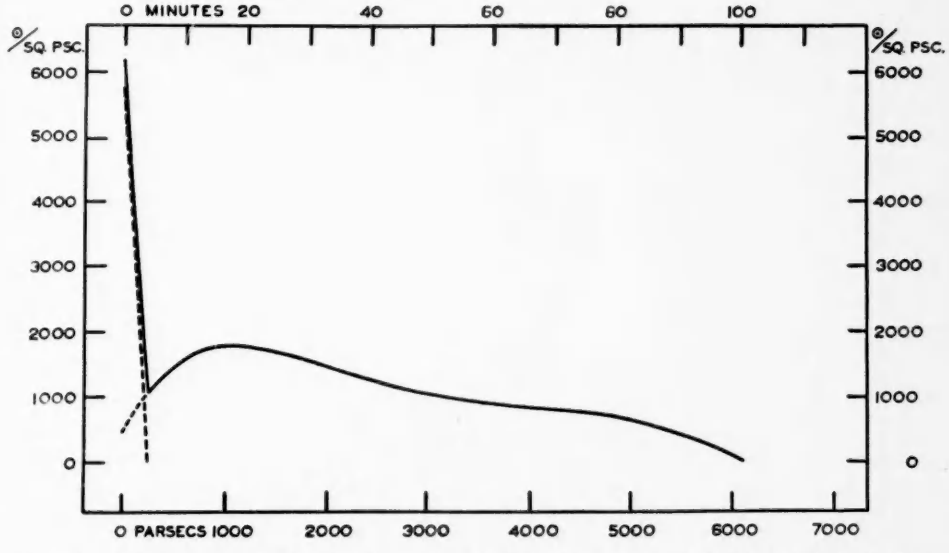

FIG. 8.—Calculated density distribution in the principal plane of M 31 (solid line). The dashed lines for the central region represent the densities of the component parts of the two-disk model used.

listed in column 2, which were transformed for this purpose into solar masses per square second of arc, and from the light densities in column 3, which were calculated from Redman and Shirley's measurements.[15]

[15] The unit of intensity in Redman and Shirley's measurements is such that when $\log I = 2$ in their tabulation, the brightness is $16^{m}.2$ pg. per square second of arc. We have converted I to the unit of the sun's absolute photographic magnitude per square second of arc, using Kuiper's value, $M_{\odot} = +5.26$ pg. (*Ap. J.*, **88**, 429, 1938), and Hubble's distance of 210,000 parsecs (*The Realm of the Nebulae*, p. 134). Since the inclination of the plane of the spiral to the plane of the sky is assumed to be 75°, we find the

The tabulated values for the ratio of mass to light, which agree quite satisfactorily with those obtained by Babcock, are unexpectedly large for the outer parts of the spiral. This result naturally raises the important question as to what kind of faintly luminous matter may be present in order to produce the large mass indicated by the observations, but the question is beyond the scope of this paper and therefore will not be further discussed.

The total mass of M 31 can be determined from equation (20). Assuming, as before, a distance of 210,000 parsecs, we find that the total mass is 9.5×10^{10} ⊙,[16] a value that agrees closely with Babcock's result, namely, 10.2×10^{10} ⊙. (In this calculation Babcock neglected the dip to zero in the rotational-velocity-curve.) The mass of the small, central disk is found to be 3.8×10^{8} ⊙. This disk is, of course, superposed upon the

TABLE 3

RATIO OF MASS TO LIGHT IN M 31

Nuclear Distance (Minutes) (1)	Mass Density (⊙/sec²) (2)	Light Density (⊙/sec²) (3)	Mass / Light (4)
0	6430	33,000	0.2*
4	1320	330	4
10	1640	128	13
20	1850	67.2	28
30	1620	42.7	38
40	1310	31.8	41
50	1060	25.5	42
60	917	17.2	53
70	811	12.7	64
80	689	9.10	76
90	431	6.18	70

* The ratio for the nucleus itself has been estimated by Hubble as 0.001 (*Ap. J.*, **69**, 154, 1929; *Mt. W. Contr.*, No. 376). The difference between this value and our estimate of 0.2 is attributable chiefly to the fact that he assumed uniform density out to a distance of 2′.5, whereas our model has a mass density increasing to the center. Hubble finds an average ratio of 0.4 within a sphere of 2′.5 radius.

central part of the large disk, which also contributes something to the mass of the central region. The total mass within the area covered by the small disk—that is to say, within a circle of 4′.15 radius—is 5.6×10^{8} ⊙, or only 0.6 per cent of the total mass of the nebula. While these figures are only rough approximations, they are probably reliable indicators of orders of magnitude, both of the total mass and of the relative amounts in the nuclear region and in the rest of the system.

With an assumption regarding the thickness and shape of M 31 we can determine the space density of matter, averaged through the thickness of the nebula, at various dis-

brightness per square second as it would appear from a direction normal to the plane of the spiral, by multiplying the observed brightness by cos 75°. Furthermore, we have increased Redman and Shirley's intensities by a factor of 1.9, in order to correct for a *total* galactic obscuration of 0.25 csc 21° = 0.7 mag., obtained from Hubble's cosecant law (*Ap. J.*, **79**, 51, 1934; *Mt. W. Contr.*, No. 485, p. 44). All the above conversions are effected by multiplying Redman and Shirley's intensities by a factor of 92. The light-density given in column 3 for the nucleus is based upon a measurement by E. G. Williams, as quoted by Redman and Shirley.

[16] This value may be compared with that derived on the simple assumption that the entire mass of the nebula is concentrated at the center. With a rotational velocity of 348 km/sec (the calculated value) for a point 100′ from the center, the point-mass model gives a total mass of 1.7×10^{11} ⊙, or nearly twice the value derived from the disk model.

tances from the center. An examination of direct photographs of several edge-on spirals,[17] similar in type to M 31, indicates that, if we neglect the central bulge, we may consider a meridian section of the nebula to be approximately elliptical, with the major and minor axes in the ratio of about 12:1. This ratio gives, with the assumed diameter of 12,000 parsecs, a central thickness (still neglecting the central bulge) of 1000 parsecs. The corresponding mean space densities, in solar masses per cubic parsec, are given in Table 4 as a function of the distance from the center in the plane of the spiral.

The tabulated densities may be compared with the space density in the solar neighborhood. Oort[18] considers 0.1 $\odot$/psc^3 to be an upper limit for the combined density of stars and interstellar material in the vicinity of the sun. The much higher densities in Table 4 lead to the inference that, if the distribution of matter in the Galaxy is at all comparable with that in M 31, then the sun is situated in the outer fringe of the Galaxy, where the density is considerably smaller than it is in the main part of the system. This conclusion has previously been advanced by Lindblad[19] on the basis of other considerations.

TABLE 4

CALCULATED SPACE DENSITIES IN M 31

Nuclear Distance		Space Density ($\odot$/Psc^3)	Nuclear Distance		Space Density ($\odot$/Psc^3)
Minutes	Parsecs		Minutes	Parsecs	
10	610	1.6	60	3670	1.1
20	1220	1.8	70	4280	1.1
30	1830	1.6	80	4890	1.1
40	2440	1.4	90	5500	0.9
50	3160	1.2	95	5710	0.7

VII. APPLICATION TO THE SPIRAL NEBULA IN TRIANGULUM (M 33)

The rotational velocities in M 33 have recently been determined by Mayall and Aller.[2] The observations show that, when due allowance is made for the uncertainties, the rotational velocities of all the observed objects, except the brightest and largest knot, NGC 604, are compatible with the existence of a smooth curve relating the velocities with the nuclear distances; that the curve is approximately symmetrical about the nucleus; and that the maximum rotational velocity, about 120 km/sec, occurs in the vicinity of 16′ from the center, after which there is a rather definite decline.

[17] The objects examined are as follows:

Nebula	Type	Major Axis	Minor Axis	Ratio
NGC 891	Sb	11′.5	0′.8	14.4
4244	Sb	12.8	1.2	10.7
4565	Sb	14.5	1.0	14.5
4631	Sc	13.4	1.5	8.9
5746	Sb	6.8	0.6±	11.3±
5906–7	Sb	11.2	0.8	14.0
Mean				12.3

[18] *B.A.N.*, **6**, 284, 1932. Oort also gives references to investigations by Kapteyn, by Jeans, and by Lindblad. In this connection, Seares's study of the density of stars in the solar neighborhood should also be consulted (*Ap. J.*, **74**, 312, 1931; *Mt. W. Contr.*, No. 437).

[19] *Festskrift Tillägnad Östen Bergstrand*, p. 30, 1938.

An examination of the models discussed in Section V suggests that the force-curve of M 33 can be adequately represented by either of the force-curves portrayed in Figures 4 and 5. The first of these, it may be recalled, corresponds to the model in which the density is given by a six-constant formula that approximates to spheroidal density distribution in the plane. The second corresponds to a similar approximation to uniform density

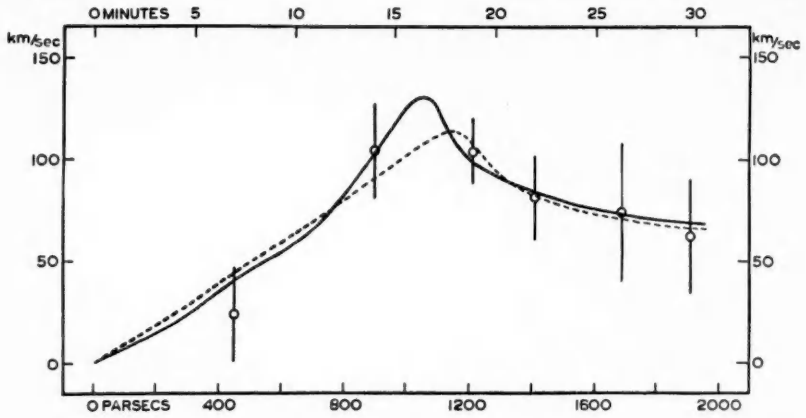

FIG. 9.—Calculated rotational velocity-curves for M 33. The solid and dashed lines correspond to those in Fig. 10. Circles and vertical lines represent observations with their probable errors.

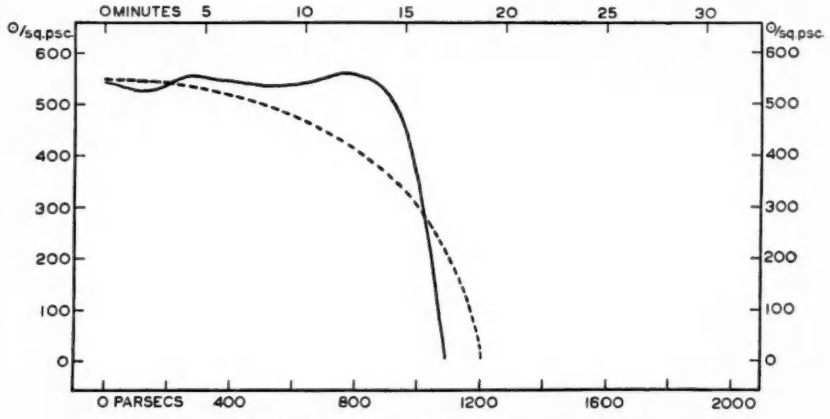

FIG. 10.—Calculated density distributions in the principal plane of M 33

---- Density varying according to the thickness of an oblate spheroid

—— Nearly constant density

in the plane. The curves of rotational velocity, which are defined by the two force-curves cited, were empirically adjusted so as to give the best fit with the observations of M 33. This adjustment of the co-ordinates included, of course, an evaluation of the radii for both models; the best radius for the "homogeneous" disk is 17′.0, and that for the "spheroidal" disk is 18′.8. The resulting velocity-curves are shown in Figure 9, together with the observed normal points and their probable errors. It is evident from Figure 9 that, while the "homogeneous" disk gives slightly the better representation of the two

models, the observations are altogether incapable of furnishing definite grounds for preferring either model to the other. In Figure 10 the corresponding surface densities are plotted. Application of equation (20) indicates a total mass,[20] for "homogeneous" distribution, of 1.8×10^9 ⊙; and for "ellipsoidal" distribution, 1.6×10^9 ⊙. We give the mean, 1.7×10^9 ⊙, as the most probable value of the total mass for M 33.

In order to estimate the space density, averaged through the thickness of M 33, we may assume, as for M 31, that the spiral is an oblate spheroid, with equatorial and polar diameters in the ratio of 12:1. The space densities, corresponding to the two distributions of surface density shown in Figure 10, are nearly independent of nuclear distance and have a value of approximately 2.7 ⊙/psc^3. This figure is probably too large, because it is based on a volume that does not include the faint outer parts of the spiral. In order to include these outlying regions, as was done for M 31, we should adopt a radius for M 33 of 30′, for reasons stated in the next paragraph. With this radius and with the same axis ratio of 12:1 the average space density for the main body becomes 1.7 ⊙/psc^3, which is comparable with the values given in Table 4 for M 31.

Although the foregoing solutions for the density distribution in M 33 indicate a negligible amount of mass beyond 18′ from the center, recent Crossley photographs[21] plainly show luminous material extending to a distance of 30′ along the major axis. The question naturally arises as to how much matter could exist in this outer region without causing too serious a departure of the rotational velocities from their observed values. The fact that the solutions described above yield zero density beyond about 18′ is a direct consequence of adopting the *most probable* values of the rotational velocities for the four normal points between 18′ and 30′ from the center (cf. Fig. 9). In order to find a model that gives an appreciable density in the outer region, we have postulated a rotational-velocity-curve which, of necessity, departs systematically from the observations but which lies well within the probable error limits of the normal points. On the basis of this hypothetical curve, and using a radius of $R = 30'$, we have made another solution for the density distribution. The points of the hypothetical curve, which were employed for the solution, are as shown in the accompanying table. It will be noted that the hypothetical curve is systematically higher and less steeply inclined in the outer regions than the observations themselves would indicate. Our experience with the thin-disk model has shown that this kind of departure is required in order to give a positive density beyond the limits of the main body.

Nuclear Distance (Minutes)	Rotational Velocity (Km/Sec)	Nuclear Distance (Minutes)	Rotational Velocity (Km/Sec)
3	14	21	92
6	33	28.5	84
12	82		

The results of this last solution may be briefly summarized. The mass of the outer region, that is to say, between 17′.5 and 30′ from the center, is 0.2 of the total mass of the nebula, which, in this case, becomes 2.0×10^9 ⊙. In the outer region the average den-

[20] The adopted distance of M 33 is 2.2×10^5 parsecs (Hubble, *The Realm of the Nebulae*, p. 143). Hubble's estimate for the mass of M 33, 1.5×10^{10} ⊙ (*Ap. J.*, **63**, 268, 1926; *Mt. W. Contr.*, No. 310, p. 33) is larger than that found here, for two reasons. First, the velocity that he used for the nucleus differed by 100 km/sec from that employed to derive the rotational velocities discussed here. Second, he made use of the velocity of NGC 604, which has, as already mentioned, been omitted from the present study on the ground that results from it are discordant with those from the other emission nebulosities observed in M 33.

[21] *Photographs Taken at Lick Observatory*, Pl. VIII, 1940.

sity in the plane is of the order of one-eighth of that in the main body, or about 60 $\odot$/psc^2. The corresponding space density, calculated as before, is 0.2–0.3 $\odot$/psc^3. Therefore, because of the nature of this solution, the evidence suggests for the outlying regions of M 33 an average space density between 0.0 and 0.3 $\odot$/psc^3, i.e., of the same order as that in the solar neighborhood.

VIII. COMPARISONS WITH THE GALAXY

The distributions of density found above for M 31 and M 33 are characterized by the lack of appreciable concentration of matter toward the center. The small, dense central region in M 31 contains but a negligible proportion of the total mass. This result appears to be at variance with the high central concentration of mass that has been estimated for the Galaxy. The discrepancy, however, is probably less real than apparent, because the usual method of deducing the mass distribution in the Galaxy involves a possible misinterpretation of the observational data. In order to bring out this point more clearly, we shall inquire into the underlying assumptions of Oort's formulation of the problem and, in particular, into the assumption commonly made for determining the distribution of mass from Oort's rotational constants A and B.

Oort's formulae for A and B possess great generality. They are based upon the simple hypothesis of circular orbital motion in the principal plane of a circularly symmetrical, rotating system. To estimate the distribution of mass within the system, however, it is necessary to introduce an additional assumption; the conventional one is that the total central force, K (in the solar neighborhood), may be resolved into two components. The first, K_1, is the force exerted by a central mass and varies inversely as the square of the distance from the center, R; the second, K_2, is the force exerted by a homogeneous oblate spheroid extending beyond the sun and varies directly as R. The observational data provide numerical values of Oort's constants A and B, from which K and dK/dR are derived. The last two quantities permit the evaluation of K_1 and K_2, from which it is customary to estimate the degree of concentration of mass. Thus, for example, Plaskett and Pearce[22] find that $K_1/K = 0.75$; they conclude that "three-fourths of the total force is due to matter concentrated towards the centre of the galaxy." Similarly, Smart,[23] who quotes the ratio K_1/K as determined by Oort and by Plaskett and Pearce, states: "The inference is that the greater part of the central force is derived from the central mass." Again, more recently, Oort[24] summarizes: "It can be inferred from the available data that as much as 85 per cent of the total gravitational force in our neighborhood may be considered as due to a central mass and as varying approximately as the inverse square of the distance from the center, while the rest can be adequately ascribed to a homogeneous mass extending beyond the sun."

All that may properly be implied by the resolution of the central force is the following: If we had a stellar system of suitable mass, of which three-fourths were concentrated at the center and the other one-fourth were spread uniformly throughout a homogeneous oblate spheroid extending beyond the sun, then the resultant force and its variation with distance would reproduce the observed values. It does not follow that the mass is actually so distributed, any more than it follows that because the sun attracts like a point-mass, it is therefore a point. That inferences regarding the mass distribution, obtained from resolution of the central force, may be quite misleading, is evident from the following three examples.

1. Consider the force exerted by the thin-disk model in which the density distribution approximates an error function (Fig. 2). For a point distant 0.87 of the radius from the

[22] *Pub. Dom. Ap. Obs.*, **5**, 302, 1934.

[23] *Stellar Dynamics*, p. 389, 1938.

[24] *Ap. J.*, **91**, 279, 1940.

center the attractive force and its variation with distance are equal, respectively, to those that would be exerted by a point-mass at the center. If we were to resolve the force in the conventional way, we should conclude erroneously that all the mass of the disk was concentrated at the center.

2. In M 33, at a distance of about 16′.4 from the nucleus, in the "homogeneous" disk model, K_1/K is 0.75, a value that has been quoted for the Galaxy. It is obvious from the discussion in Section VII that it would be wrong to infer from this ratio that the mass of M 33 is strongly concentrated toward the center.

3. In both M 31 and M 33 it is possible to find points where K_1 and K_2 are of opposite sign. Near the edge of the disk models for these systems, K_1 is positive and K_2 is negative, whereas at points halfway out from the center the signs are reversed. Thus, for a point in M 31 situated 98′ from the nucleus the resolution of the attractive force gives $K_1/K = 1.6$ and $K_2/K = -0.6$. In other words, when the force is resolved in this case, it is found that the component K_2, which is proportional to the distance from the center, is directed outward instead of inward.

It might be supposed that these results are due to the use of thin-disk models and that similar results would not be obtained for oblate spheroids. This, however, is not the case. For it is possible, even without detailed analysis, to postulate oblate spheroids in which the density diminishes monotonically from the center outward, and still to find points where K_1 and K_2 are of opposite sign.

Another consideration that might be urged in support of a high concentration of mass toward the galactic center deals with the motions of the planetary nebulae, discussed by Berman[25] and by Camm.[26] The high rotational velocities (up to 150 km/sec), exhibited by nebulae that may be close to the galactic center,[27] might suggest that a large fraction of the total mass of the system is concentrated at the center. That this is not necessarily the case may be seen from the foregoing discussion of the Andromeda nebula: in that system, rotational motions of the order of 100 km/sec are found for objects only 200 parsecs from the center, although this region contains, according to the density analysis, less than 1 per cent of the total mass.

In brief, the substance of the foregoing discussion leads us to the conclusion that, although the matter in the Galaxy *may* be highly concentrated toward the center, this property is not a *necessary consequence* of the observed ratio of K_1/K.

Finally, it may be emphasized again that the rotational velocities in M 31 and M 33 increase with nuclear distance throughout the main bodies. The decrease in rotational velocity, actually observed in M 33 and inferred for M 31, does not occur until the outermost regions of relatively low density are reached. From observations within the Galaxy it has been established that the rotational velocity in the solar neighborhood decreases outward; hence, if the density distribution in the Galaxy is at all similar to those deduced here for M 31 and M 33, it follows that the sun is situated at a considerable distance beyond the principal part of our stellar system. While this suggestion is not new, the present discussion of the observed rotational-velocity-curves and the character of the calculated density distributions may be regarded as lending considerable support to the hypothesis.

LICK OBSERVATORY
MOUNT HAMILTON, CALIFORNIA
March 15, 1941

[25] *Lick Obs. Bull.*, **18**, 57, 1937 (No. 486).

[26] *M.N.*, **99**, 71, 1938.

[27] Berman's and Camm's nebular distances are subject to considerable uncertainty, as has been pointed out by Oort (*M.N.*, **99**, 376, 1939), and by others.

ADDENDUM

Since it is possible that the integrations performed in this analysis may find additional applications in dynamical problems, we shall give in this section a brief summary of the method of simplifying equations (12), together with the detailed results of the integrations.

The first of equations (12) has been written in its explicit form as equation (13), as follows:

$$\left.\begin{aligned} M(a) = a\int_a^1 dk \int_0^{\pi/2} \frac{d\theta}{k^3\sqrt{1-k^2\sin^2\theta}} - a\int_a^1 dk\int_0^{\pi/2} \frac{1}{k^3}\sqrt{1-k^2\sin^2\theta}\,d\theta \\ + a\int_0^1 dk\int_0^{\pi/2} \frac{d\theta}{\sqrt{1-k^2\sin^2\theta}} - a\int_0^1 dk\int_0^{\pi/2}\sqrt{1-k^2\sin^2\theta}\,d\theta\,, \end{aligned}\right\} \quad (13)$$

and similarly for $N(a)$, $O(a)$, $P(a)$, and $Q(a)$. It can be shown that all four of these integrals have definite limits, provided[28] $a \neq 0$; the order of integration may therefore be interchanged. The following is a short description of the character of the integrals encountered in the simplification of equations (12).

The integrals $\int_0^1 k^n \mathcal{K} dk$ and $\int_0^1 k^n \mathcal{E} dk$ can be reduced without difficulty to give, when n is even, a rational fraction *plus* another rational fraction times $\int_0^{\pi/2} (\theta\, d\theta/\sin\theta)$. This last integral is twice Catalan's constant, which is given in Jahnke-Emde's *Tables of Functions* (p. 149) as 0.915965594. When n is odd, the integration gives simply a rational fraction.

The integrals $\int_a^1 k^{-2n}\mathcal{K} dk$ and $\int_a^1 k^{-2n}\mathcal{E} dk$ give rise to elementary integrals of trigonometric functions and to integrals of the form $\int_0^{\pi/2} \sin^{2m}\theta\sqrt{1-a^2\sin^2\theta}\,d\theta$, where n is an integer and $m = 0, 1, 2, \ldots, (n-1)$. The latter can be expressed in terms of standard elliptic integrals of the first and second kinds.

Integrals with odd negative exponents of k, namely, of the form $\int_a^1 k^{-2n-1}\mathcal{K} dk$ and $\int_a^1 k^{-2n-1}\mathcal{E} dk$, are a little more complicated. They give, in addition to the kinds of integrals mentioned in the previous paragraph, two integrals of mixed logarithmic and trigonometric functions. The first,

$$\int_0^{\pi/2} \sin^{2n}\theta \cdot \log\left(\frac{1+\cos\theta}{\sin\theta}\right) d\theta\,,$$

when integrated by parts, yields integrals that reduce to the form of a rational fraction *plus* another rational fraction times $\int_0^{\pi/2} (\theta\, d\theta/\sin\theta)$, which has already been encountered. The second,

$$\int_0^{\pi/2} \sin^{2n}\theta \cdot \log\left(\frac{1+\sqrt{1-a^2\sin^2\theta}}{a\sin\theta}\right) d\theta\,,$$

[28] As a approaches zero, the sum of the first two terms of equation (13) approaches zero, although each individually becomes infinite.

when integrated by parts, gives integrals of the following forms:

a) Elementary integrals of trigonometric functions;

b) $\int_0^{\pi/2} \frac{\sin^2\theta \cos^{2m}\theta}{t+t^2}\,d\theta$, where $m = 1, 2, 3, \ldots, n$, and $t = \sqrt{1-\alpha^2\sin^2\theta}$;

c) $\int_0^{\pi/2} \frac{\theta \sin\theta\cos\theta}{t+t^2}\,d\theta$;

d) $\int_0^{\pi/2} \theta\cot\theta\,d\theta$.

Class (*a*), of course, presents no difficulties. Class (*b*) can be reduced to elementary integrals of trigonometric functions and to standard elliptic integrals (one step of the reduction being to multiply both numerator and denominator of the integrand by $[1-t]$). In a similar manner, (*c*) can be reduced to give two integrals, of which one cancels (*d*) and the other has the form

$$I_2 = \int_0^{\pi/2} \frac{\theta\cot\theta\,d\theta}{\sqrt{1-\alpha^2\sin^2\theta}} .$$

Thus the four kinds of integrals comprised in $M(\alpha)$, $N(\alpha)$, etc., as defined in equations (12), can be reduced to functions of α involving only simple numbers, logarithms, Catalan's constant, standard elliptic integrals, and the function I_2. It remains to reduce this last expression to a form suitable for numerical calculation.

The transcendental function I_2 is apparently not expressible in terms of ordinary functions. Expanding the radical by the binomial theorem and integrating, term by term, we find

$$\left.\begin{aligned} I_2 = \int_0^{\pi/2} \frac{\theta\cot\theta\,d\theta}{\sqrt{1-\alpha^2\sin^2\theta}} &= \int_0^{\pi/2}\theta\cot\theta\,d\theta + \sum_{n=1}^{\infty} \frac{1\cdot 3\cdot 5\cdot\ldots\cdot(2n-1)}{2\cdot 4\cdot 6\cdot\ldots\cdot 2n} \\ &\qquad \cdot \alpha^{2n}\int_0^{\pi/2}\theta\sin^{2n-1}\theta\cos\theta\,d\theta , \\ &= \frac{\pi}{2}\log_e 2 \\ &\quad + \frac{\pi}{2}\sum_{n=1}^{\infty}\frac{1\cdot 3\cdot 5\cdot\ldots\cdot(2n-1)}{2\cdot 4\cdot 6\cdot\ldots\cdot 2n}\left[1 - \frac{1\cdot 3\cdot 5\cdot\ldots\cdot(2n-1)}{2\cdot 4\cdot 6\cdot\ldots\cdot 2n}\right]\frac{\alpha^{2n}}{2n} . \end{aligned}\right\} \quad (21)$$

This series does not converge very rapidly for α near unity. It may be converted into a more rapidly converging series by taking advantage of the facts that[29]

$$\sum_{n=1}^{\infty}\frac{1\cdot 3\cdot 5\cdot\ldots\cdot(2n-1)}{2\cdot 4\cdot 6\cdot\ldots\cdot 2n}\cdot\frac{\alpha^{2n}}{2n} = \log_e\left(\frac{2}{\alpha}\right) - \operatorname{sech}^{-1}\alpha ;$$

and

$$\sum_{n=1}^{\infty}\left(\frac{1\cdot 3\cdot 5\cdot\ldots\cdot(2n-1)}{2\cdot 4\cdot 6\cdot\ldots\cdot 2n}\right)^2\cdot\frac{\alpha^{2n}}{2n-1} = \frac{\pi}{2} - \mathfrak{E}\left(\frac{\pi}{2}, \alpha\right) .$$

[29] Cf. L. B. W. Jolley, *Summation of Series*, No. 515, p. 158, and No. 529, p. 162, 1925.

Equation (21) is thus reduced to the form

$$I_2 = \mathcal{E}\left(\frac{\pi}{2}, \alpha\right) + \frac{\pi}{2}\left[\log_e\left(\frac{4}{1+\sqrt{1-\alpha^2}}\right) - 1 + \sum_{n=1}^{\infty}\left(\frac{1\cdot 3\cdot 5\cdot \ldots\cdot (2n-1)}{2\cdot 4\cdot 6\cdot \ldots\cdot 2n}\right)^2 \cdot \frac{\alpha^{2n}}{2n(2n-1)}\right]. \quad (22)$$

The function I_2 has been calculated for various values of α. The results, which are given in Table 5, are believed to be correct to one unit in the seventh decimal place, except perhaps $I_2(\alpha = 0.95)$, which may be in error by two or three units in the seventh decimal.

TABLE 5

α	$I_2 = \int_0^{\pi/2} \frac{\theta \cot\theta\, d\theta}{\sqrt{1-\alpha^2\sin^2\theta}}$	α	$I_2 = \int_0^{\pi/2} \frac{\theta \cot\theta\, d\theta}{\sqrt{1-\alpha^2\sin^2\theta}}$
0.0.....	1.088 7930	0.50.....	1.144 6995
0.05.....	1.089 2844	0.60.....	1.174 9334
0.10.....	1.090 7658	0.70.....	1.217 3237
0.15.....	1.093 2581	0.80.....	1.279 9405
0.20.....	1.096 7979	0.90.....	1.385 6789
0.30.....	1.107 2538	0.95.....	1.481 4936
0.40.....	1.122 8246	1.00.....	1.831 9312

The results of the integrations required for equations (12) are given below. For convenience, let

$$L = \frac{\pi}{2}\log_e\frac{1+\sqrt{1-\alpha^2}}{\alpha}; \qquad I_1 = \int_0^{\pi/2}\frac{\theta d\theta}{\sin\theta}; \qquad I_2 = \int_0^{\pi/2}\frac{\theta\cot\theta\, d\theta}{\sqrt{1-\alpha^2\sin^2\theta}}.$$

If the modulus of $\mathcal{K}$ and $\mathcal{E}$ on the left-hand side of equations (23) is k, and if the modulus on the right-hand side is α, then the integrals appearing in equations (12) may be expressed as shown in equations (23).

Application to the thin-disk problem, i.e., substitution of equations (23) into equations (12), brings about certain cancellations, as has already been mentioned, which simplify the numerical work. The substitution yields equations (14) as the final expressions for the force coefficients.

$$\int_0^1 \mathcal{K}dk = +I_1 ; \qquad \int_0^1 \mathcal{E}dk = +\tfrac{1}{2} + \tfrac{1}{2}I_1 ;$$

$$\int_0^1 k\mathcal{K}dk = +1 ; \qquad \int_0^1 k\mathcal{E}dk = +\tfrac{2}{3} ;$$

$$\int_0^1 k^2\mathcal{K}dk = +\tfrac{1}{4} + \tfrac{1}{4}I_1 ; \qquad \int_0^1 k^2\mathcal{E}dk = +\tfrac{5}{16} + \tfrac{1}{16}I_1 ;$$

$$\int_0^1 k^3\mathcal{K}dk = +\tfrac{5}{9} ; \qquad \int_0^1 k^3\mathcal{E}dk = +\tfrac{14}{45} ;$$

$$\int_0^1 k^4\mathcal{K}dk = +\tfrac{13}{64} + \tfrac{9}{64}I_1 ; \qquad \int_0^1 k^4\mathcal{E}dk = +\tfrac{77}{384} + \tfrac{9}{384}I_1 ;$$

$$\left.\begin{aligned}
\int_a^1 k^{-3}\mathcal{K}dk &= -\frac{1}{4} + \frac{1}{4a^2}[(+1-a^2)\mathcal{K} + (+1)\mathcal{E}] + \tfrac{1}{4}(L - I_1 + I_2) ;\\
\int_a^1 k^{-3}\mathcal{E}dk &= -\frac{3}{4} + \frac{1}{4a^2}[(-1+a^2)\mathcal{K} + (+3)\mathcal{E}] - \tfrac{1}{4}(L - I_1 + I_2) ;\\
\int_a^1 k^{-4}\mathcal{K}dk &= -\frac{5}{9} + \frac{1}{9a^2}[(+2-2a^2)\mathcal{K} + (+1+4a^2)\mathcal{E}] ;\\
\int_a^1 k^{-4}\mathcal{E}dk &= -\frac{2}{9} + \frac{1}{9a^2}[(-1+a^2)\mathcal{K} + (+4-2a^2)\mathcal{E}] ;\\
\int_a^1 k^{-5}\mathcal{K}dk &= -\frac{13}{64} + \frac{1}{64a^4}[(+12-3a^2-9a^4)\mathcal{K} + (+4+9a^2)\mathcal{E}] + \tfrac{9}{64}(L - I_1 + I_2) ;\\
\int_a^1 k^{-5}\mathcal{E}dk &= -\frac{17}{64} + \frac{1}{64a^4}[(-4+a^2+3a^4)\mathcal{K} + (+20-3a^2)\mathcal{E}] - \tfrac{3}{64}(L - I_1 + I_2) ;\\
\int_a^1 k^{-6}\mathcal{K}dk &= -\frac{89}{225} + \frac{1}{225a^5}[(+36-4a^2-32a^4)\mathcal{K} + (+9+16a^2+64a^4)\mathcal{E}] ;\\
\int_a^1 k^{-6}\mathcal{E}dk &= -\frac{34}{225} + \frac{1}{225a^5}[(-9+a^2+8a^4)\mathcal{K} + (+54-4a^2-16a^4)\mathcal{E}] ;\\
\int_a^1 k^{-7}\mathcal{K}dk &= -\frac{389}{2304} + \frac{1}{2304a^6}[(+320-20a^2-75a^4-225a^6)\mathcal{K} + (+64+100a^2+225a^4)\mathcal{E}] + \tfrac{225}{256}(L - I_1 + I_2) ;\\
\int_a^1 k^{-7}\mathcal{E}dk &= -\frac{383}{2304} + \frac{1}{2304a^6}[(-64+4a^2+15a^4+45a^6)\mathcal{K} + (+448-20a^2-45a^4)\mathcal{E}] - \tfrac{525}{256}(L - I_1 + I_2) .
\end{aligned}\right\} \quad (23)$$

A NOTE ON THE DISTRIBUTION OF MASS AND LUMINOSITY IN MESSIER 33

LAWRENCE H. ALLER[1]

ABSTRACT

The observed rotational velocities in Messier 33 are compared with theoretical velocity-curves computed on two assumptions regarding the mass distribution. The observations seem to agree most closely with the model in which constant density is assumed to about a thousand parsecs from the center. Values of the mass-luminosity ratio are computed by a comparison with Miss Patterson's measures of the luminosity distribution in this object.

The purpose of this note is to call attention to a method of zonal harmonics for the estimation of the mass distribution in thin external galaxies. Instead of deriving the force and density directly from the observations by means of elliptic integrals, as do Wyse and Mayall,[2] the present procedure is to assume a set of mass distributions and to calculate the circular velocity as a function of the nuclear distance in order to find that assumption about the mass distribution which best fits the observations. Graphical methods appear to be most satisfactory.

We assume a disk model for the spiral in question and suppose it to be split into a number of elementary rings. If we wish to evaluate the potential at a particular radius, r_0, we shall suppose that over a ring of radius $r_0 - \Delta r$ to $r_0 + \Delta r$ the density is zero, in order to secure convergence of the series. The amount of mass neglected in this way can be made arbitrarily small, and we can deal with an almost uniform disk.

The expressions for the potential produced by a ring at any point in space are well known, but to complete the argument we shall sketch their derivation afresh. Consider, for the moment, a point Q upon the axis of a ring at a distance r from its plane. The distance of Q from the ring itself is therefore $\sqrt{x^2 + r^2}$, if x is the radius of the ring. The potential will be

$$V_Q = \frac{m_x}{\sqrt{x^2 + r^2}}, \tag{1}$$

where m_x is the mass of the ring. The series expression for the potential at the point Q is

$$V_Q = \frac{m_x}{x}\left[1 + \frac{r^2}{x^2}\right]^{-1/2} = \frac{m_x}{x}\left[1 - \frac{1}{2}\left(\frac{r}{x}\right)^2 + \frac{1 \cdot 3}{2 \cdot 4}\left(\frac{r}{x}\right)^4 + \ldots .\right], \tag{2}$$

if r is smaller than x, or

$$V_Q = \frac{m_x}{r}\left[1 + \frac{x^2}{r^2}\right]^{-1/2} = \frac{m_x}{r}\left[1 - \frac{1}{2}\left(\frac{x}{r}\right)^2 + \frac{1 \cdot 3}{2 \cdot 4}\left(\frac{x}{r}\right)^4 + \ldots .\right], \tag{3}$$

if r is larger than x. Furthermore, the solutions of the Laplace equation, $\nabla^2 V = 0$, for the assumed case in which the density depends only upon the distance from the center

[1] Society of Fellows, Harvard University.

[2] *Ap. J.*, **95**, 24, 1941.

in the plane of the disk, and not at all upon the longitudinal angular variable, require that, if the center of the ring be taken as origin, the solution be expressible in the form

$$V = \Sigma a_n r^n P_n (\cos \theta) , \tag{4}$$

where θ is measured from the axis toward the plane of the ring. Now $P_n(1) = 1$; and, for the point Q, $\theta = 0$ and $\cos \theta = 1$. In general, for any point in space we have the solution

$$\left.\begin{aligned} r < x , \quad V &= \frac{m_x}{x}\left[1 - \frac{1}{2}\left(\frac{r}{x}\right)^2 P_2 (\cos\theta) + \frac{1\cdot 3}{2\cdot 4}\left(\frac{r}{x}\right)^4 P_4 (\cos\theta) + \ldots .\right] , \\ r > x , \quad V &= \frac{m_x}{r}\left[1 - \frac{1}{2}\left(\frac{x}{r}\right)^2 P_2 (\cos\theta) + \frac{1\cdot 3}{2\cdot 4}\left(\frac{x}{r}\right)^4 P_4 (\cos\theta) + \ldots .\right] . \end{aligned}\right\} \tag{5}$$

In particular, if $\theta = \pi/2$,[3]

$$P_{2n}(0) = (-1)^n \frac{1\cdot 3 \ldots . (2n-1)}{2\cdot 4 \ldots . (2n)} , \tag{6}$$

which corresponds to a point in the plane of the ring. The mass of the ring is $m_x = 2\pi x \rho dx$, where ρ is the density. If r_0 is in the plane of the ring, the contribution to the potential at r_0 by a mass at a distance x from the center will be

$$\left.\begin{aligned} r_0 < x \quad dV &= 2\pi\rho dx\left[1 + P_2^2(0)\left(\frac{r_0}{x}\right)^2 + P_4^2(0)\left(\frac{r_0}{x}\right)^4 + P_6^2(0)\left(\frac{r_0}{x}\right)^6 + \ldots .\right] , \\ r_0 > x \quad dV &= 2\pi\rho dx\left[\left(\frac{x}{r_0}\right) + P_2^2(0)\left(\frac{x}{r_0}\right)^3 + P_4^2(0)\left(\frac{x}{r_0}\right)^5 + P_6^2(0)\left(\frac{x}{r_0}\right)^7 + \ldots .\right] . \end{aligned}\right\} \tag{7}$$

For different models we assume different dependencies of ρ upon x and proceed either (1) analytically or (2) by mechanical quadratures. In case (1) we integrate the series analytically, term by term, from $x = r_0 + \Delta r$ to infinity and from $x = 0$ to $r = r_0 - \Delta r$, depending on whether $r_0 \gtrless x$. In case (2) we evaluate the series (7) and integrate graphically.

The velocity, v, of a body of unit mass which moves in a circular orbit is related to the force and potential by means of the general relation

$$\text{Const}\ \frac{v^2}{r} = F = -\frac{\partial V}{\partial r} . \tag{8}$$

Accordingly, v may be computed from the calculated V and compared with the observations.

For purposes of illustration, let us consider two assumptions about the mass distribution: (*a*) For a distance of 500 parsecs from the center the mass density is taken as constant; beyond this point it is assumed proportional to the luminosity. (*b*) The density is constant from $r = 0$ to $r = 1000$ parsecs; beyond this distance it is taken as zero.

Miss Patterson[4] has measured the luminosity gradient in Messier 33. After correcting for foreshortening she finds that beyond about 6′ from the nucleus the surface brightness,

[3] Whittaker and Watson, *Modern Analysis* (4th ed.), p. 302, 1927.

[4] *Harvard Bull.*, No. 914, p. 9, 1941.

I, decreases exponentially with the nuclear distance in seconds of arc, r'', according to the formula

$$I = e^{-0.00148r''+a}$$

or

$$m = 0.00161r'' + 21.6$$

expressed in magnitudes per square second of arc. If we adopt a distance of 2.2×10^5 parsecs, the surface brightness in magnitudes per square second of arc is

$$m = 0.00150r + 21.65 ,$$

where r is now given in parsecs. Accordingly, assumption (*a*) requires

$$\rho = \rho_0 \qquad r < 0.5 \text{ kiloparsecs} ,$$

$$\rho = \rho_0 e^{-1.38(r-0.5)} \qquad r > 0.5 \text{ kiloparsecs} .$$

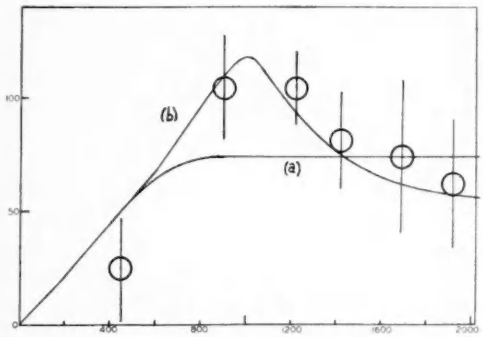

FIG. 1.—Rotational velocities in Messier 33. (*a*) Mass proportional to luminosity beyond 500 parsecs. (*b*) Constant mass density from $r = 0$ to $r = 1000$ parsecs. The circles are the velocities observed by Mayall and Aller. The lengths of the lines represent the probable errors. Abscissae are distances in parsecs; ordinates are velocities in km/sec.

In Figure 1 the mean observed rotational velocities are compared with the theoretical velocity-curves calculated on the basis of assumptions (*a*) and (*b*). Case (*b*) seems much nearer the truth than case (*a*), indicating that the distribution of luminosity in the spiral M 33 bears little relation to the mass distribution, a result in agreement with the conclusions of Babcock for M 31 and of Oort for NGC 3115. Reference to direct photographs shows that the "edge," according to model (*b*), corresponds roughly to the boundary of the main luminous body of the nebula, although spiral arms and detached nebulosities extend out even farther.

The result from case (*b*) for the mass distribution may be used in connection with Miss Patterson's luminosity gradient to estimate the mass-luminosity ratio for the outer regions of the spiral. If we choose the sun's brightness as the unit of luminosity, then the unit of surface brightness per square parsec for a distance of 220,000 parsecs will be 27.12 mag., since this would be the apparent magnitude of the sun in M 33, assuming that the sun's absolute photographic magnitude is 5.40. The surface brightness per square second of arc is then found to be

$$27.12 - 2.5 \log \left(\frac{220{,}000}{206{,}265}\right)^2 = 27.12 - 0.14 = 26.98 .$$

Miss Patterson's data are uncorrected for galactic absorption, which, for the present purpose, may be estimated with sufficient accuracy from Hubble's cosecant law.[5] Accordingly, the total galactic absorption is estimated to be $0.25 \csc 31^\circ = 0.48$ mag., and the corrected luminosities, m, in magnitudes per square second of arc are given by

$$m = 0.00150r + 21.17 .$$

[5] *Ap. J.*, **79**, 51, 1934; *Mt. W. Contr.*, No. 485, p. 44.

Finally, the luminosity, L, in suns per square second of arc, is, therefore,

$$L = 10^{-0.4[(0.00150r+21.17)-26.98]} = 10^{-0.00060r+2.32}.$$

The total mass of Messier 33 is adopted as $1.8 \times 10^9 \odot$. Since the assumed radius of the disk is 1000 parsecs, the average surface density, in suns per square parsec, is $1.8 \times 10^9/3.14 \times 10^6 = 573$; or, expressed in suns per square second of arc, it is $573 \times (220{,}000/206{,}265)^2 = 573 \times 1.14 = 654$. Thus, the mass-luminosity ratio may be calculated from the formula

$$\frac{M}{L} = \frac{654}{L}.$$

The results are given in Table 1.

TABLE 1

THE MASS-LUMINOSITY RATIO IN MESSIER 33

R (Parsecs)	Luminosity $\odot/\square''$	Mass / Luminosity	R (Parsecs)	Luminosity $\odot/\square''$	Mass / Luminosity
400	120	5.4	800	69	9.5
500	105	6.2	900	60	10.9
600	91	7.2	1000	52	12.6
700	79	8.3			

Miss Patterson has estimated the total apparent photographic magnitude of Messier 33 as 6.0. Correcting for a space absorption of 0.5 mag., the resultant absolute magnitude is -16.2, corresponding to a total luminosity of the order of $4.5 \times 10^8 \odot$. The mean mass-luminosity ratio is then about 4. If we adopt Hubble's estimate[6] of the total luminosity of Messier 33 as $1.6 \times 10^8 \odot$, we obtain a mass-luminosity ratio of 11.

HARVARD COLLEGE OBSERVATORY
September 24, 1941

[6] *The Realm of the Nebulae*, p. 143, 1936.

THE SPECTRA OF THE EMISSION NEBULOSITIES IN MESSIER 33

LAWRENCE H. ALLER[1]

ABSTRACT

The emission nebulosities in Messier 33 are similar in spectral characteristics to those of our own Galaxy and to the low-excitation planetary IC 418. The ratio of λ 5007/λ 3727 is found to be the most reliable excitation criterion for these nebulosities. The available evidence suggests that in most of these nebulosities the oxygen is predominantly in the singly ionized condition.

Astronomers have for some time recognized the presence of bright-line nebulosities in external galaxies. Seyfert[2] discovered emission nebulosities in M 101; Babcock[3] found faint emission patches at a considerable distance from the nucleus of the Andromeda nebula; while Mayall[4] has recently given a comprehensive survey of the occurrence of λ 3727 of [*O* II], and other lines as well, in the spectra of extragalactic nebulae.

Bright lines in the nebulous condensations of Messier 33 (NGC 604, 588, and 595) have been observed by Slipher,[5] by Pease,[6] and by Hubble.[7] A preliminary list of the emission patches observed in the rotational study of this spiral has been given elsewhere.[8] However, a more detailed and complete description of these emission nebulosities with respect to their excitation characteristics seems worth while. Accordingly, rough intensity estimates of the bright lines have been made whenever practicable.

The small dispersion of the spectrograms and the graininess of the fast emulsion used rendered impracticable the ordinary methods of spectrophotometry. Intensities, estimated with the aid of scale plates, seemed the best solution of the problem. Dr. Mayall and the writer made the scale plates in the following fashion.

While the spectrograph was off the telescope, we mounted an iris diaphragm between the spark and the slit. By varying the apertures of the iris diaphragm, which had been calibrated with a photoelectric cell in the laboratory,[9] we were able to make a series of exposures upon each type of emulsion with a fixed exposure time and with known intensity ratios. We developed the scale plates in the same way as the nebular plates. We then estimated the relative intensities of the lines in the nebular spectrum simply by comparing them with the lines on the scale plate.

Line intensities measured in this way, although better than estimates made on an arbitrary scale, may be affected by large systematic errors. The individual exposures were one second on the scale plates and several hours on the nebular spectra. The density-intensity curves derived from the former may not, therefore, be quite valid for the latter. More serious is the circumstance that the continuous background is often quite strong, and the scale-plate method makes no allowance for emission lines superposed on

[1] Society of Fellows, Harvard University.

[2] *Ap. J.*, **91**, 261, 1940.

[3] *Lick Obs. Bull.*, **19**, 41, 1939 (No. 498).

[4] *Lick Obs. Bull.*, **19**, 33, 1939 (No. 497).

[5] *Pop. Astr.*, **23**, 23, 1915; *Proc. Amer. Phil. Soc.*, **56**, 406, 1917.

[6] *Pub. A.S.P.*, **27**, 239, 1915.

[7] *Ap. J.*, **63**, 236, 1926; *Mt. W. Contr.*, No. 310.

[8] *Pub. A.S.P.*, **51**, 113, 1939.

[9] We are indebted to Dr. G. E. Kron for helping with this calibration.

continua. Probably the largest errors are accidental, because of the scale and graininess of the plates.

The measured intensities are given in Table 1, referred to $H\beta$ as 10. They are not corrected for plate sensitivity, instrumental transmission, or atmospheric extinction; hence, as they stand, they are useful only for intercomparisons. Unfortunately, the in-

TABLE 1

LINE INTENSITIES IN EMISSION NEBULOSITIES IN MESSIER 33*

Object	5007 [O III]	4959 [O III]	4861 $H\beta$	4340 $H\gamma$	4101 $H\delta$	3967 [Ne III] $+H\epsilon$	3889 $H\zeta$	3869 [Ne III]	3727 [O II]
Anon. 1	7	.....	10	12	.....	.....	.....	.....	14
2	5	3	10	12	8	5	5	4	30
3	12	5	10	14	7	8	4	4	20
IC 142	.....	.....	10	13	6	.....	.....	.....	20
Anon. 7	.....	.....	10	14	.....	.....	.....	.....	25
8a	.....	.....	10	14	4	.....	.....	.....	20
8b	.....	.....	10	14	4	.....	.....	.....	30
9a	4	3	10	15	8	.....	.....	.....	40
9b	.....	.....	.....	.....	.....	.....	.....	.....	12
9c	.....	.....	.....	.....	.....	.....	.....	.....	6
11	.....	.....	10	15	7	.....	.....	.....	20
14	.....	.....	10	12	5	.....	.....	.....	15
NGC 588	12	6	10	14	8	5	4	6	20
595	.....	.....	10	16	8	5	4	4	20
604	5	2	10	20	8	5	3	2	30
IC 131	5	3	10	15	8	4	5	3	40
132	20	9	10	14	10	7	5	6	20
133	11	5	10	13	8	9	4	7	30
135	.....	.....	.....	10	9	.....	.....	.....	20

* Anon. 1 shows a strong continuous spectrum, and the estimates of intensities are poor. IC 142, and Anon. 7, 8, and 11 also show continua. Anon. 16 shows only 3727, and no estimates have been made.

TABLE 1*a*

CORRECTION FACTORS FOR TABLE 1

λ	Factor	λ	Factor	λ	Factor
5007	3.0	4340	0.36	3889	0.42
4959	2.0	4101	.36	3869	.42
4861	1.0	3967	0.39	3727	0.50

strumental transmission is not known for the nebular spectrograph. In connection with the photometry of the planetary nebulae, plate-plus-instrument calibration-curves for the quartz slitless spectrograph and Imperial 1200 and Agfa Spectral Blue plates have been determined. Such calibration-curves, although not strictly valid for the nebular spectrograph, permit one to estimate the factors by which the intensities in Table 1 are to be multiplied in order to yield quantities more nearly comparable with the true intensities. The plate-plus-instrument sensitivity for an Imperial 1200 plate combined

with the atmospheric transmission calculated for a zenith distance of 30° yields the rough correction factors given in Table 1*a*. When the columns of Table 1 are multiplied by the appropriate factors, Table 2 results. The entries in the latter are deemed more nearly proportional to the true intensities than the values in Table 1.

The spectra of these emission nebulosities, as Hubble noticed for NGC 588, 595, and 604, closely resemble those of the diffuse galactic nebulae. They also resemble those of certain low-excitation planetaries, such as Campbell's hydrogen envelope star, BD+30°3639, NGC 40, or IC 418. The photometrically determined intensities of emission

TABLE 2

CORRECTED INTENSITIES OF EMISSION LINES IN MESSIER 33*

Object	5007 *O* III	4959 *O* III	4861 *Hβ*	4340 *Hγ*	4101 *Hδ*	3967 *Ne* III +*Hε*	3889 *Hζ*	3869 *Ne* III	3727 *O* II
Anon. 1	21	.....	10	4	.....	.....	.....	.....	7
2	15	6	10	4	3	3	2	2	15
3	36	10	10	5	3	3	2	2	10
7	.....	.....	10	5	.....	.....	.....	.....	12
8*a*	.....	.....	10	5	1	.....	.....	.....	10
8*b*	.....	.....	10	5	1	.....	.....	.....	15
9*a*	12	6	10	5	3	.....	.....	.....	20
9*b*	.....	.....	.....	.....	.....	.....	.....	.....	6
9*c*	.....	.....	.....	.....	.....	.....	.....	.....	3
11	.....	.....	10	5	3—	.....	.....	.....	10
14	.....	.....	10	4	2	.....	.....	.....	7
NGC 588	36	12	10	5	3	2	2	3—	10
595	.....	.....	10	6	3	2	2	2	10
604	15	4	10	7	3	2	1	1	15
IC 131	15	6	10	5	3	2	2—	1	20
132	60	18	10	5	4	3	2	3—	10
133	33	10	10	5	3	4—	2	3	15
135	.....	.....	.....	4	3	.....	.....	.....	10
142	.....	.....	10	5	2	.....	.....	.....	10
IC 418* galactic planetary	14	5	10	4.5	2.4	1.5	1.3		16

*The photometric data for the galactic planetary, IC 418, are included for comparison. The other tabular entries are eye estimates of intensity, approximately corrected for plate sensitivity, and transmission of the atmosphere and the instrument (see text).

lines in the latter object have been entered in the last row of Table 2.[10] The object of highest excitation, IC 132, more closely resembles NGC 6543, except for the weakness of λ 3727 in the latter.

By analogy with similar galactic objects, we may assume that the emission patches in Messier 33 are excited by hot O or B stars imbedded within them. Probably the excitation of the [*O* II] pair at λ 3727 occurs most often in the vicinity of one or more hot stars, although this radiation seems frequently present in the neighborhood of the nucleus, showing that the general radiation field of the spiral may play a role in the production of these lines.[11] Certain nebulosities—e.g., 9*b*, 9*c*, or 16—show only λ 3727, al-

[10] *Ap. J.*, **93**, 236, 1941.

[11] *Lick Obs. Bull.*, **19**, 38, 1939 (No. 497). It may be of significance that the [*O* III] lines seem frequently prominent in those objects which are farther from the nucleus than 20′, while in those nebu-

though the Balmer series should be visible if it is at all strong. The most obvious interpretation of the absence of the hydrogen lines is that the primary mechanism, i.e., the photoelectric ejection and subsequent recapture of electrons, is rendered inefficient owing to the low density of electrons and a relatively slow rate of photo-ionization due to the high dilution of the ionizing radiation.

As excitation criteria for the bright-line nebulosities one may conveniently employ the ratios $H\beta/\lambda\,3727$, $\lambda\,5007/H\beta$, and $\lambda\,5007/\lambda\,3727$. The first is available for all the emission nebulosities on the list; the other two may be used with such objects as show the green nebular lines. Correlation diagrams for the excitation criteria reveal that the ratios $\lambda\,5007/H\beta$ and $\lambda\,5007/\lambda\,3727$ change very appreciably for relatively small variations in the $H\beta/\lambda\,3727$ ratio.

The obvious interpretation of this result is that most of the oxygen is singly ionized and that relatively little is doubly ionized. If the intensity of the ultraviolet radiation field increases, *O* II ions will tend to become ionized, and the green nebular lines will be strengthened. Meanwhile the absolute intensity of the $\lambda\,3727$ pair may remain almost unchanged. The phenomenon is exhibited in stellar atmospheres: with rising temperature along the spectral sequence the enhanced lines of an atom may strengthen markedly before the effect on the intensities of the neutral lines is noticed. On the other hand, the character of the radiation field, as long as the exciting stars are not too hot, affects the production of the Balmer lines and the excitation of [*O* II] in much the same way. The ionization potentials of hydrogen and neutral oxygen, 13.54 and 13.56 volts, respectively, are very nearly equal. Now, the absolute intensity of the Balmer lines depends upon the number of electrons captured per second by hydrogen ions and, therefore, in a steady state, upon the rate of ionization of hydrogen. Collisions between electrons and *O* II ions produce the $\lambda\,3727$ pair, whose intensity accordingly depends upon the degree of ionization of *O* I. The intensity of the radiation field just beyond the Lyman limit at $\lambda\,912$ determines the rate at which both oxygen and hydrogen will be ionized. Unless the exciting stars are so hot that *O* II becomes appreciably ionized, or the electron density becomes sufficiently high that the Balmer lines strengthen because of the increased rate of loss and recapture of electrons, the hydrogen lines and $\lambda\,3727$ increase or decrease in absolute intensity together. Therefore, the $H\beta/\lambda\,3727$ ratio is not very sensitive to the ionization and excitation.

The $\lambda\,3727$ pair consists of two components, having wave lengths of 3726.16 A and 3728.91 A, arising from transitions from the ground $^4S_{3/2}$ level to the metastable $^2D_{3/2}$ and $^2D_{5/2}$ levels. The lifetimes of the latter levels are very long; Pasternack gives Einstein A-values of 0.00011 and 0.00014, respectively. By analogy with the theory of the excitation of the nebular lines, Menzel and Aller[12] have derived the equation of statistical equilibrium for the ^2D levels of *O* II ,viz.,

$$\left.\begin{aligned}\frac{N_A N_e}{\bar{\omega}_A}[\Omega_{Ab}+\Omega_{Ac}]e^{-\chi/kT_e}\frac{8.54\times 10^{-6}}{T_e^{1/2}}\\ = N_B N_e\left\{\frac{b}{\bar{\omega}_b}\Omega_{Ab}+\frac{c}{\bar{\omega}_c}\Omega_{Ac}\right\}\frac{8.54\times 10^{-6}}{T_e^{1/2}}+N_B[bA_{bA}+cA_{cA}],\end{aligned}\right\}\quad(1)$$

where N_A denotes the number of atoms in the ground level, $^4S_{3/2}$; it is essentially the number of *O* II atoms; N_B is the number of atoms in the ^2D term, while T_e and N_e denote, respectively, the electron temperature and density. Of the N_B atoms in the ^2D

losities nearer than 20′ these lines are often weak or missing. This result is consistent with the suggestion that the very bluest stars are in the spiral arms rather than in the central body of the nebula, as only the hottest stars are capable of emitting sufficient ultraviolet radiation to doubly ionized oxygen.

[12] *Ap. J.*, **93**, 230, 1941. Formulae (7) and (8) are analogous to equation (1) of this paper.

term, the fractions b and c are in the levels $^2D_{3/2}$ and $^2D_{5/2}$, respectively; $b + c = 1$. The value of χ is 3.31 volts; $\bar{\omega}_a = \bar{\omega}_b = 4$, and $\bar{\omega}_c = 6$ are the relevant statistical weights. By assuming that the relative populations of the two levels of the ^2D term are approximately in the ratio of their statistical weights, i.e., $b/c = 4/6$, they obtained from equation (1)

$$N_A = \tfrac{4}{10} N_B e^{\chi/kT_e} \left(\frac{\Omega_{AB} + 150 T_e^{1/2}/N_e}{\Omega_{AB}} \right) = \delta N_A^0 , \tag{2}$$

where the total target area $\Omega_{AB} = [\Omega_{Ab} + \Omega_{Ac}]$ is the sum of the individual target areas. Now N_A^0 is simply the value N_A would have if the atoms were distributed between terms A and B according to Boltzmann's law and if N_B were a known quantity. The correction factor δ depends on T_e,N_e and the unknown collisional cross-section Ω_{AB}. Since $\delta > 1$, N_A^0 is clearly the lower limit to N_A.

TABLE 3

RATIO OF $N_{O\,II}/N_{O\,III}$ FOR EQUAL INTENSITIES OF λ 3727 AND N_1+N_2

T_e	N_e		
	10^3	5×10^3	10^4
6,000	316	301	296
	34	42	51
	5.9	16	26
8,000	214	212	202
	23	28	33
	3.7	9.6	16
10,000	167	166	159
	18	21	25
	2.8	6.9	11

We should like to be able to estimate the relative numbers of O II and O III ions from the intensity ratios of the green nebular and the λ 3727 lines. Obviously, we cannot specify precise values unless we know N_e, T_e, and especially the collisional cross-section Ω_{AB}; but it may be worth while to compare the relevant equations and see exactly what role these parameters play.

The amount of energy E_{PD} radiated per unit volume per second in the green nebular lines is given by[13]

$$E_{PD} = 1.90 \times 10^{-5} \frac{N_P N_e}{T_e^{1/2}} (1 - \beta) e^{-\chi_{PD}/kT_e} h\nu_{PD} , \tag{3}$$

where N_P is the number of O III ions/cm^3, β is the fraction of O III atoms in the $^1D_2$ level collisionally de-excited, and ν_{PD} is the mean frequency of the green nebular lines. Inserting numerical values,

$$E_{PD} = 7.44 \times 10^{-17} \frac{e^{-\chi_{PD}/kT_e}}{T^{1/2}} (1 - \beta) N_P N_e . \tag{4}$$

[13] *Ap. J.*, **94**, 30, 1941. See equation (2) and text following.

Similarly, the energy radiated in the λ 3727 pair is

$$E_{3727} = N_B(bA_{bA} + cA_{cA})h\nu_{3727} = 6.75 \times 10^{-16} N_B\,, \tag{5}$$

where N_B is the number of atoms in the ^{2}D term. From equations (5) and (2)

$$E_{3727} = 1.69 \times 10^{-15} N_A e^{-\chi/kT} \left(\frac{\Omega_{AB}}{\Omega_{AB} + \frac{150 T_e^{1/2}}{N_e}} \right). \tag{6}$$

In Table 3 we list the ratio $N_{O\,II}/N_{O\,III}$ for three values of the electron temperature and density, for equal intensities of λ 3727 and $N_1 + N_2$. The three tabular entries under each pair of arguments correspond to the three assumed values of the collisional cross-section Ω_{AB}, namely, 0.1, 1.0, and 10. One readily sees that the interpretation of the intensity ratios depends most strongly upon this latter parameter. The program of theoretical studies of gaseous nebulae, carried out at Harvard under the guidance of Professor Menzel, has on its agenda the calculation of the collisional cross-sections of *O* II. Until these data are available, the relative abundance of *O* II and *O* III in low-density diffuse nebulae of the galactic type[14] cannot be determined.

By analogy with planetary nebulae of low surface brightness, one may tentatively adopt for diffuse gaseous nebulae $N_e \sim 10^3$ and $T_e \sim 8000°$. If $\Omega_{AB} \sim 1$, the ratio of *O* II to *O* III is about 20 to 1.

HARVARD COLLEGE OBSERVATORY
September 24, 1941

[14] In the planetary nebulae, especially those of high density like IC 4997, $\delta \to 1$; and Boltzmann's formula may be applied. Note that for $N_e \sim 10^4$ a hundred-fold variation in Ω_{AB} corresponds to only a tenfold variation of $N_{O\,II}$.

THE PULSATION THEORY OF LONG-PERIOD VARIABLES

R. M. Scott

ABSTRACT

In this paper the suggestion is made that the variation of the velocity of the emission material whose bright lines appear in the spectra of long-period variables indicates a variation in the velocity of the photosphere. The photospheric motions obtained from this assumption, when combined with the radiometric observations, lead to consistent absolute magnitudes and diameters for five stars.

A solution of M. Schwarzschild's pulsation equation, based upon the data made available by the knowledge of the parallax and diameter of Mira, yielded a luminosity-curve which fits the observed curve well within the error of observation. Further, the solution indicated reasonable conditions in the surface layers. The value of the ratio of the specific heats, γ, was placed by this solution at $3/2$, while the velocity of the compressional wave was found to be of the order of 6×10^6 cm/sec. Such a velocity suggests that the atmosphere extends at least 7×10^{12} cm above the photosphere. The outer layers of the star are shown to be in a state of convective instability. The pressure in these layers varies over a range of more than 70/1, while the density varies through a range of nearly 18/1; maximum density and pressure occur at maximum light.

INTRODUCTION

Several observers[1] have suggested that the emission lines, so conspicuous in the spectra of long-period variables, originate in a portion of the star's envelope below the region which gives origin to the absorption lines. Recent studies[2] of other red giants indicate that the atmospheres of these stars may be of considerable extent. The region occupied by the low-lying emission material in the long-period variable may well be quite distant from the region of greatest effect in the overlying absorption.

M. Schwarzschild[3] has shown that solutions of the pulsation equation of the progressive-wave type lead to acceptable relations between the light and radius variations in Cepheids. One may reasonably expect that such a wave will require some time to traverse the distance between the effective regions for emission and absorption, if the same type of pulsation is present in long-period variables. Hence the variation in absorption velocities may lag in phase considerably behind that of the emission velocities. Although the observations disclose a real phase difference, they do not, in themselves, indicate whether the variation of the absorption velocities lead or lag behind that of emission velocities.

Pettit and Nicholson[4] have computed diameters for several long-period variables from their observations of the luminosities and temperatures of these stars. Velocities calculated from the variations in diameter observed in this way do not agree in phase with the directly observed radial velocities from the absorption lines. I have, therefore, examined an alternate possibility: that the region in which the emission lines arise rather than the extended region where the absorption lines are formed is associated with the "radiometric" photosphere. The observed emission velocities and the variation of radiometrically computed diameters for several stars, all for which the data were sufficient, agree well with this hypothesis. There may very well be a flow of material through the actual photosphere. The radial velocity of such material would indicate the velocity of the flow and not that of the photospheric surface. Such is possibly the case with the absorption lines of Cepheids and perhaps the case with the same sort of lines in Mira-type variables. The emission lines in the latter type of star may suffer the same dis-

[1] A. H. Joy, *Ap. J.*, **63**, 281, 1926; P. W. Merrill, *Spectra of Long-Period Variable Stars*, Chicago, 1940.

[2] VV Cep, V. Goedicke, *Pub. Univ. Michigan*, **3**, 1, 1939; ζ Aur, Christie and Wilson, *Ap. J.*, **81**, 426, 1935.

[3] *Harvard Circ.*, No. 429, 1938.

[4] *Ap. J.*, **78**, 320, 1933.

placement, but I have assumed that the variation of velocity from the emission lines indicates the variation of velocity of the photosphere. The justification of such an assumption will be the results obtained by its use.

RADIOMETRIC MATERIAL

The radiometric material upon which I have based this discussion is from the observations of Pettit and Nicholson.[4] I have not used the smoothed values in Table 3 of their paper because these values are not corrected for limb darkening.

The theory of an atmosphere of gray material in local thermodynamic equilibrium leads to a predicted spectral distribution corresponding to a temperature 4 per cent higher than the mean effective temperature over the disk.[5] The value observed for the sun,

$$\frac{T_D}{T_E} = 1.044\,, \tag{2.1}$$

is in good agreement with the theory, and hence this ratio has been used.

Pettit and Nicholson drew black-body curves for numerous temperatures from which they subtracted the atmospheric and water-cell absorptions. The ratios of the areas under the water-cell transmission-curves to those under the atmospheric transmission-curves are a function of the black-body temperatures. This function is represented by the empirical relation

$$\log T_D = 3.477 - 0.623 \log WC\,, \tag{2.2}$$

where WC is the water-cell absorption, that is, the above ratio of areas expressed in magnitudes, and T_D the temperature.

Pettit and Nicholson have observed values of the water-cell absorption for stars and have used the relation (2.2) to find the stellar temperatures. A temperature so determined is that of a black body whose energy distribution most nearly approaches that of the star observed. In a like manner they have found the bolometric corrections to radiometric magnitudes, Δm_r, from the ratio of the areas under the black-body curves to those under the black-body curves corrected for atmospheric absorption. They have expressed the correction as a function of the water-cell absorption in the form

$$\Delta m_r = 0.252 + 0.234 WC\,. \tag{2.21}$$

This equation gives the correct value of the bolometric correction, since both the correction and the water-cell absorption are functions of the energy distribution, provided the distribution has approximately the form of that from a black body.

The apparent diameter of the star, d, is a function of the water-cell absorption, WC, the bolometric correction, Δm_r, the radiometric magnitude, m_r, and the effective temperature, T_E. The relation is

$$\log d = 5.276 - 2 \log T_E - 0.2(m_r - \Delta m_r)\,. \tag{2.3}$$

The temperatures which Pettit and Nicholson have used in this relation were those derived by equation (2.2), i.e., distribution temperatures rather than effective temperatures. The dependence of diameter upon temperature is

$$d = \text{const} \cdot T_E^{-2} \tag{2.4}$$

or

$$d = \text{const} \cdot T_D^{-2} \cdot 1.09\,, \tag{2.41}$$

an increase in the computed diameter of nearly 10 per cent.

[5] E. A. Milne, *M.N.*, **81**, 381, 1929.

Table 1 gives the observational data of Pettit and Nicholson. I have corrected the diameters given in the fifth column for limb darkening by equation (2.41). Figure 1 shows the diameters plotted as a function of phase. The probable error shown in Figure 1 depends upon the assumption that the probable error of a radiometric magnitude was $\pm 0^{m}.02$ and that of the water-cell absorption $\pm 0^{m}.04$.

RADIAL-VELOCITY MATERIAL

"A Spectrographic Study of Mira Ceti,"[1] by A. H. Joy, is the source for the emission-line velocities of this star. The material for the other stars discussed is derived from

TABLE 1

TEMPERATURES AND DIAMETERS OF MIRA AS DETERMINED FROM WATER-CELL ABSORPTION

JD 2420000+	Phase	m_r	WC	T_D	d
3233	0.20	−0.15	1.56	2280	0".0578
260	.28	−0.05	1.67	2186	.0613
61	.29	−0.06	1.66	2192	.0607
93	.39	+0.26	1.81	2078	.0591
95	.40	+0.28	1.80	2080	.0586
322	.48	+0.50	1.96	1980	.0595
80	.67	+0.60	1.81	2078	.0506
81	.67	+0.56	1.86	2045	.0533
411	.77	+0.65	1.75	2120	.0474
72	.97	−0.04	1.22	2664	.0389
617	.39	+0.33	1.92	2005	.0631
45	.47	+0.62	1.90	2019	.0536
706	.64	+1.01	2.18	1868	.0540
38	.74	+1.16	2.13	1890	.0496
68	.82	+0.98	1.77	2110	.0411
95	.90	+0.43	1.51	2330	.0432
4027	.64	+0.85	2.06	1927	.0538
51	.71	+0.80	1.97	1977	.0518
52	.71	+0.76	1.94	1992	.0542
86	.81	+0.65	1.78	2100	.0483
139	.96	+0.01	1.29	2570	.0410
210	.18	−0.14	1.44	2398	.0513
358	.60	+0.84	1.95	1988	.0502
80	.67	+0.76	1.89	2025	.0503
407	.75	+0.70	1.81	2078	.0483
73	.96	−0.11	1.31	2545	.0445
524	.11	−0.22	1.47	2368	.0548
64	.23	−0.22	1.60	2242	.0622
765	.87	+0.46	1.64	2210	.0469
98	.97	−0.15	1.12	2818	.0359
850	.13	−0.16	1.83	2062	.0735
83	0.23	−0.24	1.55	2294	0.0598

"Behavior of Bright Lines in the Spectra of Long-Period Variable Stars"[6] by Merrill and Burwell. Several authors have discussed the effect of limb darkening in the reduction of variable radial velocities in Cepheids to variable surface velocities.[7]

If the hypothesis of progressive waves in the outer layers of pulsating stars is correct, the time of maximum velocity should be increasingly later for increasingly higher layers

[6] *Ap. J.*, **71**, 285, 1930.

[7] Getting, *M.N.*, **95**, 141, 1934; Shapley and Nicholson, *Mt. W. Comm.*, No. 63; *Proc. Nat. Acad. Sci.*, **5**, 417, 1919.

in the atmospheres of Cepheids. An absorption line produced by material extending through a large portion of the atmosphere of such a star would be made up of contributions from successive layers of material, each with a different velocity of expansion. The resulting profiles of such lines may be so strongly distorted by this variation in velocity effect as to obscure any effect of limb darkening.

I have assumed that the emission lines for the long-period variables originate in a region closely associated with the photosphere. This region may also be of depth which is small compared with the extent of the atmosphere. If the depth is small, the velocities in the region should be homogeneous. A study of the profiles of emission lines in long-period variables might demonstrate the pulsation hypothesis in spite of the fact that absorption-line profiles have failed to do so for Cepheids. The profiles of the emission

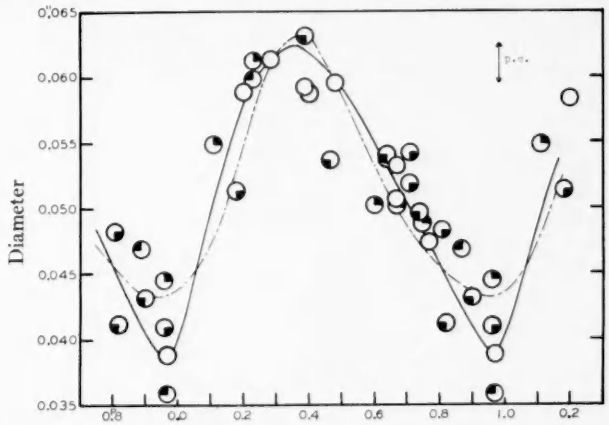

FIG. 1.—Variation of diameter of Mira Ceti; ordinate and abscissa are angular diameter and phase

lines should also indicate the amount and nature of the limb darkening for the long-period variable. Others[7] have already predicted the form of spectral lines for expanding surfaces with limb darkening.

Eddington and others[8] have suggested that the extreme range of luminosity of long-period variables may, in part, be due to "veiling." If "veiling" is present to any considerable extent near the radiating surface, it should produce very rapid and completed darkening of the limb. In such a case the measured velocities, corrected for the star's radial velocity, would be very nearly the true velocities of expansion. The case is analogous to one in which the observer sees a small portion of the surface through a tube smaller in diameter than the star.

"Veiling" however would more likely be in layers of considerable thickness and at some distance above the photosphere where the temperature is low enough to permit condensation. Material at high altitude would have much less effect upon limb darkening than material lower in the atmosphere, because the path length through the absorbing medium would not increase so rapidly with angle from the center of the disk. The emission lines, $H\beta$, $H\epsilon$, and several others that lie in portions of the spectrum where there is strong overlying absorption must suffer from a pseudo-veiling and may therefore be strongly darkened to the limb. On the other hand, those lines that seem to shine through the atmosphere unobscured by atomic or molecular line absorption would not be affected as to profile by this monochromatic veiling.

In practice the observer sets the measuring wire "upon the tips of the strongly exposed

[8] Eddington, *Internal Constitution of the Stars*, p. 207, 1926; Merrill, *op. cit.*, pp. 98 ff.

bright lines."[1] This procedure tends to reduce the systematic errors of strongly overexposed lines in comparison with the less exposed ones. The measurer thereby measures the point of maximum intensity in the line, since the tips of emission lines arise from the photographic spreading or occasional extreme excursions of the image on the slit because of "seeing."

Since no better assumption is now available, I have used as the correction factor for the conversion of radial velocity to velocity of pulsation the value that arises from the normal limb darkening.[7] The desired relation is

$$\dot{r} = 1.4(\overline{RV} - RV) . \tag{3.1}$$

Figure 2 shows the variation of the velocity of the emission surface with phase. Since no probable errors were published for the original data, the probable error shown in the

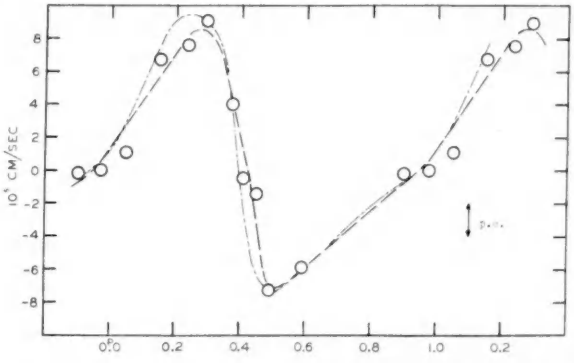

FIG. 2.—Variation of radial velocity; ordinate and abscissa are velocity and phase

figure is dependent upon the agreement of the velocities grouped together to form the normal places. This probable error therefore includes the variation of velocity at the same phase of different epochs and the dispersion of velocity in the phase interval included in each normal as well as in the errors of measurement.

PULSATION PARALLAXES

The area under the radial-velocity curve, in square centimeters, gives the radius in centimeters as a function of phase, except for an unknown additive constant—the minimum radius. The radiometric observations also give a radius-curve in seconds of arc, convertible to centimeters by a factor involving the parallax. The ratio of the increment of diameter in centimeters to the increment expressed in seconds of arc is then equal to the ratio of the radius of the earth's orbit to the parallax of the star. The only long-period variable for which the data are complete enough for a good determination of the parallax by this method is o Ceti. The smooth curve through the points of Figure 2 represents the variation in radius with phase. The solid circles in Figure 3 indicate the points resulting from the integration of the radial-velocity curve for each increment of 0.1 in phase. The open circles in this figure are the radiometric observations of diameter. A least-squares solution for the parallax of o Ceti from ten equidistant phases yielded

$$\pi = 0''.021 ,$$

and the minimum diameter,

$$D_{\min} = 3.1 \times 10^{13} \text{ cm}.$$

The probable errors resulting from the least-squares solution are meaningless, since the points used are from an already smoothed curve.

Table 2 gives the results for all the other long-period variables for which the requisite data were available. The values for these stars are not the results of least-squares solutions because the data are too meager for such treatment. These values result from a simple comparison of the maximum range of pulsation in centimeters and in seconds of arc.

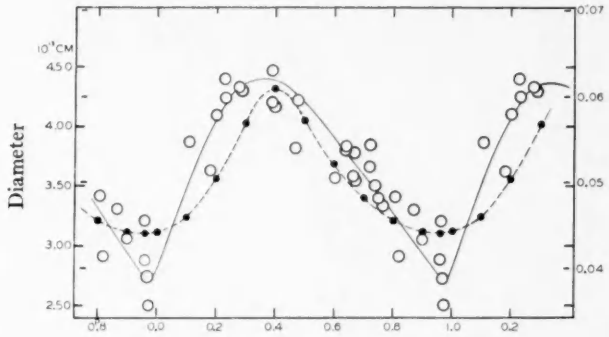

FIG. 3.—Relation between diameter and phase; open circles represent values derived from radiometric observations; filled circles, those derived by integrating the velocity-curve.

TABLE 2

RELATIVE ELEMENTS OF LONG-PERIOD VARIABLES

STAR	PERIOD	DIAMETER RANGE		PARALLAX	m_b AT MAXIMUM	DIAMETER AT MINIMUM
		Apparent	Real			
R Leo	313^d	$0''.014$	1.0×10^{13} cm	$0''.021$	$-3^m.0$	3.9×10^{13} cm
o Cet	330	.017	1.2	.021	−3.45	3.0
X Oph	337	.010	1.7	.009	−3.4	3.3
R Hyd	405	.022	1.6	.020	−3.3	3.3
χ Cyg	407	0.026	2.0	0.019	−3.0	2.8

Although the quantities in the table show no period-luminosity relation, they do indicate a slight dependence of both range of diameter and minimum diameter upon period. The range of diameter dependence is the better determined of the two and is without doubt a restatement of the well-known relation between range of brightness and period.

Recently Keivin Burns[9] has determined the parallax of Mira as $0''.020 \pm 0''.005$. This is the first determination, to my knowledge, in which the observer has allowed for the effect of the companion.

The case of X Oph is of particular interest. The long-period variable has a companion whose spectrum is Ko and does not seem to be a variable. When the red star is at minimum, the companion may be studied without interference. From an examination of the

[9] *Pub. A.A.S.*, **10**, 120, 1941.

spectrum of the companion, Adams[10] has set its absolute visual magnitude at $+2^{m}.4$; it is a subgiant. The parallax would be, then,

$$\pi = 0''.005 .$$

On the other hand, if we adopt the parallax given in Table 2 the absolute magnitude of the companion becomes $+4^{m}.0$. The star then falls just above the main sequence; it is a bit brighter than a normal K0 dwarf.[11] The investigations of the absolute magnitudes of long-period variables from proper-motion material have been numerous. A mean value for the stars of periods around 400 days is about $0^{m}.0$, absolute visual magnitude. The bolometric correction for these stars is very large and quite uncertain. The value ranges from $-3^{m}.8$ for *o* Ceti to nearly $-5^{m}.0$ for χ Cyg. It appears, then, that the absolute magnitudes in the table are considerably fainter than those resulting from studies of stellar motions.

THE APPLICATION OF THE PULSATION THEORY

Schwarzschild has shown[3] that, if the pulsation of a Cepheid is of the nature of a progressive wave in the outer layers of the star, the luminosity at any time is

$$F = \frac{10}{l}\left[\left(1 + \frac{\ddot{r}r^2}{G\mathbf{M}}\right)\left(1 + \frac{x}{\delta}\cdot\frac{r-R}{10^{11}} + \frac{y}{\delta}\frac{\dot{r}}{10^{6}}\right)^{\delta p} + q\left(\frac{r}{R}\right)^{4}\left(1 + \frac{x}{y}\frac{r-R}{10^{11}} + \frac{y}{\delta}\frac{\dot{r}}{10^{6}}\right)^{\delta(1+p)}\right] . \qquad (5.1)$$

This relation gives the luminosity as a function of the radius r, the surface velocity $\dot{r}$, and the surface acceleration $\ddot{r}$, which are all periodic functions of time. Also included in the relation are two dimensions of the star, its mean radius R and its mass $\mathbf{M}$. There remain six constants, which depend for their values upon the physical state of the outer layers of the star. They are

$$l = \frac{10}{F_0}\frac{K}{4\zeta}, \qquad x = \frac{2\gamma}{\gamma - 1} S \frac{10^{11}}{R}, \qquad y = \gamma \cdot 10^{6}\sqrt{\frac{\rho_0}{\gamma P_0}},$$
$$p = \zeta(4 + m) - \frac{n}{\gamma} - 1, \qquad q = \frac{K}{4\zeta} - 1, \qquad \delta = \frac{2\gamma}{\gamma - 1} . \qquad (5.2)$$

The notation is that of *Harvard Circular*, No. 429.

There are two possible methods for testing the theory. One might assume reasonable values of the six constants and compute the light-curve. Such a method would be more a test of the assumed values than a test of the pulsation theory, because the shape of the light-curve is critically dependent upon the values of the constants. On the other hand, a direct solution of equation (5.1) at six points on the light-curve would give the values of the constants necessary for agreement. The manner in which the constants enter equation (5.1), however, makes such a direct solution very difficult. Since the exponential constant δ is a function of the ratio of the specific heats of the stellar material in the envelope, it has a limited range of permissible values. A preliminary computation indicated that the range of possible values for q is also limited. The four remaining constants may be easily found for each assumed value of δ and q. This method insures that the function (5.1) will fit the light-curve in at least four points regardless of the values assumed for δ and q. The fit of the function to the curve at points other than these four will indicate which of the values are correct.

[10] *Ap. J.*, **59**, 97, 1924.

[11] See, e.g., *Handb. d. Ap.*, **7**, 496, 1936.

For *o* Ceti all the requisite material is now available. It would be most desirable, of course, to have sufficient material to consider only one epoch at a time; but, since the material is so meager even in this case, I have used mean curves.

I have used as the parallax of Mira $\pi = 0''.021$ upon the evidence presented above. The absolute bolometric magnitude is, then,

$$\mathbf{M}_b = m_r - \Delta m_r + 5.9 + 5 \log \pi \tag{5.3}$$

or

$$\mathbf{M}_b = m_r - 0.234WC - 2.73 , \tag{5.31}$$

where

$$\pi = 0''.021$$

and

$$\Delta m_r = 0.252 + 0.234WC . \tag{5.32}$$

The circles in Figure 4 indicate the observations reduced by equation (5.31). It is clearly seen that in this case the points from different epochs do not combine well into a mean curve.

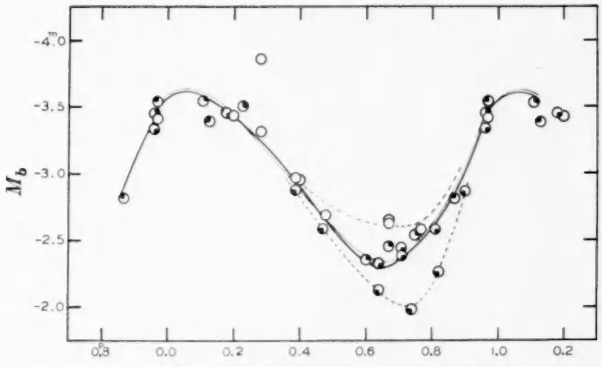

FIG. 4.—Variation of absolute magnitude of Mira Ceti with phase

While the three maxima covered by the observations are nearly of the same brightness, both visually and bolometrically, the minima show a marked disagreement. The minimum indicated by the open circles was unusually bright visually; the other three were all equally faint normal visual minima. Thus, the radiometric observations seem to exhibit the visual peculiarities except for the single minimum indicated by the circles filled in the third quadrant. At this epoch the radiometric observations made the star comparatively fainter than did the visual. Aitken observed the companion for the first time at that minimum.

The value of F in equation (5.1) is determined by

$$\mathbf{M}_b = -2.5 \log F . \tag{5.4}$$

This equation gives the correct value of the luminosity except for the factor F_0, which enters in the expression for l in equation (5.2).

The value of the mean absolute bolometric magnitude from Figure 4 is

$$\overline{\mathbf{M}}_b = -2^{\mathrm{m}}97 .$$

The empirical mass-luminosity relation[12] gives the dependence of mass luminosity in the following form:

$$\log \mathbf{M} = -0.1048(\mathbf{M}_b - 5.23) , \tag{5.5}$$

where the mass is in terms of that of the sun. If

$$\mathbf{M}_\odot = 1.983 \times 10^{33} \text{ gm} ,$$

then

$$\mathbf{M} = 1.44 \times 10^{34} \text{ gm}$$

is the mass of Mira.

Equation (5.1) requires both the radius of the surface and the velocity of the surface for each phase. Smooth curves through the observations of the two quantities would not yield constant results, since the curves of Figure 3 show that variation in slope of

TABLE 3

RADIUS, SURFACE VELOCITY, SURFACE ACCELERATION, AND LUMINOSITY OF MIRA AS FUNCTIONS OF PHASE

Phase	r	$\dot{r}$	$\ddot{r}$	F
0.00.....	1.56×10^{13} cm	$+0.75\times10^{5}$ cm/sec	$+2.75\times10^{-2}$ cm/sec^2	14.00
.05.....	1.60	+1.85	+3.50	13.96
.10.....	1.67	+2.70	+4.10	13.92
.15.....	1.75	+3.55	+4.00	13.84
.20.....	1.86	+4.55	+3.25	13.70
.25.....	2.02	+5.10	0	13.57
.30.....	2.17	+4.25	−7.00	13.42
.35.....	2.23	+1.70	−7.95	13.25
.40.....	2.23	−0.60	−7.80	13.07
.45.....	2.16	−2.65	−5.90	12.87
.50.....	2.06	−3.70	−0.60	12.67
.55.....	1.95	−3.45	+1.20	12.52
.60.....	1.86	−2.85	+1.75	12.42
.65.....	1.79	−2.45	+1.70	12.37
.70.....	1.72	−2.00	+1.70	12.42
.75.....	1.67	−1.50	+1.70	12.53
.80.....	1.62	−1.10	+1.50	12.70
.85.....	1.58	−0.70	+1.50	12.79
.90.....	1.56	−0.30	+1.50	13.19
0.95.....	1.55	−0.15	+1.75	13.56

the radius-curve does not give the surface-velocity curve. The dot-dash curves of Figures 1 and 2, determined by trial and error, are a pair of curves which are not only consistent but which fit the observations within their probable errors.

These dot-dash curves then give satisfactory values of r and $\dot{r}$ for use in equation (5.1). I have used the relation

$$\ddot{r}_{ph} = \frac{\dot{r}_{ph-0.025} - \dot{r}_{ph+0.025}}{1.43 \times 10^{6}} \tag{5.6}$$

to determine $\ddot{r}$.

The value of the fraction $\ddot{r}r^2/G\mathbf{M}$ varies between −0.07 and +0.06, so that the error in $\ddot{r}$ has very little effect upon the value of the term $1 + (\ddot{r}r^2/G\mathbf{M})$ and thus upon the luminosity.

[12] Russell and Moore, *The Masses of the Stars*, p. 112, 1940.

THE DETERMINATION OF CONSTANTS

A new variable,

$$z = 1 + \frac{y}{\delta}\left(\frac{x}{y}u + v\right), \tag{6.1}$$

reduces equation (5.1) to a more convenient form:

$$l = gz^{\delta p} + qfz^{\delta(1+p)}, \tag{6.2}$$

where

$$g = \left(1 + \frac{\ddot{r}r^2}{G\mathbf{M}}\right)\frac{10}{F}, \qquad f = \left(\frac{r}{R}\right)^4\frac{10}{F}, \qquad u = \frac{r-R}{10^{11}}, \qquad v = \frac{\dot{r}}{10^6}. \tag{6.21}$$

The substitution of the observed variables r, $\dot{r}$, $\ddot{r}$, and F, together with the constants $\mathbf{M}$ and R, into equation (6.21), gives the values of the quantities g, f, u, and v for each 0.05 in phase. The variable z is periodic and has the value 1 at two phases. If these two phases Ph_1 and Ph_2 can be found, the value of the ratio

$$\frac{v_1}{u_1} = \frac{v_2}{u_2} = -\frac{x}{y} \tag{6.3}$$

gives the ratio of two of the unknown constants; and

$$g_1 + qf_1 = g_2 + qf_2 = l.$$

I have drawn large-scale curves for the function v/u and $g + qf$, for four values of q and have determined the phases Ph_1 and Ph_2 by inspection, at which

$$\frac{v_1}{u_1} = \frac{v_2}{u_2}, \tag{6.31}$$

as well as

$$g_1 + qf_1 = g_2 + qf_2. \tag{6.4}$$

These then are the phases at which $z = 1$. The results of each step of the computation appear in Table 4.

At a pair of additional phases Ph_5 and Ph_6, at which

$$z_5 = z_6 \neq 1 \qquad \text{or} \qquad 0, \tag{6.5}$$

equation (6.2) becomes

$$g_5 + qf_5z_5^{\delta} = g_6 + qf_6z_6^{\delta}, \tag{6.51}$$

and

$$z_{5,6}^{\delta} = -\frac{1}{q}\frac{g_5 - g_6}{f_5 - f_6}. \tag{6.52}$$

From equation (6.1) it follows that the phases at which

$$z_5 = z_6 \tag{6.53}$$

will be the ones where

$$\frac{x}{y}u_5 + v_5 = \frac{x}{y}u_6 + v_6. \tag{6.54}$$

Since the ratio x/y is given by equation (6.3), the curve of $x/y(u + v)$ as a function of phase may be used to determine those phases at which equations (6.53) and (6.54) hold.

I have obtained by trial and error those phases, Ph_5 and Ph_6, given in Table 4, near which the ratio

$$\frac{g_5 - g_6}{f_5 - f_6}$$

has a maximum value. This procedure leads to a value of z of maximum accuracy. Since y is the only remaining unknown in equation (6.1), it may be easily determined for each assumed value of δ.

At Ph_4, for which $x/y(u + v)$ and therefore z is a maximum, the substitution of the values of the constants so far determined gives the value of the remaining constant p. In

TABLE 4

THE SOLUTION OF THE PULSATION EQUATION

q	1				2				3			
Ph_1	+0.209				+0.205				+0.204			
Ph_2	+ .643				+ .639				+ .635			
l	+ .157 $\times 10^{-3}$				+ .235 $\times 10^{-3}$				+ .313 $\times 10^{-3}$			
x/y	− .0868				− .108				− .115			
Ph_4	+ .965 +0.950*				+ .950				+ .950			
Ph_5	+ .600				+ .600				+ .600			
Ph_6	+0.223				+0.222				+0.221			
δ	5	6	8	14	5	6	8	14	5	6	8	14
y	+0.364	+0.360	+0.364	+0.367	+0.516	+0.522	+0.512	+0.528	+0.965	+0.983	+0.989	+1.000
x	− .0316	− .0313	− .0316	− .0319	− .0556	− .0564	− .0554	− .0571	− .111	− .113	− .114	−0.115
p	0.000	0.000	0.000	0.000	−0.326	−0.339	−0.343	−0.370	−0.597	−0.618	−0.634	−0.671
$\Sigma(\Delta m)^2$	760	786	700	526	162	62	267	501	54991	46221	29412	30891

* Approximate value of Ph_4 used in the computation of p.

general, four values of g, x, and p result from each assumed value of q, corresponding to each of the four values assumed for δ. There are then twelve solutions to choose from.

From equations (5.1) and (6.21)

$$\Delta m = 2.5 \log [gz^{\delta p} - qfz^{\delta(1+p)}] , \tag{6.6}$$

or

$$\Delta m = \frac{1.086}{l} [gz^{\delta p} + qfz^{\delta(1+p)} - l] , \tag{6.61}$$

if Δm is small.

The last row of Table 4 gives the sums of the squares of the residuals computed by equation (6.61) for five equally spaced phases starting with 0.1. Phases near 0.0, 0.2, and 0.6 were used for the determination of the constants. Thus the residuals at odd phases would be a better indicator of the goodness-of-fit to the luminosity-curve than those at even phases.

The sum of the squares of the residuals for

$$q = 2 , \qquad \delta = 6 ,$$

are so much smaller than those for any other values of the constants that there remains no doubt that these are the best values.

The values of the other constants are thus

$$y = 0.25\,, \qquad x = -0.055\,, \qquad p = -0.33\,, \qquad = 0.0235\,.$$

The data are not considered sufficiently accurate to warrant a correction of the constants by least squares. An idea of the order of accuracy may be obtained, however, from the fact that the mean absolute residual from equation (6.61) is

$$\overline{|\Delta m|} = 0^{m}032\,.$$

The lightly drawn curve in Figure 4 was computed from the above values.

INTERPRETATION OF THE CONSTANTS

The departure of the computed curve of luminosity from the observed one is well within the probable error of the observations. If, then, the values of the constants indicate physical conditions compatible with what is already known of the nature of Mira Ceti, we may assume that this pulsation theory is satisfactory.

The value of δ is related to the ratio of the specific heats by

$$\delta = \frac{2\gamma}{\gamma - 1}$$

or

$$\gamma = \frac{\delta}{\delta - 2} = \frac{3}{2}\,. \tag{7.1}$$

This value of γ corresponds to a polytropic index of 2, which implies a rather flat density gradient in the envelope. The relations

$$\frac{P}{P_0} = z^{\delta}\,, \qquad \frac{\rho}{\rho_0} = z^{\delta/\gamma} = z^{\delta-2}\,, \tag{7.2}$$

which now become

$$\frac{P}{P_0} = z^{6}\,, \qquad \frac{\rho}{\rho_0} = z^{4}\,, \tag{7.21}$$

give the variation of pressure and density with phase.

Table 5 and Figure 5 show these variations. The ranges of both pressure and density are very large, but not unacceptably so. In fact, such a large variation of density may aid in the interpretation of the spectral changes. The form of the pressure wave is much smoother than for δ Cephei.[3]

The value of y, defined by

$$y = \gamma\sqrt{\frac{\rho_0}{\gamma P_0}} \cdot 10^{6}\,, \tag{7.3}$$

is related to the velocity of the wave in the envelope. The velocity, c, of a compressional wave in an adiabatic gas is given by

$$c = \sqrt{\frac{\gamma P}{\rho}}\,. \tag{7.31}$$

Thus, from equation (7.3),

$$c = \frac{\gamma}{y} \cdot 10^{6}\,, \tag{7.32}$$

or

$$c = 6 \times 10^6 \text{ cm/sec.} \tag{7.33}$$

If we assume that the displacement of the time of zero velocity of expansion of the absorption lines from the time of zero velocity of the emission lines is a lag equal to the time required for the wave to pass from the emission region to the effective region of the absorption, it is possible from equation (7.33) to find the distance between these two

TABLE 5

VARIATION OF PRESSURE AND DENSITY OF THE SURFACE LAYERS OF MIRA WITH PHASE

Phase	z	$z^6 = P/P_0$	$z^4 = \rho/\rho_0$
0.0	1.25	3.79	2.43
.1	1.17	2.57	1.87
.2	1.01	1.06	1.04
.3	0.72	0.14	0.27
.4	0.62	0.05	0.14
.5	0.75	0.17	0.31
.6	0.95	0.73	0.81
.7	1.09	1.69	1.42
.8	1.19	2.86	2.02
0.9	1.25	3.79	2.43

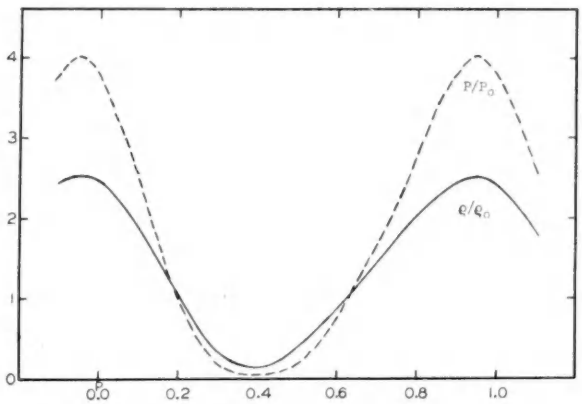

FIG. 5.—Variation of pressure and density with phase

regions. The displacement is very nearly 150 days. In this time the waves would move through 7.7×10^{12} cm!

The quantity ζ is defined by

$$\frac{1}{\zeta} = 4 - \frac{\beta^2}{4 - 3\beta}\left(3 - \frac{1}{\Gamma - 1}\right). \tag{7.4}$$

For any reasonable assumption of β, ζ is very nearly equal to $1/4$, even for the extreme value of $\Gamma = \frac{2}{3}$.

A partial check on the value of q is afforded by the relations

$$l = \frac{10}{F_0}\frac{K}{4\zeta} \tag{7.5}$$

and

$$q = \frac{K}{4\zeta} - 1 , \tag{7.51}$$

or

$$F_0 = \frac{10}{l_0}(q + 1) . \tag{7.52}$$

From the value of l and q,

$$F_0 = 12.80 .$$

The mean observed value of F_0 is 12.90, which agrees to the order of accuracy of the solution.

Equation (7.51) gives the value of K from the value of q and ζ. Then

$$K = 3 = 4\frac{P_0}{T_0}\frac{dT_0}{dP_0} .$$

The adiabatic temperature gradient is

$$\frac{P}{T}\frac{dT}{dP} = \frac{\gamma - 1}{\gamma} = \frac{1}{3} .$$

The relation indicates a condition of convective instability in the outer region since the adiabatic gradient is less than the gradient necessary for radiative equilibrium. The theory has not been developed for a star whose outer layers are in convective, rather than in radiative, equilibrium, with the result that the value obtained for K may be greatly in error.

The quantity p is related to the opacity in the outer layers. The relation between opacity, density, and pressure is

$$\chi = \chi_0 \rho^n T^{-m} .$$

Then

$$p = \zeta(4 - m) - \frac{n}{\gamma} - 1 ,$$

and

$$p = \frac{m}{4} - \tfrac{2}{3}n = -0.33 .$$

For Kramers' law $m = 3.5$ and $n = 1$; thus

$$\frac{m}{4} - \tfrac{2}{3}n = +0.21 ,$$

a discrepancy to be expected; Kramers' law would not hold in the outer regions where the temperatures are comparatively low and many of the atoms neutral.

The solution of the first-order approximation to the integral of the pulsation equation as given by Schwarzschild is

$$\frac{r - r_0}{r_0} = r_0^{-[(2/\gamma-1)S+3]} f\left(t \pm \int \sqrt{\frac{\rho_0}{\gamma P_0}}\, dr_0\right).$$

A function of the constant x has replaced the exponent of r_0 such that

$$\frac{x}{\gamma}\frac{R}{10^{11}} + 3 = \frac{2}{\gamma - 1} S + 3 = -3.6 .$$

The positive value of the exponent insures that the amplitudes of pulsation increase outward. The amplitudes indicated by the velocity-curves of the absorption and emission lines are very nearly the same. This observational fact refutes the large value for the exponent.

CONCLUSION

The results arising from the assumption that the variation of long-period variables is due to a pulsation of the stars do not conflict with the observational material at hand. A much better check upon the theory used here would be possible if radiometric and spectroscopic observations covering the same cycle were available. From such material the variations of light could be predicted for each point in the light-curve not only over a single cycle but for several succeeding ones. The values of the constants should remain unchanged from cycle to cycle.

Two points of further interest have arisen from the solution. A solution of the pulsation equation should be found for stars with a part of their envelopes in convective equilibrium, since it appears that such an equilibrium condition does exist in the atmosphere of Mira. Convective equilibrium extending through a sufficiently deep layer in the stellar envelope could bring up to the visible surface highly excited atoms. Emission lines might be the result of recombination in this material.

With the values of the radius, mass, and luminosity of Mira, found from the "pulsation" parallax, it should now be possible to form a good idea of the structure of the overlying atmosphere.[13]

I wish to express my gratitude to Dr. Menzel for his many suggestions, for reading and criticizing the manuscript, and for continual inspiration. I am also indebted to Dr. Sterne and to Dr. Schwarzschild for many conversations on obscure points which arose during this investigation.

HARVARD OBSERVATORY
August 1941

[13] See, e.g., Unsöld, *Physik der Sternatmosphären*, chap. vii, 1938.

INTENSITY ANOMALIES IN α CYGNI

LAWRENCE H. ALLER[1]

ABSTRACT

The lines of *Cr* II and *Ti* II do not fit on the curve of growth determined by the *Fe* II atoms. This curve is similar to the one determined some years ago by Struve and Elvey. Interlocking or emission arising from chromospheric effects, which the elementary curve-of-growth theory does not take into account, seems the most likely explanation of the observed discrepancy.

Deneb, or α Cygni, is an A supergiant characterized by strong, relatively sharp, metallic enhanced lines and a variable radial velocity suggestive of irregular pulsations.[2] Beals[3] considers that stars of this type are closely related to the P Cygni stars. The latter possess extensive envelopes and seem to display atmospheric turbulence.

Some years ago, Pannekoek[4] measured a number of equivalent widths in the spectrum of Deneb and used theoretical multiplet intensities to construct a curve of growth. His measures agree well with my own determinations from Mills spectrograms taken with the 36-inch refractor of the Lick Observatory. Struve and Elvey[5] have constructed a curve of growth from measures of lines of *Fe* I, *Fe* II, *Ti* II, *Cr* I, and *Cr* II in Deneb. Their intensities are consistently smaller than those obtained by Pannekoek and by myself. In the present work I have also used some intensities of Fe II lines in the visual region, measured upon Lick one-prism spectrograms.

The curve of growth relates the equivalent width, W, of a line to the number of atoms, N, acting to produce it. The kinetic or turbulent velocities of the atoms and the damping constant, Γ, fix the actual shape of the curve. The usual procedure has been to plot W against Nf, where f is the oscillator strength. Menzel[6] has shown, however, that when the lines cover a range of wave length, the correct procedure requires the plotting of W/λ, instead, as a function of X_0 rather than Nf, where X_0 is given by

$$X_0 = N \frac{\pi e^2}{mc} f \frac{c}{\pi^{1/2} v \nu_0} . \tag{1}$$

Here v is the most probable kinetic velocity of the atoms (unless turbulence exists), and ν_0 is the frequency of the line. Now N and, therefore, X_0 contain the Boltzmann factor, χ/kT. Accordingly, Menzel has also introduced the quantity, X_0', through

$$\log X_0' = \log X_0 + \frac{5040\chi}{T} . \tag{2}$$

Whereas X_0 is the effective optical depth in the center of the line, X_0' is a quantity proportional to the strength of the line and is independent of the temperature. Recently, Menzel and Goldberg[7] have derived values of log X_0' for various atoms from the solar

[1] Society of Fellows, Harvard University.

[2] *Lick Obs. Bull.*, **17**, 99, 1935.

[3] *J.R.A.S. Canada*, **34**, 169, 1940.

[4] *Proc. Kon. Akad. van Wetensch., Amsterdam*, **34**, No. 6, 1931.

[5] *Ap. J.*, **79**, 427, 1934. [6] *Ap. J.*, **84**, 462, 1936. [7] Unpublished.

data published by Allen.[8] These X_0'''s are probably superior to the theoretical line strengths computed for transition arrays with the assumption of pure LS coupling. Accordingly, I have used the solar log X_0'''s to construct empirical curves of growth for *Fe* II, *Ti* II, and *Cr* II in Deneb. An analysis of the spectrum of Gamma Geminorum suggests an excitation temperature for an A-type star as low as 6000° or 7000°. Since the excitation potentials of the lower levels of most of the involved lines of a given ion are very nearly the same, the relative X_0'''s are somewhat insensitive to the temperature chosen. I have adopted a temperature of 6000° in the computation of X_0. A few lines of sensibly different excitation potential for the lower levels fall among the others on the empirical curve of growth, i.e., they suggest that no sensible error in the empirical curve of growth can arise from this choice of temperature.

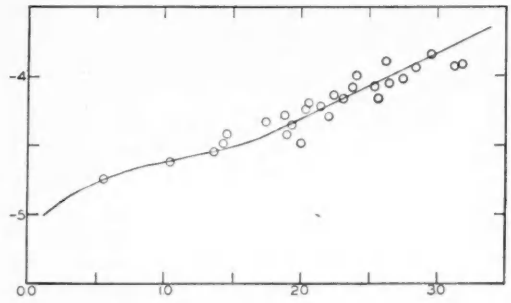

FIG. 1.—Curve of growth for *Fe* II in α Cygni

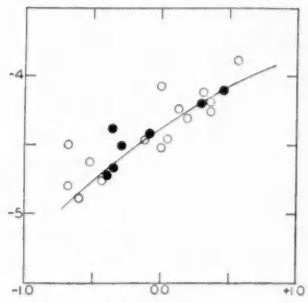

FIG. 2.—Curve of growth for *Cr* II (*filled circles*) and *Ti* II (*open circles*) in α Cygni.

Menzel's asymptotic formulae for the calculation of the theoretical curve of growth are summarized as follows:

If the value of Nf is so small that $X_0 < 1$, then

$$\frac{W}{\lambda}\frac{c}{v} \sim \sqrt{\pi} X_0 \left(1 - \frac{X_0}{\sqrt{2}} + \frac{X_0}{\sqrt{3}} \ldots .\right). \tag{3}$$

If $X_0 > 1$, but not so great that wing damping must be considered, then

$$\frac{W}{\lambda}\frac{c}{v} \sim 2[\ln X_0]^{1/2}, \tag{4}$$

while finally, if $X_0 >> 1$,

$$\frac{W}{\lambda}\frac{c}{v} \sim \frac{\pi^{1/4}}{2}\left(\frac{c}{v} X_0 \frac{\Gamma}{\nu}\right)^{1/2}, \tag{5}$$

where Γ is the quantum mechanical damping constant and c, λ, π, and ν have their usual meanings. If there is no turbulence, v is simply the most probable kinetic velocity of the atoms. Otherwise, we must use for v the turbulent velocity, as Struve and his collaborators have shown.

Figure 1 displays the curve of growth for *Fe* II. Ordinates are W/λ, abscissae are log X_0. The zero point of the empirical log X_0-scale depends on the relative number of *Fe* II ions above unit areas of the photosphere of the sun and Deneb. Accordingly, one may shift the empirical curve of growth horizontally. Now the values of c/v determine

[8] *Mem. Commonwealth Solar Obs., Canberra, Australia*, **1**, No. 5, 1934.

the position and partly also the shape of the theoretical curve. The assumption, $v \sim 2.3 \times 10^5$ cm/sec, corresponding to a kinetic temperature of about 17,000°, best fits the observations of *Fe* II. Manifestly, the lack of observations of weak lines precludes an estimate of log X_0 and the damping constant. Evidently, most of the *Fe* II lines fall in the radiation-damping portion of the curve of growth, and the turbulent velocities are not great.

The lines of *Cr* II (filled circles) and *Ti* II (open circles), plotted in Figure 2, do not fall on the curve of growth determined by *Fe* II. If we fit them to the curve of growth, we must assume turbulent velocities of the order of 10 or 12 km/sec. A change of excitation temperature cannot remove this disparity, because most of the lines have very nearly the same excitation potentials for their lower levels.

Struve and Elvey found a curve of growth very similar to the one I have obtained for *Fe* II. The indicated degree of turbulence is small for this atom. The reason for the disparity between the *Ti* II–*Cr* II curves, on the one hand, and the *Fe* II curve, on the other, is not clear. Offhand, it would indicate violent turbulence of the *Ti* II and *Cr* II ions and little turbulence of the *Fe* II ions. Such an explanation seems unlikely, as it would require stratification of the *Fe* II atoms in a nonturbulent layer separated from other metals. More likely the difficulty lies in the elementary nature of the curve-of-growth theory. As developed at present, this theory does not take into account interlocking or the possibility of incipient emission partly filling the absorption lines. The line $H\alpha$ shows a red emission component, and it is entirely possible that other lines may have emission components, overpowered by stronger absorption components.

I am indebted to the staff of the Lick Observatory for making available to me their plates of α Cygni. The equivalent widths were measured there in 1937 in connection with a search for possible line-intensity variations with radial-velocity changes.

HARVARD COLLEGE OBSERVATORY
October 18, 1941

ON THE LIMB DARKENING OF THE SUN

JULIUS ASHKIN, JOHN E. NAFE,[1] AND JEROME ROTHSTEIN

ABSTRACT

It is shown that the agreement between the limb darkening, computed in second approximation using the Schwarzschild-Milne integral equation, and the observed limb darkening in the integrated light of the sun is substantially improved by taking account of the blanketing effect.

According to Milne, the blanketing effect of the reversing layer may be taken into account by introducing an ingoing radiation $I^-(\theta)$ at the surface of the star ($\tau = 0$). The inward flux πF^- thus produced is taken to be equal to a fraction η of the outgoing flux πF^+ at the surface. Hence (with $F = F^+ - F^-$),

$$F^- = \eta F^+ = \frac{\eta}{1 - \eta} F .$$

For the angular distribution of $I^-(\theta)$, two alternative assumptions were made:
(*a*) the re-emission by the reversing layer is isotropic; i.e., $I^-(\theta) = \text{const}$. The above condition then gives

$$a) \quad I^-(\theta) = \frac{\eta}{1 - \eta} F ;$$

(*b*) the re-emission has in the first approximation the same angular dependence as the incident radiation. This leads with the above condition to[2]

$$b) \quad I^-(\theta) = \eta I_1(0, \pi - \theta) = \eta \cdot \tfrac{1}{2} F \left(\frac{1 + \eta}{1 - \eta} - \tfrac{3}{2} \cos \theta \right) .$$

The presence of ingoing radiation at $\tau = 0$ makes necessary a change in the formula (28, 7), giving the ingoing radiation at optical depth τ. This becomes

$$I(\tau, \theta) = - \int_0^\tau J(x) e^{-(x-\tau) \sec \theta} dx \sec \theta + I^-(\theta) e^{\tau \sec \theta} .$$

Formula (28, 6) for the outgoing intensity obviously remains unchanged.

Introducing the above expressions for $I^-(\theta)$ and integrating $I(\tau, \theta)$ over all directions we obtain

$$a) \quad J(\tau) = \frac{1}{2} \int_0^\infty J(x) K(|x - \tau|) dx + \tfrac{1}{2} F \frac{\eta}{1 - \eta} K_2(\tau) ,$$

$$b) \quad J(\tau) = \frac{1}{2} \int_0^\infty J(x) K(|x - \tau|) dx + \tfrac{1}{4} F \eta \left[\frac{1 + \eta}{1 - \eta} K_2(\tau) + \tfrac{3}{2} K_3(\tau) \right] ,$$

[1] Now ensign in the United States Navy at Annapolis. The opinions or assertions contained herein are the private ones of the writers and are not to be construed as official or reflecting the views of the Navy Department or the naval service at large.

[2] Unsöld, *Physik der Sternatmosphären*, eq. (32, 9); all further references will be to this book.

where the $K_n(\tau)$ are the integral exponential functions.[3] These equations are the modifications of the Schwarzschild-Milne integral equation (30, 4), appropriate to the boundary conditions (*a*) and (*b*).

By introducing $J_1(\tau) = \frac{1}{2}F([1+\eta/1-\eta] + \frac{3}{2}\tau)$ as a first approximation to J under the integral sign, a second approximation to the emissivity (corresponding to equation [30, 32]) is obtained:

$$a)\quad J_2(\tau) = \tfrac{1}{2}F\left\{\frac{1+\eta}{1-\eta}\left[1 - \tfrac{1}{2}K_2(\tau)\right] + \tfrac{3}{2}\left[\tau + \tfrac{1}{2}K_3(\tau)\right]\right\} + \tfrac{1}{2}F\,\frac{\eta}{1-\eta}\,K_2(\tau)\,,$$

$$b)\quad J_2(\tau) = \tfrac{3}{4}F\left\{\tau + \frac{2}{3}\,\frac{1+\eta}{1-\eta} - \left(\frac{\tau-1}{4} + \frac{1}{3}\,\frac{1+\eta}{1-\eta}\right)e^{-\tau} + \frac{\tau}{4}\left(\tau + \frac{4}{3}\,\frac{1+\eta}{1-\eta}\right)K(\tau)\right\}$$
$$+ \tfrac{1}{4}F\eta\left\{\frac{1+\eta}{1-\eta}\,K_2(\tau) + \tfrac{3}{2}K_3(\tau)\right\}.$$

The second approximation for the intensity of the outgoing radiation at the surface is obtained by inserting $J_2(\tau)$ into the integral relationship (28, 8). The result is (cf. eq. [30, 34]).

$$a)\quad I_2(0, \theta) = \tfrac{1}{2}F\left\{\frac{1+\eta}{1-\eta} - \tfrac{1}{8} + \tfrac{3}{4}\cos\theta + (\tfrac{1}{2}\cos\theta + \tfrac{3}{4}\cos^2\theta)\,ln\,(1 + \sec\theta)\right\},$$

$$b)\quad I_2(0, \theta) = \tfrac{1}{2}F\left\{\frac{(7+\eta)(1+\eta)}{8(1-\eta)} + \tfrac{3}{4}(1-\eta)\cos\theta\right.$$
$$\left. + (1+\eta)(\tfrac{1}{2}\cos\theta + \tfrac{3}{4}\cos^2\theta)\,ln\,(1+\sec\theta)\right\}.$$

In the following table we have listed under α the limb darkening $I(0, \theta)/I(0, 0)$ computed from equations (30, 34) (second approximation without blanketing), under β that

TABLE 1

Cos θ	1.000	0.916	0.835	0.760	0.661	0.565	0.484	0.392	0.312
α, $\eta = 0$	1.000	0.950	0.900	0.855	0.794	0.736	0.684	0.628	0.577
β	1.000	.953	.909	.867	.813	.760	.715	.664	.620
γ (*a*)	1.000	.953	.907	.866	.810	.756	.708	.657	.611
γ (*b*)	1.000	.952	.906	.865	.809	.755	.707	.656	.609
Abbott	1.000	0.955	0.912	0.871	0.822	0.769	0.722	0.665	0.612

from equations (32, 10) (first approximation with blanketing) and under γ that from the above equations (second approximation with blanketing). Milne's value, $\eta = 0.097$, was taken. The last line gives the observations of Abbott (see Unsöld's Table 5).

It will be seen that there is practically no difference in the results for (*a*) and (*b*). Mulders' value of 0.083 for η would have lowered the results by about 0.003.

We wish to thank Dr. Martin Schwarzschild for suggesting this problem.

COLUMBIA UNIVERSITY
October 1941

[3] See Unsöld, Appen. B.

ABSOLUTE *f*-VALUES FOR LINES OF *Fe* I*

ROBERT B. KING

ABSTRACT

Absolute *f*-values have been measured by the method of *total absorption* for 12 lines in 2 multiplets, $a^5D-z^5F^\circ$ and $a^5D-z^5D^\circ$, from the ground state of *Fe* I. The method has been described in a previous paper on *f*-values for *Cd* and *Cu* lines. The *f*-values for the *Fe* I lines measured are in the neighborhood of 0.01. A factor, 1.85×10^{-4}, is derived by which to multiply the relative *f*-values for *Fe* I published earlier, to place them on an absolute scale.

Relative *f*-values for 115 lines arising from the three low terms of *Fe* I, determined by the method of *total absorption*, have been published.[1] The graphite-tube electric furnace used to produce the absorbing vapor did not permit precise knowledge of the absolute number of atoms involved and the consequent determination of absolute *f*-values. To overcome this difficulty a wire-wound vacuum furnace was constructed, in which the vapor of the metal to be studied can be heated in a quartz tube to temperatures over 1300° C.[2] The temperature, measured with a platinum, platinum-rhodium (10 per cent) thermocouple calibrated by the Bureau of Standards, can be held constant to about 1° C during an exposure. With this furnace and with a tungsten lamp as the source of the continuum, measurements were made by the method of total absorption of the absolute *f*-values of the *Cd* I line λ 3261 and the *Cu* I lines λ 3247 and λ 3274.[2] The satisfactory agreement between the *f*-value for the *Cd* line and the values obtained by earlier investigators by different methods indicated that the method is capable of yielding reliable results. A detailed description of the furnace and the method used in the present investigation on lines of *Fe* I was given in the paper on *Cd* and *Cu*.

Since the measurement of absolute *f*-values by the method of total absorption demands knowledge of the number of atoms in the absorbing vapor, reliable vapor-pressure data must be available for the temperature range used. For iron, fortunately, these are available. Measurements of the rate of evaporation of iron at four temperatures between 1270° and 1580° K were made by H. A. Jones, I. Langmuir, and G. M. J. Mackay.[3] From these measurements, vapor pressures may be calculated by Langmuir's formula:[4, 5]

$$\log P = \log m - \tfrac{1}{2}\log M + \tfrac{1}{2}\log T - 1.647\,, \qquad (1)$$

where P is expressed in atmospheres, m is the rate of evaporation, M the molecular weight, and T the absolute temperature. The validity of this formula, at least for the metals which have been investigated, has been amply confirmed by the work of Langmuir and his colleagues and that of Marshall, Dornte, and Norton.[5] The concentration, i.e., the number of atoms per cubic centimeter in the vapor, can then be calculated from the formula

$$n_0 = \frac{0.973 \times 10^{19} \times 760 \times P}{T}\,. \qquad (2)$$

* *Contributions from the Mount Wilson Observatory, Carnegie Institution of Washington*, No. 655.

[1] R. B. King and A. S. King, *Mt. W. Contr.*, No. 581; *Ap. J.*, **87**, 24, 1938.

[2] R. B. King and D. C. Stockbarger, *Mt. W. Contr.*, No. 629; *Ap. J.*, **91**, 488, 1940.

[3] *Phys. Rev.*, **30**, 201, 1927.

[4] I. Langmuir, *Phys. Rev.*, **2**, 329, 1913.

[5] A. L. Marshall, R. W. Dornte, and F. J. Norton, *J. Amer. Chem. Soc.*, **59**, 1161, 1937.

K. K. Kelley, in deriving the free energy of vaporization of iron, used a smoothed result from the data of Jones, Langmuir, and Mackay in obtaining the value[6]

$$R \ln P = \frac{\Delta F^\circ}{T} = 33.85 \text{ at } 1400^\circ \text{ K}, \qquad (3)$$

where ΔF° is the free energy of vaporization and R the gas constant. He gives equations for ΔF° as a function of T for iron in different forms, from which a vapor-pressure curve can be computed with the aid of equation (3). Marshall, Dornte, and Norton measured the rates of evaporation of iron at twelve temperatures between 1317° and 1579° K and give values of the vapor pressure computed by equation (1).[5] The data from these three investigations are shown in Figure 1, where the concentration, log n_0, is plotted as

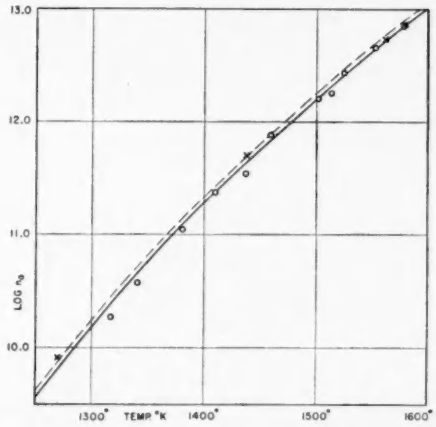

FIG. 1.—Concentration of *Fe* atoms as a function of temperature

a function of the absolute temperature. The crosses represent the points measured by Jones, Langmuir, and Mackay and the circles those of Marshall, Dornte, and Norton. The dotted curve is computed from Kelley's equation for free energy. It will be seen that there is excellent agreement between the two sets of observational data, particularly at the upper end of the temperature range covered, which happens to be that used in the present work. Marshall, Dornte, and Norton state that the deviations between the two sets of data are within the error of the temperature determinations. The full curve in Figure 1, drawn by the author through the points of both sets of experimental data parallel to the curve of Kelley, has been used in deriving values of log n_0 for the present work. It yields a value, log $n_0 = 12.546$ at 1540° K, which is about at the middle of the temperature range covered in measuring the *f*-values for iron lines.

The iron used in this experiment was hydrogen-purified carbonyl iron, obtained through the kindness of Dr. Gerhard Derge of the Metals Research Laboratory of the Carnegie Institute of Technology. This iron is from the lot described by Wells, Ackley, and Mehl,[7] and in the opinion of Dr. Derge is "the purest iron obtainable in appreciable quantities which has yet been described in the literature."[8] A sheet of this iron, carefully cleaned, was placed in a quartz absorption cell. The cell was then baked out with hydrogen, baked again at high temperature while on the pumps for degassing, and finally sealed off. Three cells, each about 25 mm in diameter, ranging in length from 34.5 to 39.5 mm, were used in the course of the experiment. Two contained pieces of the original

[6] *U.S. Bureau of Mines Bull.*, No. 383, 1935.

[7] *Trans. Amer. Soc. Met.*, **24**, 46, 1936.

[8] Personal communication.

sheet, and the third was charged with filings. No differences between the results from the three cells were detected.

The observations were made in the temperature range 1494°–1581° K. Temperatures were held constant to about 1°. As in the work on *Cd* and *Cu*, all photographs were made in the second order of the 15-foot concave-grating spectrograph. Eastman IV-O plates were used, calibrated by a tungsten lamp and step-slit. Exposure times were 10–20 minutes.

TABLE 1

ABSOLUTE *f*-VALUES FOR LINES OF *Fe I*

T	$a^5D-z^5F^o$							$a^5D-z^5D^o$				
	3705.6	3719.9	3722.6	3737.1	3745.6	3745.9	3748.3	3824.4	3856.4	3859.9	3878.6	3886.3
1494° K	.....	o.0083	.....	.....	.....	.....	.....	.....	.....	o.0059	.....	.....
1513	.....	.0168	.....	.....	.....	.....	.....	.....	.....	.0100	.....	.....
1513	.....	.0130	.....	o.0107	.....	.....	.....	.....	.....	.0058	.....	.....
1521	.....	.0135	.....	.0142	o.0144	.....	.....	.....	.....	.0095	.....	o.0048
1521	.....	.0114	.....	.0142	.0133	.....	.....	.....	.....	.0084	.....	.0049
1525	.....	.0094	.....	.....	.....	.....	.....	.....	.....	.0075	.....	.....
1529	.....	.0134	.....	.0136	.0105	.....	.....	.....	.....	.0063	.....	.0045
1538	.....	.0158	.....	.0129	.0118	.....	o.0183	o.0025	.....	.0069	.....	.0039
1538	.....	.0140	.....	.0123	.0129	.....	.0129	.0019	.....	.0076	.....	.0060
1547	.....	.0127	.....	.0135	.0144	.....	.....	.0023	.....	.0072	.....	.0052
1549	.....	.0149	.....	.0133	.0098	.....	.0164	.0022	.....	.0084	.....	.0036
1553	.....	.0080	.....	.0118	.....	.....	.....	.....	.....	.0041	.....	.....
1553	.....	.0094	.....	.0103	.....	.....	.....	.....	.....	.0070	.....	.....
1553	.....	.0139	.....	.0138	.0085	.....	.0111	.0021	o.0024	.0073	.....	.0053
1553	.....	.0142	.....	.0116	.0104	.....	.0133	.0027	.0029	.0078	.....	.0043
1559	o.0018	.0129	.....	.0110	.0105	.....	.0082	.0012	.0030	.0063	.....	.0034
1559	.0021	.0130	.....	.0119	.0104	.....	.0095	.0018	.0035	.0073	.....	.0046
1575	.....	.0118	.....	.0112	.0097	.....	.0116	.0017	.0037	.0078	.....	.0043
1575	.....	.0115	.....	.0126	.0140	.....	.0135	.0018	.0028	.0068	.....	.0037
1579	.....	.0101	.....	.0109	.0113	.....	.....	.0021	.....	.0062	.....	.0027
1580	.....	.0131	.....	.0121	.....	.....	.....	.0016	.....	.0089	.....	.0028
1581	.0024	.0144	o.0030	.0129	.0097	o.0134	.0113	.0018	.0028	.0075	o.0032	.0057
1581	.0016	.0172	.0034	.0165	.0141	.0180	.0092	.0014	.0025	.0084	.0032	.0041
1581	.0026	.0170	.0032	.0138	.0124	.0109	.0118	.0022	.0030	.0089	.0023	.0043
1581	o.0022	o.0157	o.0037	o.0145	o.0129	o.0141	o.0107	o.0018	o.0029	o.0080	o.0030	o.0046
Mean	o.0021	o.0130	o.0033	o.0127	o.0117	o.014	o.0121	o.00194	o.0030	o.0074	o.0029	o.0044

Following measurement of equivalent widths on the microphotometer tracings, the corresponding values of the total number of atoms (*nfl*) active in forming each line were read off the linear portion of a curve of growth computed for λ 3800 and $T = 1525°$ K, the $1/\lambda^2$ wave-length correction being applied to each value. The 12 lines observed lie between λ 3705 and λ 3886 and belong to two multiplets, $a^5D-z^5F^o$ and $a^5D-z^5D^o$, both arising from the ground state. The a^5D term has five sublevels, with inner quantum numbers 4–0 and a total spread of 978 cm^{-1}. The quantity n, the number of atoms per cubic centimeter in a given sublevel able to absorb a spectrum line, is determined by a Boltzmann distribution factor giving the fraction of the total number of neutral atoms per cubic centimeter, n_o, which populate the sublevel in question:

$$n = n_o \frac{g_i e^{-(E_i/kT)}}{\Sigma g_s e^{-(E_s/kT)}}, \tag{4}$$

where g_i is the statistical weight $(2j + 1)$ and E_i the excitation energy of the state measured from the ground state a^5D_4. The summation is taken over all states of the

atom. For iron, however, the contribution to the summation of the states above the a^5D is negligible at the relatively low temperatures used in this work. Also, over the temperature range covered by the measurements (1494°–1581° K), the change in the distribution factor for a given sublevel is very small. Hence a single set of factors was adopted for $T = 1540°$ K, taking into the summation only members of the a^5D term. These factors multiplied by the value of n_0 for the temperature at which the observation was made give values of n. Dividing the quantity nfl by the appropriate value of n and by l, the length of the quartz absorption cell, yields f, the absolute f-value for the line.

The results of the measures for 25 spectra are given in Table 1. The first column gives the absolute temperature at which the exposures were made. The succeeding columns contain the measured f-values for each line. At the lower temperatures only the strongest lines (largest gf-values) appear. At the highest temperature all 12 lines appear on the linear portion of the curve of growth, although the strongest are nearing the transition

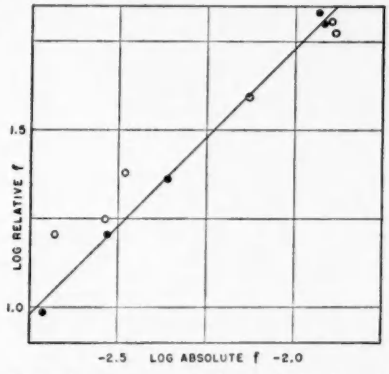

FIG. 2.—Relation between relative and absolute f-values

region. The equivalent widths varied from about 0.001 A for the faintest lines observable to 0.016 A for λ 3719 at 1581°. No systematic trends with temperature are apparent from the table, indicating that the slope of the vapor-pressure curve used and the increase in observed equivalent width with increasing temperature are in agreement.

These absolute f-values enable us to place the relative f-values, published on an arbitrary scale,[1] upon an absolute scale. Figure 2 is a plot of the logarithms of the relative f-values listed in the fifth column of Table 1 of the earlier paper[1] against the logarithms of the mean absolute f-values determined by the present investigation. The lines indicated by dots, judged to be most accurately measured in both sets of data, have relatively high weight. A line at 45° to the axes drawn through these points determines the factor by which the relative f-values should be multiplied to put them on an absolute scale. The relation is

$$\text{Absolute } f = 1.85 \times 10^{-4} \times \text{relative } f .$$

Sources of error in the method were discussed in the paper on *Cd* and *Cu*.[2] The critical points in the problem are two, namely, the reliability of the vapor-pressure data and the precision of the observed furnace temperatures. The published vapor-pressure data for iron appear to be unusually consistent and reliable. Furnace temperatures, observed with a thermocouple and potentiometer of high precision, were checked occasionally by an optical pyrometer. These readings agreed within the uncertainty of the pyrometer (5°–10°). As usual in measurements of total absorptions of faint lines, the average deviation of a single measure from the mean value is of the order of 10 per cent.

CARNEGIE INSTITUTION OF WASHINGTON
MOUNT WILSON OBSERVATORY
August 1941

ABUNDANCE OF IRON IN THE SUN*

ROBERT B. KING

ABSTRACT

A value for the abundance of neutral iron atoms in the solar reversing layer is derived from strong lines of *Fe* I by utilizing the absolute *f*-values and the solar equivalent widths. A solar damping constant ten times the classical value and an excitation temperature of 4400° were assumed. The total number of neutral iron atoms per square centimeter is found to be 4.3×10^{18}. Possible causes for apparent systematic differences in the results for various lines are discussed.

The measurement of the absolute *f*-values for several lines of *Fe* I[1] and the determination of a factor placing the relative *f*-values published earlier[2] upon an absolute scale make possible a determination, from the solar equivalent widths of these lines, of the abundance of neutral iron in the solar reversing layer. Unfortunately, the laboratory *f*-values do not extend to faint, high-level lines of *Fe*, so that a determination of abundance from faint solar lines falling on the linear portion of the curve of growth, which is unaffected by damping, is not yet possible. Hence the strong lines of neutral iron, of which there is a considerable number, have been used.

The general expression for the relation between the equivalent width and the concentration of absorbing atoms for a line formed in a stellar atmosphere by pure damping broadening[3] is

$$\frac{1}{R_c} \cdot \frac{A_\lambda}{2\Delta\lambda_D} = \frac{\pi}{2}\sqrt{\frac{aC}{2\sqrt{\pi}}}, \tag{1}$$

where A_λ is the equivalent width and $\Delta\lambda_D$ the Doppler breadth in angstrom units; $a = \gamma/\Delta\omega_D$, the damping constant divided by the Doppler breadth in frequency units; R_c the depth of the center of strong lines; and

$$C = \frac{2\pi^{3/2}e^2}{mc} \cdot \frac{1}{R_c} \cdot \frac{NHf}{\Delta\omega_D}.$$

Here NH is the number of atoms per square centimeter in the atmosphere which are in the low energy state involved in the transition, and f is the oscillator strength of the line. Equation (1) holds for values of $(1/R_c) \cdot (A_\lambda/2\Delta\lambda_D) > 7$, which, for the solar atmosphere, means lines at λ 4500 whose equivalent widths are about 0.3 A or larger.

For our purpose, equation (1) may be written in the form

$$NHf = \text{const} \cdot \frac{1}{R_c} \cdot \frac{1}{\lambda^2\gamma} \cdot \left(\frac{A_\lambda}{\lambda}\right)^2. \tag{2}$$

If this equation is to be used to determine values of NHf from measured equivalent widths, it is necessary to adopt values for R_c and γ. Recent measurements of the depth

* *Contributions from the Mount Wilson Observatory, Carnegie Institution of Washington*, No. 656.

[1] R. B. King, *Mt. W. Contr.*, No. 655; *Ap. J.*, **95**, 78, 1942.

[2] R. B. King and A. S. King, *Mt. W. Contr.*, No. 581; *Ap. J.*, **87**, 24, 1938.

[3] A. Unsöld, *Physik der Sternatmosphären*, Springer, 1938.

of strong Fraunhofer lines of neutral metallic atoms[4] show that the true residual intensities are usually only a few per cent. Therefore, for the present purpose, we may adopt a value $R_c = 0.95$, which will probably not be in error by an appreciable amount. The value for the damping constant, γ, is more difficult to decide upon. Unfortunately, with the data at hand, an independent determination of γ is impossible, since the laboratory f-values do not include *Fe* lines on the linear portion of the solar curve of growth. However, the work of Minnaert and Mulders,[5] of C. W. Allen,[6] and of Menzel, Baker, and Goldberg,[7] involving the construction of solar curves of growth from equivalent widths and theoretical multiplet intensities, indicates that a mean value of γ ten times the classical value is of the right order of magnitude for lines of *Fe*. Allen's measurements, with the aid of a curve of growth, for high-level iron lines,[8] also show that those lines which are not influenced by Stark effect have a damping constant of about this value. There is some evidence[9] that the solar damping constants for certain multiplets of iron differ by rather large amounts, but for a first approximation it is necessary to assume a single damping constant for all lines. Therefore, a value equal to ten times the classical constant has been adopted. Thus

$$\gamma = 10 \cdot \frac{8\pi^2 e^2}{3mc\lambda^2} .$$

Substitution of the adopted values of R_c and γ in equation (2) leads to the simple form

$$NHf = 6.45 \times 10^{22} \left(\frac{A_\lambda}{\lambda}\right)^2 . \tag{3}$$

NH is the number of atoms per square centimeter in the low term involved in the transition. To reduce values of NH to N_oH, the total number of neutral iron atoms per square centimeter, we must apply a Boltzmann distribution factor to NH:

$$N_oH = NH \frac{\Sigma g_s e^{-(E_s/kT)}}{g_i e^{-(E_i/kT)}} = NH \cdot B , \tag{4}$$

where g_i is the statistical weight of the lower energy-level, E_i its excitation energy measured from the ground state, and T the excitation temperature of the reversing layer. The summation in the numerator, called the partition function, is taken over all states of the neutral atom. A value for the excitation temperature of 4400° [7,10] was adopted for computing the Boltzmann factors. Contributions to the partition function of states above a^3F have been neglected (a^3F itself contributes only 1.4 per cent). With the aid of equations (3) and (4) the value of N_oH can be obtained from any *Fe* line for which measures of equivalent width and absolute f-values are available, provided the former are large enough for equation (1) to apply.

Allen's tables of equivalent widths[6,11] have been used, supplemented by my measurements in the *Utrecht Photometric Atlas of the Solar Spectrum*[12] of several strong lines beyond the violet limit of Allen's list. Allen's tables include 41 *Fe* lines, apparently free from serious blends, between λ 4045 and λ 5455, for which we have laboratory f-values.

[4] A. D. Thackeray, *M.N.*, **95**, 293, 1935; R. O. Redman, *M.N.*, **97**, 552, 1937; C. W. Allen, *Mt. W. Contr.*, No. 567, *Ap. J.*, **85**, 165, 1937; C. D. Shane, *Lick Obs. Bull.*, **19**, 119 (No. 507), 1941.

[5] *Zs. f. Ap.*, **2**, 165, 1931.

[6] *Mem. Commonwealth Solar Obs.*, **1** (No. 5), 1934.

[7] *Ap. J.*, **87**, 81, 1938.

[8] *M.N.*, **100**, 4, 1939.

[9] Unsöld, *op. cit.*, p. 277.

[10] R. B. King, *Ap. J.*, **87**, 40, 1938.

[11] *Mem. Commonwealth Solar Obs.*, **2** (No. 6), 1938.

[12] Minnaert, Mulders, and Houtgast, Amsterdam, 1940.

The author has measured the equivalent widths, in the *Atlas*, of 13 of the lines measured by Allen. The average difference, without regard to sign, is 14 per cent. Sixteen of Allen's lines and 7 of the author's fall on the square-root portion of the curve of growth, to which equation (1) applies. Table 1 lists these lines and the data used in calculating the values of N_0H from the equivalent widths. The third column contains the equivalent widths of the lines in angstrom units. Those marked with an asterisk are the author's measures; the others are Allen's. The fourth column gives logarithms of NHf derived

TABLE 1

NUMBER OF NEUTRAL IRON ATOMS PER SQUARE CENTIMETER IN THE SOLAR REVERSING LAYER GIVEN BY STRONG LINES OF *Fe* I

λ	Multiplet	A_λ	log NHf	log f†	log B	N_0H
3679.92	$a^5D-z^5F^o$ 4–4	0.483*	15.048	7.100	0.432	2.4×10^{18}
3719.95	4–5	1.874*	16.215	8.114	0.432	3.4
3758.25	$a^5F-y^5F^o$ 3–3	1.204*	15.820	8.869	1.670	4.2
3763.81	2–2	0.940*	15.605	8.824	1.845	4.2
3886.30	$a^5D-z^5D^o$ 3–3	1.015*	15.642	7.644	0.624	4.2
3895.67	1–0	0.498*	15.023	7.497	1.061	3.9
3899.72	2–2	0.543*	15.097	7.414	0.811	3.1
4045.83	$a^3F-y^3F^o$ 4–4	1.200	15.755	9.094	2.160	6.6
4063.61	3–3	0.860	15.460	9.053	2.348	5.7
4071.75	2–2	0.720	15.306	9.150	2.552	5.1
4132.07	2–3	0.380	14.736	8.610	2.552	4.8
4143.88	3–4	0.440	14.862	8.568	2.348	4.4
4202.04	$a^3F-z^3G^o$ 4–4	0.380	14.723	8.262	2.160	4.2
4250.13	3–3	0.350	14.641	8.380	2.348	4.1
4271.78	4–5	0.750	15.297	8.700	2.160	5.7
4307.91	3–4	0.697	15.228	8.940	2.348	4.3
4325.78	2–3	0.675	15.196	9.150	2.552	4.0
4383.56	$a^3F-z^5G^o$ 4–5	1.07	15.584	9.080	2.160	4.6
4404.76	3–4	0.749	15.270	8.900	2.348	5.2
4415.14	2–3	0.400	14.724	8.568	2.552	5.1
5227.19	$a^3F-z^3D^o$ 3–2	0.314	14.366	7.785(?)	2.348	8.5
5269.55	$a^5F-z^5D^o$ 5–4	0.338	14.424	7.442	1.366	2.2
5328.05	4–3	0.341	14.422	7.380	1.507	3.5

* Equivalent widths measured by author in *Utrecht Atlas*.

† Ten is to be subtracted from the characteristic of each logarithm in this column.

by equation (3). The fifth column lists logarithms of the absolute f-values of the lines. These were obtained by multiplying the relative f-values[2] by the factor 1.85×10^{-4} derived in the preceding paper.[1] In the sixth column are logarithms of the Boltzmann factor B for each line for $T = 4400°$. The last column gives the values of N_0H, the total number of neutral iron atoms per square centimeter.

Inspection of the values in the last column of Table 1 shows strong suggestions of systematic differences in the values of N_0H from various multiplets and from lines arising from various low terms. If we assume that these differences are not due to systematic errors in either the laboratory or the solar data, two possible explanations remain, namely, the value of the excitation temperature used in the reduction is incorrect, or the solar

damping constant differs for various lines. Unfortunately, it is impossible, with the present data, to distinguish definitely between these two effects. The situation is shown more clearly by Figure 1, which makes use of the strong lines listed in Table 1 and, in addition, 23 fainter lines for which solar equivalent widths and laboratory f-values are available. Here the solar equivalent widths of the lines are plotted against the value of the concentration of absorbing atoms for each line. The latter values were obtained by adopting the mean value of N_oH given by the lines listed in Table 1 (excluding λ 5227, for which the laboratory f-value is relatively uncertain) and applying the Boltzmann factors for $T = 4400°$ to obtain values of NH. The full line in the figure is a theoretical curve of growth[13] for a value of γ ten times the classical value, and a kinetic tem-

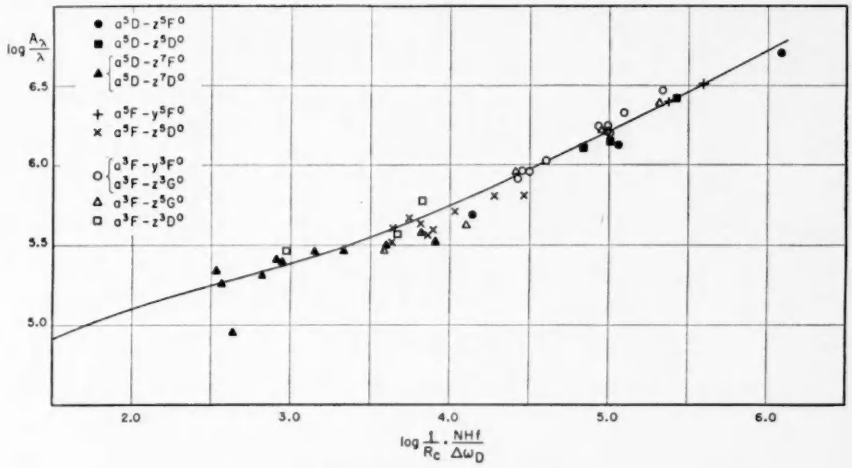

FIG. 1.—Solar curve of growth for lines of *Fe* I

perature of 5700°. Since the lines cover a considerable range in wave length the points have been adjusted to a value of $a = \gamma/\Delta\omega_D$ corresponding to λ 4500. To simplify the diagram, three multiplets represented by single lines have been omitted from the figure; and lines of two multiplets arising from the same low term, which fall on the same portion of the curve of growth and do not appear to have systematic differences, have in two instances been given the same symbol.

The scatter of the points along the square-root portion of the curve is considerably reduced if an excitation temperature of 4800° instead of 4400° is used in computing the Boltzmann factors. This has the effect of shifting the points for lines from the ground state a^5D toward the left and those from a^3F toward the right. It does not improve the fit of multiplet $a^5F - z^5D$, however; and it results in raising the weaker lines, which fall on the transition portion of the curve of growth, considerably above the theoretical curve. The latter effect argues against the validity of this procedure. The transition portion of the curve of growth is particularly sensitive to kinetic temperature as well as to R_e, the central intensity. Even with $R_e = 1.0$, the positions of the majority of the points fit a curve of growth computed for a kinetic temperature of about 7500°, which is considerably higher than the values recently determined from equivalent widths and the curve of growth (5400°)[14] and from interferometer measures of line profiles (5700°).[15]

[13] Unsöld, *op. cit.*, Fig. 85.

[14] P. J. Rubinstein, *Ap. J.*, **92**, 114, 1940.

[15] Shane, *op. cit.*, **19**, 119.

The term kinetic temperature, as commonly used in this connection, means the temperature indicated by the Doppler width of absorption lines, caused by motion of the atoms in the line of sight. In a stellar atmosphere this motion may consist of two components, motion of individual atoms in a heated gas (ordinarily called kinetic) and large-scale motions of portions of the gas (commonly called turbulence). It is of interest to note that all recent determinations yield values for the solar kinetic temperature which are higher than those for excitation temperature. Much greater differences between these two temperatures have been found from spectra of late-type giant stars.[16] These have been ascribed to turbulence in the atmospheres. If the same interpretation applies to the sun, the difference between the kinetic temperature, 5700°, and the excitation temperature, 4400°, would indicate a turbulent velocity of 0.15 km/sec for the level in the atmosphere where the absorption lines of neutral metals are formed. It should be pointed out, however, that most of the lines involved in the present work lie in a crowded portion of the solar spectrum. The effect of blends, on weaker lines particularly, is usually to increase the value of the measured equivalent width. It is entirely possible that some of the apparent systematic differences noted here, as well as accidental differences, are due to this cause. In addition, there is the complication of possible variation with wave length of a number of factors, e.g., damping constant, opacity, solar equivalent width; but the data are not extensive enough to show any clear indication of this.

If we accept the suggestions shown by Figure 1 at face value and assume 4400° to be the correct value for the excitation temperature, it appears that the damping constants for the multiplets $a^3F-y^3F^o$, $a^3F-z^3G^o$ are relatively high, while those for $a^5D-z^5F^o$, $a^5D-z^5D^o$, $a^5F-z^5D^o$, $a^5D-z^7F^o$, and probably $a^5D-z^7D^o$ are relatively low.

In view of these considerations it seems best to adopt a provisional value for the abundance of iron derived with an excitation temperature of 4400° and a mean damping constant of ten times the classical value. The mean value given by the data in Table 1 (excluding λ 5227), for the number of neutral iron atoms per square centimeter in the solar reversing layer, is

$$N_0 H = 4.3 \times 10^{18} .$$

The value of $N_0 H$ derived with an excitation temperature of 4800° is about 20 per cent less.

The author takes pleasure in thanking Professor Henry Norris Russell for his kindness in reading and criticizing the manuscript.

CARNEGIE INSTITUTION OF WASHINGTON
MOUNT WILSON OBSERVATORY
November 1941

NOTE BY R. MINKOWSKI AND R. B. KING

Results in the preceding paper raise the question whether the differences of the curves of growth for various multiplets are due to differences of the damping constants. It would be possible to compute the natural widths of the lines if the measures of *f*-values were complete. This is not yet true; but for certain terms, e.g., z^5F^o and y^5F^o, the measures are sufficient to permit a definite statement. The large values of the damping constant indicated by the curve of growth can certainly not be ascribed to the natural widths. The natural damping constants for certain lines might reach the order of magnitude of the classical value, but they will generally be much

[16] L. Spitzer, Jr., *Mt. W. Contr.* No. 619, *Ap. J.*, **90**, 494, 1939; P. Wellman, *Veröff. Universitätssternwarte Berlin-Babelsberg*, **12**, Heft 4, 1939; O. C. Wilson, *Pub. A.S.P.*, **53**, 228, 1941.

smaller. The values should spread over a considerable range, possibly as large as 1–1000. The observed range of damping constants is much smaller.

The damping constants for the iron lines, as for many other lines,[1] are evidently influenced by pressure-broadening. However, no systematic differences similar to those found for the solar lines occur when the curve of growth is plotted for lines broadened by pressure in the furnace at atmospheric pressure and at 2890° K. The order of magnitude of the pressure-broadening in the furnace suggests that under solar conditions the natural width is not quite negligible. The scatter in the points defining the curve of growth may then be due to the varying contributions of the natural widths to the damping constants. The lowest values for the damping constants would be expected for the multiplets $a^5D - z^7F^o$ and $a^5D - z^7D^o$. Whether the multiplet $a^3F - z^3D^o$ should have the largest damping constant cannot be decided at present, as the measures of *f*-values of lines with z^3D^o as upper term are quite incomplete. In conclusion it should be noted that the pressure-broadening in the sun by highly ionized gas will differ from that in the furnace by a practically neutral gas. But it seems unlikely that systematic differences too small to be noticeable in our laboratory experiments should, under solar conditions, become large enough to explain the observed scatter.

CARNEGIE INSTITUTION OF WASHINGTON
MOUNT WILSON OBSERVATORY
December 1941

[1] A. Unsöld, *Physik der Sternatmosphären*, p. 273.

THE EQUILIBRIUM AND STABILITY OF RING-SHAPED "BARRED SPIRALS"

GUNNAR RANDERS

ABSTRACT

A simple hydrodynamic model of the ring-shaped extragalactic nebulae is considered. It is shown that these nebulae are unstable in such a way that they will form mass condensations rotating with the ring. These mass condensations will grow and break up the ring. It follows that the ring-shaped nebulae, which are the only "spiral nebulae" one might possibly expect to represent a permanent stable configuration, are unstable and cannot represent any final pattern in the evolution of the spirals. The relation of the rings to other patterns of extragalactic nebulae is discussed.

I. INTRODUCTION AND CONCLUSIONS

Among the extragalactic nebulae classified by Hubble as barred spirals there exist a number of objects which appear as a circular ring with a more or less heavy central body. There are several reasons why a study of these nebulae is of interest. First, the ring-shaped nebulae are much simpler than any spiral pattern. A theoretical treatment is therefore considerably easier. Second, ring-like patterns seem to occur occasionally among spiral nebulae of practically all classifications, so that an investigation of the behavior of the rings may have some general interest. Finally, the ring pattern is the only pattern among spiral nebulae which may possibly represent stationary, stable conditions.

The most important question is, of course, whether the rings are stable. If they are stable, they may remain as rings indefinitely, and one might suspect that the rings represent the final pattern into which other types develop. If, on the other hand, they are unstable, they will break down sooner or later and then probably form other types which we observe.

In order to obtain a first, rough idea of the behavior of a rotating ring of "star gas," we shall in the present paper consider the simplest possible model. We shall study the purely hydrodynamical problem of a ring of ideal, incompressible fluid, rotating around a central body. It is obvious that in many respects this is an unsatisfactory model. However, it gives some indication of the behavior of the ring-type nebulae. In considering the stability of the liquid ring, it is obviously not permitted to draw general conclusions about the stability of the nebulae, since there are perturbations possible in a nebula which are not consistent with the liquid model. However, as long as only a certain type of perturbation is considered, the result may be applied also to the nebulae. If the model is unstable for a special perturbation, we can conclude that the nebular ring will also be so. The hydrodynamical problem treated in this paper has been treated in parts by earlier investigators, to which references are given.

We shall summarize the results and conclusions from the following analysis of the liquid ring, rotating with uniform velocity about a central body. As regards the equilibrium, there exist equilibrium configurations in which the cross-section of the ring is elliptic. For each distance from the center, there are possible two different cross-sections, one flat and one nearly circular. As we approach the central body, the two cross-sections become more and more alike and coincide at a certain distance, inside which there exists no equilibrium configuration. This minimum distance has probably no significance for the ring-shaped nebulae, because it is mainly a result of our assumption of uniform velocity of rotation. It only indicates a distance inside of which a ring must necessarily have a varying angular velocity to maintain equilibrium. As regards the

equilibrium of the central spheroidal body, there exist both an upper and a lower limit to the ellipticity, due to the attraction of the surrounding ring.

To answer the most important questions, about the stability, we apply different kinds of perturbations to the ring. A uniform expansion and contraction of the radius gives stable oscillations, as might be expected. Similarly, a deformation of the central circle of the ring—for example, an elongation—results in stable oscillations only. As regards stability against small changes in ellipticity of the cross-section, it turns out that the flat equilibrium configuration is unstable and will pass over to the configuration of nearly circular cross-section. This configuration is, however, also found to be unstable: one or more mass concentrations will form and grow until the ring is broken up. It is of interest to notice that it is essential for the mass condensations to follow the rotation of the ring if they are to cause instability. A mass condensation which is stationary in space will not be able to break up the ring, owing to the stabilizing effect of the central body. The ring is most unstable for the formation of one single mass condensation. However, most physically probable perturbations will lead to a symmetrical disturbance, so that condensations in two opposite points may be more frequent. We now must conclude that the ring-shaped nebulae are not stable and do not form any permanent configurations. A ring will sooner or later break up by the formation of one or two (or more) mass condensations, which rotate with the ring around the central body. The possible configurations resulting from the formation of mass condensations in the ring will not be discussed here. From simple general considerations, however, it is easily realized that, if some kind of spiral pattern results (which may or may not be so), then the spiral arms will trail behind in the rotation. This is because the material following the condensation point will be accelerated by the condensation and move outward from the central mass, while the mass in front is decelerated and moves inward. It is not probable that the spirals are usually formed in this way. However, the tendency toward instability by the formation of mass condensation is of interest for the formation of spiral patterns also from another angle. The view is now held by several investigators that the spiral arms are formed by condensations in already existing smooth nebulae rather than by ejection of material from a small nucleus. The tendency toward the formation of condensations in a ring is probably present also when the system consists of several concentric rings, or even when we consider a smooth nebula as composed of concentric rings. A beginning mass condensation may then be expected to induce similar condensations in neighboring rings, and the pattern will transplant itself through the whole system. This last effect has, of course, to be investigated by more appropriate models than the present one, but the results obtained by this rough approximation indicate that a closer investigation along this line will be worth while.

II. INTERNAL POTENTIAL OF A TOROID OF ELLIPTIC CROSS-SECTION

We shall in the following always assume that the diameter of the toroid is large compared to the diameter of its cross-section. As a first approximation, the gravitational force acting at the surface of and inside the toroid may then be replaced by the force at the surface and inside an infinite cylinder of the same cross-section and density. That this is correct is seen directly by the fact that, when the diameter of the toroid increases to infinity, the toroid degenerates into such a cylinder. This approximation was originally introduced by Laplace.[1] It is, however, not permissible to replace the *potential* of the toroid by the *potential* of the infinite cylinder, because the latter is infinite. Only the variable parts of the two internal potentials—the parts giving rise to the force—can be equated. The additive constant, depending upon the diameter of the toroid and its cross-section, must be determined separately. To do this we shall start with a toroid or circular cross-section.

[1] See Tisserand, *Traité de méchanique céleste*, **2**, 118, Paris, 1891.

Let the radius of the cross-section be R, and the radius of the central circle of the toroid, D. D is large as compared to R. The variable part of the internal potential of an infinite cylinder of circular cross-section is

$$V_1 = \pi\rho r^2 . \tag{1}$$

Here ρ is the (constant) density and r the distance from the axis. We assume units to be chosen so as to make the gravitational constant unity. Further, we know the asymptotic form of the potential of a circle of radius D, as we approach a point on the circle, the small distance from the circle being r,

$$V_2 = -2\sigma \log \frac{8D}{r} , \tag{2}$$

where σ is the mass density per unit length of the circular line.[2]

The complete internal potential of our toroid must, according to our approximation, have the form

$$V_i = \rho f(R, D) + \pi\rho r^2 . \tag{3}$$

The problem is now to determine the function $f(R, D)$. When $R/D \ll 1$, the potential at the surface must asymptotically become equal to the potential of a circle of radius D and density $\pi R^2\rho$ at a distance R. This potential is known by equation (2). We therefore have

$$\rho f(R, D) + \pi\rho R^2 = -2\pi R^2\rho \log \frac{8D}{R} \tag{4}$$

and

$$\rho f(R, D) = -2\pi R^2\rho \left\{ \log \frac{8D}{R} + \frac{1}{2} \right\} . \tag{5}$$

By equations (5) and (3) we obtain the internal potential of the toroid, when $R \ll D$,

$$V_i = -2\pi R^2\rho \left\{ \log \frac{8D}{R} + \frac{1}{2}\left(1 - \frac{r^2}{R^2}\right) \right\} . \tag{6}$$

We now want to pass over to a toroid of elliptical cross-section. Let the axes of the ellipse be a in the plane of the toroid, b perpendicularly to it. The variable part of the internal potential is again the same as that of an infinite elliptic cylinder of the same cross-section,

$$V_1' = \pi\rho(\alpha x^2 + \beta y^2) ; \qquad \alpha = \frac{2b}{a^2 + b^2} , \qquad \beta = \frac{2a}{a^2 + b^2} . \tag{7}$$

Here x and y are Cartesian co-ordinates in the directions of a and b, respectively, with origin in the center of the elliptical cross-section. The complete internal potential must have the form

$$V_i' = \rho f'(a, b, D) + \pi\rho(\alpha x^2 + \beta y^2) . \tag{8}$$

[2] See MacMillan, *Theory of the Potential*, p. 202, New York: McGraw-Hill, 1930.

When $a = b = R$, V_i' must reduce to V_i, or

$$V_{i_{a=b=R}}' = -2\pi\rho R^2\left\{\log\frac{8D}{R} + \frac{1}{2}\left(1 - \frac{r^2}{R^2}\right)\right\}, \tag{9}$$

and, by equation (8),

$$\rho[f'(a, b, D)]_{a=b=R} = -2\pi\rho R^2\left\{\log\frac{8D}{R} + \frac{1}{2}\right\}. \tag{10}$$

To obtain $f'(a, b, D)$ we must, therefore, substitute for R in the right-hand side of equation (10) some function of a and b which reduces to R when $a = b = R$. We must demand symmetry between a and b. This follows from the fact that, when $R/D \to 0$, V_i' becomes the potential of an infinite elliptical cylinder, which must remain invariant for a simultaneous interchange of x and y, a and b. We then have two possibilities for expressions to substitute for R, namely,

$$\sqrt{ab} \quad \text{and} \quad \tfrac{1}{2}(a + b).$$

To decide which substitution to use, let us imagine that the cross-section is deformed by decreasing b, while the total mass remains the same. Then $\pi ab\rho$ must also remain constant, or, since a is unchanged, $b\rho$ remains constant. Hence $\rho \to \infty$ when $b \to 0$. In order that the potential V_i' may remain finite at the rim ($x = a$, $y = 0$) when b decreases, it is obviously necessary to substitute ab for R^2 and to put $\frac{1}{2}(a + b)$ for R in the logarithm. Then equation (10) gives

$$\rho f'(a, b, D) = -2\pi ab\rho\left\{\log\frac{16D}{a + b} + \frac{1}{2}\right\},$$

and the complete potential (8) becomes

$$V_i' = -2\pi\rho ab\left\{\log\frac{16D}{a + b} + \frac{1}{2}\left(1 - \frac{\alpha x^2 + \beta y^2}{ab}\right)\right\}. \tag{11}$$

For future reference we shall also give here the moment of inertia I of the ring with respect to the rotational axis. We have

$$I = M_R D^2\left(1 + \frac{3}{4}\frac{a^2}{D^2}\right), \tag{12}$$

where M_R is the mass ($= 2\pi^2 abD\rho$) of the ring.

III. EQUILIBRIUM OF A RING ROTATING ABOUT A CENTRAL BODY

This problem was treated by Laplace[3] in his work on Saturn's rings. Laplace carried his calculations through in our present approximation; hence we might at this point have started our discussion directly from his final formulae. However, the calculations are short and extremely simple, and for completeness we shall give them here. We consider a spherical central body of mass M_c, surrounded by a rotating toroid, of radius D, and elliptical cross-section with semi-axes a and b. When the rotating ring is in equilibrium,

[3] *Loc. cit.*; also "Mémoire sur la théorie de l'anneau de Saturne," *Mém. Acad. sci.*, 1789.

the surface must be an equi-potential surface (centrifugal potential included). Hence we have

$$\left.\begin{aligned}\tfrac{1}{2}\omega^2(x+D)^2+\frac{M_c}{\sqrt{(D+x)^2+y^2}}\\ +2\pi\rho ab\left\{\log\frac{16D}{a+b}+\frac{1}{2}\left(1-\frac{\alpha x^2+\beta y^2}{ab}\right)\right\}=\text{const}\end{aligned}\right\}\tag{13}$$

along the surface of a cross-section of the ring. Here ω is the angular velocity, x and y, as before, Cartesian co-ordinates with origin on the central circle of the ring. Expanding equation (13), retaining terms of second order in x/D, y/D, and removing constant terms, we obtain

$$\tfrac{1}{2}\omega^2(x^2+2xD)+\frac{M_c}{D}\left(-\frac{x}{D}+\frac{2x^2-z^2}{2D^2}\right)-\pi\rho(\alpha x^2+\beta y^2)=\text{const}\tag{14}$$

along the boundary given by

$$\frac{x^2}{a^2}+\frac{y^2}{b^2}=1\,.\tag{15}$$

From equations (14) and (15) we can conclude, by the proportionality of corresponding coefficients,

$$\omega^2=\frac{M_c}{D^3}\tag{16}$$

and

$$a^2\left(\frac{3}{2}\frac{\omega^2}{\pi\rho}-\alpha\right)=-b^2\left(\frac{\omega^2}{2\pi\rho}+\beta\right).\tag{17}$$

Introducing for α and β their expressions in terms of a and b from equation (7) and solving equation (17) with respect to $\omega^2/\pi\rho$, we obtain

$$\frac{\omega^2}{\pi\rho}=\frac{4ab(a-b)}{(3a^2+b^2)(a+b)}\,.\tag{18}$$

Equations (16) and (18) are the equations given by Laplace. Let us introduce the quality γ defined by

$$\gamma=\frac{a-b}{a+b}\,,\qquad\frac{b}{a}=\frac{1-\gamma}{1+\gamma}\,.\tag{19}$$

Then equation (18) may be written

$$\frac{\omega^2}{\pi\rho}=\frac{\gamma(1-\gamma^2)}{1+\gamma+\gamma^2}\,.\tag{20}$$

Since γ is by definition less than unity, it follows from equation (20) that

$$\gamma > 0 , \tag{21}$$

which means that $a > b$, or, in other words, the cross-section is always flattened toward the plane of the toroid. We shall denote the quantity $\omega^2/\pi\rho$ by Ω. Then

$$\Omega = \frac{\omega^2}{\pi\rho} = \frac{M_c}{\pi\rho D^3} , \tag{22}$$

by equation (16). Equation (20) may now be written

$$f(\gamma) = \gamma^3 + \Omega\gamma^2 + (\Omega - 1)\gamma + \Omega = 0 . \tag{23}$$

Consider first the case $\Omega = 0$, which means that $D = \infty$ and $\omega = 0$. Then

$$\gamma = \begin{cases} 0 , \\ +1 , \\ -1 . \end{cases} \tag{24}$$

The negative solution has, as we have seen, no meaning. There are, then, two possible cross-sections for a ring in equilibrium at an infinite distance, one circular, $b/a = 1$, and one completely flat, $b/a = 0$. If we follow the run of the function $f(\gamma)$ in the case $\Omega = 0$, we see that as γ decreases from $+\infty$, $f(\gamma)$ comes down from $+\infty$, crosses the γ-axis at $\gamma = 1$, passes a negative minimum, and crosses up again at $\gamma = 0$. On the side of negative γ it bends down again, crosses at $\gamma = -1$, and drops down to $-\infty$ with γ. We are interested only in positive roots. If Ω is now increased from its zero value, it is seen that $f(\gamma)$ also increases for every positive value of γ. Therefore, as Ω increases, the two roots, originally at 0 and $+1$ draw closer together in the interval 0–1. Finally, when the minimum point of $f(\gamma)$ touches the γ-axis, the two roots will coincide. For even higher values of Ω, $f(\gamma)$ has no positive root. The negative root, originally at $\gamma = -1$, will remain negative while Ω increases, as is easily seen from the fact that $f(\gamma) > 0$ at $\gamma = 0$ for all positive values of Ω. To summarize the results, we have found that, given the central mass M_c and the density ρ of the ring, there exist either two or no equilibrium configurations of the ring for each distance D. When the distance is infinite, the ring is either circular or completely flat in cross-section. As D decreases—i.e., Ω increases—the circular cross-section becomes more and more elliptical, while the flat one becomes less and less elliptical. At a certain minimum distance D, i.e., maximum Ω, the two cross-sections become identical, and below this distance no equilibrium is possible.

To determine this critical value of Ω we apply the condition that the minimum of $f(\gamma)$ shall coincide with a root of $f(\gamma)$, which gives the two equations

$$\left.\begin{aligned} 3\gamma^2 + 2\Omega\gamma + \Omega - 1 = 0 \\ \text{and} \\ \gamma^3 + \Omega\gamma^2 + (\Omega - 1)\gamma + \Omega = 0 . \end{aligned}\right\} \tag{25}$$

Eliminating Ω, we obtain

$$\gamma^4 + 2\gamma^3 + 4\gamma^2 - 1 = 0 , \tag{26}$$

with the positive root

$$\gamma = 0.4435 . \tag{27}$$

For Ω we get from equation (25) the corresponding critical value

$$\Omega_{\max} = 0.2172 . \tag{28}$$

The limiting ratio of the axes becomes, by equation (19),

$$\left(\frac{b}{a}\right)_{\lim} = 0.3855 . \tag{29}$$

The fact that there exists a maximum value for Ω implies, according to equation (22), that for a given angular velocity of the ring there exists a lower limit to the density. We have

$$\rho_{\min} = \frac{\omega^2}{\pi\Omega_{\max}} = \frac{\omega^2}{0.2172 \cdot \pi} . \tag{30}$$

For a rotational period of the order of that of our galaxy at the sun's distance from the galactic center, which corresponds to $\omega \approx 10^{-15}$ sec^{-1}, we get

$$\rho_{\min} \approx 1.4 \cdot 10^{-30} \text{ gr/cm}^3 . \tag{31}$$

By equation (22) we also have

$$\left[\frac{M_c}{\pi\rho D^3}\right]_{\max} = 0.2172 . \tag{32}$$

Denoting the density and radius of the spherical central body by ρ_c and D_c, we have by equation (32)

$$\frac{D_c^3}{D^3} \leq 0.1629 \frac{\rho}{\rho_c} . \tag{33}$$

Consequently, the lower the density of the ring compared to the density of the central body, the larger is the radius of the ring compared to the radius of the central body. If we assume $\rho/\rho_c = 1$, we get

$$\frac{D_c}{D} \leq 0.546 . \tag{34}$$

This gives for the minimum radius of the ring approximately twice the radius of the central body. As mentioned before, these critical values have no immediate application to the ring-shaped nebulae.

IV. EQUILIBRIUM OF A SPHEROID SURROUNDED BY A RING

In the preceding section, while the equilibrium configurations of the ring were studied, the central body was assumed to be a sphere or a point mass. To study the equilibrium of the central body we can with the same approximation assume the rotating toroid

to be an infinitely thin circular ring surrounding the central body. The general effects of such a ring upon the equilibrium of a rotating spheroid, with the same axis of rotation as the ring, is rather obvious. The effect will be practically equivalent to an increase in the centrifugal force. We cannot expect to obtain much more information of value by an analytical treatment; hence we shall only briefly consider the mathematically simple case when the diameter of the spheroid is small compared to the diameter $2D$ of the ring. Consider a circular ring of mass $M_R = 2\pi D\sigma$, where σ is the density per unit length. The potential at a point z on the rotational axis is obviously

$$V_z = -\frac{2\pi D\sigma}{\sqrt{D^2 + z^2}}. \tag{35}$$

For heights z above the plane of the ring which are less than D, we can expand equation (35) thus:

$$V_z = -\frac{M_R}{D}\left\{ 1 - \frac{1}{2}\left(\frac{z}{D}\right)^2 + \frac{3}{8}\left(\frac{z}{D}\right)^4 + \dots . \right\}. \tag{36}$$

By a well-known theorem for the potential of rotationally symmetrical bodies, we obtain the general potential from equation (36) by substituting $(r/D)^n P_n$ for $(z/D)^n$. The quantity P_n is the nth zonal harmonic, r the radius vector of the point in question. We obtain

$$V = -\frac{M_R}{D}\left\{ 1 - \frac{1}{2}\left(\frac{r}{D}\right)^2 P_2 + \dots . \right\}. \tag{37}$$

The internal potential of an oblate spheroid of axes a and c, respectively, in the equatorial plane and perpendicular to it, is

$$V_{\text{spher}} = \pi\rho(\alpha_s R^2 + \gamma_s z^2 - \chi_s), \tag{38}$$

where

$$\left.\begin{aligned} \alpha_s &= (\zeta^2 + 1)\zeta \cot^{-1}\zeta - \zeta^2, & \gamma_s &= 2(\zeta^2 + 1)(1 - \zeta \cot^{-1}\zeta), \\ a &= \frac{(\zeta^2 + 1)^{1/2}}{\zeta} c, & R^2 &= x^2 + y^2. \end{aligned}\right\} \tag{39}$$

The quantity χ_s is a constant which will not concern us here. When in equilibrium, the surface of the spheroid must be an equipotential surface (centrifugal potential included). We therefore have, retaining second order in r/D,

$$\frac{M_R}{D}\left\{ 1 - \frac{1}{2}\left(\frac{r}{D}\right)^2 P_2 \right\} - \pi\rho(\alpha_s R^2 + \gamma_s z^2 - \chi_s) + \tfrac{1}{2}\omega^2 R^2 = \text{const}. \tag{40}$$

On the surface of the ellipsoid

$$\frac{R^2}{a^2} + \frac{z^2}{c^2} = 1. \tag{41}$$

Introducing

$$P_2 = \tfrac{3}{2}\cos^2\theta - \tfrac{1}{2} = \frac{3}{2}\left(\frac{z}{r}\right)^2 - \frac{1}{2}$$

and removing constant terms, equation (40) becomes

$$\frac{M_R}{D}\left\{-\frac{1}{2}\left(\frac{z}{D}\right)^2 + \frac{1}{4}\left(\frac{R}{D}\right)^2\right\} - \pi\rho(\alpha_s R^2 + \gamma_s z^2) + \tfrac{1}{2}\omega^2 R^2 = \text{const along the surface.} \quad (42)$$

Comparing equations (41) and (42), we obtain

$$\left\{\frac{1}{4}\frac{M_R}{D^3} - \pi\rho\alpha_s + \tfrac{1}{2}\omega^2\right\} a^2 = -\left\{\frac{1}{2}\frac{M_R}{D^3} + \pi\rho\gamma_s\right\} c^2, \quad (43)$$

which can also be written

$$\frac{\omega^2}{2\pi\rho} = -\frac{M_R}{4\pi\rho D^3}\left(1 + 2\frac{c^2}{a^2}\right) + \alpha_s - \gamma_s\frac{c^2}{a^2}. \quad (44)$$

When $M_R = 0$, equation (44) can always be satisfied by a real value of ω, because α_s is greater than γ_s when $a > c$. When M is finite, however, the right-hand side may become negative, in which case there does not exist any real value of ω. For ω to be real, we must have

$$\frac{M_R}{4\pi\rho D^3} \leq \frac{\alpha_s - \gamma_s\left(\frac{c}{a}\right)^2}{1 + 2\left(\frac{c}{a}\right)^2}. \quad (45)$$

This relation gives a limiting value for c/a, depending upon the mass and radius of the surrounding ring. The quantity $4\pi\rho D^3$ represents three times the mass contained in a sphere of radius equal to the radius of the ring and with density equal to that of the central spheroid. It is then obvious that the left-hand side is an extremely small quantity. The limiting value of c/a, found by taking the equality sign in equation (45), must therefore occur when the quantity $\alpha_s - \gamma_s(c/a)^2$ nearly vanishes, which is the case when $c/a \to 0$ and when $c/a \to 1$. In the first case, by equation (39), $\alpha_s = (\pi/2)(c/a)$. Neglecting squares of c/a, we therefore obtain from equation (45)

$$\frac{c}{a} \geq \frac{M_R}{2\pi^2\rho D^3}. \quad (46a)$$

In the second case ($c/a \to 1$) equation (39) gives, after a short calculation,

$$\lim_{a\to c}\left\{\alpha_s - \gamma_s\left(\frac{c}{a}\right)^2\right\} = \lim_{\zeta\to\infty}\zeta^2\left\{3(\zeta\cot^{-1}\zeta - 1) + \frac{1}{\zeta}\cot^{-1}\zeta\right\} = \frac{4}{15}\frac{1}{\zeta^2}$$

or

$$\lim_{a\to c}\left\{\alpha_s - \gamma_s\left(\frac{c}{a}\right)^2\right\} = \frac{4}{15}\left(\frac{a^2}{c^2} - 1\right).$$

Hence, by equation (45),

$$\frac{a^2}{c^2} \geq 1 + \frac{45}{16}\frac{M_R}{\pi\rho D^3}. \tag{46b}$$

We have now obtained both an upper limit (eq. [46*a*]) and a lower limit (eq. [46*b*]) to the ellipticity of a spheroid in equilibrium surrounded by a ring. Qualitatively, these results might have been anticipated. A purely spherical equilibrium configuration is not possible, even when the body does not rotate, because of the attraction of the ring, which will cause a finite ellipticity. Similarly, the additional outward attraction of the ring destroys the equilibrium for very flattened spheroids.

V. STABILITY OF A RING ROTATING AROUND A CENTRAL BODY

We have studied in the foregoing the equilibrium of a ring rotating around a central body and have found the existence of equilibrium configurations. An important question, however, still remains to be answered: Are the configurations stable, or will small perturbations result in their ultimate destruction? The stability in the case of a ring of circular cross-section, without a central body, was studied by F. W. Dyson[4] in 1893 in his work on "The Potential of an Anchor Ring." His calculations are rather long and complicated and do not include the case when the ring has a central body. The stability considerations can, however, be carried through in a rather elementary way, which is also applicable for a ring with a central body and, consequently, elliptical cross-section.

We shall consider separately four different kinds of perturbations.

1. First, we consider the simple perturbation consisting in oscillations which increase and decrease the radius D of the ring with time. The ellipticity of the cross-section remains the same during the oscillations, while the area of the cross-section varies so as to keep the volume of the ring constant.

We begin by calculating the potential energy of the ring, due to its own attraction. By equation (11) we have for the internal potential

$$V_i = -2\pi\rho ab\left\{\log\frac{16D}{a+b} + \frac{1}{2}\left(1 - \frac{\alpha x^2 + \beta y^2}{ab}\right)\right\}.$$

The potential energy of the ring is

$$U = \tfrac{1}{2}\iiint \rho V_i d\tau,$$

where the integration is extended over the whole ring. We get

$$\left.\begin{aligned} U &= -\int_0^{2\pi}\int_{-b}^{+b}\int_{-a\sqrt{1-y^2/b^2}}^{+a\sqrt{1-y^2/b^2}} \pi ab\rho^2\left\{\log\frac{16D}{a+b} + \frac{1}{2}\left(1 - \frac{\alpha x^2+\beta y^2}{ab}\right)\right\}(D+x)\,dx\,dy\,d\phi, \\ &= -2\pi^3 a^2b^2D\left\{\log\frac{16D}{a+b} + \frac{1}{2}\right\} + \tfrac{1}{2}\pi^3a^2b^2D, \\ &= -2\pi^3a^2b^2D\left\{\log\frac{16D}{a+b} + \frac{1}{4}\right\} = -\frac{M_R^2}{2\pi D}\left\{\log\frac{16D}{a+b} + \frac{1}{4}\right\}. \end{aligned}\right\} \tag{47}$$

[4] *Phil. Trans. Roy. Soc., London*, A, **184**, 1041, 1893.

The potential energy U_c due to the attraction on the ring by a spherical central body of mass M_c is

$$\left.\begin{aligned} U_c &= -M_c\rho\iiint\frac{D+x}{\sqrt{(D+x)^2+y^2}}\,dxdyd\phi\,, \\ &= -M_c\rho\int_0^{2\pi}\int_{-b}^{+b}\int_{-a\sqrt{1-y^2/b^2}}^{+a\sqrt{1-y^2/b^2}}\frac{1}{D}\left(1-\frac{x}{D}+\frac{2x^2-y^2}{2D^2}\right)(D+x)dxdyd\phi \\ &\qquad -M_c\pi ab\rho\int_0^{2\pi}\left(1-\frac{1}{8}\frac{b^2}{D^2}\right)d\phi\,. \end{aligned}\right\} \tag{48}$$

Hence

$$U_c = -\frac{M_cM_R}{D}\left(1-\frac{1}{8}\frac{b^2}{D^2}\right)\approx -\frac{M_cM_R}{D}\,, \tag{49}$$

when we neglect squares of the small quantity b/D.

The kinetic energy, T, of the oscillating ring is

$$T = \tfrac{1}{2}I\dot{\phi}^2+\tfrac{1}{2}M_R\dot{D}^2\,,$$

or, according to equation (12), neglecting the square of a/D,

$$T = \tfrac{1}{2}M_RD^2\dot{\phi}^2+\tfrac{1}{2}M_R\dot{D}^2\,. \tag{50}$$

By equations (47), (49), and (50) we obtain the kinetic potential $L = T - U - U_c$,

$$L = \tfrac{1}{2}M_RD^2\dot{\phi}^2+\tfrac{1}{2}M_R\dot{D}^2+\frac{M_R^2}{2\pi}\frac{1}{D}\left\{\log\frac{16D}{a+b}+\frac{1}{4}\right\}+\frac{M_cM_R}{D}\,.$$

Lagrange's equation for the co-ordinate D gives

$$\ddot{D}-D\dot{\phi}^2-\frac{M_R}{2\pi}\frac{\partial}{\partial D}\left[\frac{1}{D}\left\{\log\frac{16D}{a+b}+\frac{1}{4}\right\}\right]+\frac{M_c}{D^2}=0\,.$$

Since the volume of the ring and the ellipticity of its cross-section remain constant, we have, writing $b/a = \lambda$,

$$ab\cdot D = \lambda a^2D = \text{const}$$

and

$$a+b = a(1+\lambda) = (1+\lambda)\cdot\frac{\text{const}}{\sqrt{\lambda D}}\,.$$

Hence

$$\frac{\partial}{\partial D}(a+b) = -\frac{1}{2D}(a+b)\,,$$

and

$$\frac{\partial}{\partial D}\left[\frac{1}{D}\left\{\log\frac{16D}{a+b}+\frac{1}{4}\right\}\right] = -\frac{1}{D^2}\left\{\log\frac{16D}{a+b}+\frac{1}{4}\right\}+\frac{1}{D}\left\{\frac{1}{D}+\frac{1}{2D}\right\}$$
$$= -\frac{1}{D^2}\left\{\log\frac{16D}{a+b}-\frac{5}{4}\right\}.$$

Consequently,

$$\ddot{D} = D\dot{\phi}^2 - \frac{M_R}{2\pi D^2}\left(\log\frac{16D}{a+b}-\frac{5}{4}\right)-\frac{M_c}{D^2}. \tag{51}$$

From this equation we can obtain an expression for the angular velocity in the equilibrium position. Putting $\ddot{D} = 0$, we have

$$\dot{\phi}_0^2 = \frac{M_c}{D^3}+\frac{M_R}{2\pi D^3}\left(\log\frac{16D}{a+b}-\frac{5}{4}\right). \tag{52}$$

Comparing equation (52) with equation (16), we see that equation (52) contains an additional term, which takes account of the self-attraction of the ring.

To study the stability, we make use of the condition for conservation of angular momentum, which requires that

$$M_R D^2\dot{\phi} = \text{const}$$

during the motion. Lagrange's equation (51) can then be written

$$\ddot{D} = \frac{1}{D^2}\left\{\frac{\text{const}}{M_R^2 D}-\frac{M_R}{2\pi}\left(\log\frac{16D}{a+b}-\frac{5}{4}\right)-M_c\right\}. \tag{53}$$

Consider the expression on the right-hand side. In the equilibrium position it vanishes. When D is increased from the equilibrium position, the first, positive, term decreases, while the second, subtracted, term increases and the third remains constant. Consequently, the whole expression becomes negative, and the acceleration $\ddot{D}$ acts against the increase of D. Similarly, it is seen that a decrease in D from the equilibrium value makes the acceleration D positive, i.e., acting against the decrease of D. We can conclude that *the ring is stable for this type of oscillations.*

2. The second type of perturbations, which we shall now proceed to study, consists in a change of area of the cross-section along the ring. The radius D of the ring and the ellipticity of the cross-section remain constant, while the area of the cross-section varies with azimuth ϕ. The disturbance can be considered as a superposition of fundamental periodic variations of the semi-axes a and b. We shall consider such a fundamental "wave," say, one producing n maxima and minima of the cross-section along the whole ring. We have for the variation of the half-axis a

$$a = a_0(1 + A_n e^{-in\phi}). \tag{54}$$

Similarly, the axis b, having a constant ratio λ to a, has a variation

$$b = \lambda a = \lambda a_0(1 + A_n e^{-in\phi}) = b_0(1 + A_n e^{-in\phi}). \tag{55}$$

$|A_n| = (A_n A_n^*)^{1/2}$ is the infinitesimal amplitude of the relative variation of a diameter of the cross-section. The stability depends upon whether $|A_n|$ remains small or grows indefinitely after the perturbation has been started.

Since for the stability considerations a first-order approximation is not sufficient, we cannot neglect second-order terms in the perturbations. When we encounter a product of two infinitesimal periodic perturbation terms, we shall replace the product by its mean value over the ring. This means that a product of the form

$$(A_n e^{-in\phi})(A_m e^{-im\phi})$$

will be replaced by

$$\tfrac{1}{2} A_n^* A_m \cdot \delta_{m,n} ,$$

where

$$\delta_{m,n} = \begin{cases} 0 \text{ when } m \neq n , \\ 1 \text{ when } m = n . \end{cases}$$

The fluid in the ring is, as before, supposed to be incompressible so that the volume of the ring remains constant during the disturbance. The volume of the disturbed ring is

$$\int_0^{2\pi} \pi ab D d\phi = \pi \lambda a_0^2 D \int_0^{2\pi} (1 + A_n e^{-in\phi})^2 d\phi ,$$

$$= 2\pi^2 D \lambda a_0^2 (1 + \tfrac{1}{2} A_n^* A_n) .$$

By a_m we denote the mean value of a,

$$2\pi^2 D \lambda a_m^2 = 2\pi^2 D \lambda a_0^2 (1 + \tfrac{1}{2} A_n^* A_n) .$$

Hence

$$a_m^2 = a_0^2 (1 + \tfrac{1}{2} A_n^* A_n) . \tag{56}$$

To examine the stability we must calculate three quantities: (1) the potential energy of the disturbed ring due to its attraction on itself, (2) the potential energy due to the attraction of the central body on the ring, and (3) the kinetic energy of the rotating ring.

To find the potential energy U of the perturbed ring, we must know the internal potential of such a ring. Our first problem is, therefore, to obtain the internal potential of a ring of elliptic cross-section with half-axes varying with azimuth according to equations (54) and (55). For this purpose we shall make use of some elementary considerations. The potential at a point inside the ring is the energy required to bring a unit mass from infinity to that point. At infinity the force is, of course, dependent only upon the mass of the ring and not at all influenced by the small perturbation. As we approach the ring from infinity, we can come quite close before the infinitesimal perturbation of the original ring becomes sensible in the field of force. As far as these outer regions go, we can therefore replace the perturbed ring R by an unperturbed ring R_m of constant cross-section, equal to the mean value $\pi \rho \lambda a_m^2$. At points inside the ring, on the other hand, the force will, according to our approximation, be the same as that of an undisturbed ring of constant cross-section equal to the actual cross-section through the point. This will also be the case for points not too far from the ring in the outside extension of the plane of the cross-section. Thus, for a point inside the ring, or near by outside, we can replace the perturbed ring R by an unperturbed ring R_θ of constant cross-section equal

to the actual cross-section of the perturbed ring at the azimuth θ of the point in question. The outer region, where the force is effectively that of the ring R_m, and the inner region, where the force is effectively that of the ring R_θ, are separated by an intermediate region where the transition from one to the other occurs. We shall assume that this transition occurs suddenly at a certain potential surface. From infinity to this potential surface the force is that of R_m, and from here on to the internal point the force is that of R_θ. The energy required to bring a unit mass from infinity to the transition point ξ_t on the critical potential surface is equal to the potential $V_m(\xi_t)$ of R_m at this point. The energy required to bring the mass from here to the interior point ξ_i is $V_\theta(\xi_i) - V_\theta(\xi_t)$. The potential at an internal point of the perturbed ring is, therefore,

$$V_i(\xi_i) = V_m(\xi_t) - V_\theta(\xi_t) + V_\theta(\xi_i) . \tag{57}$$

The external potential of a ring of elliptical cross-section, at a point ξ_t is a function of the variables D, a, λ, ρ, and ξ_t. The first two terms in equation (57) give the difference in potential at ξ_t arising from an infinitely small change $\Delta a = a_m - a$ in a, while all the other variables are kept unchanged. We have

$$\begin{aligned} \Delta a = a_m - a &= a_0(1 + \tfrac{1}{4}A_n^* A_n) - a_0(1 + A_n e^{-in\phi}) , \\ &= a_0\{\tfrac{1}{4}A_n^* A_n - A_n e^{-in\phi}\} . \end{aligned}$$

By a Taylor expansion of the potential V we obtain, correct to the second order,

$$V(a) = V(a_m) + \left(\frac{\partial V}{\partial a}\right)_m (a - a_m) + \frac{1}{2}\left(\frac{\partial^2 V}{\partial a^2}\right)_m (a - a_m)^2$$

or

$$V_m - V_\theta = \left(\frac{\partial V}{\partial a}\right)_m a_0(\tfrac{1}{4}A_n^* A_n - A_n e^{-in\theta}) - \frac{1}{2}\left(\frac{\partial^2 V}{\partial a^2}\right)_m a_0^2 \cdot \tfrac{1}{2}A_n^* A_n .$$

It is now unnecessary to distinguish between a_m and a_0 on the right-hand side, so we can write

$$V_m - V_\theta = -\frac{\partial V}{\partial a_0} a_0 A_n e^{-in\theta} - a_0^3 \frac{\partial}{\partial a_0}\left(\frac{1}{a_0}\frac{\partial V}{\partial a_0}\right) \tfrac{1}{4}A_n^* A_n . \tag{58}$$

The potential V at a fixed external point can be expanded in the form

$$V = M_R\left\{ V_0 + V_1 \frac{a_0}{D} + V_2 \left(\frac{a_0}{D}\right)^2 + \dots . \right\} = 2\pi^2 \lambda a_0^2 D\rho \left(V_0 + V_1 \frac{a_0}{D} + \dots . \right) ,$$

where the coefficients V_0, V_1, etc., are functions of the co-ordinates of the external point and of the ellipticity, but not of a_0. When introducing this expansion into the coefficient of $A_n^* A_n$ in equation (58), we notice that the first term vanishes and only higher-order terms are left. The last term in equation (58) must therefore be neglected, and we have

$$V_m - V_\theta = -\frac{\partial V}{\partial a_0} a_0 A_n e^{-in\theta} . \tag{59}$$

The internal potential of a homogeneous ring of *constant* cross-section πab was found in section I, equation (11). Substituting from equation (11) for $V_\theta(\xi_i)$ in equation (57) and using equation (59), we can then write

$$V_i = -\left(\frac{\partial V}{\partial a_0}\right)_{\xi_t} a_0 A_n e^{-in\phi} - 2\pi ab\rho \left\{ \log \frac{16D}{a+b} + \frac{1}{2}\left(1 - \frac{\alpha x^2 + \beta y^2}{ab}\right)\right\},$$

where we write ϕ again, instead of θ, for the azimuth. In this expression a and b are functions of the azimuth. According to equations (54) and (55),

$$\left.\begin{aligned} a &= \frac{b}{\lambda} = a_0(1 + A_n e^{-in\phi}), \\ ab &= a_0 b_0 (1 + 2A_n e^{-in\phi} + \tfrac{1}{2} A_n^* A_n). \end{aligned}\right\} \tag{60}$$

Hence

$$V_i = -\left(\frac{\partial V}{\partial a_0}\right)_{\xi_t} a_0 A_n e^{-in\phi} - 2\pi a_0 b_0 \rho (1 + 2A_n e^{-in\phi} + \tfrac{1}{2} A_n^* A_n) \times \left\{ \log \frac{16D}{a_0 + b_0} - \log (1 + A_n e^{-in\phi}) + \tfrac{1}{2} \right\} + \pi\rho(\alpha x^2 + \beta y^2).$$

As usual, we retain no terms of higher order than $|A_n|^2$. Then

$$\begin{aligned} V_i = &-\left(\frac{\partial V}{\partial a_0}\right)_{\xi_t} a_0 A_n e^{-in\phi} - 2\pi a_0 b_0 \rho \left\{ \log \frac{16D}{a_0 + b_0} - A_n e^{-in\phi} + \tfrac{1}{4} A_n^* A_n + \tfrac{1}{2} \right. \\ &\left. + 2 \log \frac{16D}{a_0 + b_0} A_n e^{-in\phi} - A_n^* A_n + A_n e^{-in\phi} + \tfrac{1}{2} \log \frac{16D}{a_0 + b_0} A_n^* A_n + \tfrac{1}{4} A_n^* A_n \right\} \\ &+ \pi\rho(\alpha x^2 + \beta y^2), \\ = &-2\pi a_0 b_0 \rho \left\{ \log \frac{16D}{a_0 + b_0} + \frac{1}{2}\left(1 - \frac{\alpha x^2 + \beta y^2}{a_0 b_0}\right)\right\} \\ &- 4\pi a_0 b_0 \rho \left\{ \log \frac{16D}{a_0 + b_0} - \eta_n \right\} A_n e^{-in\phi} - \pi a_0 b_0 \rho \left(\log \frac{16D}{a_0 + b_0} - 1 \right) A_n^* A_n, \end{aligned}$$

where

$$\eta_n = -\frac{1}{4\pi b_0 \rho}\left(\frac{\partial V}{\partial a_0}\right)_{\xi_t}. \tag{61}$$

The physical meaning of η_n is obvious. It represents the rate of increase in potential at the point ξ_t, when a thin layer is added on top of the surface of the ring. This rate of increase is negative, and its numerical value falls off with increasing distance from the ring, as does the value of the potential itself. Consequently, η_n is positive and decreases when the transition point ξ_t moves away from the ring. We need not specify η_n any nearer at this point.

The potential energy U of the ring due to its own attraction is

$$U = \tfrac{1}{2} \iiint \rho V_i d\tau.$$

The integral extends over the whole ring. Written out in full, U has the form

$$\left.\begin{aligned}
U &= -\tfrac{1}{2}\rho\int_0^{2\pi}\int_{-b}^{+b}\int_{-a\sqrt{1-y^2/b^2}}^{+a\sqrt{1-y^2/b^2}}\left\{2\pi a_0b_0\rho\left[\log\frac{16D}{a_0+b_0}\right.\right.\\
&\quad\left.+\tfrac{1}{2}\left(1-\frac{\alpha x^2+\beta y^2}{a_0b_0}\right)\right]+4\pi a_0b_0\rho\left(\log\frac{16D}{a_0+b_0}-\eta_n\right)A_ne^{-in\phi}\\
&\quad\left.+\pi a_0b_0\rho\left(\log\frac{16D}{a_0+b_0}-1\right)A_n^*A_n\right\}Ddxdyd\phi\,,\\
&=-2\pi a_0b_0\rho^2\int_0^{2\pi}\int_{-b}^{+b}\left\{\left[\log\frac{16D}{a_0+b_0}+\tfrac{1}{2}+2\left(\log\frac{16D}{a_0+b_0}-\eta_n\right)A_ne^{-in\phi}\right.\right.\\
&\quad+\left(\log\frac{16D}{a_0+b_0}-1\right)\tfrac{1}{2}A_n^*A_n\Big]a\sqrt{1-\frac{y^2}{b^2}}-\frac{1}{2a_0b_0}\left[\alpha\frac{a^3}{3}\left(1-\frac{y^2}{b^2}\right)^{3/2}\right.\\
&\quad\left.\left.+\beta y^2a\sqrt{1-\frac{y^2}{b^2}}\right]\right\}Ddyd\phi\,,\\
&=-2\pi a_0b_0\rho^2\int_0^{2\pi}\left\{\left[\log\frac{16D}{a_0+b_0}+\tfrac{1}{2}+2\left(\log\frac{16D}{a_0+b_0}-\eta_n\right)A_ne^{-in\phi}\right.\right.\\
&\quad\left.\left.+\left(\log\frac{16D}{a_0+b_0}-1\right)\tfrac{1}{2}A_n^*A_n\right]\frac{\pi}{2}ab-\frac{1}{2a_0b_0}\left[\alpha\frac{\pi a^3b}{8}+\beta\frac{\pi ab^3}{8}\right]\right\}Dd\phi\,.
\end{aligned}\right\}\quad(62)$$

When we introduce ab from equation (60) and α and β from equation (7), equation (62) becomes

$$\begin{aligned}
U &= -\pi^2a_0^2b_0^2\rho^2D\int_0^{2\pi}\left\{\left[\log\frac{16D}{a_0+b_0}+\tfrac{1}{2}+2\left(\log\frac{16D}{a_0+b_0}-\eta_n\right)A_ne^{-in\phi}\right.\right.\\
&\quad\left.\left.+\left(\log\frac{16D}{a_0+b_0}-1\right)\tfrac{1}{2}A_n^*A_n\right](1+2A_ne^{-in\phi}+\tfrac{1}{2}A_n^*A_n)-\tfrac{1}{4}(1+A_ne^{-in\phi})^4\right\}d\phi\,,\\
&=-2\pi^3a_0^2b_0^2\rho^2D\left\{\log\frac{16D}{a_0+b_0}+\tfrac{1}{4}+\left(\log\frac{16D}{a_0+b_0}-1\right)A_n^*A_n\right.\\
&\qquad\left.+2\left(\log\frac{16D}{a_0+b_0}-\eta_n\right)A_n^*A_n\right\}.
\end{aligned}$$

Introducing a_m, b_m, we obtain finally

$$U=-\frac{M_R^2}{2\pi D}\left\{\log\frac{16D}{a_m+b_m}+\tfrac{1}{4}+2\left(\log\frac{16D}{a_m+b_m}-\eta_n-\tfrac{1}{2}\right)A_n^*A_n\right\}.\quad(63)$$

Consider next the potential energy U_c due to the attraction on the ring by the spherical central body M_c. We can write

$$U_c=-\int_0^{2\pi}\frac{M_c\cdot\pi ab\rho}{D}\cdot Dd\phi=-\frac{\pi\rho M_c}{D}\int_0^{2\pi}ab\,Dd\phi=-\frac{M_cM_R}{D}\,.\quad(64)$$

To determine the influence of the perturbation on the kinetic energy of the ring, we must specify the properties of the wave-perturbation applied. We shall consider two

typical cases. First, we consider that the maxima and minima of the cross-section remain stationary in space. This means that the wave is a progressing wave in the material of the ring, running against the rotational motion with the same velocity as the rotation. Second, we shall assume the density maxima to follow the rotation, in which case the wave is a standing wave in the material, moving with the rotation of the ring. This last type is probably the physically important one. The first type is the one considered by Dyson, and it is of interest to compare our result with his, to see the effect of the central body.

In the first case, where the location of the maxima and minima remains constant in space, the perturbation term has the form

$$A_n e^{-in\phi} = A_0 \cos \sigma t \cdot e^{-in\phi} , \tag{65}$$

where σ must be real if the ring is to be stable. The kinetic energy may be considered as consisting of two parts. The first part, T_ϕ, is the kinetic energy due to the rotational velocity $v_\phi = D\dot{\phi}$. The second, T_A, is the kinetic energy of the motion in the plane of a cross-section, due to the variation of the diameter. Consider, first, T_ϕ. We must then know the effect of the perturbations on the velocity v_ϕ. As we approach the stability limit, the frequency σ of the oscillations becomes very small, so that the local change in cross-section is slow. To study the stability we may therefore assume

$$abv_\phi = \text{const} = C . \tag{66}$$

Then

$$\left.\begin{aligned} T_\varphi = \int_0^{2\pi} \pi ab \cdot \tfrac{1}{2}\rho v_\phi^2 \cdot Dd\phi = \frac{\pi}{2} D\rho C^2 \int_0^{2\pi} \frac{d\phi}{ab} = \frac{\pi D\rho C^2}{2a_0 b_0} \int_0^{2\pi} \Big(1 - 2A_n e^{-in\phi} \\ + 3\frac{A_n^* A_n}{2} \Big) d\phi = \frac{\pi^2 D\rho C^2}{a_0 b_0} (1 + \tfrac{3}{2} A_n^2) = \frac{\pi^2 D\rho C^2}{a_m b_m} (1 + 2A_m^2) . \end{aligned}\right\} \tag{67}$$

To calculate the part T_A, we must know the velocity component in a meridional cross-section of the ring. As we follow the motion around the ring, we assume that each particle has a meridional velocity component v_A, directed from the center of the cross-section, proportional to the distance from the center, and in phase with the motion of the outer boundary. This assumption must give a good approximation to the real motion. The mean value of v_A^2 over a circular cross-section with radius expanding at the rate da/dt would be $\frac{1}{2}(da/dt)^2$. In the case of an elliptic cross-section, the mean value becomes

$$\overline{v_A^2} = \frac{1}{4}\left\{ \left(\frac{da}{dt}\right)^2 + \left(\frac{db}{dt}\right)^2 \right\} = \frac{1 + \lambda^2}{4} \left(\frac{da}{dt}\right)^2 . \tag{68}$$

Now we have

$$\frac{da}{dt} = a_0 \frac{d}{dt} (1 + A_0 \cos \sigma t \cdot e^{-in\phi}) = - a_0 (\sigma \sin \sigma t + in\dot{\phi} \cos \sigma t) A_0 e^{-in\phi} , \tag{69}$$

and, with our usual approximation,

$$\left(\frac{da}{dt}\right)^2 = a_0^2 \left(\frac{\sigma^2}{2} \sin^2 \sigma t + \dot{\phi}^2 \frac{n^2}{2} \cos^2 \sigma t \right) A_0^2 , \tag{70}$$

squaring the real part of equation (69). For the kinetic energy T_A we then get

$$\left.\begin{aligned} T_A &= \frac{1}{2}\int_0^{2\pi} \pi ab\rho\overline{v_A^2} D d\phi = \frac{1}{2}\int_0^{2\pi} \pi ab\rho \cdot a_0^2 \frac{1+\lambda^2}{4}\left[\left(\frac{\dot\phi^2 n^2}{2} - \frac{\sigma^2}{2}\right)\cos^2 \sigma t \right.\\ &\qquad\qquad \left. + \frac{\sigma^2}{2}\right] A_0^2 D d\phi\,, \\ &= M_R \frac{a_m^2 + b_m^2}{16}\{(\dot\phi^2 n^2 - \sigma^2)A_n^2 + \sigma^2 A_0^2\}\,. \end{aligned}\right\} \quad (71)$$

The total energy is the sum of equations (63), (64), (67), and (71):

$$\left.\begin{aligned} U + U_c + T_\varphi + T_A &= -\frac{M_R^2}{2\pi D}\left\{\log\frac{16D}{a_m+b_m} + \tfrac{1}{4} + 2\left(\log\frac{16D}{a_m+b_m} - \eta_n - \tfrac{1}{2}\right)A_n^2\right\} \\ &\quad - \frac{M_c M_R}{D} + \frac{\pi^2 D\rho C^2}{a_m b_m}(1 + 2A_n^2) + \frac{M_R(a_m^2+b_m^2)}{16}\{(\dot\phi^2 n^2 - \sigma^2)A_n^2 - \sigma^2 A_0^2\}\,. \end{aligned}\right\} \quad (72)$$

Since the total energy remains constant during the motion, the coefficient of the time variable factor A_n^2 must vanish. Hence

$$-\frac{M_R^2}{\pi D}\left(\log\frac{16D}{a_m+b_m} - \eta_n - \tfrac{1}{2}\right) + 2\pi^2 D^3 a_m b_m \rho\dot\phi_0^2 + \frac{M_R(a_m^2+b_m^2)}{16}(\dot\phi^2 n^2 - \sigma^2) = 0 \quad (73)$$

where, by means of equation (65), we have introduced the equilibrium value $\dot\phi_0^2$ from the relation

$$a_m b_m D\dot\phi_0 = C\,.$$

The value of $\dot\phi_0$ is known by equation (52). Equation (73) then takes the form

$$\left.\begin{aligned} -\frac{M_R^2}{\pi D}\left\{\log\frac{16D}{a_m+b_m} - \eta_n - \tfrac{1}{2}\right\} + M_R\left\{1 + \frac{n^2}{16D^2}(a_m^2+b_m^2)\right\} \\ \times\left\{\frac{M_c}{D} + \frac{M_R}{2\pi D}\left(\log\frac{16D}{a_m+b_m} - \frac{5}{4}\right)\right\} = \frac{a_m^2+b_m^2}{16} M_R\sigma^2\,. \end{aligned}\right\} \quad (74)$$

The condition for stability is that $\sigma^2 > 0$, which gives

$$-\frac{M_R}{\pi D}\left\{\log\frac{16D}{a_m+b_m} - \eta_n - \tfrac{1}{2}\right\} + \left\{\frac{M_c}{D} + \frac{M_R}{2\pi D}\left(\log\frac{16D}{a_m+b_m} - \frac{5}{4}\right)\right\} > 0\,, \quad (75)$$

neglecting the term of second order in a_m/D.

Before we can draw any conclusions from equation (75), we must determine η. We remember that η is positive and that it decreases when the transition point moves away from the ring. It is easily realized that the distance of the transition point from the ring must increase with increasing wave length of the perturbation. Consequently, as the wave length increases, η decreases. From equation (75) it is seen that the instability is greatest for the smallest value of η, which, then, means for the longest wave length. Hence we need only study the stability of the wave $n = 1$, which produces one maxi-

mum and minimum of thickness around the ring. To determine η we shall make use of equation (57), which by means of equations (59) and (61) can be written

$$\eta_1 \cdot 4\pi\rho a_m b_m \cdot A_1 e^{-i\theta} = V_i(\xi_i) - V_\theta(\xi_i) . \tag{76}$$

The right-hand side gives the difference in potential at the internal point, ξ_i, between the actual, perturbed ring and a ring of constant cross-section equal to that of the perturbed ring at the azimuth of θ. Equation (76) is obviously also valid for an external point ξ_e close to the ring. We shall consider equation (76) for such a point. Since a zero-order determination of η_1 is sufficient in equation (75), we may disregard the actual cross-section of the ring and assume the mass to be concentrated along the central circle. The potential $V_e(\xi_e)$ is then the potential of a circle with density per unit length given by the expression $\pi a_0 b_0 \rho(1 + A_1 e^{-i\varphi})^2$, while $V_\theta(\xi_e)$ is the potential of a ring with constant density along the ring equal to $\pi a_0 b_0 \rho(1 + A_1 e^{-i\theta})^2$, where θ is the azimuth of the point ξ_e. The left-hand side of equation (76) is the difference between these potentials, or the difference between the potentials at azimuth θ of the two rings with density distributions

$$\pi a_m b_m \rho \cdot 2A_1 e^{-i\varphi} \tag{77}$$

and

$$\pi a_m b_m \rho \cdot 2A_1 e^{-i\theta} . \tag{78}$$

Replacing a_0 by a_m introduces only third-order terms here. (Notice that φ is the varying azimuth along the ring, while θ is a constant.) The potential of the homogeneous ring (78), as the distance r from the ring tends to zero, is, by equation (2),

$$-4\pi a_m b_m \rho \cdot \log \frac{8D}{r} \cdot A_1 e^{-i\theta} . \tag{79}$$

The potential of a circle of density distribution (77) is, close to the circle at azimuth θ,[5]

$$-4\pi a_m b_m \rho \left\{ \log \frac{8D}{r} - 2 \right\} A_1 e^{-i\theta} . \tag{80}$$

Introducing the difference between (79) and (80) into the left-hand side of equation (76) gives

$$\cdot \quad \eta_1 = \dot{2} .$$

The condition for stability, (eq. [75]), then becomes finally

$$\frac{M_c}{M_R} > \frac{1}{2\pi}\left(\log \frac{16D}{a_m + b_m} - \frac{15}{4} \right) . \tag{81}$$

We can now conclude that any ring is stable if the central mass is sufficiently great compared to the mass of the ring. If we put $M_c = 0$, and $a_m = b_m$, we have the condition for stability of a ring of circular cross-section without any central mass. The equation (81) then agrees with Dyson's result,[6] apart from the term $1\frac{5}{4}$, which in Dyson's

[5] See Cayley, *Elliptical Functions*, p. 54, or Dyson, *op. cit.*, p. 53.

[6] *Op. cit.*, p. 1070.

work is given as $1\frac{3}{4}$. The difference arises from an error in Dyson's equation (33). According to equation (81), a ring without central body is unstable only if $D > 5.2a$, where a is the radius of the circular cross-section. If the central mass is equal to the mass of the ring, the diameter of the ring must already be more than 10,000 times the mean diameter of the cross-section before the ring is unstable. We must therefore consider the ring as stable as long as there is any appreciable central mass present.

The second case, where the thickening of the ring follows the rotation, is very easily treated. As before, the potential energy of the attraction by the central body is not affected by the perturbation. Further, the rotational motion in this case gives rise to no change in cross-section and, consequently, to no extra kinetic energy. The stability is then determined wholly by the variation in potential energy of the ring itself. For stability this potential energy must be a minimum in the equilibrium position. According to equation (63), introducing for η_1 its value 2, this means that

$$\log \frac{16D}{a_m + b_m} - \tfrac{5}{2} < 0 ,$$

if the ring is stable. Denoting the mean radius $\frac{1}{2}(a + b)$ by $\bar{a}$, we get (approximately)

$$\frac{\bar{a}}{D} > \frac{2}{3} . \tag{82}$$

The accurate value of this limit has no significance, since our approximations are invalid for a ring of such thickness. The practical result, however, is that the rings we consider are all unstable for the perturbation in question. The central mass does not affect this instability at all. Whether the ring is large or small, whether there is a central body or not, the ring will have a tendency to form mass condensations, which increase and break up the ring into separate masses.

In spite of the fact that the ring has been proved unstable for a certain perturbation, it is of interest to study other types of perturbations in order to obtain some knowledge about the way in which the ring breaks down. We know that the formation of mass condensations rotating with the ring is one possible way. We still do not know whether a small deformation, e.g., an elongation of the ring, without any change in the cross-section, will lead to destruction of the ring. We shall therefore consider a third type of perturbation.

3. The cross-section by a plane through the axis is left unchanged by the perturbation, while the radius D varies slightly with azimuth ϕ. Again we consider a fundamental wave disturbance, letting D vary according to the equation

$$D = D_0(1 + A_n e^{-in\phi}) . \tag{83}$$

The volume of the disturbed ring is

$$\pi ab \int_0^{2\pi} D_0(1 + A_n e^{-in\phi}) d\phi = 2\pi^2 ab D_0 . \tag{84}$$

The mean value of the radius in the disturbed ring is therefore D_0.

To discuss the stability, exactly the same method as before can be applied. We then start by obtaining the internal potential U_i of the perturbed ring. Bringing a unit mass from infinity to the interior point ξ_i, we pass first through a region where the infinitesimal

perturbation does not affect the field of force to our approximation and where we may replace the perturbed ring by an unperturbed ring of constant radius D_0. Inside a "transition point," ξ_t, the force is that of a ring of constant radius D, equal to the actual radius of the perturbed ring at the azimuth θ of the point in question. The potential of the ring of radius D_0, at the point ξ_t is $V_0(\xi_t)$. The potential of the ring of radius $D_0(1 + A_n e^{-in\theta})$ at the points ξ_t and ξ_i is $V_\theta(\xi_t)$ and $V_\theta(\xi_i)$. For the internal potential $V_i(\xi_i)$ of the disturbed ring we then can write, analogous to equation (57),

$$V_i(\xi_i) = V_0(\xi_t) - V_\theta(\xi_t) + V_\theta(\xi_i) . \tag{85}$$

The first two terms may be written

$$V_0(\xi_t) - V_\theta(\xi_t) = -\left[\frac{\partial V(\xi_t)}{\partial D}\right]_0 \Delta D = -\left[\frac{\partial V(\xi_t)}{\partial D}\right]_0 D_0 A_n e^{-in\theta} . \tag{86}$$

Introducing the internal potential $V_\theta(\xi_i)$ from equation (11) and making use of equation (86), we can write equation (85) in the form

$$V_i = -\left[\frac{\partial V(\xi_t)}{\partial D}\right]_0 D_0 A_n e^{-in\phi} - 2\pi ab\rho\left\{\log\frac{16D}{a+b} + \frac{1}{2}\left(1 - \frac{\alpha x^2 + \beta y^2}{ab}\right)\right\} . \tag{87}$$

We write ϕ instead of θ for the arbitrary azimuth of the point ξ_i. As usual, x and y are rectangular co-ordinates in a meridional plane, with origin at the center of the elliptical cross-section. D is a function of φ according to equation (83), and we get

$$\left.\begin{aligned} V_i &= -\left[\frac{\partial V(\xi_t)}{\partial D}\right]_0 D_0 A_n e^{-in\phi} - 2\pi ab\rho\left(\log\frac{16D_0}{a+b} + A_n e^{-in\phi} - \tfrac{1}{4}A_n^* A_n\right) \\ &\qquad + \frac{1}{2}\left(1 - \frac{\alpha x^2 + \beta y^2}{ab}\right), \\ &= -2\pi ab\rho\left\{\log\frac{16D_0}{a+b} + \frac{1}{2}\left(1 - \frac{\alpha x^2 + \beta y^2}{ab}\right) - (\vartheta - 1)A_n e^{-in\phi} - \tfrac{1}{4}A_n^* A_n\right\} , \end{aligned}\right\} \tag{88}$$

where

$$\vartheta = -\frac{D_0}{2\pi ab\rho}\left[\frac{\partial V(\xi_t)}{\partial D_0}\right] . \tag{89}$$

In order to obtain the potential energy of the ring, due to its own attraction, we must integrate equation (88) over the whole interior of the ring. We have for the potential energy

$$\begin{aligned} U &= \tfrac{1}{2}\iiint V_i \rho dx dy D d\phi , \\ &= -\frac{\rho}{2}\int_0^{2\pi}\int_{-b}^{+b}\int_{-a\sqrt{1-(y^2/b^2)}}^{+a\sqrt{1-(y^2/b^2)}} 2\pi ab\rho\left\{\log\frac{16D_0}{a+b} - (\vartheta - 1)A_n e^{-in\phi} - \tfrac{1}{4}A_n^* A_n \right. \\ &\qquad \left. + \frac{1}{2} - \frac{1}{2ab}(\alpha x^2 + \beta y^2)\right\} D_0(1 + A_n e^{-in\phi}) dx dy d\phi . \end{aligned}$$

An elementary integration over x and y, introducing the expressions for α and β from equation (7), gives

$$\left.\begin{aligned} U &= -\pi ab\rho^2 \int_0^{2\pi} \left\{ \log \frac{16D_0}{a+b} - (\vartheta - 1)A_n e^{-in\phi} - \tfrac{1}{4}A_n^* A_n + \tfrac{1}{4} \right\} \\ &\qquad \times (1 + A_n e^{-in\phi}) D_0 d\phi \,, \\ &= -2\pi^3 a^2 b^2 \rho^2 D_0 \left\{ \log \frac{16D_0}{a+b} + \tfrac{1}{4} - (\vartheta - \tfrac{1}{2})\tfrac{1}{2}A_n^* A_n \right\} . \end{aligned}\right\} \quad (90)$$

We shall determine ϑ in exactly the same way as we determined η for the last perturbation. By equation (9c) we see that if $\vartheta > \frac{1}{2}$, the potential energy is *increased* by the perturbation. Such an increase means a stabilizing effect. A large value of ϑ, therefore, corresponds to a higher degree of stability than a small value of ϑ. The smallest possible ϑ will give the most unstable case. It is seen by equation (89), however, that ϑ is positive and decreases when the transition point moves away from the ring. But the distance of the transition point increases with the wave length of the perturbation, and the largest distance, i.e., the smallest value of ϑ, will therefore occur for the perturbation with $n = 1$. By equations (85) and (89) we have

$$2\pi ab\rho\vartheta_1 \cdot A_1 e^{-i\theta} = V_i(\xi_i) - V_\theta(\xi_i) \,. \quad (91)$$

Again, instead of the internal point, ξ_i, we take an external point, ξ_e, close to the ring. The ring shall, further, be considered as an infinitely thin mass-circle. $V_e(\xi_e)$ is the external potential close to the perturbed ring, which has a radius varying with azimuth as $D = D_0(1 + A_1 e^{-i\phi})$. To a first approximation this perturbed ring is simply the original ring displaced a small distance $|A_1|$. The potential at a small distance r from a point on the ring is therefore simply

$$V_e(\xi_e) = -2\pi ab\rho \log \frac{8D_0}{r} \,. \quad (92)$$

The potential $V_\theta(\xi_e)$ is the potential close to a ring of radius equal to that of the perturbed ring at the azimuth of the point ξ_e, which is $D_0(1 + A_1 e^{-i\theta})$. The distance of ξ_e from this ring is, of course, also r, and the potential is

$$\left.\begin{aligned} V_\theta(\xi_e) &= -2\pi ab\rho \log \frac{8D_0(1 + A_1 e^{-i\theta})}{r} \,, \\ &= -2\pi ab\rho \log \frac{8D_0}{r} - 2\pi ab\rho A_1 e^{-i\theta} \,. \end{aligned}\right\} \quad (93)$$

Equations (91), (92), and (93) now give

$$\vartheta_1 = 1 \,. \quad (94)$$

Hence, by equation (90), the potential energy of the perturbed ring is

$$U = -2\pi^3 a^2 b^2 \rho^2 D_0 \left\{ \log \frac{16D_0}{a+b} + \tfrac{1}{4} - \tfrac{1}{4}A_1^* A_1 \right\} . \quad (95)$$

The potential energy due to the attraction of the central body, M_c, is

$$U_c = -\int_0^{2\pi} \frac{\pi ab\rho M_c}{D} \cdot Dd\phi = 2\pi^2 ab\rho M_c \,, \tag{96}$$

which is constant, unaffected by the perturbation. We therefore have the result that the whole potential energy of the system is increased by the perturbation. For perturbations of larger n, i.e., for perturbations causing several maxima and minima of the radius D around the ring, the increase in potential energy is still greater. We can, then, without further calculations, conclude that the ring is always stable for such perturbations. The rotation will only increase the stability.

4. Finally we shall consider a perturbation which is of interest in connection with our results about the equilibrium configurations in section II. We found that for each distance outside a certain limit there are two different elliptical cross-sections possible. The question is whether both are stable or not. To investigate this point, we shall consider a perturbation which consists in a variation of the ellipticity of the cross-section, while the radius D and the volume of the ring remain constant. Then the area πab of the cross-section also remains constant. We put

$$a = a_0(1 + A) \,, \tag{97}$$

where A is the infinitesimal relative perturbation of the half-axis a_0. Now we have

$$ab = \text{const} = c^2 \,,$$

and consequently

$$a + b = a + \frac{c^2}{a} = a_0(1 + A) + \frac{c^2}{a_0}(1 - A + A^2) = a_0 + b_0 + (a_0 - b_0)A + b_0A^2 \,,$$

and

$$\left.\begin{aligned} \log(a + b) &= \log(a_0 + b_0) + \frac{a_0 - b_0}{a_0 + b_0} A + \frac{b_0}{a_0 + b_0} A^2 - \frac{1}{2} \frac{(a_0 - b_0)^2}{(a_0 + b_0)^2} A^2 \\ &= \log(a_0 + b_0) + \frac{a_0 - b_0}{a_0 + b_0} A - \frac{a_0^2 - 4a_0b_0 - b_0^2}{2(a_0 + b_0)^2} A^2 \,. \end{aligned}\right\} \tag{98}$$

The potential energy of a uniform ring of elliptical cross-section is, by equation (47),

$$U = -\frac{M_R^2}{2\pi D}\left\{\log\frac{16D}{a + b} + \frac{1}{4}\right\} \,. \tag{99}$$

Introducing equation (98), we obtain the potential, after a small change in ellipticity corresponding to the change (eq. [97]) in a,

$$U = -\frac{M_R^2}{2\pi D}\left\{\log\frac{16D}{a_0 + b_0} - \frac{a_0 - b_0}{a_0 + b_0} A + \frac{a_0^2 - 4a_0b_0 - b_0^2}{(a_0 + b_0)^2} A^2\right\} \,. \tag{100}$$

The coefficient of A in equation (100) is the quantity γ from section II, equation (19). In equilibrium we have the following equation for γ:

$$\frac{M_e}{\pi\rho}\frac{1}{D^3} = \frac{\gamma(1-\gamma^2)}{1+\gamma+\gamma^2}, \tag{101}$$

according to equations (16) and (20). Now let our ring be one of extremely large radius D. Then, by equation (101) we have either $\gamma \approx 0$ or $\gamma \approx 1$. We consider each case separately.

If $\gamma \approx 0$, then $a_0 \approx b_0$. The linear term in A of equation (100) disappears, and we have

$$U = -\frac{M_R^2}{2\pi D}\left\{\log\frac{16D}{a_0+b_0} - A^2\right\}. \tag{102}$$

The potential energy due to the attraction by the central body is not affected when we neglect b^2/D^2. The moment of inertia of the ring also remains constant to the same approximation, so that the angular velocity and, consequently, the kinetic energy of rotation are unaffected. Since, by equation (102), the potential energy increases by the perturbation, it is therefore clear that the ring is stable. Hence the configuration with nearly circular cross-section is stable.

Let us now consider the configuration with highly elliptical cross-section. We have then $\gamma \approx 1$ or $b_0/a_0 \approx 0$. The potential energy becomes

$$U = -\frac{M_R^2}{2\pi D}\left\{\log\frac{16D}{a_0+b_0} - A + A^2\right\}. \tag{103}$$

It is seen that when A is negative the potential energy has been decreased by a first-order term. There are no terms in the expressions for the attraction of the central body or for the kinetic energy of rotation which could balance this decrease, and it follows that the ring is unstable for a small decrease of a. The configuration with very elliptical cross-section is therefore unstable. The ellipticity will decrease and the configuration go over to the nearly circular one.

YERKES OBSERVATORY
September 1941

THE SPECTRA OF WOLF-RAYET STARS AND RELATED OBJECTS*

P. SWINGS

ABSTRACT

New observational data are given for the spectra of several Wolf-Rayet stars. Evidence is produced for the presence of *C* IV in the WN sequence and for a central reversal of the *H*, *He* I, and *He* II lines. The spectra of two Of stars are described, and some properties of the Of shells are discussed, especially the ionization conditions and the excitation process. The absence of well-marked dilution effects and other considerations suggest that the size of a Wolf-Rayet shell is not much larger than that of the photospheric surface, so that an occultation effect should be expected in certain cases. The relative abundances of carbon and nitrogen in the ejected shells of Wolf-Rayet, Of, and P Cygni stars, as well as of novae, are discussed, since W objects have been observed which are intermediate between the pure nitrogen and carbon sequences. Suggestions are made concerning the classification, absolute magnitudes, temperatures, and radii of Wolf-Rayet stars and planetary nuclei, as well as concerning the application of Zanstra's theory to the nebulae with a Wolf-Rayet nucleus or to the Wolf-Rayet stars themselves.

In the last twelve years considerable progress has been made in the interpretation of the spectra of the Wolf-Rayet stars, especially through the work of Beals.[1] The subdivision into nitrogen and carbon sequences, which originated mainly in the papers by Perrine,[2] Lunt,[3] and J. S. Plaskett,[4] was discussed in considerable detail by Beals on the basis of the laboratory work by Edlén[5] and gave rise to the classification officially adopted by the International Astronomical Union at the 1938 meeting (notations WN and WC).[6] Simultaneous work by C. H. Payne dealt with the same subject.[7] Recent papers by O. C. Wilson[8] and by S. Gaposchkin[9] on the eclipsing binary BD+38°4010 (HD 193576, HV 11111; WN5+B1) have also thrown some new light on the physical characteristics of the Wolf-Rayet stars.

Two years ago the spectroscopic group at the Yerkes and McDonald observatories engaged in a large program of observations of all types of outer envelopes which are not accounted for by the elementary theories of stellar atmospheres. The problem of the Wolf-Rayet stars was included in this program, as it was believed that additional observational material might clarify our general ideas regarding the chemical constitution, the geometrical and dynamical picture, and the essential physical processes of these hot stars.

Additional observations were especially desirable in four directions: the southern Wolf-Rayet stars, some of which had been obtained with slitless spectrographs, and dis-

* *Contributions from the McDonald Observatory, University of Texas*, No. 40. This paper was presented at the symposium on astronomical spectra held at the Yerkes Observatory in celebration of the Fiftieth Anniversary of the University of Chicago on September 10–12, 1941.

[1] *Pub. Dom. Ap. Obs.*, **4**, 271, 1930; **6**, 95, 1934; *M.N.*, **90**, 202, 1929; **92**, 577, 1932; *J.R.A.S. Canada*, **34**, 169, 1940; *Observatory*, **64**, 42, 1941.

[2] *M.N.*, **81**, 142, 1920. Perrine already considers in some detail the different behavior of λ 4634 and λ 4641 (*N* III), on one hand, and of λ 4650 (*C* III), on the other.

[3] *M.N.*, **80**, 534, 1920.

[4] *Pub. Dom. Ap. Obs.*, **2**, 346, 1924.

[5] *Zs. f. Ap.*, **7**, 378, 1933; this paper contains the applications of Edlén's laboratory work to the identification of lines in W stars.

[6] *Trans. I.A.U.*, **6**, 248, 1938.

[7] *Zs. f. Ap.*, **7**, 1, 1933.

[8] *Pub. A.S.P.*, **51**, 55, 1939; *Ap. J.*, **91**, 379, 1940, and **91**, 394, 1940.

[9] *Ap. J.*, **93**, 202, 1941.

cussed by C. H. Payne during the period 1927–1933;[10] the Wolf-Rayet nuclei of planetary nebulae, which had been the object of the remarkable pioneering investigations by Wright[11] but for which further progress was anticipated in view of the recent instrumental advances; the objects intermediate between the pure absorption O stars and the W stars, to supplement earlier work by Wright,[12] H. H. Plaskett,[13] J. S. Plaskett,[14] and C. H. Payne;[15] and the Wolf-Rayet characteristics in novae, especially those of the slow type.[16]

In collaboration with O. Struve, we have already collected and discussed a fairly large amount of observational material.[17] Although our program has not yet been completed, we shall give here the main general results as they appear at the present stage, together with a description of some new observational material. From the beginning of our program in 1939 we planned to investigate the profiles of the emission and absorption lines and this photometric work will be carried on in the near future.

I. NEW OBSERVATIONAL DATA ON SOME WOLF-RAYET STARS

For physical discussions of Wolf-Rayet stars it is useful to possess, besides the general table of Wolf-Rayet lines as published by Beals, detailed descriptions of individual objects. Such descriptions have been published by J. S. Plaskett for six stars (three WN's and three WC's, including Campbell's object $+30°3639$), by Wright for several planetary nuclei, by C. H. Payne for several southern stars, and by Struve and Swings for the nuclei of $+30°3639$, NGC 6543, IC 418, NGC 40, IC 4997, and HD 167362.

In this section we shall give additional data for several Wolf-Rayet stars which are not surrounded by visible nebulosity.

HD 151932.[18]—This star is located in the cluster NGC 6231 in Scorpius, as are also three other objects described in this and in the following section.[19] The spectrum was described by C. H. Payne,[20] together with several other stars in which both emission and absorption lines are present, the latter being strong and significant. Spectrograms of this star have been published by Beals,[21] who classified it as WN 7.[22] For possible discussions of line widths, we have collected in Table 1 our measurements of this spectrum; these data could be added to the values of the line widths as given by Beals, and they confirm the well-established decrease in width with increasing ionization of the same atom. The sharpness of the *N* v lines is particularly conspicuous (Pl. IV, *a*).

[10] *Harvard Bull.*, Nos. 834, 836, 842, 843, 844, 855, 874, 878; *Zs. f. Ap.*, **7**, 1, 1933.

[11] *Pub. Lick Obs.*, **13**, 193, 1918; see also Stoy, *Pub. A.S.P.*, **47**, 162, 1935.

[12] *Op. cit.*, 206.

[13] *Pub. Dom. Ap. Obs.*, **1**, 325, 1922.

[14] *Loc. cit.*

[15] *Harvard Bull.*, Nos. 842, 843, 844, 1927.

[16] See Edlén's report to the Paris conference on novae and white dwarfs, 1939.

[17] Papers published on this problem in collaboration with O. Struve: *Ap. J.*, **91**, 546, 1940; **92**, 289, 1940; **92**, 295, 1940; **93**, 349, 1941; **93**, 356, 1941; *Proc. Nat. Acad. Sci.*, **26**, 454, 1940; **26**, 458, 1940; **26**, 548, 1940; **27**, 225, 1941; *Pub. A.S.P.*, **52**, 394, 1940; **53**, 35, 1941.

[18] CD $-41°10972$; $m_v = 6.56$; α (1900) $= 16^h45^m.3$; δ (1900) $= -41°41'$; WN7 according to Beals. I most sincerely thank Mrs. C. Payne Gaposchkin, who called our attention to the W and O stars in NGC 6231.

[19] For investigations of this cluster see D. A. MacRae, *Harvard Bull.*, No. 914, p. 21, 1940, and references to earlier publications mentioned in this paper. The distance of the O stars appears to be 300 parsecs, and the photographic absorption amounts to 1.7 mag.

[20] *Harvard Bull.*, No. 843, 1927.

[21] *Trans. I.A.U.*, **6**, 248, Pl. I, 1938; *J.R.A.S. Canada*, **34**, Pl. VIII, 1940.

[22] WN6 would seem better, according to our spectrograms.

TABLE 1

SPECTRUM OF HD 151932 (WN7)

λ	Intensity	Violet Edge	Red Edge	Identification			Width		Notes
				Element	λ	Intensity	In A	In Km/Sec	
3888	1E			*He* I	88.65	10			
				H_8	89.05				
				He II	87.47				
3969	1E			$H\epsilon$	70.08				
				He II	68.47				
4026.4	1E			*He* I	26.19	5			
4056.5	3E			*N* IV	57.80	2			
4100	3En			*N* III	97.31	10			1
				N III	103.37	9			
				$H\delta$	101.75				
				He II	100.08	2			
4199.9	2E			*He* II	99.87	2			2
4335.2	2A	32.40	38.16	$H\gamma$	40.48		5.76	398	
4341.2	4E	38.16	50.43	*He* II	38.71	3	12.27	848	
4388	1E			*He* I	87.93	3			
4475.3	1E	64.33	84.14	*He* I	71.48	6	19.81	1329	3
4515.3	2E	06.2	22.4	*N* III	10.92	6			
				N III	14.89	7			
4537.4	1A	34.74	38.84	*He* II	41.63	5	4.10	271	
4544.1	3E	38.84	48.96				10.12	668	
4602.49	3A	599.44	04.42	*N* V	03.2		4.42	288	
4606.41	2E	04.42	08.77				4.35	284	
4619	1E			*N* V	19.4				
4638.50	8E	27.76	47.84	*N* III	34.16	9	20.08	1299	4
				N III	40.64	10			
				N III	41.90	7			
4671.87	4A	66.22	76.91	*He* II	85.81	300	10.69	684	
4686.67	8E	76.91	96.47				19.56	1252	
4735.5	0+E			*N* IV	33.				
4853.95	1A			*He* II	59.36	7			
4862.18	4E	55.58	68.96	$H\beta$	61.34		13.38	825	

TABLE 1—*Continued*

λ	Intensity	Violet Edge	Red Edge	Identification			Width		Notes
				Element	λ	Intensity	In A	In Km/Sec	
5405.01	2A	.....	.....						
5412.07	3E	.....	.....	*He* II	11.57	50			5
5416.89	3E	.....	.....						
5876	4E	.....	.....	*He* I	75.62	10	.....	.....	6
6561	5E	.....	.....	*Hα*	62.32	.....	.....	.....	
				He II	60.16	100			

NOTES TO TABLE 1

The wave lengths given in the first column correspond to the maxima of the emission or absorption lines.

1. Very broad feature.
2. Possibly double.
3. Violet absorption probably present.
4. In λ 4638, two maxima are observed corresponding to *N* III 4634 and *N* III 4641. The presence of a faint line near *C* IV 4658 is not excluded.
5. Double emission; central minimum at λ 5413.9.
6. Strong violet absorption present.

HD 192163.[23]—Although this star is a typical representative of class WN6, all the lines are not identified with certainty (Pl. IV, *b*). This is especially true of a fairly strong line situated to the blue of *He* I 5876. The wave length of this line was measured by J. S. Plaskett in HD 192163 at λ 5812 (intensity 4, compared to intensity 6 for *He* I 5876 and intensity 14 for *He* II 5411). The other measures collected by Beals were λ 5807 (Campbell), λ 5807 (Wright), and λ 5806 (Beals), and he finally adopted the value λ 5806. We measured the same band on an excellent spectrogram and obtained λ 5803 for the center of the emission.

The exact wave length is certainly very near λ 5805, and it cannot be shifted appreciably in either direction, since the violet-absorption component of the measured line is absent or extremely weak and since the violet-absorption component of D_3 5876 is fairly sharp and does not extend to the blue beyond λ 5842.

The line is observed in the nitrogen sequence where it reaches its maximum in the subclass WN6; it is still observed in WN7. It has been attributed by Beals to a predicted transition of *N* IV, whereas Edlén[24] had identified it tentatively with *C* IV(?). The predicted multiplet of *N* IV considered by Beals is $3p'\ ^3P - 3d'\ ^3P^o$ (excitation potential of upper level 63.1 volts). Although the transition has not been observed in the laboratory, the relative values of the levels are fairly well known; actually $3d'\ ^3P^o$ combines with $2p'\ ^3P$ (strong group at λ 298), which in turn combines with $2p^3P^o$ (strong group near λ 923) and $3s'\ ^3P^o$ (intense lines near λ 345). Finally, the transitions between these last two levels and $3p'\ ^3P$ have been observed in the laboratory. The uncertainty in the relative positions of the levels $3p'\ ^3P$ and $3d'\ ^3P^o$ thus results mostly from possible errors of measurement in the vacuum ultraviolet multiplets. But, considering the precision of

[23] BD+ 37°3821; α (1900) = 20^h8^m4; δ (1900) = +38°03′; WN6 according to Beals.

[24] *Zs. f. Ap.*, **7**, 378, 1933.

Edlén's measures of the *N* IV spectrum, it does not appear possible to accept an error of more than 5 A in the predicted wave lengths. These are given in Table 2.[24] The center of gravity of the three broad lines should thus be around λ 5830,[25] and it does not seem possible to explain the difference of 25 A between the predicted wave lengths and the wave length measured in HD 192163. The predicted multiplet should be much weaker than the "unprimed" transition $3s^3S - 3p^3P^o$ (near λ 3481) and $3p^1P^o - 3d^1D$ (λ 4057.8). Additional laboratory work would be most valuable.

Under the present conditions it appears more logical to attribute the line to the $3s^2S - 3p^2P^o$ transition of *C* IV (excitation potential of $3p^2P^o$, 39.5 volts); the laboratory wave lengths are λ 5801.51 (intensity 4) and λ 5812.14 (intensity 3). This doublet is the most striking characteristic of *C* IV in WC stars, the other (corresponding to the much higher excitation potential of 58 volts and to higher *n*-values) being $5g^2G^o - 6h^2H$ at λ 4658.64 and $5f^2F - 6g^2G^o$ at λ 4656.5. Unfortunately, in nitrogen stars, these blue

TABLE 2

PREDICTED WAVE LENGTHS AND THEORETICAL RELATIVE INTENSITIES OF THE $3p'\ ^3P - 3d'\ ^3P^o$ TRANSITIONS IN *N* IV

	λ	Intensity		λ	Intensity
$3p'\ ^3P_1 - 3d'\ ^3P^o_2$	5812	5	$3p'\ ^3P_2 - 3d'\ ^3P^o_2$	5846	15
$3p'\ ^3P_2 - 3d'\ ^3P^o_1$	5828	5			

lines would fall between *He* II 4686 and the group of nitrogen lines λλ 4603 (*N* V), 4619 (*N* V), 4634 (*N* III), 4641 (*N* III), so that their detection is extremely difficult.[26] Besides, if lower excitation enhances a line in an outer shell, the doublet λλ 5802–5812, which corresponds to an excitation potential 19 volts lower than λ 4658, would be relatively enhanced. In their theoretical synthesis of supernova spectra, Whipple and C. P. Gaposchkin consider λ 5806 as very much stronger than the group near λ 4658,[27] this being in consequence of the lower *n*-values.

The ionization potential of C^{+++} being 64.2 volts as compared to 47.2 volts for N^{++} and 77.0 volts for N^{+++}, it is natural that the line λ 5805, if due to *C* IV, should reach its maximum in the same subclass as *N* IV (WN6) but should still be present in WN7.

The *C* IV doublet is usually observed as a broad band in WC stars; but in some cases the two components are well separated, i.e., in the nuclei of NGC 6543[28] and in Campbell's envelope star. In the latter case Wright[29] measured three lines at λλ 5801, 5812, and 5828; the first two belong to *C* IV and the third to *C* III.

[25] This value was also adopted by Whipple and C. P. Gaposchkin in their theoretical synthesis of the supernova spectra, *Proc. Amer. Phil. Soc.*, **84**, 1, 1941.

[26] According to our measurements, the red wing of the broad emission observed in HD 192163, with maximum around 4638 A seems to extend too far to be attributed to *N* III only; there may thus be some blending effect by *C* III and *C* IV in the red wing. Actually, in the same spectrum, J. S. Plaskett measured two maxima in the broad band near λ 4640, one of intensity 10 at λ 4631 (*N* III), the other of intensity 6 at λ 4652 (*C* III, *C* IV); but this difficult observation remains somewhat doubtful.

[27] Because of blends, the only $6 \rightarrow 5$ transitions of *C* IV observed by Edlén in the laboratory were $5g^2G - 6h^2H^o$ at λ 4658.64 (lab. int. 5) and $5p^2P^o - 6d^2D$ at λ 4441.81 (lab. int. 0). The other $6 \rightarrow 5$ transitions have been predicted by Edlén at λλ 4656.5 ($5f^2F^o - 6g^2G$), 4646.5 ($5d^2D - 6f^2F^o$), 4659.38 ($5g^2G^o - 6f^2F^o$), and 4664.5 ($5f^2F^o - 6d^2D$). By analogy to the relative laboratory intensities observed among the $5 \rightarrow 4$ transitions, it appears that λ 4658.64 must be the strongest of the $6 \rightarrow 5$ transitions, the intensities among the lines to the blue of λ 4658.64 decreasing with decreasing quantum number *L*. This is opposite to what Whipple and C. P. Gaposchkin have adopted in their work on supernovae.

[28] R. H. Stoy, *Lick Obs. Bull.*, **17**, 179, 1935; P. Swings, *Ap. J.*, **92**, 289, 1940.

[29] *Op. cit.*, p. 193, 1918.

PLATE IV

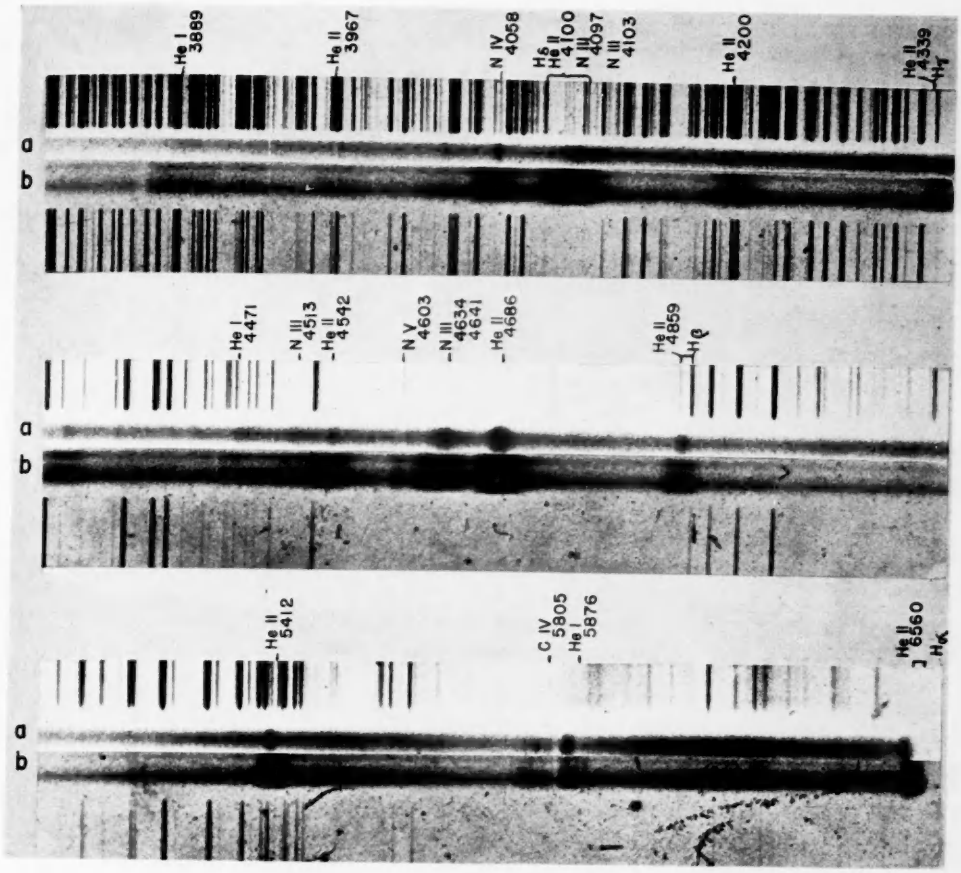

Spectra of two Wolf-Rayet stars belonging to the nitrogen sequence: (*a*) HD 151932 (WN6+); (*b*) HD 192163 (WN6).

PLATE V

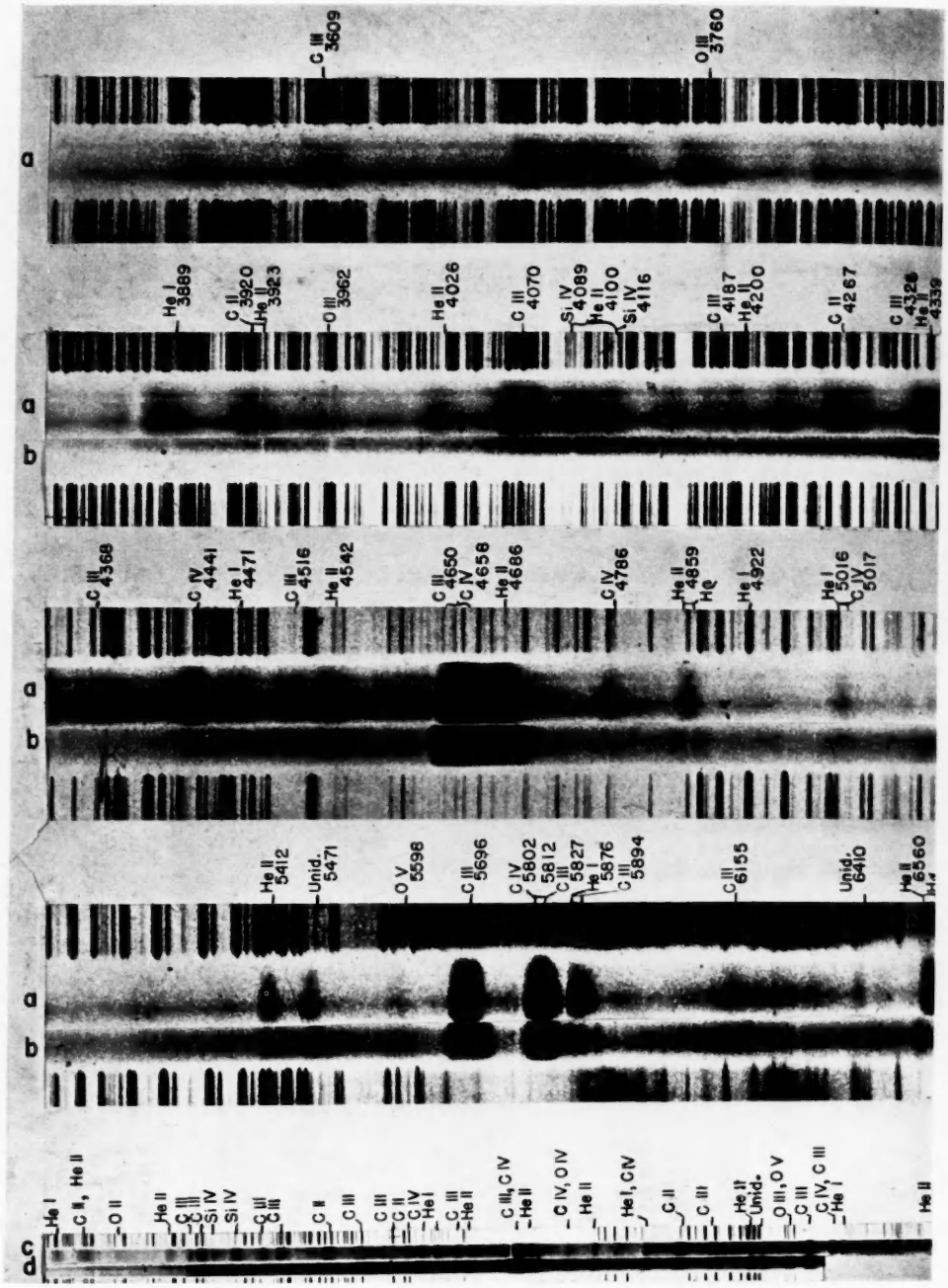

Spectra of Wolf-Rayet stars belonging to the carbon sequence: (*a*) HD 192103 (WC7); (*b*) HD 152270 (WC6+) (central reversal in $H\beta$); (*c*) HD 164270 (WC8); (*d*) HD 156385 (WC6).

PLATE VI

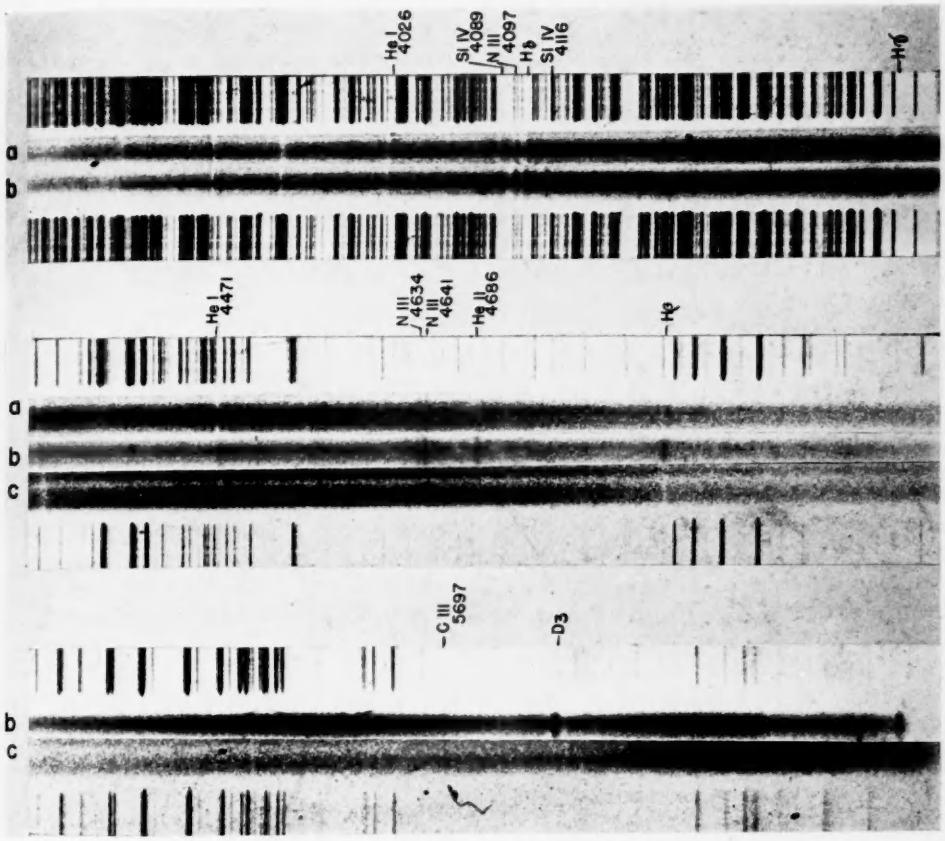

Spectra of three O7f stars: (*a*) HD 151804; (*b*) HD 152408; (*c*) HD 192639

PLATE VII

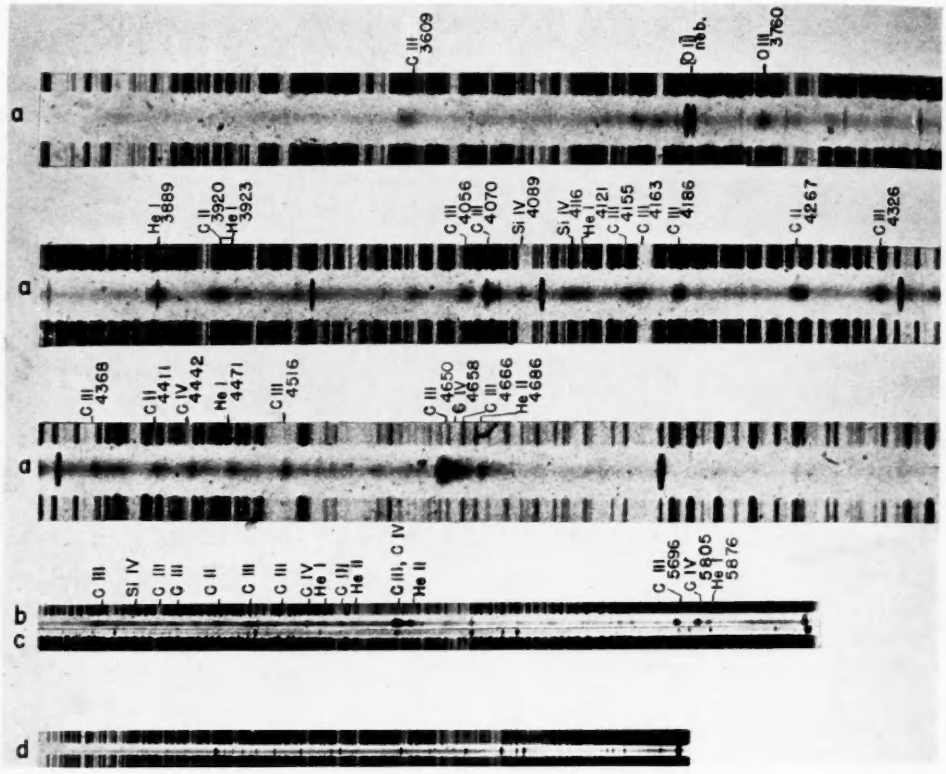

Spectra of planetary nebulae and their nuclei: (*a*) BD+30°3639; (*b*) NGC 40; (*c*) HD 167362 ($\lambda > 4000$); (*d*) HD 167362 (including ultraviolet region).

The conclusion to be drawn is that in some WN stars there is rather conclusive evidence in favor of the presence of carbon lines, although nitrogen is more abundant: only additional laboratory work would settle the matter definitely. But it will be shown in section III that the simultaneous presence of *C* and *N* is by no means exceptional in planetary nuclei of Wolf-Rayet type.

HD 152270.[30]—This object is also located in the cluster NGC 6231. Its spectrum was described by C. H. Payne,[31] who identified *He* II, *C* III, *C* IV, *N* IV, and *N* V. Although these identifications have to be revised, the description by Miss Payne is very important, because she called attention to the central reversals which were present in certain lines, in addition to the violet absorptions. This observation, which will be discussed in section III, has not received the attention it deserves and will eventually help in understanding the physical processes involved.

The following lines are observed on our spectrograms (Pl. V, *b*):

C II	4267 (1–0)
C III	4070 (3); 4187 (1); 4326 (1); 4516 (1 blended); 4650 (20, blended with *C* IV); 5696 (15); 5894 (1); 6155 (2)
C IV	4441 (1); 4650 (20, blended with *C* III); 4786 (1) 5806 (20)
He I	5876 (3)
He II	4542 (1 blended); 4686 (8); 4859 (1); 5412 (3)
O V	5114 (1–2); 5590 (2)

The central undisplaced reversal is present in all Balmer lines and in several lines of *He* I (λ 4471 and λ 5016) and *He* II (λλ 4200, 4542, 5412); a comparison of $H\gamma$ and *He* I 4471 shows that the central absorption is sharper in *He* I than in *H*. Similarly the central absorptions are sharper for *He* II than for *H*. In the region of the higher members of the Balmer series the wings of the Balmer emissions overlap, so that only the central absorptions appear clearly, and these may be followed to H_{13}. There is no appreciable reversal in *C* III 4070, *C* III + *C* IV 4650, *C* III 5696 or *He* II 4686.

As usual, the *C* III lines are much broader (width of *C* III 5696: 72.5 A or 3800 km/sec) than the *C* IV lines (width of the blend of λ 5801 and λ 5812 of *C* IV: 51.8 A; this width would have been reduced to about 45 A or about 2300 km/sec if the line had been simple).

According to the intensity ratios (and to the line widths), the star should really be considered as intermediate between WC6 and WC7 and might be called WC6+. According to the intensity criteria adopted by the International Astronomical Union, the object is later than WC6; but compared with the typical WC7 star—HD 192103(Pl. V, *a*)—the intensity ratio of *He* I 5876 and *C* IV 5806 is smaller in this star.

HD 164270.[32]—This object has a remarkable Wolf-Rayet spectrum in which both emission and absorption lines are present (Pl. V, *c*). It was described by C. H. Payne,[33] who noticed that the widths of the lines were of the order of 10 A. Since our material appears to be better than Payne's and since the identifications may now be improved, our measured wave lengths are collected in Table 3. Unidentified lines have been measured at λλ 4451.6 (1), 5092.9 (1), and 5471.0 (5); they are also present in BD+30°3639. Another unidentified line at λ 6410.5 was also observed in HD 192103. Except for the fact that the lines are broader, the present object is very similar to +30°3639 and constitutes an excellent example of a WC8 star.

[30] CD− 41°11041; m_v = 6.72; α (1900) = $16^h47^m.3$; δ (1900) = 41°40′; classified WC6 by Beals.

[31] *Harvard Bull.*, No. 844; *Zs. f. Ap.*, **7**, 1, 1933.

[32] CD− 32°13623; m = 8.8; α (1900) = $17^h55^m.2$; δ (1900) = − 32°43′; classified WC8 by Beals.

[33] *Harvard Bull.*, No. 843, 1927.

TABLE 3

SPECTRUM OF HD 164270 (WC8)

λ	Intensity	Violet Edge	Red Edge	Identification			Width		Notes
				Element	λ	Intensity	In A	In Km/Sec	
3888.7	3E	81.72	94.40	*He* I	88.65	10	15.68	1209	1
				C III	89.18	4			
				C III	85.99	3			
3923.3	3E	12.32	33.41	*C* II	18.98	9	21.09	1611	
				C II	20.68	10			
				He II	23.51	.....			
3960.9	1Enn	.....	.....	*O* III	61.59	8	.....	.....	
				He I	64.73	4			
4026.5	2–3E	20.38	35.63	*He* II	25.64	.....	15.25	1136	
				He I	26.19	5			
4055.5	3E	50.61	59.80	*C* III	56.06	5	9.19	680	
4071.6	5E	64.94	78.06	*C* III	67.87	9	13.12	967	2
				C III	68.97	10			
				C III	70.30	10			
				O II	75.87	10			
				C II	76.00	7			
				C II	74.89	5			
				C II	74.53	6			
4088.8	2E	84.85	93.11	*Si* IV	8.86	10	8.26	606	
4099.1	1E	95.24	101.86	*Hδ*	101.76	.....	6.62	484	
				He II	100.08	.....			
4122.7	4E	12.85	29.54	*Si* IV	16.10	8	16.69	1213	
				He I	20.81	3			
				C III	22.05	3			
4161.2	4E	49.34	70.15	*C* III	62.80	5	20.81	1500	
				C III	56.50	4			
4186.8	5E	81.31	93.33	*C* III	87.05	10	12.02	861	2
				O II	89.79	10			
4200.0	1E	.....	.....	*He* II	199.87	.....	.....	.....	
4267.5	8E	58.23	77.78	*C* II	67.27	20	19.55	1374	
				C II	67.02	19			
4325.0	6E	16.05	33.50	*C* III	25.70	8	17.45	1209	
4339.4	1E	.....	.....	*He* II	38.71	.....	.....	.....	
				Hγ	40.48	.....			
4367.3	3E	61.75	72.51	*C* III	68.14	4	10.77	740	
4385.8	3E	75.71	95.65	*He* I	87.93	3	19.96	1365	
				C III	88.24	2			
				C III	83.24	1			

TABLE 3—*Continued*

λ	Intensity	Violet Edge	Red Edge	Identification			Width		Notes
				Element	λ	Intensity	In A	In Km/Sec	
4414.1	2–3E	06.03	21.84	*C* II	11.52	5	15.81	1073	
				C II	11.20	5			
				O II	14.89	10			
				C II	10.06	4			
4441.2	4E	35.61	45.85	*C* IV	41.81	0	10.24	691	
4451.6	1E	45.85	56.28	.....	.....	.....	10.43	702	3
4461.7	2A	58.56	64.59	*He* I	71.48	6	6.03	405	
4472.4	5E	64.59	80.72				16.13	1082	
4516.7	5E	09.36	23.56	*C* III	16.93	4	14.20	943	
				C III	16.02	3			
4542.2	2E	37.04	56.69	*He* II	41.63	5	.....	.....	
4554.1	2E			*Si* III	52.61	9	.....	.....	
				O V	54.28	0			
4572.8	0–1E	.....	.....	*Si* III	67.83	7	.....	.....	
				Si III	74.75	4			4
4594.8	0–1E	.....	.....	*C* III	93.47	2d	.....	.....	
				O II	90.98	9			
				O II	96.19	8			
4638.0	5A	33.85	41.51	*C* III	47.40	20	7.66	495	
				C III	50.16	19			
4650.8	20E	41.51	75.04	*C* III	51.35	18	33.53	2166	5
				O II	49.15	10			
				Si IV	54.14	4			
				C IV	58.64	5			
				C IV	56.5	4			
				C IV	46.5	2			
4686.4	6E	80.39	96.29	*He* II	85.81	300	15.90	1018	
4711.1	1E	.....	.....	*He* I	13.14	3	.....	.....	
4783.9	2E	79.68	89.24	*C* IV	85.6	.....	9.56	599	
				O IV	83.4	2			
4858.2	4E	54.66	66.15	*He* II	59.36	.....	11.49	709	
				Hβ	61.34	.....			
4922.6	2E	14.51	30.46	*He* I	21.93	4	15.95	971	
5002.2	3A	999.12	05.11	*He* I	15.67	6	5.99	358	
				C IV	15.9	.....			
5015.7	5E	05.11	26.63	*C* IV	17.7	.....	21.52	1287	6
5092.9	1E	86.52	100.05	.....	.....	.....	13.53	797	3

TABLE 3—*Continued*

λ	Intensity	Violet Edge	Red Edge	Identification			Width		Notes
				Element	λ	Intensity	In A	In Km/Sec	
5133.2	7E	24.16	42.63	(C II	32.96	3)	18.47	1080	7
				(C II	33.29	2)			
5244.3	1E	40.37	56.42	C III	44.5	0	.....	.....	
5252.1	3E			C III	53.55	1	.....	.....	
				C III	49.6	0			
5272.3	3E	65.88	76.37	C III	72.56	2	10.49	597	
5304.67	4E	298.24	09.30	(O IV	05.	pr)	11.06	626	3
5343.3	1E	.....	.....	(C II	36.7	0)	.....	.....	
5413.9	5E	05.59	21.20	He II	11.57	.....	15.61	866	8
5471.0	5E	64.62	75.30	.....	.....	.....	10.68	586	9
5596.1	3E	88.00	601.74	O III	92.37	6	13.74	736	
				O V	97.9	.....			
5650.8	1E	33.12	65.05	C II	48.08	3	31.93	1695	
				C II	62.51	4			
5668.8	1A?	.....	.....	C III	96.0	8	.....	.....	
5697.2	15E	76.53	714.23				37.70	1987	
5789.2	4A	82.67	94.54	C IV	01.51	4	.....	.....	10
				C IV	12.14	3			
5822.2	10E	794.54	41.93	C III	27.1	1	47.39	2442	
5860.3	2A	.....	.....	He I	75.62	10	.....	.....	
				C II	91.65	3			
5880.2	10E	65.65	905.45	C II	89.97	4	39.80	2030	11
				C III	71.6	pr			
				C III	94.1	pr			
6102.8	1E	.....	.....	C II	98.62	3	.....	.....	
				C II	95.37	2			
6154.8	4E	.....	.....	C III	54.4	pr	.....	.....	
				C III	55.4	pr			
				C III	56.7	pr			
6207.1	2E	.....	.....	.....	.....	.....	.....	.....	3
6410.5	2E	.....	.....	.....	.....	.....	.....	.....	12
6464.2	4E	.....	.....	.....	.....	.....	.....	.....	3

TABLE 3—*Continued*

λ	Intensity	Violet Edge	Red Edge	Identification			Width		Notes
				Element	λ	Intensity	In A	In Km/Sec	
6519.9	1E								
6561	6E			*Hα*	62.82				13
				He II	60.16				
				C II	78.03	10			
				C II	82.85	9			
				C III	92.3	pr			

NOTES TO TABLE 3

1. Fairly strong violet absorption.
2. May have a weak violet absorption.
3. Also present in BD+30°3639.
4. Uncertain.
5. A secondary maximum at λ 4665.9 corresponds to λλ 4665.90 (*C* III, int. 6), 4663.53 (*C* III, int. 4), 4664.5 (*C* IV, int. 1), and 4661.65 (*O* II, int. 9).
6. Probably a broad line to the red of λ 5026.
7. λ 5133 is superposed on a broader line of intensity 1En extending from 5114.3 to 5164.3 and due (at least partly) to a blend of *C* II lines (λλ 5114.07 [2], 19.55 [2], 21.69 [1], 43.49 [2], 45.16 [5]). In BD+30°3639, Wright mentions a group of two or more faint emission bands below λ 5131 and extending to about λ 5162.
8. Weak violet absorption present.
9. One of the strongest unidentified lines.
10. The three components are separated in BD+30°3639.
11. Violet edge much sharper than red edge.
12. Also present in BD+35°4013 (HD 192103, WC7).
13. Broad and complex band.

HD 156385[34] *and HD 168206.*[35]—These objects were described by C. H. Payne,[36] and the second was also observed by Beals. In agreement with Beals, they must be classified as carbon stars (Pl. V, *d*). No nitrogen line was observed in our spectrograms, contrary to identifications suggested by C. H. Payne.[37]

In HD 168206 there may be a central reversal in *He* II 4542. The spectrum of this star is mainly characterized by strong *C* III, λ 5696 being stronger than *C* IV 5806; *He* II is weak, and *He* I, as well as *H*, is very weak.

II. NEW DATA ON THREE OBJECTS INTERMEDIATE BETWEEN WOLF-RAYET AND ABSORPTION O STARS

Several typical examples of objects showing an absorption spectrum of O type, on which are superposed vestiges of emission, have been described previously,[38] for example,

[34] CD− 45°11392; m = 7.2; α (1900) = 17^h12^m1; δ (1900) = − 45°32′; classified as WC6 by Beals.

[35] BD− 11°4593; m = 8.9; α (1900) = 18^h13^m5; δ (1900) = − 11°40′; classified as WC7 by Beals.

[36] *Harvard Bull.*, No. 844, 1927.

[37] *Zs. f. Ap.*, **7**, 1, 1933.

[38] *Ap. J.*, **91**, 553, 1940, and earlier references mentioned there; *Pub. A.S.P.*, **52**, 394, 1940 (HD 192639); **53**, 35, 1941 (HD 108); *Proc. Nat. Acad.*, **27**, 225, 1941 (IC 418).

9 Sagittae, BD+35°3930*N*, 29 Canis Majoris, the nucleus of NGC 2392, the nucleus of IC 418, HD 192639, HD 108, and several southern stars.

To supplement the descriptions given by C. H. Payne[39] of spectra of southern stars of a similar type, we shall give here some additional data on two O stars situated in the cluster NGC 6231, i.e., HD 151804 and HD 152408.

HD 151804.[40]—This star (Pl. VI, *a*),usually referred to as O9f,[41] has an absorption spectrum which is very similar to that of 9 Sagittae, and it should thus be classified as O7f. Emission is observed in the following lines: *Hα* and *Hβ* (the latter with violet absorption); *He* I 5876; *He* II 4686; *N* III 4634 and 4641; *C* III 5696. As in 9 Sagittae, *N* III 4097 and 4103 are present only as strong absorptions; an unidentified line measured at λ 4485 is also present in 9 Sagittae. The peculiar selectivities observed among the *N* III lines in the shell of 9 Sagittae are also observed in HD 151804. The *C* III line has about the same intensity as *N* III 4640, so that the relative intensities of *C* III and *N* III in the present star are intermediate between those in 9 Sagittae (*N* III strong, *C* III weak) and HD 192639 (*C* III strong, *N* III weak [Pl. VI, *c*]).

HD 152408.[42]—As in 9 Sagittae, all the lines of the Pickering series of *He* II are observed in pure absorption; they are seen clearly to λ 3769.3 ($n = 22$) and certainly belong to the underlying star (Pl. VI, *b*). On the contrary, the strong emission at λ 4686 belongs to an outer shell. The Balmer lines are observed in emission to *Hε*, the line *Hα* being about of the same intensity as D_3; no part is being played in the Balmer emission by *He* II, since λ 4541 and λ 5412 of *He* II are present in pure absorption. Many *He* I lines have both an emission and an absorption component (i.e., λλ 5876, 4026, 4121, 4471). Five lines of *N* III are observed in the shell (emission and violet absorption), but our spectrograms do not show any trace of *N* IV. *C* III 5696 is an emission of intensity (4*E*), comparable to the lines λλ 4097 (4*E*), 4103 (4*E*), and 4634 (5*E*) of *N* III.[43] An unidentified line, which was also present in 9 Sagittae, was measured near λ 4503 (1 A, 1*E*). The width of the "nuclear" line λ 4542 (5 A) is 6.13 A or 405 km/sec. For future discussions, it is useful to tabulate the widths and displacements of a number of lines of the shell. These are given in Table 4.

Some characteristics of the shells in Of stars.—Striking variations have been observed recently in the spectrum of the Of star HD 108.[44] Less conspicuous variations have taken place in 9 Sagittae, BD+35°3930*N*, HD 34656, and HD 190864. This is probably true also for some of the southern stars previously described by C. H. Payne but for which recent McDonald spectrograms differ appreciably from Miss Payne's description. These variations concern only the outer shells which give rise to emission and displaced absorption lines, and they emphasize the temporary character of certain of these shells.

Previous investigations of Of stars have emphasized the strong selection shown by the emission and absorption lines in the shells of 9 Sagittae,[45] BD+35°3930*N*,[45] HD 192639,[46] the nucleus of IC 418,[47] and some other peculiar stars. This selection is summarized in Table 5.

It appears at once that this selection has no connection either with the metastability of certain spectral terms or with the excitation potential. A similar, yet unexplained,

[39] *Harvard Bull.*, Nos. 842, 843, 878, 1927; *Zs. f. Ap.*, **7**, 1, 1933.

[40] CD− 41°10957; $m_v = 5.4$; α (1900) = 16^h44^m5; δ (1900) = − 41°04′.

[41] The suffix *f* used by the Victoria observers refers to the emission at λλ 4634, 4640, and 4686.

[42] CD− 40°10919; $m = 6.03$; α (1900) = 16^h48^m0; δ (1900) = − 41°00′.

[43] The observation of *C* III in HD 151804 and HD 152408 is in disagreement with the inclusion of these stars by C. H. Payne in a group of stars without carbon (*Zs. f. Ap.*, **7**, 1, 1933).

[44] *Pub. A.S.P.*, **53**, 35, 1941.

[45] *Ap. J.*, **91**, 569, 1940.

[46] *Pub. A.S.P.*, **52**, 394, 1940.

[47] *Proc. Nat. Acad.*, **27**, 225, 1941.

TABLE 4

SHELL OF HD 152408

Element	Wave Length	Absorption			Emission			Distance between Centers of Absorption and Emission Components (in Km/Sec)
		Intensity	Width in A	Width in Km/Sec	Intensity	Width in A	Width in Km/Sec	
H.....	*Hγ*	2	2.95	204	3	2.07	143	208
He I.....	4026.2	2	2.73	203	1	2.17	162	171
	4120.81	0–1	.....	.....	0	.....	.....	153
	4471.48	3	.....	.....	3	.....	.....	202
He II.....	4865.81	1	4.18	267	10	4.75	304	290
N III.....	4097.31	5	3.33	244	4	3.24	237	233
	4103.37	5	3.30	241	4	3.49	255	228
	4634.16	No abs.		.....	5	3.99	258	.....
	4640.64	No abs.		.....	6	3.79	245	.....
	4379.1	1	.....	.....	0	.....	.....	.....
Si IV.....	4088.86	2	.....	.....	2	.....	.....	166
	4116.10	1	.....	.....	3	2.91	212	179

TABLE 5

EMISSION LINES OBSERVED IN THE SHELL OF Of STARS

Element	Wave Lengths	Notations	Term Values (in Volts)
N III.....	4634.2–4640.6	$3p^2P^o-3d^2D$	30.3–33.0
N IV.....	4057.8	$3p^1P^o-3d^1D$	49.9–53.0
N V.....	4603 –4619	$3s^2S-3p^2P^o$	56.3–59.0
C III.....	5696	$3p^1P^o-3d^1D$	32.0–34.1
Si IV.....	4089 –4116	$4s^2S-4p^2P^o$	24.0–27.0
Hα, *Hβ*.....	6563 –4861	$2p^2P^o-3, 4d^2D$	10.2–12.0 (12.7)
He I.....	5876	$2p^3P^o-3d^3D$	20.9–23.0
He II.....	4686	$3d^2D-4f^2F^o$	48.2–50.8

selection is also well apparent in P Cygni stars, which represent a stage of excitation lower than the Of objects. For example, in P Cygni all the observed transitions of *Si* III, for which the terms $4p^1P^o$ or $4p^3P^o$ are the upper level, are present in absorption; whereas those transitions for which these terms $4p^{1,3}P^o$ are the lower level are in emission.[48]

The selection is present in the spectrum of HD 151804, but it has almost disappeared in HD 152408. In this latter Of star, the emission is much more pronounced than in 9 Sagittae, HD 151804, and other Of's considered before. For example, λ 4097 and λ 4103 of *N* III appear in the shell, together with λ 4634 and λ 4641 of *N* III. This observation shows that in the Of stars the selection decreases when the emission and absorption in the shell increase. It has actually disappeared in Wolf-Rayet atmospheres.

The temperature of the underlying star in 9 Sagittae and other O7f objects is approximately 40,000°. This value may be obtained, for example, by considering that the strongest observed absorption lines of *N* IV and *N* III have about the same intensity, despite a difference of excitation of about 20 volts. The mean electron density in the reversing layer of the underlying star may be readily estimated by determining the quantum number n of the line where the Pickering series terminates; in 9 Sagittae and HD 152408, $n = 22$. Inglis and Teller[49] in their investigation of the termination of spectral series, brought about by static Stark effect due to charged particles, obtained the following formula:

$$N = 0.027 \times a_0^{-3} \times n^{-15/2},$$

where a_0 is the Bohr radius and N the density of positive ions. For $n = 22$ (underlying star),

$$N = 1.55 \times 10^{13} \text{ per cm}^3.$$

The absence of any strong dilution effect in an Of shell shows that the dilution factor is not small (see sec. III). The electron density in the shell must be lower than 1.5×10^{13}. For further calculations of ionization, let us adopt for the shell a dilution factor 0.2 and an electron density $N_e = 1.5 \times 10^{13}$ per cm³. In these conditions *He* is almost completely in the doubly ionized state He^{++}, N^+ is practically nonexistent, N^{+++} is more abundant than N^{++} (by a factor of the order of 100),[50] and N^{++++} is somewhat less abundant than N^{+++}. Similarly, C^{+++} is much more abundant than C^{++}, and this in turn is more abundant than C^+.

Under these conditions it seems difficult to escape the conclusion that the emission lines observed in the shells arise in the capture of electrons by ions. It is difficult to understand how collisional excitations could be sufficiently efficient. For example, if the stellar temperature is 40,000°, we may, as a working hypothesis, adopt an electron temperature of about 34,000°. Under such conditions only a very small percentage of the number of electrons (less than 0.3 per cent) would have energies higher than 33 volts, required to excite the N^{++} atoms. As, on the other hand, nitrogen is mostly in the trebly ionized state, the excitation of *N* III lines by collisions of N^{++} ions with electrons of high kinetic energy has a very small probability. It is thus likely that the emission is due to a recombination of ions and electrons, which under the physical conditions of the Of shells takes place according to definite selections. These selections disappear in the Wolf-Rayet envelopes characterized by much more powerful emission compared with absorption and by the disappearance of the spectrum of the underlying star.

[48] *Pub. A.S.P.*, **52**, 394, 1940.

[49] *Ap. J.*, **90**, 439, 1939.

[50] This was the basis for our estimation of the stellar temperature.

An electron density of 10^{13} or even one lowered by a factor of 10^3 or 10^4 is much too high to permit forbidden lines to appear with any appreciable intensity in an Of shell. Similar results may be obtained for pure Wolf-Rayet stars, which never show forbidden lines unless they are surrounded by a nebula.

In the case of the outer shell of γ Cas, which grew steadily weaker in 1940 and 1941, it has been shown that the optical thickness for continuous radiation of the shell near its maximum development was about $\tau_1 = 0.2$.[51] If the Of shells have opacities of the same order of magnitude—which is likely, considering the intensities of the emission lines of *H*, *He* II, *N* III, and *C* III—we should expect a difference between the opacities of the shells of 9 Sagittae and HD 152408. It has been planned to investigate such differences.

III. SOME GENERAL GEOMETRICAL AND PHYSICAL PROPERTIES OF WOLF-RAYET STARS AND RELATED OBJECTS

Dimensions of the shell.—It has often been assumed that the radius of a Wolf-Rayet envelope is large compared with the radius of the photospheric surface. This picture was mostly based on the fact that no appreciable occultation effect has been observed in the profiles of the Wolf-Rayet emission lines. Against such a picture, Chandrasekhar, in 1934, wrote the following: "Any dynamical theory for the ejection of the atoms would not provide stellar atmospheres so extensive as to justify our regarding the parent star as of negligible dimensions."[52] Consequently, Chandrasekhar computed the effect of an occultation in a line profile.

Despite the failure to observe an occultation effect, several types of evidence, besides the absence of forbidden lines, lead to the result that the radius R of the shell is not much larger than the radius of the photosphere, say, in any case, not larger than $5r$ (probably less).

1. The violet-displaced absorption components observed in Wolf-Rayet spectra do not show any appreciable dilution effect. The best criteria for dilution in Wolf-Rayet atmospheres are the following *He* I lines:

$2s^3S - np^3P^o$ ..... (λ 3889)	$2p^3P^o - nd^3D$ ..... ($\lambda\lambda$ 5876, 4471, 4026)
$2s^1S - np^1P^o$ ..... ($\lambda\lambda$ 5016, 3965, 3613)	$2p^1P^o - nd^1D$ ..... ($\lambda\lambda$ 6678, 4922, 4388, 4144)

The lines having the lower level $2s^3S$ or $2s^1S$ (metastable states) are enhanced in a diluted atmosphere, compared to those having the lower level $2p^3P^o$ and $2p^1P^o$. As is evidenced by Struve and Wurm's calculations,[53] the dilution effect decreases with increasing temperature.[54] Yet at a temperature of 25,000° the easily observable lines $\lambda\lambda$ 3889, 5016, and 3965 are enhanced three times compared to $\lambda\lambda$ 5876, 4471, and 4026 when we pass from $W = 1$ to $W = 0.1$ (W = dilution factor). Even at temperatures as high as 75,000°, it does not seem possible to accept a dilution $W \leqslant 0.01$ for the average position of the absorbing layer. Further quantitative photometric investigations are planned in this direction.

2. Let us consider the case of a pure phenomenon of ejection and assume that the width of the violet-absorption component is mostly due to the range in the component of the ejection along the line of sight, inside the star's cylinder of sight. We may then very easily determine the mean distance of the absorbing layer. This will give only a minimum value of R, since other causes of broadening may exist, but the order of magnitude will probably be correct. Such a procedure was followed previously by O. C. Wilson

[51] *Ap. J.*, **94**, 291, 1941.

[52] *M.N.*, **94**, 522, 1934.

[53] *Ap. J.*, **88**, 84, 1938, Table 4.

[54] Mr. P. Ledoux has kindly computed the dilution effects for $T = 75{,}000°$ and has found that for $W = 0.1$, λ 5876 will still be reduced by a factor of 2 compared to λ 3888.

for three Wolf-Rayet stars[55] and by Struve and Swings for 9 Sagittae.[56] If V is the ejection velocity and ΔV the width of the absorption line, a first approximation will be[57]

$$R_{\text{shell}} = r_{\text{nucleus}} \times \sqrt{\frac{V}{2\Delta V}} . \tag{1}$$

Applying this formula to HD 192163 (WC7), O. C. Wilson gets $R = 1.9r$; for two other stars he obtains $R = 1.4r$ and $2.1r$. We shall see farther on that our values are slightly smaller than these.

The application of formula (1) may lead to the right order of magnitude in certain cases of Wolf-Rayet stars where the lines are very broad and where the essential process is assumed to be the continuous ejection of high-speed atoms from the stellar surface. It becomes much less reliable when the lines become sharper, such as in the Of stars, where rotation and turbulence may play an important part in the broadening of the line. The determination of R must proceed by successive approximations. The value of the ejection velocity may not be obtained so easily from the profiles of the emission and the absorption components. On the red side of the emission the profile is being reduced by the occultation effect, and this must be compensated by some reduction not yet accounted for in the violet part of the emission. Considering the complexity of the interpretation of profiles, it appears best to find a first approximation of R by taking for V half of the distance from the red end of the emission to the blue end of the absorption. In a second approximation, V may be corrected for the occultation effect.

The first approximation is equivalent to

$$R = \frac{r}{2}\sqrt{\frac{\Delta_t}{\Delta_a}} , \tag{2}$$

Δ_t and Δ_a being respectively the total width and the width of the absorption line. Applying formula (2) to our spectrograms and using various well-defined lines, we obtain

for HD 192163.....$R = 1.25r$ (Wilson found $R = 1.9r$)
for HD 164270.....$R = 1.14r$; $1.05r$; $1.1r$ and $1.5r$
for BD30°3639.....$R = 1.28r$

A second approximation, taking into account the occultation effect, would give values of R about 10 or 15 per cent larger. On the whole, a value $R = 1.4r$ or $1.5r$ appears to be of the right order of magnitude. A similar value or slightly larger ($2r$) would be found for 9 Sagittae. The dilution factor corresponding to $R = 1.5r$ is $W = 0.11$. At a temperature of the order of 50,000° such a dilution factor has no conspicuous effect on the relative intensities of characteristic lines, whereas it would already be important in a star of lower excitation, like P Cygni. Besides the technical difficulties, the limitations of the method are obvious and appear very strikingly when we try to apply formula (2) to certain stars, such as HD 152408, which would give a value of R equal to or smaller than r. This simply means that the other causes of broadening (rotation, turbulence, range in ejection velocity within the absorbing layer) are not negligible in such cases. For very broad lines (as in HD 192163), the main objection to the method is obviously that it neglects the range in ejection velocity within the layer giving rise to absorption lines. But the neutral *He* atoms exist only in the very outer parts of the Wolf-Rayet shells and a variation of about 30 per cent of the ejection velocity of *He* I in this probably

[55] *Ap. J.*, **91**, 403, 1940.

[56] *Ap. J.*, **91**, 566, 1940.

[57] Neglecting $(\Delta V/V)^2$ compared to $2\Delta V/V$.

thin layer appears rather unlikely. The method is evidently too crude to provide evidence in favor of the stratification of elements, which is strongly suggested by various other observations.

The essential result of this discussion is the relatively small size of the Wolf-Rayet shells compared to the photospheric surfaces. A value $R = 1.5r$ seems to be a good approximation, and it does not appear logical to accept values exceeding $5r$ (which would give $W = 0.01$). This is similar to the result of the discussion by O. C. Wilson.

Line profiles.—Despite the numerous theoretical and observational investigations of line profiles in Wolf-Rayet stars,[58] the question is far from solved. The violet edge of the emission lines, which have an absorption component, is usually sharper than the red edge, as it appears in HD 164270 on Plate V, *c*. This may be easily understood by combining a smooth symmetrical emission profile with a continuous background cut by an absorption line which sets in at a distance from the center equal to $V_{ej}\sqrt{1 - (r/R)^2}$. This absorption should begin and end rather abruptly, if the ejection velocity does not vary much in the absorbing layer.

Obviously, this is only a crude treatment of the problem. It neglects any darkening toward the limb and any occultation effect. Moreover, the simple addition of a line-emission profile and of a background depleted by an absorption line is only a rough approximation to a problem which should require the solution of the equation of transfer corresponding to the present case.

But two main points which require special attention at present are the occultation effect and the central reversals. If we adopt, for example, $R = 1.45r$, 28 per cent of the red wing must be lost. How is it that the lines do not show any definite asymmetry or any very peculiar radial velocities? The absorption line displaced to the violet and affecting the background is not always present and therefore could not explain all cases. There is no escaping the conclusion that in the violet part of the emission lines some reabsorption process compensates approximately for the occultation[59] if R is not larger than $3r$. On the other hand, if we adopt $R = 5r$, only 2 per cent of the red wing is lost by obscuration, which would be unobservable. Actually, the obscuration effect may be different for different stages of ionization of the same atom.

Central reversals are rarely observed in Wolf-Rayet stars but are well apparent in many lines of HD 152270. These central absorption lines are undisplaced, and it seems highly improbable that they are absorption lines belonging to some other star.[60] In HD 152270, microphotometer tracings of $H\beta$, which has a width of 54.9 A (or 3387 km/sec), give for the central absorption a width of 17.25 A (or 1064 km/sec). According to C. H. Payne,[61] the central absorptions have been regarded by Gerasimovič as "confirming the idea that the bright lines are formed at low levels in the atmosphere, and are broadened by pressure." This hypothesis is hardly tenable now. Rosseland has given another interpretation.[62] The reabsorption effect would occur preferentially near the

[58] Beals, *Pub. Dom. Ap. Obs.*, **6**, 111, 1934; Gerasimovič, *Zs. f. Ap.*, **7**, 335, 1933; Chandrasekhar, *loc. cit.*; O. C. Wilson, *Ap. J.*, **80**, 259, 1934; Araki and Kurihara, *Zs. f. Ap.*, **13**, 89, 1936.

[59] The asymmetry would be removed if we assume that the atoms, after ascending to a certain distance, begin to fall back toward the photosphere; we have, moreover, to assume that these descending atoms are equally efficient in contributing to the emission. But then how could we explain the violet absorption? This matter was discussed by Chandrasekhar (*loc. cit.*), who concluded that it is best to neglect the emission by descending atoms.

[60] They cannot be attributed to a stationary shell, since this latter would not show any trace of dilution (reversal in *He* I 4471 as strong as in *He* I 5016) and would have to lie very near the region of line emission. Beals's suggestion (*Pub. Dom. Ap. Obs.*, **4**, 295, 1929) to attribute the absorption lines to the underlying star does not appear very probable, since we should assume that the ionization of the nucleus should be higher than in the shell. On the contrary, the central absorption is very pronounced in the Balmer lines, which would require a high percentage of neutral hydrogen in the underlying star.

[61] *Harvard Bull.*, No. 874, p. 25, 1930.

[62] *Theoretical Astrophysics*, p. 294, Oxford, 1936.

center of the line, where the line of sight passes the luminous shells tangentially and the optical paths in the shell are a maximum. It is easily seen that the reversal may not take place when the envelope is uniformly accelerated outward, but it may take place when the outward motion of the atmosphere is uniformly decelerated. If further investigation proves the correctness of Rosseland's suggestion, the central reversals will bring the first clear evidence regarding the deceleration or acceleration of specific ejected atoms.

Araki and Kurihara[63] have investigated theoretically the effect of absorption upon the band profiles in expanding shells and their work shows conclusively how wide a variety of profiles may be obtained, including some with a minimum in the center. But no satisfactory general conclusions appear possible yet from a comparison of their theoretical profiles to the observed ones.

Chemical constitution of the ejected layers.—There is no doubt that certain Wolf-Rayet stars show only carbon, the best example being the nucleus of Campbell's envelope star. It is quite certain also that in certain W stars, the nitrogen lines are much stronger than the carbon lines. But we have now also conclusive evidence that there are intermediate objects, showing simultaneously carbon and nitrogen with various intensity ratios.

In the typical WN6 star, HD 192163, the line λ 5805 is in all likelihood due to *C* IV and not to *N* IV, as was shown in section I. Our investigation of the nucleus of NGC 6543 has shown that *C* IV and *N* IV have similar intensities. The description of the nuclear spectrum of NGC 6572 by Wright[64] shows that the characteristic lines λ 4634 and λ 4641 of *N* III, λ 4650 of *C* III, λλ 4659, 5802, and 5812 of *C* IV are present. There is also definite evidence of the simultaneous presence of *C* and *N* with similar intensities in the Wolf-Rayet nucleus of NGC 6826. We have observed the characteristic lines of *N* III and *C* III with similar intensities in the nucleus of IC 4997. In the nucleus of IC 418 we observed very strong bright lines of *N* III (λ 4634.16 and λ 4640.64), *C* III (λλ 4647.40, 4650.16–4651.35, 4665.90, 5696, 4325), and weaker lines of *C* II (λ 4267) and *N* IV (λ 4058). This nucleus constitutes an intermediate between the 9 Sagittae type and the pure Wolf-Rayet type stars, the emission being much stronger than in 9 Sagittae, but undisplaced absorption lines of *He* II (Pickering series only, λ 4686 being bright) are still present.

Variations in the relative intensities of the emission lines of *N* and *C* are also very striking in the Of stars. Typical examples are: (*a*) Of shells showing nitrogen lines, but no trace of carbon: BD+35°3930.*N*, nucleus of NGC 2392, HD 152386;[65] (*b*) Of shells showing nitrogen lines and weaker carbon: 9 Sagittae, HD 108 (in 1941); (*c*) Of shells showing *N* III 4641 and *C* III 5686 of approximately the same intensity: HD 151804, HD 152408;[66] and (*d*) Of shells in which *C* III 5686 is much stronger than *N* III 4641: HD 192639.

It is interesting to consider also the shells of novae with regard to the relative abundance of *C* and *N*.[67] In the case of N Her, many lines of *C* II, III, IV, and *N* II, III, are still observed, whereas in the present spectrum of N Ser, the *N* III lines are strong, but

[63] *Loc. cit.* [64] *Op. cit.*, p. 213.

[65] This interesting spectrum has been described by C. H. Payne (*Harvard Bull.*, No. 842, 1937) and by Seyfert and Popper (*Ap. J.*, **93**, 461, 1941). The latter authors mention the following bright lines: *Hα*, *Hβ*, *He* II (4686), *N* III (4634, 4640, 4097), *Si* IV (4088 and 4116). Our spectrograms reveal also bright D_3 (*He* I 5876) and a weak emission at *He* II 4542. *C* III is absent.

[66] The nucleus of IC 418 may possibly be considered as belonging to this category.

[67] See the report of Swings at the Paris conference on novae and white dwarfs, 1939. Some examples which seem to indicate peculiar abundances in nova shells are the tremendous intensity of [*Fe* VII] in Nova Pictoris 1925, the strength of [*Ne* III] in N Per and N Ser, of [*Fe* III] in N Ser and in DO Aquilae 1925; the absorption lines of *O* I and *C* I were especially strong in N Herculis. A lower abundance of hydrogen is not excluded in nova shells.

there is no trace of carbon.[68] In the spectrum of Z Andromedae in August, 1940, one year after the outburst of 1939, the lines *N* III 4634.2 and 4640.6 were of intensities similar to *C* III 4647.4 and 4650.2. The chemical constitution of the layers ejected in nova outbursts seems to differ from that of ordinary reversing layers,[67] and the relative behavior of *C* and *N* should be investigated carefully.

The analysis of the spectrum of P Cygni has also shown[69] that this post-nova is much more closely related to the nitrogen than to the carbon sequence. This is also true of BD+11°4673 and CD−27°11944, both of P Cygni type.

Classification of Wolf-Rayet spectra.—The classification suggested by Beals and adopted by the I.A.U.[70] is based on the following criteria of excitation: (*a*) in the WN stars: *N* III/*He* II; *N* V/*He* II and *He* I/*He* II; and (*b*) in the WC stars: *C* III/*C* IV; *C* III/*O* V, *C* III/*He* II, *He* I/*He* II, and band widths.

Some additions or modifications may possibly appear advisable for the following reasons:

1. Certain objects contain both *C* and *N* and can obviously not be listed among the WC or among the WN stars.
2. Observational difficulties arise in the case of the planetary nuclei observable only with low dispersion. Fairly narrow nuclear lines have sometimes been observed: in this case the lines of *H*, *He* I, and *He* II (sometimes also *N* III) may belong both to the nucleus and to the nebula, and it may be difficult to separate the two contributors.
3. We have noticed different relative abundances of carbon and nitrogen; it is not certain that the relative abundances of carbon and helium, or of nitrogen and helium, are constant for all Wolf-Rayet stars.

For these reasons, the following suggestions are tentatively made:

1. Continue to use the WN and WC notations whenever the predominance of *N* or *C* is definitely ascertained; in case of simultaneous presence of *N* and *C* with similar intensities, simply use the notation W.
2. Devise criteria not involving *He* I and *He* II lines for the planetary nuclei,[71] in a way agreeing quantitatively with the presently adopted criteria.
3. Avoid comparisons between intensities of lines belonging to different elements and concentrate as much as possible on different stages of ionization of one element.

The application of these suggestions would require further photometric work and would probably be best performed under the auspices of the I.A.U.

The correlation of band width (of certain lines) and spectral type, especially in the carbon sequence, has often been emphasized. But here again great caution should be exercised in applying this excitation criterion, which holds only statistically. In some stars intermediate between Wolf-Rayet and Of stars, such as the nucleus of IC 418, which has strong emission lines of *N* III, *C* III, and *He* II, the lines have only a width of 155 km/sec, corresponding to an ejection velocity of the order of 80 km/sec. In W stars of very early type, such as the nucleus of NGC 6543, the two carbon lines λ 5801.5 and λ 5812.1 are very well separated on our spectrograms, whereas the average band width for class WC6 is 70 A. The nucleus of IC 4997 has also fairly sharp lines.

[68] Because the fluorescence process of *N* III excited by *He* II (via the *O* III resonance line) has a great efficiency, the comparison between the intensities of *N* and *C* lines must be made carefully.

[69] Struve, *Ap. J.*, **81**, 66, 1935.

[70] *Trans. I.A.U.*, **6**, 250, 1938.

[71] It should be noted that the careful classification of the planetary nuclei is an important and urgent problem, especially in order to determine the temperatures of many nuclei, to discuss the excitation conditions in the nebulae, and to try to relate the chemical constitution of the nuclei to that of their surrounding nebulosities (e.g., it has been shown that several pure carbon nuclei are surrounded by a nebulosity which is very rich in nitrogen).

At this stage a short comparison between Wolf-Rayet and P Cygni stars may be interesting. It is often assumed that the lines in P Cygni stars are narrower than in novae and in Wolf-Rayet stars, but there are many cases in which this assumption does not hold. For comparison, here are a few approximate values of the ejection velocities:

P CYGNI STARS

	Km/Sec
P Cygni	~ 120
BD+11°4673	~ 125
BD+47°3487	~ 180
CD−27°11944	~ 350
ZCMa	~ 350

WOLF-RAYET STARS

BD30°3639	~ 300 (*He* II)
HD 167362	~ 185 (C III)

Of STARS

9 Sagittae	~ 250
BD+35°3930*N*	~ 300

NOVAE

Very low velocities in Z And, TCBr, RS Oph

The process of ejection of matter is essentially the same in Wolf-Rayet objects, P Cygni stars, Of stars, and novae. In all four cases there is a wide range in the velocity of ejection. An Of star differs from a Wolf-Rayet object in that the ejected layer is optically thin so that the spectrum of the underlying star itself may appear, although encountering continuous and line absorption in the shell; but for the essential properties (similar excitations, absence of forbidden lines) this thin layer is similar to a Wolf-Rayet envelope. The P Cygni stars have simply a lower excitation. The P Cygni shells may have widely different opacities, so that the underlying star may not be observed (as in P Cygni, CD−27°11944, and many novae) or may partly shine through (as in BD +47°3487, 17 Leporis, HD 190073, and novae at certain stages).[72] The P Cygni shells have a wider variety of dilution than the Wolf-Rayet stars; consequently, the dilution effects may be more pronounced in the P Cygni stars,[73] and some of them present forbidden lines (e.g., BD+11°4673, Z CMa, RY Scuti, etc., and novae, e.g., in the λ Carinae or RY Scuti stages).

Absolute magnitudes, temperatures, radii.—As is well known, there seems to exist a difference in absolute magnitude, of the order of three magnitudes,[74] between the Wolf-Rayet stars and the planetary nuclei; and this is commonly considered as very strange, since it is usually assumed that there is no appreciable spectroscopic difference between Wolf-Rayet stars and planetary nuclei. That these nuclei have high temperatures has been established clearly by Wright, who emphasized the considerable extension of their continuous spectra into the ultraviolet and the occurrence of bright bands due to the same atoms as those identified in Wolf-Rayet stars. But a detailed examination of the spectra reveals that, except in rare cases, the spectra of planetary nuclei have not exactly the typical Wolf-Rayet type corresponding to their excitation. R. Minkowski

[72] All the dilution effects observed at certain stages of novae have their equivalent among the P Cygni, Of, or Wolf-Rayet stars.

[73] As was mentioned before, the dilution effects on absorption lines are greater for lower temperatures.

[74] Beals, *J.R.A.S. Canada*, **34**, 179, 1940.

has found a very high ejection velocity in the nucleus of NGC 6571, but this appears to be an exception. Here are some general indications concerning the best-known nuclei:

IC 418.....nucleus intermediate between W and Of, contains *N* and *C*
NGC 2392.....nucleus of type Of
NGC 6543.....nucleus containing *C* and *N;* nuclear lines unusually sharp for observed excitation
NGC 6572.....nucleus containing *C* and *N;* lines λλ 4634, 4641, 4650, 4568 well separated; width of λ 4686 only 15 A
BD+30°3639.....lines rather sharp (Pl. VII, *a*)
NGC 6826.....nucleus containing *C* and *N;* width of λ 4686 only about 8 A
IC 4997.....nucleus containing *C* and *N;* lines rather sharp
NGC 40.....normal WC8 (Pl. VII, *b*)
HD 167362.....lines very sharp (Pl. VII, *c* and *d*)

On the whole, the planetary nuclei with emission lines seem to have lower ejection velocities than the W objects of similar excitation. Many nuclei have also a pure continuous spectrum. When we compare pure W stars and planetary nuclei, the smaller velocity of ejection would thus correspond to the objects of lower absolute magnitude. This is probably equivalent to lower surface gravity for the W stars, since the difference of radius would probably not be compensated by the difference of mass.

According to Sanford and Wilson[75] the mean absolute magnitudes of the Wolf-Rayet stars are: for WC (6 stars), −2.8; for WN (12 stars), −2.1. From his data, Beals suggested a value of −2.0 to represent the intrinsic luminosity of the Wolf-Rayet stars as a class.

In sections I and II we have described the spectra of four stars in NGC 6231, the parallaxes of which are probably nearly identical. After correction for interstellar absorption,[76] the absolute magnitudes obtained are as follows:

HD 151932 (WN6).....$M_v = -2.54$
HD 152270 (WC6+).....$M_v = -2.38$
HD 152408 (O7f, with numerous, strong emission lines).....$M_v = -3.07$
HD 151804 (O7f, emission rather weak).....$M_v = -3.7$

Even if the numerical values of the M_v's are in error, the differences should be correct. There is thus some indication that the Of stars are intrinsically brighter than the W objects. But such a comparison may have little meaning, since the temperatures and atmospheric structures of the W6 and O7f stars are so different.

In using the absolute magnitudes for determinations of radii or for similar calculations, the values adopted should refer only to the continuous background. In many cases the contribution of the emission lines to the visual or to the photographic magnitude may become very important. Before computing the photospheric radii in these cases, the magnitudes should be corrected, and this may be rather difficult and uncertain. For the stars in NGC 6231, the contribution of the line emission is small compared to the continuum, except for HD 152270, in which a correction of a few tenths of a magnitude should be applied ($M_{\text{cont}} \sim -1.8$ or -2.0). But the correction may amount to much more in many cases.

Assuming as a first approximation a black-body distribution for the continuous spectrum in the visual region, the following values of the radius are obtained:

HD 151932 (assuming $M_v = -2.54$, $T = 80{,}000°$); $R = 2.0\odot$
HD 152270 (assuming $M_v = -2.0$, $T = 100{,}000°$); $R = 1.4\odot$
HD 152408 (assuming $M_v = -3.07$, $T = 40{,}000°$); $R = 3.9\odot$
(assuming $M_v = -3.07$, $T = 50{,}000°$); $R = 3.3\odot$
HD 151804 (assuming $M_v = -3.7$, $T = 40{,}000°$); $R = 5.2\odot$
(assuming $M_v = -3.7$, $T = 50{,}000°$); $R = 4.5\odot$

[75] *Ap. J.*, **90**, 235, 1939.

[76] MacRae, *op. cit.*

The values obtained for the W stars are similar to those obtained by Beals.[77] The two Of stars have definitely larger radii.

The application of the theory of Zanstra to the determination of temperatures of Wolf-Rayet stars.—The temperatures adopted for HD 151932 and HD 152270 are the photo-ionization temperatures obtained by Beals by applying Zanstra's theory and by assuming that the photospheric surface radiates like a black body. It seems appropriate to make a few comments regarding this application, aside from the question of the applicability of black-body radiation.

a) The case of a nebula excited by a nucleus of Wolf-Rayet type.—Several years ago Bowen called attention to two important effects which might influence the photo-ioniza-

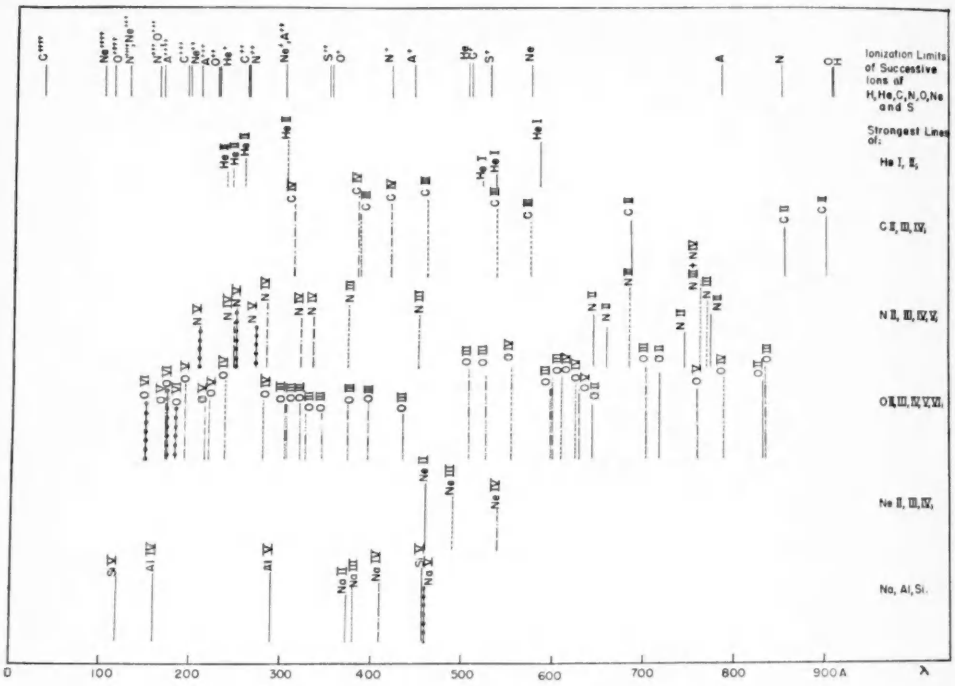

FIG. 1.—Region λλ 30–912 A in Wolf-Rayet stars

tion of certain atoms and, consequently, the intensity of the observable lines resulting from the recombination process. These are (1) the effect of the overlapping regions of photoelectric absorption and (2) the photo-ionization by the emission lines present in the extreme ultraviolet region of the spectrum of the nucleus and of the nebula.

To simplify the discussion of these effects, we have prepared a diagram (Fig. 1), giving the ionization limits of the different abundant atoms or ions between λ 30 and λ 912 A, together with the strongest lines of *He* I, *He* II, *C* II–IV, *N* II–V, *O* II–VI, *Ne* II–IV, *Na* II–V, *Al* IV and V, *Si* IV and V. According to the spectral type of the Wolf-Rayet nucleus, it is easy to make a synthesis of the line emission most likely to be present. It should be noticed that the incomplete multiplets of *O* III and *N* III, which may be excited

[77] In the binary HD 193576, the Wolf-Rayet component of type WN5 has a radius of 5.8⊙, according to S. Gaposchkin (*Ap. J.*, **93**, 202, 1941). Similarly, large radii would be obtained for HD 151932 and HD 152270 by adopting a temperature of the order of 20,000°.

by *He* II 304, are not enhanced in the Wolf-Rayet stars, as compared with the other transitions of *O* III and *N* III. Actually, *O* III is always very weak or absent in the WN stars, and it does not show any selection in the WC stars. This seems to indicate that, in the Wolf-Rayet stars, practically all the intensity of the line emission is due to recombination and not to line excitation.

Applying this observation to the case of *He* II itself, we may infer that in W stars *He* II 304 does not build up a very high intensity at the expense of the higher members of the $1s^2\ S - np^2P^o$ series (λλ 256.31, 243.02, 237.33), which may still retain an appreciable intensity when they leave the Wolf-Rayet star. For radial-velocity reasons, we may expect that only a minor part of the intensities of the lines λλ 256, 243, 237 will be absorbed by the *He* II atoms in the nebula and by successive emissions will be transformed into λ 304. Despite the fact that the absorption coefficient of line absorption is ordinarily greater than that for the photoelectric absorption below a series limit, a great part of the energy concentrated in the Wolf-Rayet lines λλ 256.31, 243.02, 237.33, of *He* II will thus be used to ionize C^{++} and N^{++}.

On the other hand, the ionization of O^{++} is not favored by these lines of *He* II. On the contrary, since He^+ and O^{++} have almost the same ionization potential and since He^+ is more abundant than O^{++}, the ionization of O^{++} may be slowed down.

This effect is observed in the nebula NGC 6543,[78] in which fairly strong permitted lines of *C* III and *N* III are present, but no permitted *O* III line. The general decrease of the continuous spectrum toward short wave lengths (about a factor of 2 between λ 260 and λ 226) is not sufficient to explain the observed enhancement of *C* III and *N* III compared with *O* III.

b) The case of the Wolf-Rayet star.—The stratified distribution of the elements which Bowen pointed out in the case of the nebulae[79] is also present in the Wolf-Rayet envelope itself, as was shown especially by Beals.[80] Hence the radiation which reaches a certain outer region of the W envelope has already suffered transformations in the deeper layers, part of the ultraviolet photospheric continuum having been absorbed photoelectrically and transformed into longer wave lengths.[81] Thus photo-ionization by emission lines may become possible in the outer layers. Evidently the effect of overlapping regions of photoelectric absorption is the same inside the Wolf-Rayet envelope or in a nebula.

Other examples may easily be found in addition to the one concerning He^+, O^{++}, N^{++}, and C^{++}, for example, on the basis of the quasi-coincidence of the ionization potentials of neutral *H* and *O*. It is quite certain that, even assuming a black-body photospheric radiation, the numerical values of the temperature obtained when applying Zanstra's theory may be different for different atoms.

In conclusion, I express my cordial gratitude to Dr. O. Struve for his interest in this work, his valuable suggestions, and his great help in securing the observational material.

YERKES OBSERVATORY
AND
MCDONALD OBSERVATORY
August 1941

[78] *Ap. J.*, **92**, 289, 1940.

[79] *Ap. J.*, **67**, 1, 1928.

[80] E.g., *J.R.A.S. Canada*, **34**, 169, 1940.

[81] Stratification is actually a general feature for all stellar envelopes, including shells of P Cygni and Be types.

EXTENDED STELLAR ATMOSPHERES: A REVIEW OF THE PROBLEMS OF GASEOUS SHELLS*

OTTO STRUVE

ABSTRACT

The properties of the gaseous shells which surround many early-type stars are discussed. The questions to be answered are: (1) Why do some stars have shells, while others, of similar spectral type, do not? (2) Why do some shells expand, while others are stationary, both types occurring in different stars of similar class, or even in a single star? (3) Why do the shells vary in a more or less irregular manner? The observational data are classified, and it is shown that there are in an ideal case three observable layers: (1) a stationary, main-sequence reversing layer, (2) above it a stationary α Cygni type layer with or without dilution, and (3) on top an expanding P Cygni type layer of varying optical thickness. The origin of the two upper layers may in some cases be ascribed to rapid rotation of the reversing layer. The structure of these layers—the stationary lower layer and the upper P Cygni type layer—is interpreted in terms of radiation pressure from the Lyman α flux of the shell. This flux is directed inward in the lower levels of the shell and outward in the higher levels.

INTRODUCTION

The principal questions which require answers are the following:

1. Why do some stars possess tenuous outer atmospheres or shells, while other stars, apparently of identical physical characteristics, do not have such shells?

2. What is the origin of a shell and how is it supported, in apparent violation of the laws of mechanics?

3. How can we account for the remarkable tendency of nearly all shells to vary either periodically or, more often, in an irregular manner?

4. Why do some shells expand, while others are stationary?

There has been, in recent years, a growing realization that some of the peculiar phenomena generally ascribed to a tenuous outer atmosphere in some early-type stars are not confined to a few freaks in the stellar population but are probably characteristic, in a small degree, of the majority of stars in certain stages of their evolution. Beals has called attention on several occasions[1] to the fact that there exist certain definite similarities between such widely different groups of stars as those of classes Be, W, P Cygni, and α Cygni. The tendency to show bright lines of the P Cygni type is pronounced in class A supergiants, and probably even a few members of class F show them. It is common among the W stars and occasionally is seen in stars normally designated as Be. Swings and I have called attention to the fact[2] that several O stars with emission lines also show indications of P Cygni type structure. My own studies of dilution effects have led to the recognition of a considerable number of stars which are surrounded by outer shells or extended atmospheres, where the pressure is low and the dilution factor of the order of 0.1–0.01. Some of these shells expand, as in 17 Leporis. Others are stationary, as in ζ Tauri, ϕ Persei, γ Cassiopeiae, Pleione, etc.

The different types of shells are not yet clearly related to one another. But we do know the following facts: (*a*) Shells of the Be type may become transformed into shells producing strong absorption lines (γ Cassiopeiae, Pleione). (*b*) Normal B stars without emission lines may become at times Be stars, and vice versa. (*c*) Expanding shells of the P Cygni type stars may become transformed into peculiar Be stars without P Cygni type

* *Contributions from the McDonald Observatory, University of Texas*, No. 41. This paper was presented at the symposium on astronomical spectra, held at the Yerkes Observatory in celebration of the Fiftieth Anniversary of the University of Chicago, on September 10–12, 1941.

[1] *Observatory*, **64**, 42, 1941; *J.R.A.S. Canada*, **34**, 169, 1940.

[2] *Ap. J.*, **91**, 569, 1940.

structure in their lines (Z Andromedae), and vice versa. (*d*) A-type supergiants with P Cygni type lines may at times lose the P Cygni lines (β Orionis) or show marked variations in their intensity and structure (α Cygni). (*e*) All phenomena of outer shells are more or less violently variable (17 Leporis, P Cygni, V/R variation in Be stars, etc.).

The question arises whether any star of early type may be regarded as being free of these peculiarities, or at least of a certain predisposition to develop them from time to time. This question is of great importance because upon its answer will depend the degree of confidence which we are prepared to bestow upon discussions of "normal" reversing layers, built up according to the standard procedure, where mechanical equilibrium is assumed by setting equal gravitational acceleration and gas pressure *plus* ordinary continuous radiation pressure.[3] This doubt affects especially our ideas concerning the structure of a supergiant reversing layer. Three independent lines of investigation tend to confirm the suspicion.

I. Pannekoek[4] has called attention to the fact that if g_{eff} is determined for α Cygni with the help of the Stark effect, as computed by Verwey, a value is obtained which is smaller by a factor of about 100 than the corresponding value, g, computed from the mass given by the mass-luminosity relation and the temperature. He has suggested that this discrepancy is typical for most supergiants and that it is a consequence of radiation pressure. A similar result was obtained by Shajn[5] for β Orionis. Pannekoek also called attention to the very remarkable fact that in several cases known to him the radiation pressure computed from g and g_{eff} amounts to 98 or 99 per cent of the gravity. This is rather surprising, since there should not be any obvious relation between these two quantities (see accompanying table). Hence he suggested that the atmospheres may not be in equilibrium but may expand and that the expansion may then impose upon the atmosphere a density distribution which, if interpreted as for an atmosphere in equilibrium, may lead one to believe that the observed value of g is a small percentage of the dynamical value. The computations gave promising results suggesting velocities of expansion of the order of 10 km/sec. But observations in double stars—ζ Aurigae by Christie and Wilson, and β Orionis by Shajn—failed to confirm the expansion.

Star	Dyn. Gr.	Obs. Gr.	Rad. Pr.
α Cygni	800 cgs	10 cgs	790 cgs
Cepheids	320	1	319
ζ Aurigae	10	0.2	9.8

Dr. Kuiper, who has investigated all available data in their relation to the mass-luminosity relation, informs me that we have as yet no actual mass determination for any supergiant of the type of α Cygni; hence a direct test of the anomaly is not possible. Nevertheless, the departure of the effective gravity from the dynamical gravity is almost certainly real.

II. Swings and I have recently shown[6] that the similarity of the periods of velocity variation of β Canis Majoris and β Cephei suggests a greater degree of similarity of internal structure than may be expected from the spectra: β CMa has a supergiant (or near-supergiant) spectrum with large turbulence; β Cep has a normal, low-luminosity, B-type spectrum with strong forbidden *He* I 4470.

III. The Mount Wilson studies by Adams and others have revealed the existence of currents in the atmospheres of many supergiants which affect certain atoms but not others.

[3] Unsöld, *Physik der Sternatmosphären*, p. 141, Berlin, 1938.

[4] *B.A.N.*, **8**, No. 301, 1937.

[5] *Poulkovo Obs. Circ.*, Nos. 26–27, p. 5, 1939.

[6] *Ap. J.*, **94**, 99, 1941.

In order to help elucidate some of these questions Dr. Swings and I have been engaged during the last two years in a study of stars having different types of shells. We hoped that by investigating objects in which the peculiar effects are very prominent we might throw light upon the less conspicuous effects in otherwise normal stars.

SUMMARY OF OBSERVATIONAL DATA

The observations are now so numerous that it is possible to systematize and classify them (see Table 1). Broadly speaking, we distinguish between two major groups of shells: group A, stationary shells, whose radial velocities are identical, within the precision of the measurements, with the velocities of the stars themselves—γ Cassiopeiae, ζ Tauri, ϕ Persei, Pleione, ϵ Capricorni, etc., are examples of this group; group B, expanding shells, showing negative radial velocities from the absorption lines and normal stellar velocities or slightly positive velocities from the emission lines—P Cygni, 17 Leporis, etc., are typical examples. Group A may be divided into three subdivisions:

a) Normal Be and Oe stars, of line characters *s* and *n*—κ Draconis, ω Orionis, etc., are typical examples. These stars show a conspicuous correlation between rotational broadening of the stellar absorption lines and width of the emission lines. The latter, being proportional to λ, strongly suggest that rotation accounts for their broad contours. Variation in V/R and in $V + R$ emission intensities are outstanding features of the majority of these stars. The stellar reversing layer is always clearly visible, but in some stars with very strong emission lines the continuous absorption of the shell may cause some veiling. Probably the quantity τ_1, which measures the optical depth of the shell for the Lyman continuum, is not excessively large. In some cases the emission lines have more or less conspicuous central reversals, relating them with subdivision (*c*) of group A. A few, as Beals has emphasized,[7] combine the characteristics of Be and P Cygni type objects. These include HD 108, MW 374 ($+47°3487$), HD 190073, 17 Leporis, 29 Canis Majoris, 9 Sagittae, etc. Dilution is probably conspicuous: *Mg* II 4481 is usually very faint, even when the emission lines of *Fe* II are strong. There are indications of stratification—inferred from the fact that the widths of the emission lines are not the same for all elements. The latest statistical results by R. E. Wilson[8] indicate that the Be stars are very little, if at all, more luminous than normal main-sequence B stars. Formerly they were believed to be slightly more luminous, but all investigators agree in placing them near the main sequence and very far from the supergiant group. With regard to the origin of these shells, rapid rotation is the only positive clue we have. Gerasimovič[9] has objected to the hypothesis that rotation is responsible for the emission but has admitted that rotation probably acts as a trigger mechanism aiding in the formation of shells by radiation pressure. Incidentally, some of Gerasimovič's objections are no longer valid. For example, he uses in the case of γ Cass (prior to the recent outbursts) a width of 6.3 A for $H\gamma$ in absorption and 4.0 A in emission. The constancy of rotational momentum requires that the velocity of axial rotation be proportional to r^{-1}. Hence the dilution factor, according to Gerasimovič, should be about 0.4. As a matter of fact, since

$$\frac{r}{R} = \frac{6.3}{4.0} = 1.6 ,$$

we find for the dilution factor

$$W = \frac{\omega}{4\pi} = \frac{1}{2}\left\{ 1 - \sqrt{1 - \frac{R^2}{r^2}} \right\} = \tfrac{1}{2}\{1 - \sqrt{1 - 0.4}\} = 0.1 .$$

[7] *Observatory*, **64**, 44, 1941.

[8] *Ap. J.*, **94**, 12, 1941.

[9] *M.N.*, **94**, 744, 1934.

This is not as bad as it might have looked to Gerasimovič, who thought that we should expect $W = 10^{-3}$–10^{-5}. We now know that in reality W is usually close to 0.1. The remaining discrepancy may well be due to the fact that the width of an absorption line is a poor measure of rotational velocity. Gerasimovič also remarked that the rotational hypothesis demands that the total emissions should be the same in Bne and Bse stars, because the line-widths are considered to be largely an effect of inclination. It seems to me that this discrepancy, which rests upon a well-established summary by Merrill,[10] may be the result of the inclusion among the Bse stars of true supergiants, which unquestionably show a real tendency toward emission, often of the P Cygni type. I have in mind such stars as β Orionis and 55 Cygni. There is no doubt that rapid rotation does not explain the emission lines of these stars. This fact by itself does, of course, weaken the rotational hypothesis. But it is perhaps not necessary that it should explain all types of bright lines. The final objection that "Laplacian rings rotating around the stars can hardly appeal to a modern astrophysicist" is not very deep. Against the theory of Gerasimovič—convincing as it is in many respects—is the fact that *normally* the Be stars show no trace of a violet absorption-border, such as we observe in P Cygni stars and in many W stars. Whenever absorption lines are present, they fall centrally or nearly centrally over the emission lines. Gerasimovič would regard these as the result of absorption in the outermost layers of a shell whose velocity of expansion is decelerated outward. But the absence of violet wings in all but a few objects of the type mentioned by Beals cannot be overlooked. Forbidden lines are not normally observed in these shells. The degree of ionization represented by the emission lines is almost always appreciably lower than that of the reversing layer: it is normal to observe in the same star *Fe* II in emission and *He* I in absorption. The widths of emission lines of any one atom are proportional to λ, but lines of different atoms may have different widths. On the rotational hypothesis this is interpreted as the consequence of the r^{-1} relation for the rotational velocities. *Mg* II is usually abnormally weak in emission—probably a result of dilution—and in some cases it definitely suggests origin at a relatively low level, because the width of λ 4481 is greater than that of *Fe* II. But apparently it is not possible to use the r^{-1} relation without reservation. For example, in the case of π Aquarii the widths of the emission lines suggest a rotational velocity of about 200 km/sec, while the absorption lines give 100 km/sec. The latter value may be seriously in error. Nevertheless, it is difficult to see how the result can be reconciled with the r^{-1} relation. Among the earlier O stars this type of emission in *He* II, *N* III, *H*, etc., is the rule rather than the exception.

b) The second subdivision of group A consists of a number of peculiar emission-line objects, which show many strong emission lines, including those of forbidden transitions. These objects, like Z Andromedae, RX Puppis, R Aquarii, RW Hydrae, and others, are closely related to the P Cygni type stars, and some of them exhibit P Cygni lines in certain stages of their evolution. Some have nova-like outbursts (T Coronae, Z Andromedae), and nearly all are more or less variable in light. As to origin, they all seem to consist of binaries having one late-type component and one early-type component (α Scorpii). In some as yet obscure manner these wide pairs stimulate the formation of large, tenuous shells, which are excited by the otherwise normal (or even under-luminous: α Scorpii) hot components. In some of these stars the red components are variable in an apparently normal manner (R Aquarii), while in others the hot components are subject to violent outbursts (T Coronae, Z Andromedae). There is rarely any doubt as to whether an emission-line star belongs to this subdivision or to the preceding. The great intensity of the forbidden lines and the tremendous development of all emission features show that the dilution factor is very much smaller than that found for the preceding subdivision and that the nebula in which the lines originate is probably more closely related to

[10] *Pub. A.S.P.*, **45**, 49, 1933.

TABLE 1

SUMMARY OF OBSERVATIONS

	Extended Stellar Atmospheres (Shells)							
	A. Stationary (γ Cas)			B. Expanding (P Cyg)				
	a) Normal Be and Oe π Aqr, κ Dra, ω Ori, $+35°3930$	*b*) High-Excitation Objects Z And, AX Per, CI Cyg, RX Pup, RW Hya, R Aqr WY Gem, HD 45677	*c*) Absorption Shells ϕ Per, ζ Tau, γ Cas, Pleione	*a*) Novae	*b*) W Stars	*c*) P Cygni Stars		
						1. Absorption Predominant 17 Lep	2. Emission and Absorption P Cyg	3. Peculiar Binaries β Lyr, 29 CMa, RY Scu
Dilution	$W = 10^{-1}$	$W = 10^{-6}$	$W = 10^{-1}$ to 10^{-2}	W varies (10^{0} to 10^{-6})	$W = 10^{-1}$	$W = 10^{-1}$ to 10^{-2}	$W = 10^{0}$ to 10^{-2}	$W = 10^{-1}$
Spectrum (Star	B and O	Hot	A and B	.....	.....	A	B, A, F	B and O
Spectrum (Shell	A, B, O	Nebular	F, A, B	.....	.....	A	A and B	B and O
Ionization of shell compared with star	Less	.....	Less	.....	.....	Same?	Decreases outward	Sometimes greater (β Lyr)
Forbidden lines	Absent	Very strong	Absent (exception, HD 45677)	Strong	Absent	Absent	Sometimes present; [*Fe* II] in $-27°11944$ Absent in P Cyg	Sometimes present; [*Fe* III]in RY Scu Absent in β Lyr
Luminosity of star	Main sequence	?	Main sequence	.....	.....	m.s. or s.g. 17 Lep HD 160529	m.s. or s.g. HD 190073 υ Sgr $+47°3487$ α Cyg β Ori ϵ Aur	Supergiant
Doppler broadening of emission	Large (rotation)	Small (no rotation)	Large (rotation)	Large (expansion)	Large (expansion)	Intermediate (em. weak)	Intermediate (expansion)	Large or Small (β Lyr) (RY Scu) Exp. and orb. motion
Rotation of star	Rapid	?	Very rapid	?	?	Intermediate	Fast $+47°3487$ Slow HD 190073	Intermediate
Binary nature	Single	Binary	Single Binary 14 Com ϕ Per Pleione ζ Tau	?	?	Single Binary 17 Lep. ?	Single Binary P Cyg $-27°11944$	Binary
Opacity of shell (continuous)	Small	?	Intermediate veiling	?	?	Interme- Small diate 17 Lep HD 160529	Interme- Large diate HD 190073 P Cyg $+47°3487$ Z CMa	Interme- Large diate β Lyr RY Scu

TABLE 1—*Continued*

	Extended Stellar Atmospheres (Shells)					
	A. Stationary (γ Cas)			B. Expanding (P Cyg)		
	a) Normal Be and Oe π Aqr, κ Dra, ω Ori, $+35°3930$	*b*) High-Excita-Objects Z And, AX Per, CI Cyg, RX Pup, RW Hya, R Aqr WY Gem, HD 45677	*c*) Absorption Shells ϕ Per, ζ Tau, γ Cas, Pleione	*a*) Novae	*b*) W Stars	*c*) P Cygni Stars
						1. Absorption Predominant 17 Lep
Variations	V/R and $V+R$	Changes in ionization; $[O\,III]/O\,III$; Aur/Neb	Changes in int. and vel. of abs. lines. Var. α Cyg abs. (ι8 Lib, ϵCap)	.....	.....	Outbursts Changes (17 Lep) in Int. (HD 160529)
Transformations	Into Ac (γ Cas) or normal B stars	Into Bc2 (Z And)	Into Aa (Pleione) (γ Cass)	.....	.....	.....
Special features	.....	Nova-like outbursts (Z And, T CrB, RS Oph) Late-type variable	Variation in sharp *He* I triplets (ϕ Per)	.....	.....	Stat. *Mg* II partly in inner shell (17 Lep)

	B. Expanding (P Cyg)
	2. Emission and Absorption P Cyg
Variations	Variable α Cyg absorption (HD 45910, HD 163296? AB Aur?)
Transformations	Into Ab (Z And)
Special features	*E*/*A* measures distance from star

	B. Expanding (P Cyg)
	3. Peculiar Binaries β Lyr, 29 CMa, RY Scu
Variations	Complex (binary motion, etc.)
Transformations	.....
Special features	.....

planetary nebulae than to the true shells. In the case of the B-type companion of α Scorpii, the emission of forbidden [*Fe* II] is concentrated in a small nebulosity surrounding the B star. Adopting a distance of 100 parsecs, a radius of the nebula of 3″, and a radius of the B star of $10R_\odot \approx 10^{12}$ cm, we find an average dilution factor of roughly $W = 10^{-6}$, or even less.

c) The third subdivision of group A consists of stationary shells producing sharp absorption lines. The spectra of these shells show conspicuous dilution effects: in fact, the latter were first recognized from the fact that *He* I 3965 is sharp in ζ Tauri and ϕ Persei, while most other *He* I lines are broad and diffuse[11] and from their appearance suggest excessively rapid axial rotation.[12] The stellar reversing layer is always visible through the shell, but in some cases there is a large amount of veiling due to continuous absorption and emission in the shell (γ Cassiopeiae, ϕ Persei, ζ Tauri), while in others the veiling is imperceptible (Pleione). Several stars show marked effects of stratification, if the amounts of rotational broadening of different lines are so interpreted. In ζ Tauri the effect is especially pronounced: the normal *He* I lines and the *H* wings are produced in the lowest levels, where rotation is largest and where Stark effect widens the Balmer lines; *Si* II and *Mg* II occur higher in the shell, *Fe* II lies still higher, and the cores of *H*, *Ni* II, *He* I 3965—which are the sharpest of all—occupy the highest levels. A similar picture of stratification can be outlined for 48 Librae, ϵ Capricorni, HD 218393, etc. In all these stars the normal lines of *He* I and the wings of *H* lie lowest and the cores of *H* and *He* I 3965, originating from a metastable level, lie highest. The principal lines used for the determination of the dilution factor are *Mg* II 4481 and *Si* II 4128, 4131. These lines originate from normal levels, which connect by means of strong transitions with the ground level. Hence these lines are greatly weakened by dilution. However, it is significant that in Pleione a *Mg* II line of low, but nevertheless appreciable, intensity, having intermediate rotational broadening came into existence with the rest of the shell. This line is definitely produced in the lower strata of the shell and not in the reversing layer, where a line of excessive width was present before the formation of the shell. Also, we notice that, in ζ Tauri, *Mg* II 4481 originates above the reversing layer, though lower than most other lines of the shell. Qualitatively, we explain this effect as the result of the opposing trends of dilution (which favors the lower strata) and ionization (which favors the higher strata). In all cases the ionization decreases outward. The excitation temperatures of the shells are lower than those of the reversing layers. Of particular interest is the shell of 14 Comae, which resembles the spectrum of ϵ Aurigae, except that the *H* lines are very weak. The exciting stars probably all belong to the main sequence (14 Comae, Pleione). The pressures and thicknesses of the shells suggest structures which resemble reversing layers of normal supergiants or may be less dense than the latter by a factor of about 10. There are individual differences, some stars having large optical thicknesses and others small. All known absorption shells form a more or less uniform spectral sequence, which runs parallel to the usual sequence, with the shell nearly always showing a lower degree of ionization than the exciting star. This suggests that the average pressures of the shells are all roughly of the same order. There is a pronounced tendency for the shells to form around main-sequence stars of classes B3 to B5. The latest shell is that of 14 Comae, the star being of class A5n, the shell roughly F2. The earliest is that of γ Cass, the star being of class Bon and the shell about B1. As to origin, axial rotation almost certainly plays an important role. No shells of this kind have been observed in connection with any well-established supergiants. The shells are subject to large variations of an irregular character (Pleione) or of a periodic character (ϕ Persei). In a few (14 Comae) no changes have been observed. There are a number of stars which show stationary shells, together

[11] Struve and Wurm, *Ap. J.*, **88**, 84, 1938; Struve, *Proc. Amer. Phil. Soc.*, **81**, 211, 1939.

[12] Morgan, see *Annual Report of the Yerkes and McDonald Observatories for 1940–41; Pub. A.A.S* in press.

with P Cygni type lines. The best representative of this class is HD 45910. Another example is HD 160529.

We next consider group B, representing the expanding shells. These may be divided into three subdivisions: (*a*) novae and supernovae, (*b*) Wolf-Rayet stars, and (*c*) P Cygni type stars.

Since subdivisions (*a*) and (*b*) have already been the subject of the discussion by Dr. Swings,[13] I shall deal only with subdivision (*c*). This may again be broken up into three classes.

1. Expanding shells showing strong violet-displaced absorption lines with either no emission or very little of it. 17 Leporis is an example. The recognition of expansion in such cases rests upon (*a*) the large negative velocity, (*b*) the difference between this velocity and that given by the broad wings of the *H* lines and by other lines produced in the reversing layer, and (*c*) the irregular variations in velocity and intensities of the lines. In 17 Leporis the lines become double at times.

2. Expanding shells showing strong emission as well as absorption (P Cygni). These shells are sometimes opaque to the lower layers (P Cygni, $-27°11944$, Z Canis Majoris), or they are nearly transparent (α Cygni, β Orionis). Some permit us to recognize through the expanding shell the Stark wings of *H* lines of normal main-sequence reversing layers (HD 190073, 17 Leporis, $+47°3487$), while others show below the expanding shell a stationary supergiant reversing layer (α Cygni, β Orionis, 55 Cygni, HD 160529, υ Sagittarii, ϵ Aurigae). None of the latter reversing layers gives any indication of rapid rotation, and few of the main-sequence reversing layers do ($+47°3487$). In fact, the widths of *Mg* II 4481 in 17 Leporis and HD 190073 give an indication of appreciable, but by no means excessive, axial rotation. It must, however, be borne in mind that in 17 Leporis at least a part of *Mg* II 4481 originates in a low stratum of the shell, which, paradoxically, must be stationary or nearly so. It is a remarkable thing that some objects show simultaneously the characteristics of groups A and B (HD 45910). Binary nature may be important in the formation of the shells ($-27°11944$). The red color, at least, partly due to the Kosirev mechanism, is conspicuous (P Cygni, $-27°11944$). Several P Cygni stars show conspicuous stratification: in P Cygni, and probably in most others, the ionization decreases outward. The range of ionizations represented is usualiy large, and the ratio of emission to absorption increases with increasing distance from the star. The strong absorption lines nearly always show larger velocities of expansion, even when they are not complicated by emission lines (17 Leporis, HD 160529), and this is interpreted as a result of outward acceleration. The effects of dilution are present for some lines (*Fe* III in P Cygni) but are absent or inconspicuous in others (*Mg* II 4481 in P Cygni). This is adequately explained by the great extent of the expanding shell—some lines originating at low levels where dilution is inconspicuous, while others come from higher levels where it is prominent.

3. In this class we combine various peculiar binaries which at times show P Cygni lines. We have already mentioned under group A(*b*) such objects as Z And. Somewhat arbitrarily we add β Lyrae, RY Scuti, 29 Canis Majoris, etc., which show lines of the P Cygni type. It is of interest that 29 CMa, β Lyrae, and, according to unpublished results by Popper, also RY Scuti are close spectroscopic binaries with rapid orbital motion. But, of course, not all close binaries of type B develop expanding shells (α Virginis).

The properties of the expanding shell in β Lyrae, which gives rise to the B5 absorption component and also to the emission component, have been discussed by Kuiper and by Struve.[14] In 29 Canis Majoris the observational evidence is somewhat fragmentary. The absorption spectrum shows only one binary component, and the emission lines are in phase with it. This rather definitely indicates that the shell is associated with the bright component. The emission lines show a large red shift, the origin of which has not been

[13] *Ap. J.*, **95**, 112, 1942.

[14] *Ap. J.*, **93**, 133, 1941; *ibid.*, p. 104.

fully explained. The cutting-down of the violet edge of the emission line by diffuse absorption of the P Cygni type may account for the phenomenon. Red shifts of emission lines in P Cygni stars are not unusual. For example, *Hα* in α Cygni has, according to W. H. Wright,[15] an emission line shifted about 1.2 A to the red from the normal position and an absorption line shifted about 1.4 A toward the violet. It is reasonable to suppose that this red shift is due in some manner to self-absorption.

The spectrum of 29 Canis Majoris shows P Cygni absorption lines during certain phases but not during others. There are also marked changes in the width and in the intensity of the emission line *He* II 4686. From the observations by Struve and Sherman[16] we infer that the violet absorption-line first becomes visible about a half-day before inferior conjunction of the bright component. This is about 0.1 of a complete cycle (p = 4.39351 days). The absorption remains visible until about 1.2 days, or about 0.25 period, after inferior conjunction, and then rapidly disappears. We conclude that the gases stream out of the *brighter* component of 29 CMa in a manner which is quite similar to that predicted by Kuiper for the *fainter* component of β Lyrae. The conservation of momentum then tends to curve the outward-moving stream, so that it will lag behind the rapidly revolving O star. Maximum intensity of the absorption line comes somewhere near the following surface of the O star—a situation which resembles that of β Lyrae. Minimum intensity of emission and greatest haziness of it come at phase 0.80 p. This is almost diametrically opposite to the phase of maximum development of the violet absorption. Occultation easily accounts for the effect. There is also a faint central absorption near phase 0 p. Its origin remains obscure.

The proposed interpretation demands that the gas be emitted by the brighter component. It is reasonable to suppose that this component is also the more massive. But Kuiper's theory requires a stream of matter from A to B and from B into space. Hence we cannot directly apply Kuiper's theory. The question arises as to whether the effect of radiation pressure may not alter the theoretical picture. We shall see later that radiation pressure plays a fundamental role in the P Cygni type stars. 29 CMa is an O star, and the effect of radiation pressure from the star itself and from the shell has not yet been considered.

INTERPRETATION OF THE OBSERVATIONS

It is very difficult to understand why the shell of a star like γ Cassiopeiae or Pleione is stationary, while that of 17 Leporis or of +47°3487 expands. Both have main-sequence exciting stars, and temperature considerations would rather favor expansion in the first pair. It is even more difficult to see how we can have simultaneously, in a star, (*a*) a stationary reversing layer of the main sequence and an expanding shell (17 Leporis); (*b*) a stationary reversing layer of supergiant character and an expanding shell (α Cygni); and (*c*) a stationary reversing layer, a stationary shell, and an expanding shell (HD 45910).

Nevertheless, there are definite indications that we are not dealing with objects of altogether different character. For example, it is suggestive that variable α Cygni absorption lines occur in stationary shells (ζ Tau, 48 Lib, ε Cap) and also in P Cygni stars (HD 45910). There seems to be a pronounced difference between the binaries and the single stars, in the sense that the former often tend to produce large tenuous shells giving forbidden lines. But the groups of single stars merge into one another and often pass even from one group to another. It is tempting to consider them as representatives of a single physical phenomenon. In order to provide a basis for the theoretical interpretation of this phenomenon I shall suggest a working hypothesis, which may tend to oversimplify the actual conditions but which will probably be found useful as a preliminary step in the discussion. We shall disregard, for the time being, those objects which are complicated

[15] *Lick Obs. Bull.*, **8**, 1, 1913.

[16] *Ap. J.*, **93**, 90, 1941.

by binary structure. We shall assume that fundamentally the outer layers of the stars which we are considering are alike: that a supergiant like υ Sagittarii or α Cygni differs from a main-sequence star surrounded by a shell, like γ Cassiopeiae or Pleione, by the optical depth of the outer layers. In the former this optical depth is sufficient to obliterate completely the denser strata below; in the latter the veiling effect is not sufficient to hide the broad wings of the *H* lines. Perhaps we may attribute in some stars the origin

TABLE 2

CLASSIFICATION OF SHELLS

1. Reversing Layer: Stationary, in rapid rotation	2. Chromosphere: Inner, stationary shell	3. Corona: Outer, expanding shell
a) Little veiling 17 Lep Pleione 14 Com Be stars	Small τ_1 *Mg* II in 17 Lep	$\tau_1=0$ Pleione 14 Com Be stars Small τ_1 .....
	Intermediate τ_1 Pleione, Be stars, 14 Com	Intermediate τ_1 17 Lep
	Large τ_1	Large τ_1 .....
b) Strong veiling ζ Tau 48 Lib γ Cas HD 45910 +47°3487 υ Sgr	Small τ_1 +47°3487 HD 45910	$\tau_1=0$ ζ Tau Small τ_1 48 Lib υ Sgr
	Intermediate τ_1 ζ Tau 48 Lib	Intermediate τ_1 HD 45910
	Large τ_1 γ Cas υ Sgr	Large τ_1 +47°3487
c) Invisible P Cyg Z C Ma −27°11944 α Cyg β Ori HD 160529?	Invisible P Cyg Z CMa −27°11944	Small τ_1 α Cyg β Ori
	Intermediate τ_1	Intermediate τ_1 HD 160529?
	Large τ_1 α Cyg β Ori HD 160529?	Large τ_1 P Cyg Z CMa −27°11944

of the tenuous shells to rapid rotation of the main-sequence nucleus. This would produce a shell (or reversing layer) in which the dynamical gravity is partly balanced by centrifugal acceleration and radiation pressure. The inner strata of such a shell do not expand. But it is premature to lay any stress upon the mechanism of shell formation. It must suffice, for the present, that observations prove the existence of such shells.

We are led, therefore, to consider in each star three layers: (1) the main-sequence reversing layer which does not appreciably expand, (2) an inner stationary shell which we may designate as the chromosphere and which has the same radial velocity as the revers-

ing layer, and (3) an outer, expanding shell which we may identify with the corona and which produces the P Cygni type lines. On this basis we can now classify the observational data, using for this purpose the parameter τ_1, the optical thickness of each layer for continuous radiation in the observable region of the spectrum. This classification is presented in Table 2.

This classification is an attempt to overcome the difficulty presented by the frequent occurrence of stationary and expanding shells surrounding ordinary, main-sequence stars; it was formerly believed that only in supergiants is the surface gravity low enough to permit the formation of a shell. At the same time the proposed scheme has the advantage of combining this difficulty with that encountered by Pannekoek and by Struve and Swings in accounting for the support of the reversing layer in a supergiant star. In effect, both difficulties are now reduced to the problem of chromospheric support. However, I want to emphasize that, by postulating that the outer layers of supergiants and of shell-surrounded, main-sequence stars are fundamentally alike, I do not mean to suggest that their internal structure is the same. It certainly is not: the very existence of an opaque stationary shell in α Cygni and υ Sagittarii must affect the structure of the inner layers.

The usefulness of the proposed scheme depends upon one very important tacit assumption, namely, that the three layers are continuous and overlie one another and that we are not concerned with radially moving prominences which are essentially opaque to the underlying gases, while the stationary reversing layer is seen between the prominences. In the case of 17 Leporis, where the bottoms of the violet-displaced lines of *Ca* II are very deep, there can be no doubt that the expanding layer covers essentially the entire disk of the star and that the stationary wings of *H* are seen through the expanding shell. But it must be admitted that for the other stars there is as yet no evidence on this point. This is unquestionably the weakest link in our chain of arguments.

FORCES ACTING UPON THE SHELLS

In order to explain the origin of the three layers, we shall consider three forces: (1) gravity, (2) centrifugal acceleration, and (3) radiation pressure.

CENTRIFUGAL ACCELERATION

In rapidly rotating stars the effective gravity is reduced by rotation:

$$g_{\text{rot}} = \frac{V^2}{r} .$$

For $V = 200$ km/sec, $r = 10\odot = 7 \times 10^{11}$ cm, we obtain

$$g_{\text{rot}} \approx 10^3 \text{ cm/sec}^2.$$

This is of the same order as $g = 10^3$ or 10^4 cm/sec^2.

RADIATION PRESSURE

The acceleration due to radiative pressure is

$$g_r = \frac{\kappa \pi F}{c} ,$$

where κ is the mass-absorption coefficient, F is the net flux of the radiation, and c is the velocity of light.

The effect of the radiation pressure upon the outer layers of a star has been computed many times. We must distinguish between radiation pressure from the continuous spectrum of the photosphere absorbed by (*a*) photoelectric ionizations and (*b*) line formation. Because of the very high abundance of *H* the radiation pressure upon other atoms is negligible if the density is sufficient to produce a uniform velocity of expansion. In most stellar shells this seems to be the case. In the following section we shall consider the radiation field of the shell itself.

Following Gerasimovič,[17] we compute the acceleration gained, on the average, by an *H*-atom in the forward direction from photoelectric ionizations from the ground level,

$$g_r = \frac{(1 - x)\pi}{m_H c} \int_{\nu_1}^{\infty} \kappa(\nu) I(\nu) d\nu \, .$$

The factor $(1 - x)$ measures the ionization. After some changes,

$$g_r \approx \frac{p_e}{(kT)^{3/2}} \times 2.6 \times 10^{-17} \, .$$

For $p_e = 10^{-3}$ atm. Gerasimovič finds the figures shown in the accompanying table.

T	g_r	T	g_r
50,000	1.4×10^3 cgs	15,000	8.8×10^3 cgs
30,000	3.0×10^3	10,000	4.2×10^3
20,000	5.8×10^3	7,000	6

The decrease at low temperatures results from the low intensity in the continuous spectrum. The decrease for higher temperatures results from the increased ionization.

It is a question as to whether in a shell these values of p_e are correct. Of course, the pressures are much lower, but the dilution of radiation causes a reduction in the ionization which tends to cancel the effect of the lowered pressure.

Remembering that $g \sim 10^4$ for a main-sequence star, we conclude that the g_r and g are roughly of the same order of magnitude. A somewhat similar result is obtained for the absorption of $L\alpha$ by atoms, in the continuous spectrum of the star. Both computations presuppose that the star radiates as a black body and that absorption in the reversing layer has not already produced a depletion of those radiations to which the *H* atoms of the shell are sensitive.

It is difficult to see how in stars of similar surface gravity this effect of radiation pressure can lead to stationary shells in some stars and to expanding shells in others.

TRANSFER OF RADIATION THROUGH A SHELL

The problem of the radiative equilibrium of a tenuous shell of gas resembles that of a planetary nebula. The latter problem has been exhaustively treated by Milne,[18] Chandrasekhar,[19] Ambarzumian,[20] Zanstra,[21] and others.[22]

[17] *Op. cit.*, p. 740.

[18] *Zs. f. Ap.*, **2**, 337, 1931.

[19] *Zs. f. Ap.*, **9**, 266, 1935; *M.N.*, **94**, 456, 1934.

[20] *M.N.*, **93**, 50, 1932; *Bull. Poulkovo Obs.*, **13**, No. 3, 1933.

[21] *M.N.*, **95**, 84, 1934; *ibid.*, **97**, 1936.

[22] Rosseland, *Theoretical Astrophysics*, p. 325, Oxford, 1936.

The fundamental physical considerations underlying the theory go back to the work of Zanstra. Consider a shell which consists mostly of hydrogen. If the dilution of the radiation is sufficient, we can neglect line absorptions and photoelectric ionizations from excited levels. We can then make use of Zanstra's argument that essentially all absorption from the ground level will result in (*a*) re-emissions of ultraviolet quanta in the Lyman continuum and (*b*) Lyman α quanta. Recombinations to higher levels and subsequent cascadings downward are all ultimately converted into Lyman α quanta, provided the optical depth τ of the shell for continuous hydrogen absorption beyond the Lyman limit is appreciable. Zanstra's theory presupposes that τ is large. But for our purpose it need not be excessive because the average absorption coefficient within $L\alpha$ is roughly ten thousand times larger than the absorption coefficient for the Lyman continuum; while for higher members of the Lyman series it is, though not so large, still amply large enough that after every emission of $L\beta$, $L\gamma$, etc., there will follow new absorptions with ultimate cascading leading to $L\alpha$.

If we designate by p the probability that an ultraviolet quantum is re-emitted with the same wave length, then $(1 - p)$ is the probability that it will appear in the diffuse nebular radiation as $L\alpha$. In the three-state problem, where 3 designates the continuum, we may write approximately

$$p = \frac{a_{31}}{a_{31} + a_{32}} .$$

According to Cillié,[23] the fraction of electrons captured into the ground level is very nearly 0.5, this quantity being only very slightly affected by temperature.[24] We shall therefore assume

$$p = 0.5 .$$

If we disregard the curvature of the layers and make the usual approximation of the Schwarzschild-Schuster type, where the average intensity of the outward radiation is $I(\tau)$ and that of the inward radiation is $I'(\tau)$, the equations of transfer are

$$\frac{1}{2}\frac{dI(\tau)}{d\tau} = I(\tau) - B(\tau) ,$$

$$\frac{1}{2}\frac{dI'(\tau)}{d\tau} = B(\tau) - I'(\tau) .$$

These equations hold for the ultraviolet diffuse radiation as well as for the $L\alpha$ radiation, provided I and B are properly defined. In the first case $4\pi B(\tau)d\tau$ is the amount of energy emitted in the form of ultraviolet quanta by the layer $d\tau$ within 1 second. In the second problem it is the amount of energy emitted within $L\alpha$ by the layer $d\tau$, where τ is now the optical depth for $L\alpha$, while in the former case it referred to the Lyman continuum. We count τ from the outer boundary of the shell inward. According to Milne, the problem has usually been solved with the following boundary conditions:

$$I'(0) = 0 , \qquad I(\tau_1) = I'(\tau_1) .$$

The latter is equivalent to $F(\tau_1) = 0$, because

$$\pi F = \int_0^{\pi}\int_0^{2\pi} I \cos\theta \sin\theta \, d\theta \, d\phi = I - I' .$$

[23] *M.N.*, **92**, 820, 1932.

[24] Ambarzumian, *Bull. Poulkovo Obs.*, **13**, No. 3, p. 6, 1933.

The condition for the inner boundary means that at each point of the inner surface of the nebula the diffuse radiation in the forward direction is equal to that which this point receives from all other parts of the inner boundary of the nebula. In other words, the star is supposed to be negligibly small as compared to the inner radius of the nebula.

In adapting the theory to the case of a shell we find three main differences between the case of a planetary nebula and that of a shell.

1. The dilution is of the order of 10^{-1} or 10^{-2} instead of 10^{-13}. The importance of this difference has been stressed by Ambarzumian,[25] who has pointed out that the partial compensation of the direct cycle $1 \rightarrow 3 \rightarrow 2 \rightarrow 1$ by the reverse cycle $1 \rightarrow 2 \rightarrow 3 \rightarrow 1$ leads to an important difference in the ionization. However, he remarks: "It seems to us that for the question of the final intensities of the emission lines, it is of little difference whether we take into account the reverse processes or not." The same conclusion is reached by Gerasimovič,[26] who specifically applies Zanstra's reasoning to expanding shells, like that of P Cygni. He states:

> In the idealized nebular problem we may neglect $L\beta$, etc., thus supposing that the whole radiation field is composed of C (continuous UV) and $L\alpha$ quanta. Such a simplifying supposition is, however, not legitimate in our case. In the lower part of an expanding chromosphere with density law $\sim r^{-2}v^{-1}$ the conditions cannot differ much from thermodynamic equilibrium. With increasing r these deviations increase more and more until the nebular conditions are actually reached, where $L\beta$, etc., are being gradually transformed into $L\alpha$ . . . . . It appears therefore practical and reasonable to consider only these nebular strata, where $L\beta$, etc., fields can be neglected.

We shall follow Gerasimovič and idealize our stellar atmosphere by assuming that there exists a sharply defined boundary where conditions approaching thermodynamic equilibrium (the photosphere and the normal reversing layer) suddenly give way to conditions approaching the requirements of Zanstra's theory.

2. The second principal difference arises from the fact that the diameter of the star is not negligibly small as compared to the inner diameter of the shell. Hence Milne's boundary conditions are of no value to us, and we must introduce new ones. The logical modification consists in assuming that the inner boundary of the shell and the outer edge of the normal reversing layer coincide. In that case the boundary conditions become

$$I'(0) = 0 \qquad \text{and} \qquad I(\tau_1) = 0 .$$

These are essentially the conditions used by Gerasimovič.[27] But since his formulae are rather complicated it is convenient to use the derivation by Ambarzumian, who solved precisely this problem for a different purpose.[28]

3. The last serious difference consists in the neglect of curvature of the gaseous layers of the shell. In a relatively thin shell of a planetary nebula at great distance from the nucleus this approximation appears reasonable. It may not hold for a shell whose inner layer has a diameter similar to that of the reversing layer and whose outer radius may be several times larger. In spite of this obvious difficulty we shall discuss the theory for the case of a plane parallel slab.

The solution of the differential equations by Ambarzumian is straightforward. He considers two cases.

[25] *M.N.*, **95**, 469, 1935.

[26] *Op. cit.*, p. 746. [27] *Ibid.*, p. 749.

[28] *Bull. Poulkovo Obs.*, **13**, No. 3, 16, 1933. Ambarzumian used the boundary condition $I(\tau_1) = 0$ in order to allow for the fact that in a uniformly expanding nebula the gas is transparent for $L\alpha$ radiation from behind, because this radiation is shifted by the Doppler effect into frequencies which the atoms we are considering are not capable of absorbing.

A. The optical thickness of the nebula for continuous Lyman radiation, τ_1, is small. In this case the net flux is

$$\pi F_a = \frac{\nu_a}{\nu_c}(1 - p)\pi S\left(\frac{\tau_1}{2} - \tau\right),$$

where ν_a is the frequency of La; νc is the mean frequency corresponding to the Lyman continuum; and πS is the amount of ultraviolet light incident on 1 cm² of the inner surface of the shell. Since $p = 0.5$, the net flux at the inner surface is

$$\pi F_a(\tau_1) = -0.25\pi \frac{\nu_a}{\nu_c} S$$

and is directed inward. At the outer boundary it is

$$\pi F_a(0) = +0.25\pi \frac{\nu_a}{\nu_c} S .$$

The two quantities are equal in amount and are directed in opposite directions.

B. The optical thickness τ_1 is large. In this case the approximation for the inner boundary is

$$\pi F_a(\tau_1) = -\pi \frac{\nu_a}{\nu_c} S .$$

The outward flux at the outer boundary is

$$\pi F_a(0) = 0 ,$$

because the sum of the absolute values of the two fluxes must be, for $\tau_1 = \infty$, equal to $\pi (\nu_a/\nu_c) S$.

The important thing here is that there is a large flux directed inward. The physical meaning for the disappearance of the outward flux when τ_1 is very large is, in the case of Ambarzumian's expanding shell, that the inward radiation is freely transmitted by those portions of the nebula which lie behind the star, because the Doppler effect prevents the atoms from absorbing them. In our case the inward radiation is lost within the star, where it is ultimately transformed into black-body radiation. As such it is already accounted for in our value of S.

The theory has been developed by Chandrasekhar, who has given simple formulae for both sets of boundary conditions and has actually computed the flux in La for different values of p and of τ_1.[29] For boundary conditions of the type $2J(\tau_1) = F(\tau_1)$; $2J(0) = F(0)$, which correspond to the expanding nebula case, he gives the following values of the flux in units of $(\nu_a/\nu_c)S$, when the total optical thickness τ_1 in ultraviolet light beyond the Lyman limit is 2 (see accompanying table). The table shows a large negative flux at the

τ	$F_a^*(\tau)$ for $\tau_1 = 2$ and $p = 0.5$	τ	$F_a^*(\tau)$ for $\tau_1 = 2$ and $p = 0.5$
0	+0.293	1.25	−0.050
0.25	+ .253	1.50	− .174
0.50	+ .201	1.75	− .324
0.75	+ .135	2.00	−0.501
1.00	−0.051		

[29] *Loc. cit.*

inner boundary and a small outward flux at the outer boundary. It is rather obvious that this result will be retained even after the curvature of the layers has been allowed for.

There remains one further complication. The formulae apply to the case of a stationary nebula or of a nebula which expands with a uniform velocity (Ambarzumian). They require modification if the expansion is accelerated or decelerated. Zanstra[30] has shown that for an expanding nebula, in which the mechanical velocity V is proportional to the optical depth, the net flux is only $\frac{1}{3}(W/V_L)^2$ of what it would be for a stationary nebula having the same thermal width W, if V_L is the range in velocity of expansion within the principal luminous portion of the nebula. But in the cases which we are considering V_L is always relatively small, while W is large because of turbulence. Gerasimovič[31] completely disregarded the Doppler effect in his computation of the Lyman flux. He assumed a velocity of expansion decreasing from $V = 250$ km/sec at $\tau = \tau_1$ to 0 km/sec at $\tau = 0$. He also assumed $\tau_1 = 10$ and found that $\Delta V = 0.1$ km/sec corresponds to $\Delta\tau_u = 4 \times 10^{-3}$ or to $\Delta\tau_a = 27$. Hence, even disregarding thermal velocities, La is practically opaque for distances which correspond to very small changes in the velocity of expansion. We can probably conclude that the reduction in La flux due to accelerated or decelerated expansion is relatively unimportant in the case of an expanding shell.

RADIATION PRESSURE OF La FLUX

For large τ_1 in a nebula in which the entire Lyman continuum of the star's continuous spectrum is converted into outward La flux we have

$$\pi F_a = \frac{r_1^2}{r_2^2}\,\frac{2\pi h\nu_a}{c^2}\int_{\nu_0}^{\infty}\frac{\nu^2 d\nu}{e^{h\nu/kT}-1}\,.$$

The acceleration per H atom in the normal state is

$$\frac{\kappa\pi F_a}{c} = \frac{r_1^2}{r_2^2}\,\frac{2\pi\kappa h\nu_a}{m_H c^3}\int_{\nu_0}^{\infty}\frac{\nu^2 d\nu}{e^{h\nu/kT}-1}\,,$$

and the ratio to gravity, $g\,(r_1^2/r_2^2)$, is, after allowing for ionization,

$$\mu = \frac{g_r}{g} = \frac{\kappa\pi(1-x)2h\nu_a}{mgc^3}\int_{\nu_0}^{\infty}\frac{\nu^2 d\nu}{e^{h\nu/kT}-1}\,.$$

Ambarzumian has computed this quantity and finds for $n_2/n_1 = 500$, $T = 40{,}000°$,

$$\mu = \frac{10^{10}}{g}\,.$$

This is too large by a considerable factor because (1) τ_1 is not ∞ and (2) the Lyman continuum is already partly depleted in the reversing layer. But it is difficult to see how we can escape a value of μ which is much larger than 1.

The equation of motion of the shell under the influence of gravity, radiation pressure, and density gradient is

$$v\,\frac{dv}{dr} = \frac{g}{r^2} - \frac{g_r}{r^2} + \frac{RT}{m_0}\,\frac{1}{\rho}\,\frac{d\rho}{dr}\,.$$

Disregarding the density gradient and gravity, we find

$$\tfrac{1}{2}v^2 = \frac{g_r}{r^2}\,(r_2 - r_1)\,.$$

[30] *Op. cit.*, **95**, 96, 1934. [31] *Op. cit.*, p. 750.

Consider a shell whose average radius is five times the radius of the star. Then, if $g = 10^3$ cm/sec^2,

$$\frac{g_r}{r^2} \approx 4 \times 10^5 \text{ cm/sec}^2 ,$$

and, for $r_2 - r_1 = 10R\odot = 7 \times 10^{11}$ cm,

$$v = 8 \times 10^8 \text{ cm/sec} \approx 10{,}000 \text{ km/sec} .$$

Even in the middle of the shell the velocity is of the order of 5000 km/sec. Although the force of gravity and the density gradient will tend to reduce these velocities, they are still very much too large in comparison with the values which we have observed. It is difficult to estimate the influence of factors 1 and 2.

If we adopt the result of Ambarzumian for small τ_1 and allow for an appreciable depletion of the Lyman continuum in the deeper parts of the reversing layer, we may estimate

$$g_r = +10^4 \text{ cm/sec}^2 \qquad \text{(inside layers)},$$

$$g_r = -10^4 \text{ cm/sec}^2 \qquad \text{(outside layers)}.$$

The structure of the shell inside will resemble that of a normal star. The *H* and *He* lines may even show some Stark effect. For the outside layers we then obtain

$$v = 400 \text{ km/sec} .$$

This is no longer quite so excessive. In several P Cygni stars the velocity of expansion approaches this value. However, in most stars the observed expansion is absent or very small. How shall we explain this? The problem may be resolved in one of two ways.

1. We have seen that, when τ_1 is large, the outward flux is small and radiation pressure outward is negligible. The radiation pressure inward would be very large, and it is difficult to see how the density of the inner atmosphere can be low enough to give rise to such sharp *H* lines as those of ϕ Per, ζ Tau, etc.

2. The quantity τ_1 refers to absorption of the Lyman continuum. Hence the critical value $\tau_1/2$, at which the flux of *La* radiation changes sign, refers also to *La*. However, because of the high excitation potential of the Balmer lines, on one side, and the relative weakness of these lines, on the other, we should expect that they would be produced in much deeper layers and would come predominantly from the inner, stationary shell.

INTERPRETATION OF THE OBSERVATIONS

1. We at once understand the origin of three distinct layers: (*a*) the normal reversing layer, often showing rapid axial rotation; (*b*) the stationary α Cygni type layer, having sharp lines and often showing signs of moderate dilution; and (*c*) an outer P Cygni type layer, where the atoms are accelerated outward and where dilution should be conspicuous.

In some stars we observe all three layers: HD 45910 is an excellent example. In others we observe only (*b*) and (*c*). HD 160529 is an example. Still others show only layer (*c*): for example, P Cygni. Some show layers (*a*) and (*c*), with but a trace of (*b*); an example is 17 Leporis. This is essentially the scheme which we proposed as a working hypothesis on page 143.

2. We do not yet understand why the optical thicknesses of the two shells are so very different in different stars. But one or two clues are present. Whenever the optical thickness of the entire shell (both stationary and expanding) is very small, we have almost no expansion, we see only the stationary shell, and the reversing layer is that of a main-se-

quence star. Presumably, ionization and excitation of the *observable* shell lines favor the inner regions. There are not enough excited H atoms in the outer regions to show P Cygni lines, although there must be plenty of H atoms in the ground state. When the optical thickness of the entire shell is large, then we may have either an expanding shell (P Cygni) or predominantly a stationary layer (α Cygni). Perhaps this is somehow connected with the ratio of g_r/g in the inner regions.

3. We do not yet account for the variations, although there is reason to believe that the mechanisms considered by Gerasimovič[32] and by McLaughlin may account for some of them. In particular, Gerasimovič succeeded in giving a plausible explanation for the V/R variation in Be stars. It is tempting to consider the phenomenon of doubling of lines in 17 Leporis. This suggests that at certain times a new shell, having a larger velocity of expansion, is formed. Such a formation may result from one of two causes: (*a*) a sudden increase in the amount of UV light in the star and (*b*) an increase in the $L\alpha$ flux of the shell. The former is improbable because no conspicuous changes in visible light have been recorded. The latter is entirely plausible and may be the consequence of one of two effects: the density of H may increase, leading to an increase in τ_1, or the opacity of the nebulous matter may increase because of a reduction in the outward acceleration. The latter idea is essentially that of Zanstra. It is characteristic that the outbursts occur when the velocity of expansion of the shell is least. But there is not enough material at present to pursue this interesting speculation.

UNSOLVED PROBLEMS

Beals and I have independently given a number of strong reasons for believing that in an expanding shell the ratio of emission to absorption is a good measure of the diameter of the shell. For example, in the case of P Cygni this criterion gives consistent results and permits us to study the stratification of ions in the shell. But the purely geometrical factor does not explain why the emission lines are strong in P Cygni and weak in 17 Leporis; and there are other similar inconsistencies.

The difficulty becomes even more apparent when we compare the relative importance of emission in a W star and in a shell, like that of γ Cassiopeiae (in the sharp absorption-line stage). Swings has shown that the dilution factors of the W stars are substantially the same as those of typical stellar shells ($W \sim 0.1$). Hence it is difficult to see how the geometrical factor *plus* dilution effect can cause the emission to be so enormously more important in the W stars than in the shells. The only suggestion that now offers itself is that turbulence, which presumably is correlated with the velocity of expansion, tends to introduce cyclic processes which favor the production of visible emission lines. There is some unrelated evidence in different stars that turbulence can superexcite the atoms to an appreciable degree.[33]

In the discussion of the observations it has not been possible to give specific references to all the many papers which I have consulted. I therefore express here my indebtedness to those investigators whose work has laid the foundations of our knowledge of extended atmospheres, especially to Dr. P. W. Merrill and his associates at the Mount Wilson Observatory, Dr. J. S. Plaskett and Dr. C. S. Beals and their associates at the Dominion Astrophysical Observatory, and Dr. D. B. McLaughlin of the University of Michigan Observatory. The theoretical interpretation rests almost entirely upon the brilliant work of V. A. Ambarzumian and S. Chandrasekhar.

McDonald Observatory
September 1941

[32] *Observatory*, **58**, 115, 1935.

[33] The solar corona, according to Edlén; the atmosphere of ζ Aurigae, according to Wellmann (*Veröff. Berlin-Babelsberg*, **12**, No. 4, 1939).

SPECTROGRAPHIC OBSERVATIONS OF PECULIAR STARS. III*

P. SWINGS AND O. STRUVE

ABSTRACT

This paper describes recent changes in the spectra of AX Per, Z And, AG Peg, and R Aqr. There is also a description of recent spectrograms of the unusually red bright-line star MWC 349.

Our understanding of the physical, dynamical, and geometrical conditions prevailing in peculiar objects which combine bright lines of high excitation and late-type spectra will eventually be based on the spectroscopic variations in these stars. CI Cygni is the only complex object known which shows forbidden lines of high excitation which do not seem to have varied appreciably in recent years, although the late-type companion is variable. As far as the bright lines of high excitation are concerned, our spectrograms of CI Cygni since September, 1939, do not differ from the ones taken by Merrill in 1931 and 1932.[1] The present paper is concerned with the description and discussion of recent spectral changes in AX Persei, Z Andromedae, AG Pegasi, and R Aquarii. It also provides some additional information on the peculiar bright-line star MWC 349.

AX Persei.—This object, which in 1939 was similar to CI Cygni to such an extent that one could hardly distinguish their spectra, has suffered conspicuous variations. The 1939 spectrum corresponded to a much higher ionization than that of 1931–1932, when it was described by Merrill.[1] But on our spectrograms of January, 1941, the forbidden lines of [*Fe* VII], which were extremely intense in 1939,[2] had disappeared, and other changes had also occurred.[3] Now our spectrograms of August 2 and 8, 1941, have reversed the situation, the star having recovered a bright-line spectrum very similar to that of September, 1939. [*Fe* VII], practically absent in January, 1941, had recovered in August, 1941, its intensity of 1939. A comparison of line intensities in the region λλ 3869–6560 on January 5, 1941, and August 8, 1941, is given in Table 1; intermediate intensities are observed on a spectrogram secured on May 30, 1941. It is apparent that the general trend after January, 1941, has been toward an increase in excitation, which had reached a minimum around January, 1941. This increase is evidenced by the following changes in the intensities relative to *He* II and *H:* (*a*) the large increase of [*Fe* VII] and [*Ne* V]; and (*b*) the decrease in intensity of *He* I, *N* III, *C* III, [*O* III], and [*Ne* III]. It should be noticed that the *He* I triplets have been reduced less than the singlets (compare, for example, λ 4388 and λ 4471).

Z Andromedae.—After its 1939 outburst to a mean maximum magnitude of 7.9, Z Andromedae declined to a mean minimum brightness of 9.6 in 1940 and then increased again in 1941, reaching magnitude 8.7 in August, 1941.[4] We noticed this recent outburst at the 82-inch telescope on July 25 and August 6. Our spectrograms reveal very striking changes in this binary since August, 1940, and even since January 5, 1941.

With regard to line intensities and structures, the evolution of the emission lines may be summarized as follows: (*a*) Increases in the following intensity ratios: *Fe* II/*N* III, *C* III, *C* IV; *O* III fl./[*Ne* V]; *He* I/[*Ne* III]; *Fe* II/*He* I; *Fe* II/[*O* III]; *Si* II/Continuum; *Mg* II/Continuum. (*b*) No variation in the structure of the "nuclear" features in the region λλ 4632–4658, but a general weakening, compared to *Fe* II. (*c*) A general intensity decrease of the forbidden lines [*O* III], [*Ne* III], [*Ne* V]. (*d*) A slight decrease in

* *Contributions from the McDonald Observatory, University of Texas*, No. 42.

[1] *Ap. J.*, **77**, 44, 1933. [2] *Ap. J.*, **91**, 607, 1940. [3] *Ibid.*, **94**, 298, 1941.

[4] *Harvard Announcement Card*, Nos. 595 and 598; Leon Campbell, *Pop. Astr.*, **49**, 446, 1941.

the ratio of the auroral to the nebular transitions of [*O* III] since 1940 (no appreciable change since January, 1941). (*e*) A very strong Balmer continuum in emission.

The measured lines are shown in Table 2; the wave lengths have been corrected to the sun but have not been corrected for the motion of the star. For the identifications extensive use was made of our new table of wave lengths in α Cygni.[5] In the region be-

TABLE 1

COMPARISON OF THE LINE INTENSITIES IN AX PERSEI ON JANUARY 5, 1941, AND AUGUST 8, 1941

Element and λ	Intensities		Element and λ	Intensities	
	January 5 1941	August 8 1941		January 5 1941	August 8 1941
3869 [*Ne* III]	4	2	4641 *N* III	4–5	1
3889 H_8 + *He* I	2	5	4646 *C* III	3	1–0
3967 [*Ne* III]	2	1	4649 *C* III	3n	
Hε	3	4	4686 *He* II	10	8
4009 *He* I	1	abs.	4713 *He* I	2	1
4026 *He* I	2	1	*Hβ*	10	15
4097 *N* III	4	1–0	4922 *He* I	2–3	1
Hδ	3	4	N_2 [*O* III]	2	0
4144 *He* I	2–3	1	N_1 [*O* III]	4	1–2
4200 *N* III + *He* II	1n	0	5016 *He* I	1	1
Hγ	7	8	5158 [*Fe* VII]	abs.	1–2
4351 *Fe* II	abs.	0–1	5275 [*Fe* VII]	abs.	1–0
4363 [*O* III]	5	2–3	5412 *He* II	2	2
4388 *He* I	2–3	1	5721 [*Fe* VII]	0	3
4471 *He* I	3	2	D_3 *He* I	7	7
4634 *N* III	2–3	1–0	6086 [*Fe* VII]	0	6
			Hα	15	15

tween the Balmer limit and λ 3445, the very strong continuous hydrogen emission is interrupted only by the absorption lines 2p $^3P^\circ$ – 8, 9, 10d ^3D of *He* I (λλ 3634, 3587, and 3554); no trace is observed of *He* I 3613, which means that the dilution effect is not important. This latter result is in agreement with the observations of a violet absorption component of the lines 2p $^3P^\circ$ – 5, 6, 7 d ^3D. *He* I 3634 cuts deeply into the Balmer continuum. The continuous spacings between the higher members of the Balmer

[5] *Ap. J.*, **94**, 344, 1941. According to the variable-star observers of the Milwaukee Astronomical Society, the apparent visual magnitude of Z And was 8.8 at the time of our spectroscopic observations.

TABLE 2

SPECTRUM OF Z ANDROMEDAE (JULY–AUGUST, 1941)

λ	Int.	Identification			λ	Int.	Identification		
		Element	λ	Int.			Element	λ	Int.
3420.83	0E	*Cr* II	1.20	75	3712.21	5En	H_{15}	1.97	5
							Cr II	2.97	35
3422.71	1E	*Cr* II	2.74	125			*Cr* II	3.04	15
3426.05	1–0E	[*Ne* V]	5.8	.....	3714.73	1E	*Cr* II	5.19	20
							Cr II	5.45	20
3443.45	4E	*O* III	4.10	5			*V* II	5.48	1200
							O III	5.08	6
3554	0A	*He* I	4.39	7					
					3719.83	0E	*Fe* I	9.93	1000
3587	1A	*He* I	7.25	10					
		He I	7.40	2	3722.05	5E	H_{14}	1.94	6
3633.45	3A	*He* I	4.24	15	3724.04	0E	*Cr* II	3.40	15
		He I	4.37	2					
					3726.88	1E	[*O* II]	6.12	.....
3664.37	0–1E	H_{28}	4.68	.....			*Cr* II	7.37	40
							V II	7.35	1000
3665.86	1E	H_{27}	6.10	.....					
					3728.55	0–1E	[*O* II]	8.91	.....
3667.59	2E	H_{26}	7.68	.....					
					3734.51	6E	H_{13}	4.37	8
3669.40	2E	H_{25}	9.47	.....					
					3737.03	2E	*Cr* II	7.55	10
3671.39	3E	H_{24}	1.48	.....			*Fe* I	7.13	1000
3673.90	3–4E	H_{23}	3.76	.....	3739.19	0–1E	(*Cr* II	8.38	25)
3676.38	3–4E	H_{22}	6.36	.....	3741.58	2E	*Ti* II	1.65	200
3677.34	2E	*Cr* II	7.69	40	3745.71	2–3E	*V* II	5.81	800
		Cr II	7.86	50			*Fe* I	5.56	500
		Cr II	7.93	30					
					3748.00	2E	*Fe* II	8.49	8
3679.42	4E	H_{21}	9.35	.....			*Fe* I	8.26	500
3681.02	1E	.....	.....	.....	3750.30	6E	H_{12}	0.15	10
3682.66	4E	H_{20}	2.81	.....	3754.60	2E	*Cr* II	4.59	20
							O III	4.67	7
3684.71	1E	*Cr* II	4.25	25			*N* III	4.62	6
		Ti II	5.20	700					
					3757.48	1E	*Ti* II	7.69	100
3686.93	4E	H_{19}	6.83	.....			*O* III	7.21	5
3691.57	4E	H_{18}	1.56	2	3759.23	2E	*Fe* II	9.46	6
							Ti II	9.30	400
3697.18	5E	H_{17}	7.15	3			*O* III	9.87	9
3700.01	0E	*V* II	0.34	200	3760.83	1E	*Ti* II	1.32	300
3703.42	5E	H_{16}	3.85	4	3764.22	1–0E	*Fe* I	3.79	500
3705.55	4En*	*He* I	5.00	30	3766.74	0E	*Fe* I	7.19	500
		He I	5.14	3			(*Cr* II	6.65	4)

* Faint violet absorption.

TABLE 2—*Continued*

λ	Int.	Identification			λ	Int.	Identification		
		Element	λ	Int.			Element	λ	Int.
3770.73	7E	*H* II	0.63	15	3895.83	1E	*Fe* I	5.66	400
3783.14	2E	*Fe* II	3.35	4	3900.12	2E	*Ti* II	0.54	50
							Al II	0.68	200
3795.47	1E	*Fe* I	5.00	500	3903.19	1E	*V* II	3.26	250
3797.96	7E	*H* 10	7.90	20	3905.57	2E	*Si* I	5.53	15
3806.26	0–1En	*He* I	5.76	3			*Cr* II	5.64	25
		(*Si* III	6.56	5)	3913.84	2–3E	*Ti* II	3.46	70
3813.73	2En	*Fe* II	4.12	4	3926.57	1–2E	*He* I	6.53	7
		Cr II	4.00	12	3930.31	2–3E	*Fe* I	0.31	600
3818.66	3A	*He* I	9.61	50	3933.78	3E	*Ca* II	3.67	600
3820.12	3E				3938.31	3–4E	*Fe* II	8.29	2
3824.88	1E	*Fe* II	4.91	4	3943.38	1–0E	(*Al* I	4.03	2000)
3827.11	0E	*Fe* II	7.08	4	3945.15	2E	(*Cr* II	5.11	1)
3829.60	1–0E	*Mg* I	9.35	100	3951.50	0En	*V* II	1.97	500
3832.90	1E	*Mg* I	2.31	250			*Fe* I	1.17	150
3835.55	6E	*H* 9	5.39	40	3961.00	1En	*Fe* II	0.89	3
3838.24	1–2E	*Mg* I	8.26	300			*Al* I	1.53	3000
							O III	1.59	8
3845.23	1E	.....	.....	.....	3965.01	4E	*He* I	4.73	50
3848.39	1E	*Mg* II	8.24	10	3967.89	2E	[*Ne* III]	7.5	.....
3849.80	1–2E	*Mg* II	0.40	5			*Ca* II	8.47	500
		Fe I	9.97	500	3970.32	8E	*He*	0.08	80
3854.84	1A	*Si* II	6.03	8	3973.78	1–2E	*Fe* II	4.16	3
3856.12	4E						*V* II	3.64	300
							O II	3.27	125
3859.73	0–1E	*Fe* I	9.91	1000	3978.32	1–0E	(*Fe* I	7.75	300)
3861.23	1A	*Si* II	2.59	6	3981.89	1–0E	(*Fe* I	1.77	150)
3862.40	4E				3987.20	1–0E	.....	.....	.....
3865.45	1E	*Cr* II	5.59	75	3991.56	0–1E	(*Si* II	1.77	2n)
3868.64	4E	[*Ne* III]	8.7	.....	3997.87	0–1E	(*Si* II	8.00	1n)
3872.35	1E	*He* I	1.82	5			*Fe* I	8.05	150
3878.71	2E	*V* II	8.71	300	4002.35	1E	*Fe* II	2.55	3
3887.76	2A†	*He* I	8.65	1000	4005.36	0–1E	*V* II	5.71	800
3889.03	9E	*H* 8	9.05	60	4009.58	2E	*He* I	9.27	10

† The absorption component is due to *He* I only.

TABLE 2—*Continued*

λ	Int.	Identification			λ	Int.	Identification		
		Element	λ	Int.			Element	λ	Int.
4012.60	1–2E	*Cr* II	2.50	30	4227.35	0E	*Ca* I	6.73	500
							Al II	6.81	35
4015.51	1E	*Ni* II	5.48	1			*Al* II	7.50	30
							Al II	7.98	20
4025.61	2A	*He* I	6.19	70			*Fe* I	7.43	300
4026.65	5E				4232.89	5E*	*Fe* II	3.17	11
4054.02	1E	*Cr* II	4.11	8	4267.37	1E*	*C* II	7.02	350
							C II	7.27	500
4063.80	0E	*Cr* II	4.05	.....					
		Fe I	3.60	400	4286.85	1E	[*Fe* II]	7.40	
4066.97	1E	*Ni* II	7.05	30	4289.81	1E	*Ti* II	0.23	60
4069.28	0E	[*S* II]	8.5	.....	4293.53	1E	*Ti* II	4.12	80
		C III	7.87	6			*Fe* I	4.13	700
		C III	8.94	7					
		C III	0.43	8	4296.56	1E	*Fe* II	6.58	6
4071.56	1E	*Fe* I	1.74	300	4307.42	1E	*Ti* II	7.90	100
		(*Cr* II	0.90	10)			*Fe* I	7.91	1000
4075.87	2E	*O* II	5.87	800	4313.12	1E	*Ti* II	2.87	100
		Si II	5.45	2					
					4315.07	1E	*Ti* II	4.98	20
4097.40	4E	*N* III	7.31	10			*Fe* I	5.09	500
4102.20	10E	*Hδ*	1.75	100	4320.97	1E	*Ti* II	0.96	40
		N III	3.37	9			*Sc* II	0.74	40
4121.16	1–2E	*He* I	0.81	25	4331.36	1E	*Fe* II	1.53	3
4122.46	1–2E	*Fe* II	2.64	4	4340.79	10E	*Hγ*	0.48	200
4124.88	0E	*Fe* II	4.79	1	4351.60	4E	*Fe* II	1.76	9
							Mg I	1.91	15
4128.15	1–2E	*Si* II	8.05	20					
		Fe II	8.73	3	4358.66	1E	[*Fe* II]	9.34	.....
4131.19	1E	*Si* II	0.88	25	4363.21	5E	[*O* III]	3.20	.....
4143.71	3E	*He* I	3.76	15	4368.22	0E	*O* I	8.30	1000
							Fe II	8.26	1
4161.27	0–1E	*Ti* II	1.54	30			*Ti* II	7.66	25
4163.71	2E	*Ti* II	3.65	150	4384.30	2–3E	*Fe* II	5.38	7
							Fe I	3.55	1000
4166.11	1–0E	.....	.....	.....			(*Mg* II	4.64	8)
4169.00	1–0E	*He* I	8.97	7	4387.47	3E	*He* I	7.93	30
4171.51	1–0E	*Ti* II	1.90	70	4390.48	1–0E	*Mg* II	0.58	10
4173.68	2–3E	*Fe* II	3.45	8	4394.91	2En	*Ti* II	5.04	150
4178.63	3E	*Fe* II	8.85	8	4399.60	2E	*Ti* II	9.77	100

TABLE 2—*Continued*

λ	Int.	Identification		
		Element	λ	Int.
4404.88	1E	*Fe* I	4.75	1000
4414.70	1E	[*Fe* II]	3.78	.....
		O II	4.89	300
4417.08	3En	*Fe* II	6.82	7
		[*Fe* II]	6.28	.....
		Ti II	7.72	80
4443.20	1E	(*Ti* II	3.80	125)
4468.40	1E	*Ti* II	8.50	150
4472.12	5E*	*He* I	1.48	100
4480.93	3E	*Mg* II	1.33	100
4488.75	1–2E	*Fe* II	9.18	4
		Ti II	8.32	125
4491.62	1–2E	*Fe* II	1.40	5
4501.21	1E	*Ti* II	1.27	100
4508.73	2E	*Fe* II	8.28	8
4515.43	2E	*Fe* II	5.34	7
4520.54	2E	*Fe* II	0.22	7
4522.86	2E	*Fe* II	2.63	9
4529.11	1E	*Ti* II	9.46	40
		V II	8.51	300
4534.17	2E	*Ti* II	3.97	150
		Fe II	4.17	2
		Mg II	4.26	4
4541.46	2En	*Fe* II	1.52	4
		He II	1.63	5
4549.74	3–4E	*Fe* II	9.47	10
		Ti II	9.63	200
4555.95	3E	*Fe* II	5.89	8
4558.19	1E	*Cr* II	8.66	100
4564.04	0E	*Ti* II	3.77	200
4571.57	0E	*Mg* I	1.10	20
		Ti II	1.98	300
4576.89	0E	*Fe* II	6.33	4
4583.93	4E	*Fe* II	3.84	11
4589.29	1–0En	*Cr* II	8.22	75
		Cr II	9.89	3
		Ti II	9.95	100
4619.87	2Enn	*Cr* II	8.83	35
		Fe II	0.51	3
4629.53	4E	*Fe* II	9.34	7
4635.06‡	3–4E	*N* III	4.16	8
		Fe II	5.33	5
		Cr II	4.11	25
4641.23‡	4–5E	*N* III	0.64	10
		N III	1.90	3
4649.19‡	3Enn§	*C* III	7.40	10
		C III	0.16	9
		C III	1.35	8
4657.53‡	1E	*C* IV	8.64	5
		C IV	6.5	4
4685.58	12E	*He* II	5.81	300
4709.65	1–0E	(*Fe* II	8.97	3)
4713.99	3E†	*He* I	3.14	40
		He I	3.37	7
4732.17	1E	*Fe* II	1.44	3
4861.95	15E	*Hβ*	1.34	500
4919.64	1A	*He* I	1.93	50
4922.80	6E	*Fe* II	3.92	12
4936.55	1E	.....	.....	.....
4959.36	4E	[*O* III]	8.91	.....
4993.96	1E	*Fe* II	3.35	1
5007.05	6E	[*O* III]	6.84	.....
5017.33	5E	*He* I	5.67	100
		Fe II	8.43	12
5040.16	1–0E	(*Si* II	1.13	8)
5048.01	1E	*He* I	7.74	15

‡ These "nuclear" features have a violet absorption component, and their general structure has not changed since August, 1940.

§ Extends from λ 4646.3 to λ 4651.9.

TABLE 2—*Continued*

λ	Int.	Identification			λ	Int.	Identification		
		Element	λ	Int.			Element	λ	Int.
5168.82.....	3E	*Fe* II	9.03	12	5283.95.....	1E	*Fe* II	4.09	3
5183.66.....	1–oEn	*Mg* I	3.62	500	5316.92.....	4E	*Fe* II	6.61	8
5197.60.....	2E	*Fe* II	7.57	6	5362.82.....	2E	*Fe* II	2.86	5
5226.66.....	oE	*Ti* II	6.55	50	5534.79.....	2E	*Fe* II	4.86	4
		Fe I	7.19	400	5876.....	10E	*He* I	5.62	1000
5234.64.....	1–2E	*Fe* II	4.62	7	6563.....	20E	*Hα*	2.82	2000
5275.16.....	3E	*Fe* II	5.99	7					

series are faint; this shows that the continuous spectrum at λ 3613 is practically all due to the Balmer continuum. Hence, this continuum is absorbed by overlying *He* I atoms.

The radial velocities on August 6, 1941, have the following values:

H: Mean $V_{em} = +5$ km/sec; from *Hγ* and *Hε* alone: $V_{em} = +20$ (against +16 in 1940)

He I: Mean $V_{em} = +21$ km/sec; individual values in the $2p\ ^3P^\circ - nd\ ^3D$ series:
$n = 5$, λ 4026, $V_{abs} = -43$, $V_{em} = +34$, $V_{em} - V_{abs} = 77$
$n = 6$, λ 3820, $V_{abs} = -75$, $V_{em} = +40$, $V_{em} - V_{abs} = 115$
$n = 8$, λ 3634, $V_{abs} = -59$
Mean $V_{em} - V_{abs} = 96$ (against a mean value +81 in 1940)

Si II: $V_{abs} = -99$; $V_{em} = +10$, $V_{em} - V_{abs} = 109$ km/sec

Metallic ions: V_{em} of *Fe* II: −2; *Ti* II: −13; *Cr* II: −11; *Mg* II: −27; *Ca* II: +8

High excitation features: $V_{em} = +9$ (against +6 in 1940)

Nuclear features: No variation in either V_{em} or V_{abs} since 1940

On the whole, we may say that all the emission lines not accompanied by violet absorptions have about the same radial velocity; that the velocity of expansion of *He* I is essentially the same as in 1940; that *He* I and *Si* II have practically the same ejection velocities; and that the "nucleus" and the "forbidden nebular lines" have, as a whole, simply become fainter in the course of 1941.

Whatever may be the true origin of the "nuclear" features—either an exciting Wolf-Rayet nucleus or deep layers in the nebula—their intensity decrease, which was simultaneous and similar to that of the forbidden nebular lines, is easily understood. The other spectroscopic variations observed in 1941 are presumably due to the fact that more abundant matter was ejected with practically the same velocity as last year. Part of the emissions and violet absorptions (excluding the "nuclear" features) arise in the new

shell, which is still fairly close to the photospheric surface. The opacity of the new shell reduces the excitation in the nebula.

This general picture is crude and qualitative; but it is hoped that additional observations may provide data for a more or less quantitative treatment.

AG Pegasi (*BD* + 11°4673).—The general trend toward higher excitation has continued.[6] Comparing our 1941 spectrograms[7] with those of 1939–1940, it is apparent (1) that *Si* I 3905 has disappeared; (2) that *Ca* II and *Fe* II have decreased in intensity; and (3) that *He* II, *N* III, and *Si* IV have increased appreciably.

R Aquarii.—Spectrograms of this object secured on July 30 and August 12, 1941, when the late-type companion was near minimum,[8] reveal that this peculiar star has recovered its [*Fe* III] stage.[6] The [*Fe* III] lines were observed by Merrill from 1919 to 1926, inclusive, when the nebular spectrum was strong, as a whole. On a 1924 plate, λ 4658 was "probably accompanied by λ 4701 and λ 4733." In 1939 there was no trace of [*Fe* III]. The emission lines observed on our spectrograms of August, 1941, are:

H: *Hα* (20), *Hβ* (12), *Hγ* (6), *Hδ* (4), *Hε* (4, bl), H_8 (4, bl)
He I: D_3 (3), 4471 (1–2), 4144 (0–1), 3889 (4 bl)
[*O* II]: 3727 (2)
[*O* III]: N_1 (15), N_2 (6), 4363 (5)
[*S* II]: 4069 (3), 4076 (1)
[*Ne* III]: 3869 (6), 3967 (4 bl)
Fe II: 4303 (1–2), 4352 (1–2)
[*Fe* II]: 4244 (1), 4287 (1), 4414–4416 (2)
[*Fe* III]: 4658 (2), 4702 (1), 4755 (0)
Mg I (or unidentified): 4571 (3)

The presence of the transitions of nebular type of [*O* II] is interesting, since they have an extremely low transition probability; they must undoubtedly arise in a nebular region of extremely low density.

MWC 349.[9]—The line emission in this star has been described by Merrill, Humason, and Burwell as follows:[10] "In addition to the hydrogen lines, the bright nebular line at λ 4658 is well marked and the companion line λ 4701 is visible. Bright lines of neutral helium are also present and possibly λ 4583 of ionized iron."

MWC 349 bears a striking spectral analogy to MWC 17[11] and should also be compared to the star of slightly higher excitation, RY Scuti.[12] It is located in a dark region of the Milky Way and is reddened to a considerable extent; the total absorption is probably of the order of 10 mag.

[6] This was also observed by Dr. P. W. Merrill (communication at the Yerkes Observatory Symposium on Stellar Spectra, September 10–12, 1941).

[7] According to the Milwaukee observers, the magnitude of AG Peg was 7.7 at the time of our spectroscopic observations in July and August, 1941.

[8] According to the Milwaukee observers, the magnitude of R Aqr was 11.0 at the time of our spectroscopic observations.

[9] $\alpha(1900)$: 20^h29^m2; $\delta(1900)$: +40°19′; 22^s preceding and 3′ north of BD+40°4226. Magnitude given by Merrill in 1932: 13.2; the star was fainter than the fourteenth magnitude when observed on July 31 and August 1, 1941. Galactic co-ordinates: $l = 47°$, $b = 0°$.

[10] *Ap. J.*, **76**, 156, 1932, star MW 203.

[11] *Ap. J.*, **93**, 349, 1941.

[12] *Ap. J.*, **91**, 581, 1940.

The lines observed on our spectrograms are:

H:	$H\alpha$ (20), $H\beta$ (3), $H\gamma$ (1)
He I:	D_3 (7)
[*O* I]:	6300 (2)
[*N* II]:	5755 (5)
Fe II:	5169 (1), 5317 (1–0)
[*Fe* III]:	5270 (3), 5010 (2), 4658 (1), 4701 (0)

The reddening is especially noticeable in the [*Fe* III] lines. In unreddened stars, λ 4658, which is the leading component of the $^5D - {}^3F$ multiplet, is always at least as strong as λ 5270, which is the strongest $^5D - {}^3P$ transition, and λ 5010 is always weaker than λ 4658. But in MWC 349, λ 5270 and λ 5010 are appreciably more intense than λ 4658. This gives conclusive evidence in favor of a considerable color excess (of the order of 2 mag.) and consequently of a tremendous general absorption. The general intensity distribution in the continuous spectrum is similar to a late M star, but no late-type absorption feature is apparent. By comparison with RY Scuti we should expect the spectral type to be early B.

In RY Scuti the [*Fe* III] lines are also strong, but *He* II is present and *Fe* II is absent; in MWC 17 both *Fe* II and [*Fe* III] are present, and *He* II is absent.

McDONALD OBSERVATORY
September 1941

THE SPECTRUM OF α CARINAE*

JESSE L. GREENSTEIN

ABSTRACT

The wave lengths and identifications of nearly one thousand lines measured on McDonald coudé spectrograms of α Car, a supergiant Fo star, are given in Table 1. The measured equivalent widths for three hundred lines are also included. The spectrum is noteworthy for strong hydrogen lines, in spite of an absolute magnitude of -3^m5. Ionized metals and *Fe* I dominate; *C* I, *N* I, *S* I, and *Si* II are present. A curve of growth, based on semitheoretical intensities communicated by Menzel and Goldberg, has been constructed for *Fe* I and also for the ionized metals. The excitation temperature is between 4900° and 6000°; the former value is adopted for the curves of growth. The curves of growth, Figures 2 and 3, are represented by a turbulent velocity of 3.5 km/sec and a damping constant ten times the classical value.

The hydrogen wings correspond to log $N \approx 18$; the opacity of the reversing layer is then found to be completely explained by the hydrogen atoms. The hydrogen lines produce a weakening of other lines located in the Stark wings; the weakening is shown in Figure 4 and is interpreted theoretically. An attempt has been made to derive the central intensities of lines as a function of equivalent width by correction for instrumental effects. Preliminary values are given in Table 9, together with predicted values for a Milne-Eddington model atmosphere. The ionization equilibria have been studied quantitatively and lead to an ionization temperature of 7300° and log $P_e = 1.0$. Estimates of the abundance of the lighter elements are made; some evidence for stratification is found in the abnormally high abundance of hydrogen.

The star α Car, Canopus, is a representative of supergiants of intermediate luminosity; the spectral type, near Fo, indicates that the spectrum must be relatively simple, since the neutral metals are weak. In connection with a general investigation of high-dispersion spectra of supergiants the wave lengths and intensities have been measured in α Car to provide a guide for more complex spectra. The identifications should prove useful in problems of blending on shorter-dispersion spectra of A and F stars.

OBSERVATIONAL MATERIAL

The coudé spectrograph of the McDonald Observatory consists of an autocollimating prism train and a lens having a focal length of 213 cm and an aperture of 12.7 cm. Two prism settings cover the region λλ 3800–6700, with considerable overlap. The "blue" setting has a dispersion ranging from 2.5 to 4 A/mm and reaches λ 4700. The "red" setting starts at λ 4430, and the dispersion drops from 2.5 to 4 A/mm at $H\beta$. Several exposures on the fast, contrasty, but coarse-grained Eastman Ia-O emulsion have been obtained. Proper exposure for α Car is difficult, since the star is at $\delta = -52°.6$; the image is nearly a centimeter long, because of atmospheric dispersion; and seeing conditions are of extreme importance. The present investigation is based on two excellent plates: Cd 125, red setting, 80-minute exposure on February 24, and Cd 132, blue setting, 100-minute exposure on February 26, 1941. The lines were found to be extremely sharp, without rotation or obvious turbulence. A single plate, therefore, yields sufficiently accurate wave lengths.

The spectrograms were measured in a long-screw measuring engine provided with a field-projection device designed by Dr. G. Van Biesbroeck. For reduction, Hartmann formulae covering up to 50 mm in a single run were computed; the iron-arc comparison lines define correction-curves with an accuracy of ±0.003 A. The comparison wave lengths, taken from Burns and Walter,[1] were also used to determine the radial velocity (including the curvature correction) for each section of the plate separately. The mean

* *Contributions from the McDonald Observatory, University of Texas*, No. 43.

[1] *Pub. Allegheny Obs.*, **6**, No. 11, 1929.

error of the measured $\delta\lambda$ between star and laboratory position of the *Fe* lines ranges from ± 0.014 to ± 0.027 A. An overexposed section of Cd 132 gave a discordant apparent velocity, and the measured wave lengths were corrected to zero velocity, using this apparent velocity. As a consequence, a small systematic deviation of perhaps 0.03 A may appear in the wave lengths between λ 4280 and λ 4430. The systematic errors in other regions of the plate should be less than 0.02 A; the accidental mean errors for good lines are less than ± 0.02 A. Approximately one-third of the lines were measured on overlapping plates or during overlapping measuring sessions. To check the reality of the faintest lines, an independent run of both plates was made. Lines of intensity 1–0 are almost certainly real, and more than half of the weaker lines are probably real. A few lines measured only once, either direct or reverse, are included, with colons, in the final tabulation.

The wave lengths and intensities of almost one thousand lines are given in Table 1. The identifications have been made completely independent of previous investigations. They are based on the usual sources supplemented by the kind loan of unpublished lists of new observed and predicted lines of *Fe* II, *Cr* II, *Ti* II, and *Mn* II prepared by Mrs. Sitterly. Weak *Fe* I lines are taken from the M.I.T. tables; intensities of such lines and of lines of other elements taken from a different source than the majority of lines of that element are placed in parentheses. The last column of Table 1 contains the symbol (−) when the identification given may not contribute largely to the observed line; the symbol (− −) is used when the laboratory identification is certainly insufficient. In the last column is also the quantity $-\log W/\lambda$, derived from the measured equivalent widths. Abbreviations used are: n, diffuse; nn, very diffuse; w, winged; v, blended on the violet side; r, blended on the red side; pr, predicted; colon (:), uncertain wave length or intensity.

A comparison of the wave lengths with those measured by Dunham[2] in α Per, a cF_5 star, shows no important wave-length differences. The present material has slightly better resolving-power, mainly because of the sharpness of the lines in α Car. Fewer lines are found in α Car than in α Per because of the higher temperature of the former. The rare-earth lines are considerably weakened in α Car. Plates VIII–XI show reproductions of the spectrum of α Car, from λ 3900 to $H\beta$, together with coudé plates of δ CMa. The latter star, an extremely luminous F8 supergiant with extreme turbulence, is under investigation by Struve and Swings.

[2] *Contr. Princeton Obs.*, No. 9, 1929; also manuscript of unpublished wave lengths in the violet.

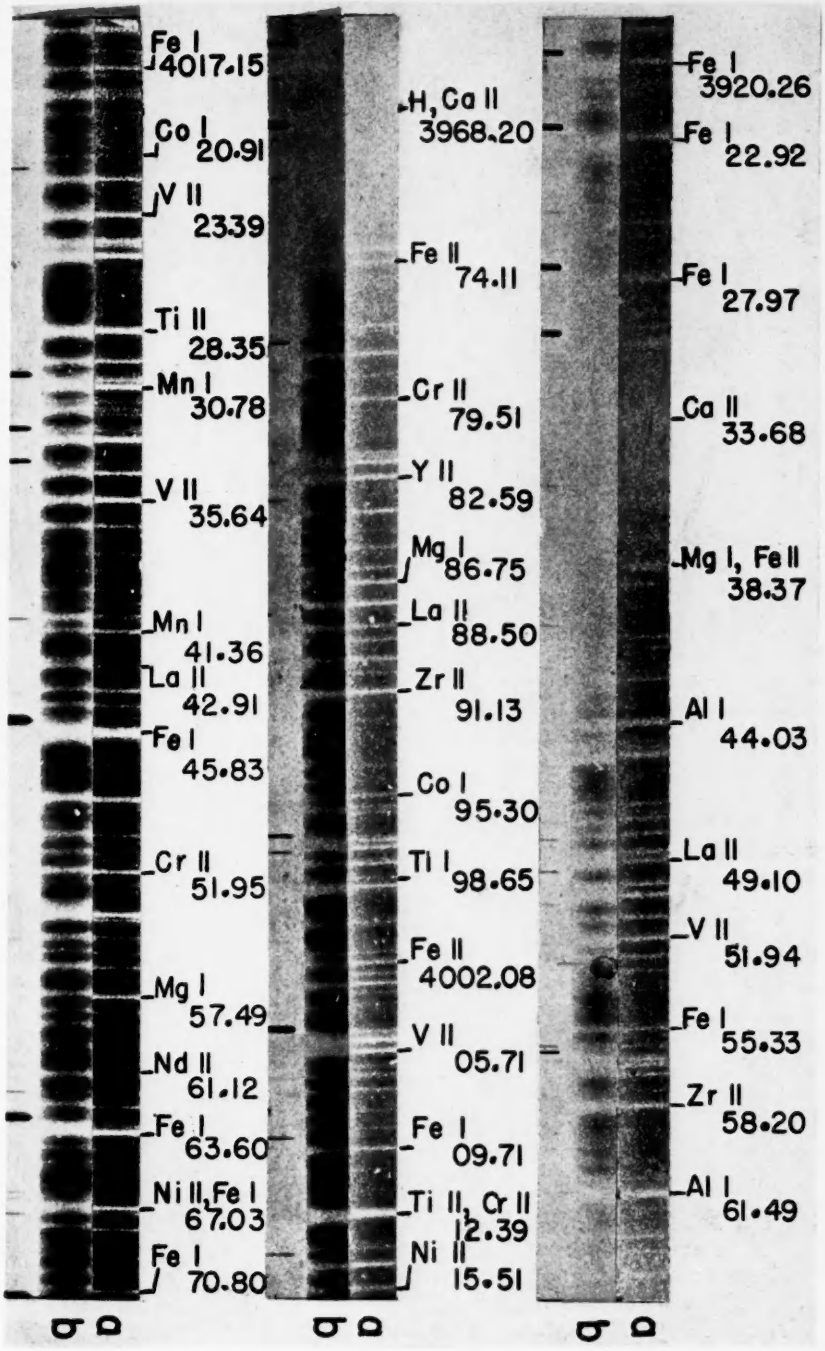

PLATES VIII–XI

THE SPECTRA OF α CAR AND δ CMA REPRODUCED FROM MCDONALD OBSERVATORY COUDÉ SPECTROGRAMS, WITH AN ENLARGEMENT OF 7.6 TIMES

The identifications refer to α Car. The comparison spectrum is that of the iron arc. The plates of δ CMa were taken by Struve and Swings; this star shows extreme turbulent broadening.

(*a*) α CARINAE 1941, FEB. 26; (*b*) δ CANIS MAJORIS 1941, JAN. 22

PLATE IX

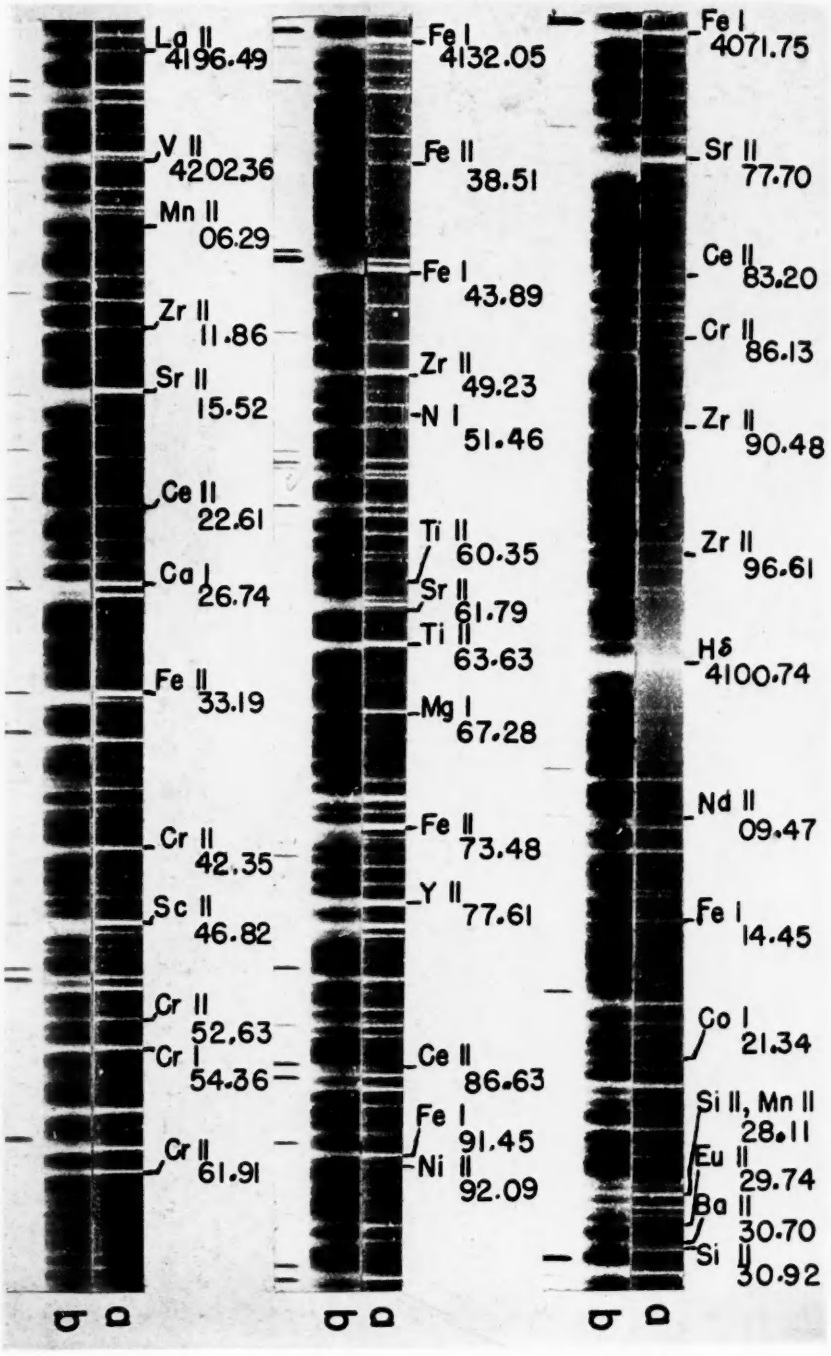

(*a*) α Carinae 1941, Feb. 26; (*b*) δ Canis Majoris 1941, Jan. 22

PLATE X

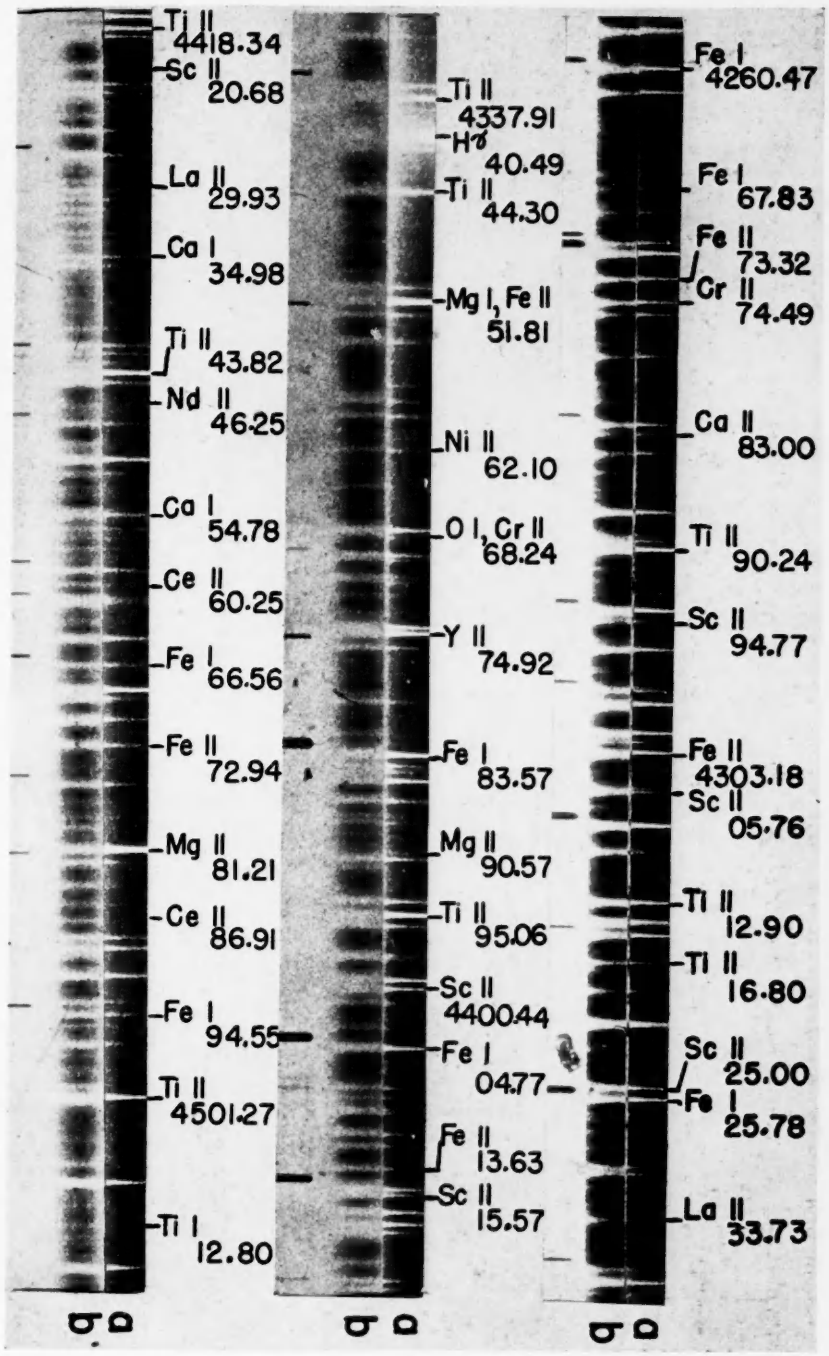

(*a*) α Carinae 1941, Feb. 26; (*b*) δ Canis Majoris: (1) 1941, Jan. 22; (2) and (3) 1941, Feb. 12

PLATE XI

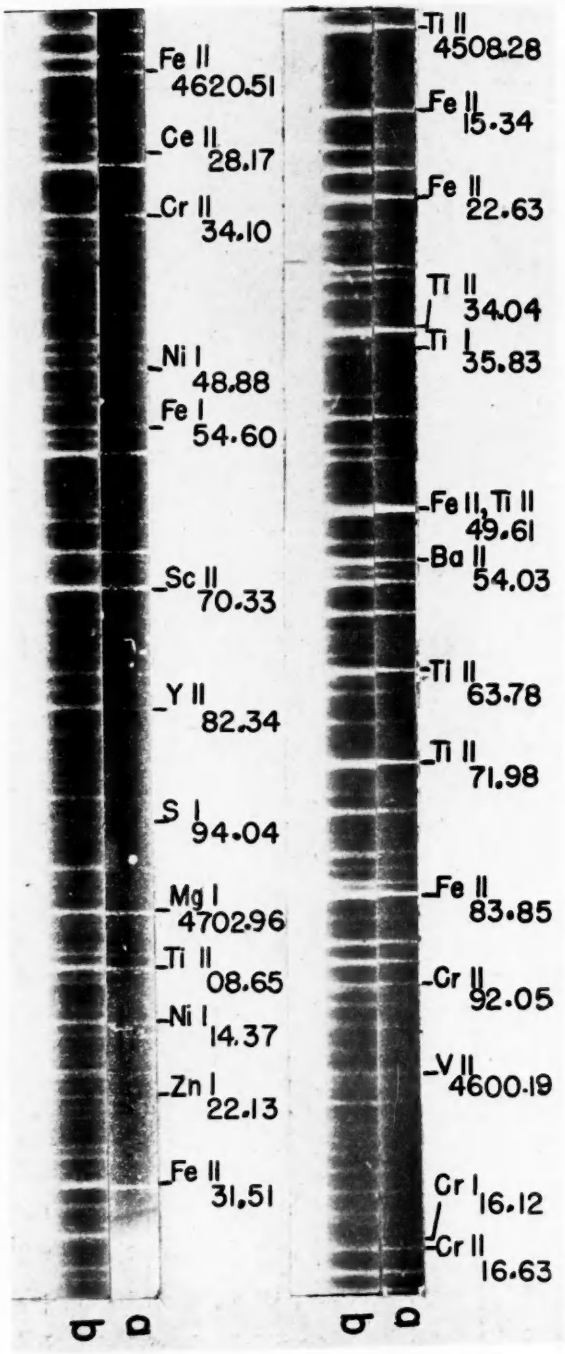

(*a*) α CARINAE 1941, FEB. 26; (*b*) δ CANIS MAJORIS 1941, JAN. 22

TABLE 1

IDENTIFICATIONS AND INTENSITIES IN α CAR

STAR		LABORATORY			REMARKS	STAR		LABORATORY			REMARKS
λ	*I*	Elem.	λ	*I*	− log *W*/λ	λ	*I*	Elem.	λ	*I*	− log *W*/λ
3899.12	1	*V* II	0.14	200	.....	3914.24	6r	*V* II	0.33	250	.....
		Fe I	.03	2	.....			*Zr* II	.34	7	.....
3899.78	2n	*Fe* I	.71	30R	.....	3914.53	2v	*Fe* II	.48	2	.....
3900.54	4	*Ti* II	.54	70	.....	3915.96	3n	*Zr* II	.94	25	.....
3901.32	0–1	.....	.....	.....	.....			*La* II	.07	300	—
3902.93	3	*Fe* I	.95	20	.....	3916.39	3	*V* II	.42	200	.....
3903.26	2	*V* II	.27	250	.....	3916.73	2	*Fe* I	.73	6	.....
3903.51:	0–1	.....	.....	.....	.....	3917.18	3	*Fe* I	.18	8	.....
3903.88	2	*Fe* I	.90	5	.....	3918.03	0	*Hf* II	.10	100	— —
3904.82	0	*Ti* I	.79	40n	.....	3918.34	4n	*Fe* I	.31	3	.....
3905.55	7	*Cr* II	.64	25	.....			*Fe* I	.42	(15)	—
		Si I	.53	10	—	3918.62	5	*Fe* I	.65	6	—
3906.03	0	*Fe* II	.04	5	.....	3919.11	4	*Fe* I	.07	3	—
3906.45	2	*Fe* I	.48	8	.....			*Cr* I	.17	35	—
3907.50	1	*Sc* I	.48	75	—	3920.26	5	*Fe* I	.26	20R	.....
		Fe I	.48	1	—	3920.59	1	*Fe* I	.63	1	.....
3907.95	2	*Fe* I	.93	4	.....	3921.02	2nn	*Fe* I	.84	1n	—
3908.43	1–0	*Ce* II	.41	30	—			*Cr* I	.05	20	—
		Pr II	.20	1–0	—	3922.92	10	*Fe* I	.91	25R	.....
3908.68	1	*Cr* I	.76	25	—	3925.21	1	*Fe* I	.20	1	.....
3908.98	1	*Ni* I	.93	8n	.....	3925.66	1	*Fe* I	.64	4	.....
3909.28	1	*Cr* II	.25	pr	.....	3925.98	3	*Fe* I	.95	6	.....
3909.58	2	*Fe* I	.67	1	—	3926.48	1	*V* II	.50	10	—
3909.85	2	*Fe* I	.84	3	.....	3927.97	10n	*Fe* I	.92	30R	.....
3910.85	2	*Fe* I	.84	2	.....	3929.19	2n	*Ti* II	.15	pr	.....
3911.30:	1n	*Cr* II	.32	3	.....			*La* II	.23	300	.....
3911.93	1–0	*Sc* I	.83	100	—			*Fe* I	.21	(15)	.....
		Ni I	.30	8n	—	3929.72	2	*V* II	.73	50	.....
3913.48	10nn	*Ti* II	.47	60	.....	3930.32	4	*Fe* I	.30	25R	.....
		Fe I	0.63	4	—	3933.6:	50w	*Ca* II	0.68	400R	2.9:

TABLE 1—*Continued*

Star		Laboratory			Remarks	Star		Laboratory			Remarks
λ	*I*	Elem.	λ	*I*	− log *W*/λ	λ	*I*	Elem.	λ	*I*	− log *W*/λ
3935.89	2	*Fe* II	0.94	6	.....	3951.94	7	*V* II	0.97	500	4.43:
		Fe I	.81	8	.....						
		Zr II	.06	7	.....	3952.64	5	*Fe* I	.60	8	4.56:
3937.31:	1	*Fe* I	.34	3	.....	3953.17	3	*Fe* I	.15	4	4.84:
3938.37	8	*Mg* I	.41	3	—	3953.88	1	*Fe* I	.86	(8)	.....
		Fe II	.29	2	— —						
						3955.33	2	*Fe* I	.34	3	—
3938.96	2	*Fe* II	.97	4	.....						
						3955.97	1	*Fe* I	.97	2	.....
3940.88	2	*Fe* I	.89	5	4.74:						
						3956.43	2	*Fe* I	.47	9	.....
3941.27	1	*Fe* I	.28	3	.....			*Ti* I	.34	60	—
3942.11:	on	*Sc* II	.07	pr	.....	3956.68	3	*Fe* I	.69	12	.....
3942.44	2	*Fe* I	.44	6	.....	3957.03	2	*Fe* I	.04	4n	.....
								Ca I	.04	10	—
3942.76:	1–0	.....	.....	.....	.....						
						3958.20	5	*Zr* II	.22	50	.....
3944.03	15	*Al* I	.02	10R	4.33:			*Cr* II	.10	1	—
								Ti I	.22	80	— —
3944.69	0	*Fe* I	.74	2	.....						
		Dy II	.69	600	.....	3960.26	1n	*Fe* I	.29	(30)	.....
3944.91	1	*Fe* I	.89	3	.....	3960.90	0–1	*Fe* II	.90	3	.....
3945.19	10	*Cr* II	.12	1	— —	3961.13:	0	*Fe* I	.14	2	5.40::
		Fe I	.13	(30)	—						
						3961.49	8	*Al* I	.54	10R	4.37:
3945.85	1nn	*Fe* I	.05	pr	—						
						3962.12:	1nn	*Fe* I	.35	2	.....
3946.99	2	*Fe* I	.00	4n	4.98:			*Fe* I	.09	pr	—
3947.32:	0–1	*Fe* I	.38	1	.....	3963.08	2	*Fe* I	.10	6n	.....
		O I	.33	10	—						
						3963.65	1	*Cr* I	.70	30	5.05:
3947.55	3n	*Fe* I	.53	5	.....						
		O I	.51	7	— —	3964.15	2	*Ti* I	.28	35	— —
3948.09	4	*Fe* I	.11	6n	4.69:	3966.08	1n	*Fe* I	.06	10	4.86::
3948.77	4n	*Fe* I	.78	10	.....	3968.—	100w	*H*ε	.08	.....	.....
		Ti I	.68	60	— —			*Ca* II	.49	350R	2.7:
3949.10	4n	*La* II	.06	600	.....	3973.58	4	*V* II	.64	300	.....
		Fe I	.15	pr	—			*Ni* I	.56	25	—
								Fe I	.66	3	—
3949.97	4	*Fe* I	.95	10	4.76:						
						3974.11	5	*Fe* II	.16	3	4.60:
3950.35	8	*Y* II	.36	200	4.53:						
						3974.76	1–0	*Fe* II	.03	2	.....
3951.17	6	*Fe* I	.16	9	4.71:			*Ni* I	.64	1on	.....
								Fe I	.76	1	.....
3951.58:	1	*Y* II	0.63	5	5.34::			*Fe* I	0.65	1	.....

TABLE 1—*Continued*

Star		Laboratory			Remarks — log W/λ	Star		Laboratory			Remarks — log W/λ
λ	*I*	Elem.	λ	*I*		λ	*I*	Elem.	λ	*I*	
3976.60	3	*Fe* I	0.62	4	4.68::	3995.30	3	*Co* I	0.32	60	4.91:
3976.83	1	*Fe* I	.87	1	—	3995.74	2	*La* II	.75	400	.....
		Cr I	.70	25	—	3995.97	1	*Fe* I	.98	4	.....
3977.72	5	*Fe* I	.74	12	4.71:	3996.95	1r	*Fe* I	.97	2	.....
3978.60	1	*Fe* I	.46	1	—	3997.12	5	*V* II	.13	200	.....
3979.51	3	*Cr* II	.51	20	.....	3997.40	5	*Fe* I	.39	15	.....
3980.92	1nn	*Fe* I	.64	1	—	3997.89	1–or	*Co* I	.91	40	.....
		Ce II	.88	35	—	3998.05	2	*Fe* I	.05	10	4.62:
3981.63	2r	*Fe* II	.63	pr	.....	3998.65	1	*Ti* I	.65	100r	.....
3981.80	2v	*Fe* I	.77	7	.....	3998.96	4	*Zr* II	.97	30	.....
		Ti I	.78	70r	.....	3999.21	1–0	*Ce* II	.23	500	.....
3982.00	5	*Ti* II	.00	tr	—			*V* II	.20	30	.....
3982.59	6	*Y* II	.60	150	.....	4000.46	2	*Fe* I	.47	2	.....
3983.93	5	*Fe* I	.96	10	4.50:			*Dy* II	.45	600	.....
3984.13:	0	*Ni* I	.15	8n	.....	4001.48	0–1	.....	.....	.....	.....
3984.69	1	*Ce* II	.68	40	.....	4001.67	2	*Fe* I	.66	5	.....
3985.35	2	*Fe* I	.40	3	.....	4002.08	4	*Fe* II	.07	2	.....
3986.16	3	*Fe* I	.17	5	4.78:	4002.54	2	*Fe* II	.55	3	.....
3986.75	5	*Mg* I	.76	4	4.59:			*Cr* II	.48	5	.....
3987.59	6	.....	.....	.....	.....	4002.93	4	*V* II	.94	80	.....
3988.50	3	*La* II	.52	500	.....	4003.29	1	*Cr* II	.33	25	.....
3989.05	2	*Sc* II	.09	1	4.97:	4003.75	1	*Fe* I	.77	2	.....
3989.79	4	*V* II	.80	15	—	4004.89	3	*Fe* I	.84	(10)	—
		Ti I	.76	(80)	—	4005.25	9	*Fe* I	.24	25	.....
3990.37	1	*Fe* I	.38	2	5.18:	4005.71	8	*V* II	.71	800	.....
3991.13	5	*Zr* II	.13	40	.....	4006.32	1	*Fe* I	.32	3	.....
3993.32	0–1n	*Ce* II	.39	50	.....	4006.69	3n	*Fe* I	.64	2	—
3992.91	0	*Cr* I	.83	15	.....			*Fe* I	.76	1n	—
3994.10	1n	*Fe* I	.12	2	5.04::	4007.29	2	*Fe* I	0.27	6	4.89
3994.68	0–1	*Pr* II	.82	200	—	4007.97:	0	.....	.....	.....	.....
		Nd II	0.68	80	—						

TABLE 1—*Continued*

Star		Laboratory			Remarks	Star		Laboratory			Remarks
λ	*I*	Elem.	λ	*I*	− log *W*/λ	λ	*I*	Elem.	λ	*I*	− log *W*/λ
4008.20	1	*V* II	0.18	20	.....	4024.52	4r	*Zr* II	0.45	12	.....
								Fe II	.55	5	.....
4008.88	1	*Ti* I	.94	35	.....						
						4024.72	2v	*Fe* I	.72	6n	.....
4009.17	1–0	.....	.....	.....	.....						
						4025.15	10	*Ti* II	.14	2	4.45
4009.71	3	*Fe* I	.71	10	.....						
		Ti I	.66	15	— —	4025.85	1	.....	.....	.....	.....
4009.96:	1–0	.....	.....	.....	.....	4027.66:	0n	.....	.....	.....	.....
4010.59	1–0	*Fe* I	.78	1	.....	4028.35	12	*Ti* II	.35	7	4.37
4011.40:	0n	*Fe* I	.41	1	5.40::	4029.49:	0	.....	.....	.....	.....
		Fe I	.72	1	—						
						4029.68	5	*Zr* II	.65	20	.....
4012.39	20	*Ti* II	.39	4	.....			*Fe* I	.65	3n	—
		Cr II	.50	30	.....						
						4030.49	3n	*Fe* I	.49	6	.....
4013.64	1–0r	*Fe* I	.64	2	.....			*Fe* I	.18	3	—
4013.82	1	*Fe* I	.78	2	.....	4030.78	10	*Mn* I	.77	200R	4.42:
4014.51	7	*Sc* II	.53	8	.....	4031.42	2	*Fe* I	.24	2	—
		Fe I	.53	10	.....			*Fe* II	.46	1	—
								Zr II	.35	2	—
4015.51	5n	*Ni* II	.48	1	.....						
						4031.73	2n	*La* II	.72	300	—
4015.60:	0v	.....	.....	.....	.....						
						4031.99	1	*Fe* I	.97	4	.....
4016.41	1	*Fe* I	.42	2	5.37						
		Fe I	.54	1	—	4032.49	1	*Fe* II	.50	3	.....
						4032.65	2	*Fe* I	.63	4	.....
4016.81	0–1	*V* II	.82	20	.....						
						4033.03	10n	*Mn* I	.08	150R	.....
4017.15	3	*Fe* I	.15	6	4.84			*Fe* II	.95	3	.....
4017.52	2	.....	.....	.....	.....						
						4034.09	1	*Zr* II	.10	5	.....
4018.09	2r	*Mn* I	.09	20	.....						
		Cr II	.96	3	.....	4034.49	5	*Mn* I	.49	100R	4.64
4018.33	3v	*Zr* II	.39	10	.....	4035.64	10	*V* II	.63	400	4.44
		Fe I	.27	4	.....			*Mn* I	.74	15	— —
4020.26:	0	.....	.....	.....	.....	4036.77	4	*V* II	.78	60	4.96
4020.55:	0	*Sc* I	.40	75	—	4037.98	3	*Cr* II	.03	25	.....
4020.91:	0–1n	*Co* I	.91	20	5.45	4038.80	1	.....	.....	.....	.....
4021.86	4	*Fe* I	.87	12	4.68	4039.58	2	*V* II	.57	20	5.16
4023.39	7	*V* II	.39	600	.....	4040.12	1nn	*Zr* II	.27	4	.....
								Fe I	0.94	1	—
4024.07:	0n	*Fe* I	0.10	1	5.79:						

TABLE 1—*Continued*

Star		Laboratory			Remarks	Star		Laboratory			Remarks
λ	*I*	Elem.	λ	*I*	− log *W*/λ	λ	*I*	Elem.	λ	*I*	− log *W*/λ
4040.71	3n	*Fe* I	0.64	4	.....	4054.99	1v	*Fe* I	0.04	3	.....
		Ce II	.76	300	—			*Fe* I	.87	1	.....
4041.36	4	*Mn* I	.38	50r	.....	4055.56	3	*Mn* I	.55	20	4.98
4041.68:	0	*Fe* II	.64	pr	.....	4056.20	4	*Ti* II	.20	1	4.68
4042.59	0–1	*Ce* II	.58	50	.....	4057.49	6	*Mg* I	.63	5	4.54
4042.91	2	*La* II	.91	300	—			*Fe* II	.46	2	— —
						4058.23	2	*Fe* I	.22	4n	.....
4043.95	4	*Fe* II	.01	2	.....						
		Fe I	.89	3	—	4058.76	2	*Fe* I	.75	3	.....
4044.61	3	*Fe* I	.61	6	4.91	4058.98	1n	*Mn* I	.94	10	.....
4045.13	1	*Fe* I	.12	pr	.....	4059.73	1	*Fe* I	.72	3	5.44
4045.63	3r	*Zr* II	.60	15	.....	4061.12	2	*Nd* II	.09	200	—
4045.83	15v	*Fe* I	.81	60r	4.10	4061.74	0–1	*Mn* I	.74	5	.....
								Cr II	.77	pr	.....
4046.03:	1v	*Fe* I	.06	.....	—						
						4061.98	1	.....	.....	.....	.....
4046.30:	0	*V* II	.27	50	.....						
						4062.45	3	*Fe* I	.44	10	4.70
4048.73	8nn	*Zr* II	.67	25	.....						
		Fe II	.83	3	— —	4063.29	1	*Fe* I	.28	3	.....
		Mn I	.76	15	— —						
						4063.60	12	*Fe* I	.59	45	4.29:
4049.09	1	*Cr* II	.14	18	.....						
						4064.03	0–1	*Cr* II	.94	pr	.....
4049.37	1	*Fe* I	.33	1	5.50						
						4064.38	2	*Ti* II	.37	1	.....
4049.90	0–1	.....	.....	.....	.....			*Fe* I	.45	2	—
4050.34	3	*Zr* II	.33	15	4.96	4065.25	2nn	*V* II	.07	100	.....
								Fe I	.29	2	.....
4050.70	1	*Fe* I	.69	(5)	—			*Fe* I	.38	2	.....
4051.07	2	*V* II	.06	20	.....	4066.60:	0–1	*Fe* I	.59	(40)	5.40:
4051.27	1	*V* II	.34	100	.....	4067.03	5	*Ni* II	.04	3	.....
		Fe II	.21	pr	.....			*Fe* I	.97	6	.....
4051.95	6	*Cr* II	.97	12	.....	4067.30	2	*Fe* I	.27	4	.....
4052.52	1	*Fe* I	.29	1	.....	4067.98	4	*Fe* I	.98	8n	4.69
		Fe I	.65	1	.....						
		Fe I	.72	1	.....	4069.92	or	*Fe* II	.88	1	.....
4053.29	0–1	*Fe* I	.27	(6)	—	4070.03	1v	*Fe* II	.02	pr	—
		Cr II	.45	1	.....						
						4070.80	3	*Fe* I	.77	5n	4.60:
4053.83	8	*Ti* II	.83	3	.....						
						4071.07	1	*Cr* II	.90	10	.....
4054.11	2	*Cr* II	0.11	8	.....			*Zr* II	0.10	4	.....

TABLE 1—*Continued*

Star		Laboratory			Remarks	Star		Laboratory			Remarks
λ	*I*	Elem.	λ	*I*	− log *W*/λ	λ	*I*	Elem.	λ	*I*	− log *W*/λ
4071.58:	or	*Fe* I	0.52	1	.....	4084.99	2	*Fe* I	0.01	4	.....
4071.75	10	*Fe* I	.74	40	4.25	4085.29	4	*Fe* I	.30	4	—
4072.54	4	*Cr* II	.56	4	.....	4085.64:	on	*Zr* II	.73	5	5.14:
		Zr I	.70	100	— —			*V* II	.67	10	—
		Fe I	.50	2	—	4086.13	3	*Cr* II	.14	8	.....
4073.46	o–1	*Fe* II	.45	(8)	.....	4086.70	3	*La* II	.72	350	4.87
4073.77	3	*Fe* I	.76	4n	4.84	4087.10	1	*Fe* I	.09	1	.....
4074.77	3	*Fe* I	.79	5	4.77	4087.28	2	*Fe* II	.28	pr	.....
4075.10	1–o	.....	.....	.....	.....	4087.59	1	*Cr* II	.63	2	.....
4075.68	1–o	*Cr* II	.63	pr	.....	4087.95	o	*Cr* II	.80	pr	—
4075.92	2	*Fe* II	.95	pr	—	4088.61	1r	*Fe* I	.57	(7)	.....
4076.62	3	*Fe* I	.63	8n	.....	4088.77	3v	*Fe* II	.76	pr	—
4076.82	2	*Cr* II	.87	3	.....			*Cr* II	.90	1	—
4077.32	1	*Fe* II	.16	3	—	4089.20	1	*Fe* I	.23	1	5.50
		La II	.35	300	.....	4090.48	4	*Zr* II	.52	10	4.82
4077.70	15	*Sr* II	.73	400r	4.10	4090.99	2	.....	.....	.....	.....
4078.38	3	*Fe* I	.35	4	4.77	4091.55	2	*Fe* I	.55	1	—
4079.22	2	*Mn* I	.24	12	.....	4092.35	1–o	*Co* I	.40	25	.....
		Fe I	.25	2n	.....	4092.64	1–o	*Ca* I	.67	8	.....
4079.40:	1n	*Mn* I	.42	10	.....			*Fe* I	.52	1	—
4079.84	2	*Fe* I	.84	4	4.96	4093.12:	on	*Co* I	.04	(10)	.....
4080.20	2	*Fe* I	.21	2n	.....			*Hf* II	.16	150	— —
4080.86	1–o	*Fe* I	.88	(5)	5.41:	4094.51:	o–1	.....	.....	.....	.....
4081.25	1	*Cr* II	.21	1	.....	4094.89:	1–o	*Ca* I	.94	12	5.38
4082.27	3nn	*Cr* II	.30	10	.....	4095.28:	o	.....	.....	.....	.....
		Fe II	.59	1	.....	4095.77:	1–o	.....	.....	.....	.....
		Fe I	.12	(10)	—	4095.97	2	*Fe* I	.97	4	4.87:
4082.92	2	*Mn* I	.95	12	5.15	4096.61	1	*Zr* II	.65	4	.....
4083.20	1	*Ce* II	.23	35	—	4097.09	2	*Ca* II	.12	1	—
4083.65	5n	*Mn* II	.67	pr	—			*Fe* I	.08	1	—
		Mn I	.64	12	—						
4084.47	3	*Fe* I	0.49	6	4.72	4098.17	2	*Fe* I	0.18	4n	4.99

TABLE 1—*Continued*

Star		Laboratory			Remarks — log W/λ	Star		Laboratory			Remarks — log W/λ
λ	*I*	Elem.	λ	*I*		λ	*I*	Elem.	λ	*I*	
4098.50	1	*Ca* I	0.54	15	.....	4120.24	2	*Fe* I	0.21	5	.....
		Cr II	.44	8	.....						
4100.15:	0	*Mg* I	.77	2	—	4121.34	2	*Co* I	.33	60	4.93
		Fe I	.17	(10)	.....	4121.84	2	*Fe* I	.80	5	4.89
4100.76:	0	*Fe* I	.74	3	5.34:	4122.67	10	*Fe* II	.64	4	4.34
4101.74	50w	*Hδ*	.75	.....	2.7:	4123.24	2n	*La* II	.24	400	.....
								Zr II	.38	1	—
4103.29	0	*Dy* II	.31	500	.....	4123.81	1n	*Fe* I	.76	1	.....
4104.16	2	*Fe* I	.12	3	5.36			*Sa* II	.95	(10)	.....
4105.03	1	*Fe* I	.94	1	—	4124.85	6n	*Fe* II	.79	1	— —
								Y II	.92	15	—
4106.48	1–0	*Fe* I	.42	1	5.39	4125.65	1	*Fe* I	.63	(80)	.....
4107.51	4	*Fe* I	.49	12	4.74						
4108.54	0–1	*Ca* I	.54	10N	.....	4125.91:	0	*Fe* I	.88	2	.....
4109.08	1	*Fe* I	.05	1	5.15	4126.20	2	*Fe* I	.18	3n	.....
4109.47:	1–0	*Nd* II	.46	200	.....	4126.55	0	.....	.....	.....	.....
4109.83	4	*Fe* I	.80	9	.....	4127.07	0	*Cr* II	.08	3	.....
		Zr II	.04	3	—	4127.60	2	*Fe* I	.61	7	.....
		Ca II	.83	1	— —	4127.84	1	*Fe* I	.81	3n	.....
4111.02	5	*Cr* II	.00	18	4.53	4128.11	7	*Si* II	.05	8	4.36::
4111.85	1n	*Fe* II	.90	1	—			*Mn* II	.14	2?	.....
		V I	.79	100R	—	4128.76	4	*Fe* II	.74	3	4.54
4112.36	0–1	*Fe* I	.32	1	5.44:			*Mn* II	.87	pr	—
4112.55	1	*Cr* II	.59	1	.....	4129.16	2	*Ti* II	.15	pr	.....
4112.96	2	*Fe* I	.97	3n	.....			*Fe* I	.19	1	—
4113.25	3	*Cr* II	.24	5	.....	4129.74	1n	*Eu* II	.73	4000	4.93:
4114.45	2	*Fe* I	.45	5	4.86	4130.70	2r	*Ba* II	.66	80	.....
4114.94:	1–0	*Fe* I	.96	1	.....	4130.92	3	*Si* II	.88	10	4.53:
4117.86:	0	*Fe* I	.85	1	.....	4132.05	8	*Fe* I	.06	25	4.32:
4118.14:	0	.....	.....	.....	.....	4132.45	2	*Cr* II	.41	7	.....
4118.56	5	*Fe* I	.55	15	4.50:	4132.92	3	*Fe* I	.90	8	4.76
4118.86	0–1	*Fe* I	.89	1	.....	4133.85	2	*Fe* I	.86	2	4.86:
		Co I	.78	50	.....	4134.44	1–0	*Fe* I	.43	1	.....
4119.53	3	*Fe* II	0.53	pr	—			*Fe* I	0.34	1	.....

TABLE 1—*Continued*

Star		Laboratory			Remarks — log W/λ	Star		Laboratory			Remarks — log W/λ
λ	*I*	Elem.	λ	*I*		λ	*I*	Elem.	λ	*I*	
4134.70	4	*Fe* I	0.68	12	4.54	4154.50	3	*Fe* I	0.50	12	.....
4136.49:	1–0	*Fe* I	.52	1	5.06	4154.82	3	*Fe* I	.81	9n	.....
4137.00	3	*Fe* I	.00	7	.....	4156.27	3	*Zr* II	.23	15	4.48
4137.46	0	.....	.....	.....	.....	4156.80	3	*Fe* I	.80	12	4.52
4137.64	1	*Ce* II	.64	400	.....	4157.79	3	*Fe* I	.78	8n	4.61
4138.21	1–0	*Fe* II	.21	pr	.....	4158.33	0n	*Fe* II	.44	pr	.....
4138.51	2	*Fe* II	.40	pr	—	4158.81	2	*Fe* I	.79	5n	4.75
4139.83:	0n	*Fe* I	.93	2	.....	4159.20	2	.....	.....	.....	.....
		Fe I	.84	1	.....	4160.35	1–0	*Ti* II	.37	.....	5.26:
4140.41	0n	*Fe* I	.40	1	5.05:	4160.66	1	.....	.....	.....	.....
4141.85	0n	*Fe* I	.87	1	5.03:	4161.19	2	*Zr* II	.21	20	.....
4142.48	1–0n	.....	.....	.....	.....			*Cr* II	.05	2	—
4143.42	5	*Fe* I	.41	15	4.52	4161.54	4	*Ti* II	.52	1	.....
4143.89	8	*Fe* I	.87	30	4.36	4161.79	1	*Sr* II	.80	30	.....
4144.50	0n	*Ce* II	.49	10	—	4163.63	8	*Ti* II	.66	40	4.26
4144.99	0n	*Ce* II	.00	10	—	4165.57	1n	*Fe* I	.42	(12)	.....
4145.14	1n	*Fe* I	.20	1	—			*Ce* II	.61	40	.....
4145.79	3	*Cr* II	.77	25	.....	4165.99:	0v	*Ba* II	.00	20	.....
4146.39:	0	*Cr* II	.50	pr	.....	4167.28	4	*Mg* I	.28	10n	4.47
		Fe I	.07	2	.....	4167.93	1	*Fe* I	.86	(8)	.....
4147.70	3	*Fe* I	.67	10	4.64			*Fe* I	.96	(10)	.....
4149.23	5r	*Zr* II	.20	75	.....	4168.66	1	*Fe* I	.62	1n	—
4149.37	2v	*Fe* I	.37	5n	.....			*Fe* II	.66	pr	—
4149.92	1–0	*Fe* I	.76	1	—	4168.97	0–1	*Fe* I	.95	(10)	.....
4150.29	1	*Fe* I	.25	4	4.85	4169.93	1nn	*Fe* I	.77	1n	—
4150.98	3	*Cr* II	.00	5	.....			*Fe* II	.97	pr	—
		Zr II	.97	10	.....	4170.63	1–0	*Cr* II	.58	pr	.....
4151.46:	0–1	*N* I	.46	12	5.25	4170.99	3nn	*Fe* I	.90	5	.....
4152.07	4nn	*Fe* I	.17	4	.....			*Cr* II	.86	1	—
		Fe II	.77	pr	—	4171.90	6	*Ti* II	.91	30	4.23:
4153.89	3	*Fe* I	0.90	10n	4.50			*Cr* II	.92	3	— —
						4172.09	1v	*Fe* I	.14	5	.....
								Ga I	0.05	30R	— —

TABLE 1—*Continued*

Star		Laboratory			Remarks	Star		Laboratory			Remarks
λ	*I*	Elem.	λ	*I*	− log *W*/λ	λ	*I*	Elem.	λ	*I*	− log *W*/λ
4172.65	3n	*Cr* II	0.60	2	.....	4188.74	2	.....	.....	.....	.....
		Fe I	.75	4	.....	4189.58	1n	*Pr* II	0.52	125	− −
4173.48	10	*Fe* II	.45	8	.....	4190.27	2nn	*Ti* II	.24	1	.....
		Ti II	.55	1	—			*V* II	.40	15	.....
4174.07	2	*Ti* II	.08	2	.....	4191.45	4	*Fe* I	.43	15	4.51
4174.33	1	*Mn* II	.31	pr	.....	4191.68	0	*Fe* I	.68	2	.....
4174.93	2	*Fe* I	.91	5	4.85	4192.09	1	*Ni* II	.02	1	.....
4175.62	3	*Fe* I	.64	10	4.57	4193.17	0n	.....	.....	.....	.....
4176.59	2	*Fe* I	.57	7n	.....	4193.80	0n	*Ce* II	.87	35	.....
4177.61	10n	*V* II	.54	125	4.19	4195.37	4	*Cr* II	.41	10	.....
		Fe II	.70	pr	− −			*Fe* I	.33	5	.....
4178.06	1−0	.....	.....	.....	.....	4196.20	2	*Fe* I	.21	4	.....
4178.42	1	*V* II	.39	60	.....	4196.49	1	*La* II	.55	250	.....
4178.84	7	*Fe* II	.86	8	4.27	4198.11	1	.....	.....	.....	.....
4179.40	3	*Cr* II	.43	12	.....	4198.30	5	*Fe* I	.34	20	.....
4179.81	1	*Zr* II	.82	15	5.12	4198.63	1	*Fe* I	.64	4n	.....
4181.76	3	*Fe* I	.75	15	4.38	4199.11	5	*Fe* I	.10	20	.....
4181.95	1−0	.....	.....	.....	.....			*V* II	.28	5	− −
4182.38	1	*Fe* I	.39	4	4.90	4199.89	0n	*Fe* I	.98	1	5.30
4182.74	0−1	*Fe* II	.69	pr	.....	4200.48:	0	*Ti* II	.40	pr	.....
4183.18	0−1	*Fe* II	.20	pr	.....	4200.92	2	*Fe* I	.92	3n	4.87
4183.44	3	*V* II	.44	250	.....	4202.03	6	*Fe* I	.03	30	.....
4184.00	2	.....	.....	.....	.....	4202.36	2	*V* II	.35	150	.....
4184.32	3	*Ti* II	.31	0	.....	4202.89	1−0n	*Ce* II	.94	40	.....
		Lu II	.31	120	− −	4204.00	3n	*Fe* I	.98	10	.....
		Gd II	.25	300	− −			*V* II	.20	20	—
4184.90	2	*Fe* I	.89	10	4.68	4204.70	1	*Y* II	.73	10	.....
4186.63	1n	*Ce* II	.60	600	.....	4205.07	3	*V* II	.08	250	.....
4187.04	4	*Fe* I	.04	20	4.49			*Eu* II	.05	6000	.....
4187.62	1r	*Fe* I	.59	(3)	—	4205.41	2n	*Mn* II	.37	pr	.....
4187.81	5	*Fe* I	0.80	20	4.37			*Fe* I	0.54	2	.....

TABLE 1—*Continued*

Star		Laboratory			Remarks — log W/λ	Star		Laboratory			Remarks — log W/λ
λ	*I*	Elem.	λ	*I*		λ	*I*	Elem.	λ	*I*	
4206.29	0–1	*Mn* II	0.38	0N	.....	4225.43	2	*Fe* I	0.45	6n	.....
		Ca II	.21	.....	—	4225.94	1	*Fe* I	.96	3	5.21:
4206.74	1	*Fe* I	.70	3	5.11	4226.46:	1r	*Fe* I	.43	2	.....
4207.15	2	*Fe* I	.13	4	.....	4226.74	7	*Ca* I	.74	500	4.29:
		Mn II	.23	pr	.....	4227.39	6	*Fe* I	.43	30	4.33
4207.38	2	*Cr* II	.35	4	.....	4228.33	1	.....	.....	.....	.....
4208.60	2	*Fe* I	.61	3n	.....	4229.65:	1nn	*Fe* I	.75	1	.....
4208.99	4	*Zr* II	.99	30	4.53			*Cr* II	.81	1	.....
		Cr II	.02	3	—	4231.65	1	*Zr* II	.61	8	.....
4209.75	1	*V* II	.83	10	—	4232.00	1	*V* II	.07	80	.....
		Cr II	.84	pr	—	4233.19	8	*Fe* II	.17	11	4.24:
4210.35	5	*Fe* I	.34	15	4.45	4233.63	3	*Fe* I	.60	18	.....
4211.86	4	*Zr* II	.89	12	4.63	4234.29:	1–0	*V* II	.23	7	5.28:
4212.36	1–0	.....	.....	.....	.....	4234.55:	0–1	*V* II	.55	40	.....
4213.67	3	*Fe* I	.65	5	.....	4235.23	1	*Mn* I	.27	8	.....
4215.52	15	*Sr* II	.55	300R	4.15			*Mn* I	.15	6	.....
4216.21	2	*Fe* I	.18	8	4.79	4235.78	1r	*V* II	.74	20	.....
4217.07	1	*Cr* II	.07	1	5.11	4235.94	4	*Fe* I	.94	25	4.44::
4217.54	3	*Fe* I	.55	7n	.....	4236.44:	0–1	*Zr* II	.56	5	.....
4219.36	3	*Fe* I	.36	12	.....	4237.15:	0	*Fe* I	.18	2	.....
4220.09	1	*V* II	.04	10	—	4238.05	1	*Fe* I	.02	4	4.87::
		Ca II	.13	.....	—	4238.39:	0–1	*La* II	.40	400	5.48
4220.35	1	*Fe* I	.34	4	.....	4238.79	4	*Fe* I	.81	10n	4.58
4222.22	3	*Fe* I	.21	12	4.58			*Mn* II	.79	pr	—
4222.61	0–1	*Ce* II	.60	300	.....	4239.80	3nn	*Fe* I	.84	2	—
4223.23:	0n	.....	.....	.....	.....			*Mn* I	.73	5	—
4224.20	3	*Fe* I	.17	6n	.....	4240.36	1	*Ti* II	.27	pr	.....
		Zr II	.22	3	—			*Fe* I	.37	(30)	.....
4224.52	2	*Fe* I	.51	3n	.....	4242.35	5	*Cr* II	.38	30	.....
4224.86	2	*Cr* II	.85	20	.....	4244.80	1	*Ni* II	.81	1	.....
4225.21	2	*V* II	0.23	120	.....			*Fe* II	0.58	pr	— —

TABLE 1—*Continued*

Star		Laboratory			Remarks — log W/λ	Star		Laboratory			Remarks — log W/λ
λ	*I*	Elem.	λ	*I*		λ	*I*	Elem.	λ	*I*	
4245.30	3	*Fe* I	.26	6	4.81	4266.96	1	*Fe* I	0.97	2	5.01
4246.08	1	*Fe* I	.09	3	4.99:	4267.83	2	*Fe* I	.83	5	4.85
4246.82	8	*Sc* II	0.84	100	4.28	4268.75	1–0	*Fe* I	.74	2	.....
4247.42	3	*Fe* I	.43	12	4.66	4269.01	1n	*Cr* II	.93	1	—
4248.22	1	*Fe* I	.22	4	4.95:	4269.27	3	*Cr* II	.28	10	.....
4248.68	0–1	*Ce* II	.68	60	.....	4271.14	4	*Fe* I	.15	20	4.47
4250.14	4	*Fe* I	.12	25	4.45	4271.78	8	*Fe* I	.76	35	4.29
4250.81	6	*Fe* I	.81	25	4.36	4273.32	5	*Fe* II	.32	3	4.42
4251.70	1–0n	*Fe* II	.54	pr	—	4274.79	5	*Cr* I	.81	400R	4.48
		Gd II	.76	300	—	4275.58	5	*Cr* II	.57	20	.....
4252.10:	0n	*Ti* II	.05	pr	.....			*La* II	.66	100	— —
4252.63	3	*Cr* II	.62	10	4.65	4276.68	0–1n	*Fe* I	.68	1	5.28
4254.36	5	*Cr* I	.35	500R	4.36	4277.45	1n	*Zr* II	.39	4	—
4255.45	0	*Fe* I	.50	(5)	.....	4278.15	4	*Cr* II	.10	1	.....
4256.17	0n	*Fe* I	.20	3	.....	4278.85	1–0	*V* II	.89	60	.....
		Cr II	.16	5	.....			*Cr* II	.94	pr	.....
4258.12	6	*Fe* II	.16	3	.....	4279.90	0–1	*Fe* I	.87	1	.....
		Zr II	.05	12	—			*Sc* II	.95	1	.....
4258.25	2v	*Fe* I	.32	2	.....	4281.10	1–0	*Cr* II	.03	pr	.....
		Fe II	.35	pr	.....			*Mn* I	.10	6	—
4259.16	1	*Mn* II	.20	0n	.....	4282.40	5	*Fe* I	.40	12	.....
4260.04	1	*Fe* I	.01	2	.....			*Zr* II	.22	6	—
		Fe I	.14	1	.....	4283.00	3	*Ca* I	.02	40	4.62
4260.47	6	*Fe* I	.47	35	4.35:	4284.18	4	*Cr* II	.21	20	4.54
		Mn II	.47	pr	—	4285.42	2	*Fe* I	.44	3	.....
4261.91	5	*Cr* II	.92	20	4.40	4286.95	1	*Fe* I	.99	1	.....
4263.15	1	*Ti* I	.14	15	—			*Fe* I	.86	1	.....
4263.85	1–0	.....	.....	.....	.....			*La* II	.01	300	.....
4264.19	1	*Fe* I	.21	2	.....	4287.90	6	*Ti* II	.89	2	4.29
		Cr II	.18	pr	.....	4289.35	1	*Ca* I	.37	40	.....
4265.25	0	*Fe* I	.27	2	5.41:	4289.72	2	*Cr* I	.73	350R	.....
4265.94	0–1	*Mn* I	0.93	6	—	4290.24	8	*Ti* II	0.23	50	.....

TABLE 1—*Continued*

Star		Laboratory			Remarks — log W/λ
λ	I	Elem.	λ	I	
4290.90	1–0	*Fe* I	0.87	1	.....
		Ti I	.96	22	—
4291.47	1	*Fe* I	.46	4	5.06
4292.24	1	*Mn* II	.25	0N	.....
		Fe I	.29	1	—
4293.11	1–0	*Zr* II	.13	7	.....
4294.11	9	*Ti* II	.12	40	.....
		Fe I	.13	15	—
4294.77	3	*Sc* II	.78	5r	4.63
4296.58	6	*Fe* II	.57	6	4.34
4298.03	1	*Fe* I	.03	2	5.03
4299.04	2	*Ca* I	.00	30	.....
4299.24	4	*Fe* I	.23	18	.....
4300.05	10	*Ti* II	.06	60	4.17
4301.11	0	*Ti* I	.11	50	5.09:
		V II	.18	40	—
4301.95	7	*Ti* II	.93	15	4.26
4302.53	3	*Ca* I	.54	60	4.62
4303.18	6	*Fe* II	.17	8	4.32
4304.58	1–0	*Fe* I	.54	1	.....
4305.48	2	*Sr* II	.46	40	.....
		Fe I	.45	3	.....
4305.76	3	*Sc* II	.72	6	.....
4306.81	2nn	*Fe* I	.58	1	—
		Fe I	.08	pr	—
		Ce II	.72	30	—
4307.86	15	*Fe* I	.90	35	.....
		Ti II	.91	40	.....
4308.97	1	*Zr* II	.94	4	.....
4309.44	1	*Fe* I	.37	4	.....
4309.64	2	*Y* II	.63	50	.....
4312.90	8	*Ti* II	.88	35	4.22
4314.12	7r	*Sc* II	0.09	30	.....
4314.27	2v	*Fe* II	0.29	4	.....
4315.03	9	*Ti* II	.98	40	.....
		Fe I	.09	10	— —
4316.80	3	*Ti* II	.80	1	4.54
4317.33	1	*Zr* II	.33	12	5.20
4318.66	2	*Ca* I	.66	45	4.60
4320.86	10nn	*Sc* II	.75	20	.....
		Ti II	.96	1	—
4322.50	0–1	*La* II	.51	100	—
4325.00	6	*Sc* II	.00	20	4.34
4325.78	10	*Fe* I	.76	35	4.22
4326.69	2	*Mn* II	.76	3	4.95
		Fe I	.75	2	—
4327.12	2	*Fe* I	.11	3	—
4330.25	3	*Ti* II	.25	0	.....
4330.71	3	*Ti* II	.71	0	.....
4331.60	0	*Ni* I	.65	12	.....
4333.73	1	*La* II	.77	500	4.94
4337.09	2n	*Fe* I	.05	10	.....
		Ti II	.26	1	.....
4337.91	8	*Ti* II	.93	8	4.28
4338.69	1n	*Fe* II	.70	pr	.....
		Fe I	.26	2	.....
4340.49	50w	*Hγ*	.48	.....	2.7:
4341.37	3n	*Ti* II	.37	1	4.71
4343.26	1	*Fe* I	.27	(20)	—
4344.30	5n	*Ti* II	.29	2	4.30:
		Mn II	.99	2N	— —
4350.83	4	*Ti* II	.84	1	4.48
4351.81	20	*Fe* II	.76	9	.....
		Mg I	.92	30	.....
4352.73	4	*Fe* I	0.73	9	4.55

TABLE 1—*Continued*

Star		Laboratory			Remarks — log W/λ	Star		Laboratory			Remarks — log W/λ
λ	*I*	Elem.	λ	*I*		λ	*I*	Elem.	λ	*I*	
4353.44	0	.....	.....	.....	.....	4385.42	10	*Fe* II	0.38	7	4.41:
4354.50	3	*Sc* II	0.62	5	.....	4386.87	5	*Ti* II	.86	10	4.44
		Mg I	.52	1	— —						
4355.08	1	*Ca* I	.10	25	5.12	4387.84	1	*Fe* I	.89	3	.....
4357.56	2	.....	.....	.....	.....	4388.43	2	*Fe* I	.41	4n	.....
4358.69	4n	*V* II	.72	30	.....	4389.25	0–1	*Fe* I	.25	2	5.44
		Fe I	.50	3	—	4390.57	2	*Mg* II	.59	10	.....
4359.70	4	*Zr* II	.75	10	4.61	4391.03	5	*Ti* II	.04	tr	.....
		Ni I	.63	10	— —			*Fe* I	.95	4	—
								Sa II	.86	600	—
4361.33	1n	*Fe* II	.25	2	.....	4394.07	5	*Ti* II	.07	2	4.41
4362.10	2	*Ni* II	.10	1	.....	4395.06	15	*Ti* II	.04	60	4.23
4367.67	7	*Ti* II	.68	15	4.45	4395.84	4	*Ti* II	.85	2	4.43
		Fe I	.58	5	— —	4398.02	2	*V* II	.02	50	.....
4368.24	1	*O* I	.30	10	—	4398.28	1	*Ti* II	.30	1	.....
		Cr II	.20	pr	— —	4399.80	7	*Ti* II	.78	35	4.31
4369.42	3	*Fe* II	.40	2	.....	4400.44	6	*Sc* II	.40	20	4.35
4369.77	2	*Fe* I	.77	7	.....	4401.46	3nn	*Fe* I	.29	5	.....
4370.96	2	*Zr* II	.99	8	4.84			*Fe* I	.45	2	—
4371.35	3	*Cr* I	.29	20	— —			*Ni* I	.55	30	.....
4372.23	1	*Fe* II	.22	pr	.....	4402.83	1–on	*Fe* II	.88	2	.....
4373.52	0	*Fe* I	.56	2	5.03	4403.33	1–on	*Zr* II	.34	6	.....
4374.47	9	*Sc* II	.47	30	.....	4404.77	8	*Fe* I	.75	30	4.22
4374.92	12	*V* II	.95	300	.....	4407.70	3	*Fe* I	.71	5	.....
		Ti II	.83	1	—			*Ti* II	.65	1	.....
4375.94	3	*Fe* I	.93	9	.....	4408.42	2	*Fe* I	.41	6	.....
4379.25	0–1	*V* I	.24	150r	5.22			*V* I	.53	90	—
4379.76	2	*Zr* II	.77	9	.....	4409.30	2r	*Ti* II	.25	tr	.....
4382.82	0	*Fe* I	.77	(10)	.....	4409.51	2v	*Ti* II	.53	tr	.....
4383.57	15	*Fe* I	.54	45r	4.26	4411.10	4	*Ti* II	.08	15	4.49
4384.31	2	*Fe* II	.33	pr	.....	4411.98	3	*Ti* II	.94	1	4.73
4384.80	2	*Sc* II	.83	5	.....	4413.63	2	*Fe* II	.60	0	—
		V I	.71	125r	—						
		Mg II	0.64	8	—	4414.54	0	*Zr* II	0.56	5	5.16

TABLE 1—*Continued*

Star		Laboratory			Remarks	Star		Laboratory			Remarks
λ	*I*	Elem.	λ	*I*	− log *W*/λ	λ	*I*	Elem.	λ	*I*	− log *W*/λ
4415.14	7	*Fe* I	0.12	20	.....	4438.38:	0	*Fe* I	0.35	1	5.48:
4415.57	5	*Sc* II	.57	20	.....	4440.47	2	*Zr* II	.48	10	.....
								Fe I	.48	1	—
4416.84	8	*Fe* II	.82	7	4.24	4441.74	5	*Ti* II	.72	pr	—
4417.74	9	*Ti* II	.73	40	4.30	4442.36	4	*Fe* I	.34	12	4.67
4418.34	4	*Ti* II	.34	1	4.54	4443.09	4nn	*Fe* I	.19	7	.....
4420.68	1	*Sc* II	.67	2	5.13			*Zr* II	.00	25	.....
4421.94	4	*Ti* II	.95	1	4.64	4443.82	15	*Ti* II	.81	50	4.26
4422.59	3	*Fe* I	.57	6	.....	4444.57	6n	*Ti* II	.56	1	.....
		Y II	.58	40	.....			*Fe* II	.56	1	— —
4423.26	1	*Ti* II	.27	pr	5.09	4446.25	1–0	*Fe* II	.25	1n	.....
								Nd II	.39	200	—
4424.36	0	*Sa* II	.34	600	.....	4447.75	5	*Fe* I	.72	9	4.64
4425.45	2	*Ca* I	.45	50	4.77	4450.51	12	*Ti* II	.49	10	4.32
4427.32	4	*Fe* I	.31	10	4.61	4451.57	3	*Fe* II	.55	4	.....
4427.94	1	*Ti* II	.92	pr	5.15			*Mn* I	.59	15	.....
		Mg II	.00	7	—			*Nd* II	.57	400	— —
4428.50	0	*Cr* I	.52	5	— —	4453.32	1	*Ti* I	.32	30	5.06:
4429.93	1	*La* II	.91	400	.....	4454.42	2	*Fe* I	.38	5	.....
4430.65	3	*Fe* I	.61	6	.....	4454.78	4	*Ca* I	.80	80	.....
4431.38	3	*Sc* II	.37	3	4.87			*Zr* II	.80	10	—
4432.11	3	*Ti* II	.09	tr	—	4455.19	3nn	*Ti* I	.32	30	—
								Fe I	.03	2n	— —
4432.65	1–0	*Fe* I	.56	3	.....	4455.89	3	*Ca* I	.90	40	4.78
4433.22	3	*Fe* I	.27	3n	—	4456.66	2	*Ti* II	.64	tr	4.93::
		Fe I	.39	pr	—			*Ca* I	.63	10	— —
4433.93	2n	*Fe* I	.78	2n	.....	4457.44	2	*Zr* II	.44	8	.....
		Sa II	.89	300	—			*Ti* I	.44	40	—
4434.41:	0	*Sa* II	.32	400	.....	4458.18	1n	*Fe* I	.08	3	.....
								Mn I	.26	12	.....
4434.98	6	*Ca* I	.97	60r	4.62	4459.10	6	*Fe* I	.12	10	.....
4435.67	4	*Ca* I	.69	40	4.83			*Ni* I	.04	20	.....
4436.38	0–1	*Mg* II	.48	5	—	4460.23	1	*Ce* II	0.21	400	.....
		Mn I	0.35	80	.....						

TABLE 1—*Continued*

Star		Laboratory			Remarks — log W/λ	Star		Laboratory			Remarks — log W/λ
λ	*I*	Elem.	λ	*I*		λ	*I*	Elem.	λ	*I*	
4461.49	8nn	*Zr* II	0.21	10	.....	4493.53	3	*Ti* II	0.53	1	4.71
		Fe I	.65	8	.....	4494.55	5	*Fe* I	.56	12	.....
4462.00	1	*Fe* I	.97	4	.....			*Zr* II	.39	8	—
		Mn I	.01	20	.....	4495.46	2	*Ti* II	.43	pr	.....
4464.47	9	*Ti* II	.46	1	4.33			*Zr* II	.43	3	—
								Fe II	.52	pr	—
4465.75	0	*Cr* II	.78	4	.....			*Fe* I	.57	1	—
		Ti I	.82	20	.....	4496.06	0n	*Fe* I	.95	1	.....
4466.56	5	*Fe* I	.55	12	4.55			*Ti* I	.16	20	—
4468.50	15	*Ti* II	.50	50	4.25	4496.95	4	*Zr* II	.98	15	4.68
4469.26	7nn	*Ti* II	.16	tr	.....	4497.66	1n	.....	.....	.....	.....
		Fe I	.38	5n	.....	4500.34	2n	.....	.....	.....	.....
4470.86	5	*Ti* II	.86	tr	4.40	4501.27	15	*Ti* II	.28	40	4.25
4472.94	6	*Fe* II	.92	2	.....	4506.75	0	*Ti* II	.74	pr	5.04:
4476.04	4	*Fe* I	.02	8	.....	4508.28	10	*Fe* II	.28	8	4.31
		Fe I	.08	4	.....	4512.80	1	*Ti* I	.75	40	5.36
4477.49	1n	.....	.....	.....	.....			*V* II	.72	60	—
4478.67	1n	.....	.....	.....	.....	4514.37	0n	*Fe* I	.37	(2)	.....
4480.10	0n	*Fe* I	.13	2	.....	4515.34	9	*Fe* II	.34	7	4.26
4481.21	30	*Mg* II	.14 .34	100	4.08	4518.35	4	.....	.....	.....	.....
4482.23	4	*Fe* I	.25	6	.....	4520.24	8	*Fe* II	.23	7	4.30
		Fe I	.17	4	.....	4522.63	10	*Fe* II	.63	9	4.21
4482.85	0n	*Fe* I	.74	2	.....	4524.73	1	*Ti* II	.69	1	.....
4484.25	2	*Fe* I	.22	4	4.86	4525.18	2	*Fe* I	.14	5n	.....
4485.67	1n	*Fe* I	.68	2n	.....			*Ti* II	.25	pr	.....
		Zr II	.42	2	—			*Ba* II	.95	35	—
4486.91	0–1	*Ce* II	.91	300	.....	4526.46	1	*Fe* II	.58	1	.....
4488.32	4	*Ti* II	.33	15	4.46			*Cr* I	.46	15	.....
4489.18	6	*Fe* II	.19	4	4.37	4526.91	1–0	*Ca* I	.94	30	5.26:
4489.71	1–0	*Fe* I	.74	3	5.43:	4527.31	1–0	*Ti* I	.33	35	5.09:
4490.11	1	*Fe* I	.08	2	.....	4528.59	6	*Fe* I	.61	18	4.34
4490.71	1	*Fe* I	.78	2n	5.35			*V* II	.51	300	—
4491.42	7	*Fe* II	0.40	5	4.39	4529.51	5	*Ti* II	.49	1	4.44
						4530.71	1	*Cr* I	0.74	20	.....

TABLE 1—*Continued*

Star		Laboratory			Remarks — log W/λ	Star		Laboratory			Remarks — log W/λ
λ	*I*	Elem.	λ	*I*		λ	*I*	Elem.	λ	*I*	
4531.15	2	*Fe* I	0.15	8	.....	4566.95	0	*Fe* I	0.88	1	—
		Co I	.96	30	—						
4533.18	2nn	*Ti* I	.25	80	—	4568.32	2	*Ti* II	.33	1	4.65
4534.04	20	*Ti* II	.97	30	4.09	4571.10	1–0	*Mg* I	.10	5	5.37
		Fe II	.17	(2)	— —	4571.98	12	*Ti* II	.98	50	4.15
4534.79	1–0	*Ti* I	.79	60	5.26	4576.34	5	*Fe* II	.33	4	4.36
4535.83	1nn	*Ti* I	.58	50	.....	4578.53	1	*Ca* I	.56	30	4.87
		Ti I	.93	40	.....						
		Ti I	.06	40	.....	4579.51	1	*Fe* II	.52	1	.....
4539.63	2	*Cr* II	.62	2	.....	4580.04	3	*Fe* II	.06	1	—
								Cr I	.06	20	—
4540.57	1–on	*Cr* I	.50	12	.....						
		Cr I	.72	10	.....	4580.48	1	*Ti* II	.47	1	.....
4541.53	6	*Fe* II	.52	4	4.38	4581.45	2n	*Ca* I	.41	40	.....
								Fe I	.51	2	.....
4544.02	3	*Ti* II	.02	tr	.....	4582.83	4	*Fe* II	.84	3	.....
4544.67	1	*Ti* I	.70	30	—						
		Cr II	.69	pr	—	4583.48:	1r	*Ti* II	.42	1	.....
4545.15	3	*Ti* II	.15	tr	4.56:	4583.85	12	*Fe* II	.83	11	.....
4545.96	1–0	*Cr* I	.96	20	.....						
						4585.91	2	*Ca* I	.88	50	4.70
4547.83	1	*Fe* I	.85	4	4.96:	4587.16	1	*Fe* I	.13	2	.....
4549.61	30	*Fe* II	.47	10	.....						
		Ti II	.64	60	.....	4588.20	6	*Cr* II	.22	75	4.29
4550.74	1–0	*Fe* I	.77	2	.....	4589.94	6	*Ti* II	.96	2	.....
								Cr II	.89	3	— —
4552.35	2	*Ti* II	.29	pr	.....						
						4592.05	4	*Cr* II	.09	20	4.46:
4554.03	6	*Ba* II	.04	1000R	.....	4592.62	2	*Fe* I	.65	5	.....
		Zr II	.96	12	—			*Ni* I	.53	10	—
4555.00	4	*Cr* II	.02	20	4.52						
						4593.81	1	.....	.....	.....	.....
4555.95	7	*Fe* II	.89	8	4.19						
		Fe I	.14	4n	—	4595.55	1	*Fe* II	.68	pr	.....
4558.66	8	*Cr* II	.66	100	4.22	4596.03	2	*Fe* I	.06	2n	—
4562.30	0	*Ce* II	.35	400	.....	4598.25	1–on	*Fe* I	.12	2n	.....
4563.78	10	*Ti* II	.77	30	4.23	4599.83	1–0	*Fe* I	.90	1	—
4564.61	2	*V* II	.59	200	.....	4600.19	2	*V* II	.19	150	.....
4565.65	3	*Cr* II	.78	10	.....	4600.75	1–0	*Cr* I	0.75	20	.....
		Fe I	0.66	2	—						

TABLE 1—*Continued*

Star		Laboratory			Remarks — log W/λ	Star		Laboratory			Remarks — log W/λ
λ	*I*	Elem.	λ	*I*		λ	*I*	Elem.	λ	*I*	
4601.38	1	*Fe* II	0.34	pr	4.97	4646.21	2	*Cr* I	0.17	40	— —
4602.92	2	*Fe* I	.94	9	4.73	4647.48	2	*Fe* I	.43	6	4.82
4604.96	1–0	*Ni* I	.00	12	4.67::	4648.01	1	.....	.....	.....	.....
4607.65	1	*Fe* I	.65	3n	4.84	4648.88	3nn	*Ni* I	.66	15	—
								Fe II	.93	0	.....
4609.32	1	*Ti* II	.27	pr	.....	4650.18	1–on	.....	.....	.....	.....
4610.54	1	.....	.....	.....	.....	4652.17	1	*Cr* I	.17	30	.....
4611.27	2	*Fe* I	.28	5n	4.64			*Fe* II	.28	tr	—
4613.23	1	*Fe* I	.24	2n	4.89	4654.60	3	*Fe* I	.50	5	.....
								Fe I	.62	5	.....
4616.12	1–0	*Cr* I	.13	25	.....	4655.75	2n	*Ti* II	.71	3	.....
4616.63	4	*Cr* II	.64	18	4.51:			*La* II	.46	400	—
4618.80	6	*Cr* II	.83	35	.....	4656.44	1	*Ti* I	.47	25	5.22:
4619.31	1–0	*Fe* I	.29	3n	.....	4657.13	8n	*Ti* II	.21	tr	—
								Fe II	.98	1	— —
4620.51	5	*Fe* II	.51	3	4.41	4663.75	3	*Fe* II	.70	0	—
4625.00	1	*Fe* I	.05	3	4.86:			*La* II	.80	300	—
4626.06	1–0	*Fe* II	.91	1	.....	4664.92	1–on	.....	.....	.....	.....
		Cr I	.18	20	.....	4665.93	1n	.....	.....	.....	.....
4628.17	0–1	*Ce* II	.16	500	.....	4666.78	6	*Fe* II	.75	2	4.39:
4629.36	12	*Ti* II	.34	15	.....	4667.48	2	*Fe* I	.45	6	.....
		Fe II	.34	7	.....	4668.17	2	*Fe* I	.13	6	4.72:
4632.91	1–0	*Fe* I	.91	2	5.03	4669.26	1	*Fe* I	.17	3	.....
4634.10	5	*Cr* II	.11	25	4.42			*Sa* II	.40	500	.....
4634.76	0–1	*Fe* I	.71	.....	—	4670.33	8	*Sc* II	.42	10	4.35
4635.34	2	*Fe* II	.33	5	4.67			*Fe* II	.17	0	— —
4636.38	1	*Ti* II	.33	1	4.99	4671.29:	1–0	*Cr* II	.36	pr	—
4637.51	1–0	*Fe* I	.51	3	5.07:	4672.31	1	.....	.....	.....	.....
4638.04	1	*Fe* I	.01	3	4.95:	4673.25	1	*Fe* I	.16	4	.....
								Fe I	.27	pr	—
4641.25	0–1	.....	.....	.....	.....	4678.15	1–0	*Cd* I	.15	10R	—
4643.41	0–1	*Fe* I	0.46	2	4.91:	4678.86	2	*Fe* I	0.85	7	.....
4644.98:	0	.....	.....	.....	.....						

TABLE 1—*Continued*

Star		Laboratory			Remarks	Star		Laboratory			Remarks
λ	*I*	Elem.	λ	*I*	− log *W*/λ	λ	*I*	Elem.	λ	*I*	− log *W*/λ
4682.34	2	*Y* II	0.35	20	4.85	4723.28	1–0	.....	.....	.....	.....
4686.13	1	.....	.....	.....	.....	4727.33	1n	*Fe* I	0.40	3n	.....
4690.13	1	*Fe* I	.14	3	.....			*Mn* II	.90	pr	.....
4691.45	2n	*Fe* I	.41	6	.....	4728.50	2	*Fe* I	.55	3n	—
		Ti I	.35	20	—	4731.51	6	*Fe* II	.44	3	.....
4694.04	1n	*S* I	.18	10	5.08	4732.50	1–0	.....	.....	.....	.....
4695.42	1	*S* I	.51	8	5.13:	4733.63	1–0	*Fe* I	.59	4	5.19:
4698.54	2n	*Cr* I	.47	20	.....	4734.15:	0	*Ti* II	.18	pr	—
		Sc II	.28	1	—						
		Cr II	.64	pr	—	4735.83	1	*Fe* I	.85	(10)	—
		Ti I	.77	20	—	4736.74	3	*Fe* I	.77	12	4.55:
4700.18:	0n	*Fe* I	.16	2n	.....	4738.26	1n	*Mn* II	.29	pr	.....
4701.54	1–0	.....	.....	.....	.....	4739.46:	0	*Mn* I	.12	8	.....
4702.96	5	*Mg* I	.01	40	4.49			*Zr* I	.45	100	— —
								Mg II	.59	5	—
4704.87	0	*Fe* I	.95	5	.....	4740.41	0	*Fe* I	.34	1	.....
4706.57	0–1	.....	.....	.....	.....			*Ti* II	.52	pr	.....
4707.25	2	*Fe* I	.27	8	.....	4741.59	1	*Fe* I	.53	3	.....
4708.01	1	*Cr* I	.02	15	5.40:	4743.85	0	.....	.....	.....	.....
4708.65	4	*Ti* II	.67	tr	4.51:	4744.36	2	.....	.....	.....	.....
4710.32	1n	*Fe* I	.28	5	.....	4745.76	2	*Fe* I	.80	3n	.....
		Mn I	.72	10	—			*Sa* II	.68	500	—
4713.17	1–0	*Fe* II	.19	pr	—	4748.11	3	*Sc* II	.12	pr	— —
4714.37	3	*Ni* I	.42	25	4.74	4752.27	1–0	.....	.....	.....	.....
4715.09	0	*Cr* II	.10	1	.....	4754.06	2n	*Mn* I	.04	50	4.75
4715.74	1	*Ni* I	.77	8	4.99:	4754.83	0–1	.....	.....	.....	.....
4716.56	0	.....	.....	.....	.....	4755.74	3n	*Mn* II	.73	0n	.....
4718.42	1–0	*Cr* I	.43	20	5.12	4756.50	1	*Ni* I	.52	10	5.20:
4719.51	2	*Ti* II	.51	1	4.88:	4761.53	0nn	*Mn* I	.53	10	.....
4720.16	1	*Fe* II	.16	pr	.....			*Cr* II	.42	1	.....
4721.01	1n	*Fe* I	.00	1	—	4762.42	5r	*Mn* I	.38	30	.....
								C I	.41	4	—
4722.13	1	*Zn* I	0.17	10R	.....	4762.77	4v	*Ti* II	0.78	1	.....

TABLE 1—*Continued*

Star		Laboratory			Remarks	Star		Laboratory			Remarks
λ	*I*	Elem.	λ	*I*	− log *W*/λ	λ	*I*	Elem.	λ	*I*	− log *W*/λ
4763.94	5	*Ti* II	0.84	pr	− −	4806.89	0	*Ni* I	0.00	4	−
4764.55	4r	*Ti* II	.54	1	.....	4810.56	1n	*Zn* I	.54	10R	.....
4764.74	1v	*Mn* II	.7	pr	.....	4812.34	5	*Cr* II	.35	25	4.68
4765.50	1−0	*Fe* I	.48	1	5.04:	4813.04:	0	*C* I	.84	1	−
4765.88	1−0	*Mn* I	.87	10	.....	4823.43	3	*Mn* I	.52	50	.....
4766.54	2nn	*C* I	.62	2	.....			*Y* II	.31	30	.....
		Mn I	.43	20	.....	4824.14	8	*Cr* II	.13	75	.....
4768.40	1n	*Fe* I	.40	3n	4.94	4825.65	1	*Fe* II	.71	pr	.....
4770.05	2n	*C* I	.00	2	4.84			*Nd* II	.48	150	− −
4771.71	6	*C* I	.72	4	4.59	4826.79	0−1	*C* I	.73	1	.....
4772.95	1	*Fe* I	.82	3	.....	4829.06	2	*Ni* I	.03	15	5.15
4775.88	3n	*C* I	.89	3	4.75	4831.13	2	*Ni* I	.18	10	5.09
4780.00	10	*Ti* II	.99	1	−	4833.18	2	*Fe* II	.21	pr	.....
4781.18:	0	.....	.....	.....	.....	4836.21	5	*Cr* II	.22	25	4.53
4783.40	3	*Mn* I	.43	50	4.78	4838.55:	1n	*Fe* I	.51	2n	5.04:
4786.59	4nn	*Y* II	.54	20	.....	4840.06	2nn	*Co* I	.27	25	.....
		Fe I	.81	5	−			*Fe* II	.00	pr	−
		Ni I	.54	15	−	4848.26	10	*Cr* II	.24	60	.....
		Yb II	.62	500	−	4849.13	2	*Ti* II	.17	pr	−
4788.83	0	*Fe* I	.76	4	.....	4852.52:	1−0	.....	.....	.....	.....
4789.40	0−1	*Cr* I	.34	20	.....	4854.84	4	*Y* II	.88	150	.....
4789.64	2	*Fe* I	.65	7	.....	4855.51	3	*Fe* I	.68	3	.....
4791.11	1	.....	.....	.....	.....			*Ni* I	.42	15	.....
4792.38	3	*Ti* II	.39	pr	−	4856.12	5n	*Cr* II	.19	20	.....
4793.49	1−0	.....	.....	.....	.....	4859.81	0	*Fe* I	.74	15	5.34::
4798.51	5	*Ti* II	.54	2	4.63	4861.29	75w	*Hβ*	.34	.....	2.9:
4799.98	1	*Ti* II	.99	1	.....	4864.35	4	*Cr* II	.32	50	4.70
		Cd I	.91	10R	− −	4865.16	0	.....	.....	.....	.....
4802.92:	0−1	*Sc* II	.95	pr	.....	4865.61	2	*Ti* II	.62	tr	4.91
		Fe I	.88	3	.....	4871.32	6	*Fe* I	0.32	25	4.62:
4805.08	12	*Ti* II	0.10	2	.....						

TABLE 1—*Continued*

Star		Laboratory			Remarks	Star		Laboratory			Remarks
λ	*I*	Elem.	λ	*I*	− log *W*/λ	λ	*I*	Elem.	λ	*I*	− log *W*/λ
4872.14	5	*Fe* I	0.14	20	4.77:	4901.63	1	*Cr* II	0.65	15	.....
4874.04	5	*Ti* II	.02	tr	4.78	4903.29	2	*Fe* I	.31	12	.....
4876.47	8	*Cr* II	.41	50	.....	4904.44	0–1	*Ni* I	.42	10	.....
4878.20	4	*Fe* I	.21	12	4.66	4911.16	4	*Ti* II	.20	0	.....
		Ca I	.13	50	—	4918.96	4	*Fe* I	.99	30	.....
4883.69	7	*Y* II	.69	200	4.61	4920.48	6	*Fe* I	.50	60	.....
4884.66	3	*Cr* II	.57	10	4.97	4921.96:	on	*La* II	.79	200	.....
4885.40	1–0	*Fe* I	.43	2	5.36:			*Cr* I	.27	20	.....
4886.42	1	*Fe* I	.34	1	—	4923.94	12	*Fe* II	.92	12	.....
4887.05	2	*Cr* I	.01	20	—	4924.90:	0	*Fe* I	.77	3	.....
4888.74	2n	*Fe* I	.10	2	—	4932.05	1	*C* I	.00	5	.....
		Fe I	.64	1	—	4934.08	8	*Ba* II	.10	700R	.....
4889.97	1–0	.....	.....	.....	.....	4935.76	1–0	.....	.....	.....	.....
4890.75	4	*Fe* I	.76	25	.....	4938.78:	0–1	*Fe* I	.81	10	.....
4891.53	6	*Fe* I	.49	50	.....	4957.50	1on	*Fe* I	.60	60	.....
4893.78	1–0	*Fe* II	.78	on	.....			*Fe* I	0.30	20	—
4900.09	6n	*Y* II	0.13	150	4.57						

The elements identified in the spectrum of α Car are listed in Table 2; the last column contains a rough estimate of the intensity of the lines of the element in α Car as compared with α Per. Such estimates can be made only when the effect is large. A plate of the latter star was kindly loaned by Dr. Struve.

Table 3 contains a list of some of the stronger unidentified lines. The identifications in α Per given by Dunham[2] are in columns 3, 4, and 5. Singly ionized metals are probably responsible for the majority of these lines, although the strength of several lines in the sun is rather surprising.

SPECTROPHOTOMETRY

The plates were calibrated by means of a tube photometer provided with filters; the effective wave lengths of the calibrations were about λ 3850 and λ 4500. The tube photometer gives about ten usable densities over a range of 3.5 mag. The Yerkes microphotometer has been used to obtain calibrated tracings with a magnification of thirty times, i.e., a final dispersion of 0.1 A/mm. In spite of the graininess of the Ia-O emulsion, the width of the analyzed portion of the spectrum is such that tracing deflections are relatively smoothed and can be read to less than 1 mm, corresponding to about 0.02 mag. The Ia-O emulsion has high contrast and fortunately shows small variation of characteristic curve with wave length—at least over the range of the tube-photometer effective wave lengths.

The lines measured, approximately 325, were selected for freedom from blends, for interest, and for availability of estimates of relative or absolute *f*-values. The lines with $\lambda < 4000$ A are in a relatively underexposed region; lines with $4431 < \lambda < 4471$ A are measured on two plates; lines with $\lambda > 4835$ A are in an underexposed region. Approximately one-half of the lines were measured twice, either on overlapping tracings or

TABLE 2

ELEMENTS IDENTIFIED IN α CAR

Element	Remarks	Relative to α Per	Element	Remarks	Relative to α Per
*H**	Very strong	+ +	*Fe* I§	Strong	−
C I	Present	+	*Fe* II	Strong	.....
N I†	One line	+	*Co* I	Present	−
O I	Masked	.....	*Co* II	No data	.....
Mg I	Present	−	*Ni* I	Weak	−
Mg II	Strong	+	*Ni* II	Present	.....
Al I	Present	−	*Zn* I	Present	−
Si I	Masked	.....	*Sr* II	Strong	−
Si II‡	Present	+	*Y* II	Strong	−
S I	Present	+	*Zr* II	Present	.....
Ca I	Strong	−	*Cd* I‖	Possible?	−
Ca II	Strong	−	*Ba* II	Present	−
Sc I	Possible, weak	−	*La* II¶	Present	− −
Sc II	Strong	.....	*Ce* II	Present	− −
Ti I	Very weak	−	*Pr* II	Very weak	− −
Ti II	Very strong	.....	*Nd* II	Very weak	− −
V I	Very weak	−	*Sa* II	Very weak	− −
V II	Present	.....	*Eu* II	Weak	−
Cr I	Present	−	*Gd* II	Weak, absent?	.....
Cr II	Strong	.....	*Dy* II	Very weak	−
Mn I	Present	−	*Yb* II	Weak, absent?	.....
Mn II	Present	.....	*Lu* II	Weak, absent?	.....
			Hf II	Weak, absent?	.....

* The hydrogen lines are very strong with broad Stark wings and a relatively sharp core. They resemble lines in a dwarf.

† The single possible *N* I line, λ 4151.46 ($I = 0-1$) is unblended and at exactly the laboratory wave length (Duffendack and Wolfe, *Phys. Rev.*, **34**, 409, 1929) of the strongest line ($I = 12$), $3s^4P_{5/2} - 4p^4S^0_{3/2}$. The line is absent in α Per. The presence of *N* I is unusual in the photographic region; infrared lines are known, and I have found *N* I strong in the visual region of υ Sgr. The excitation potential is 10.3 e.v.

‡ The *Si* II lines are badly blended, as can be seen from the relative intensities; λ 4128.11 has as dominant component a new *Mn* II line, found by Mrs. Sitterly; it is also close to a blend of *Fe* II and *Mn* II; λ 4130.92 is fairly close to an *Fe* I line. It is possible that this complex blending will explain the anomalous variation of the ratio 4128/31 found by W. W. Morgan (*Ap. J.*, **75**, 423, 1932; also unpublished description of 21 Aql) in a peculiar A star with variable spectrum and also in 21 Aql.

§ *Fe* I is strong with respect to other neutral metals.

‖ The two possible *Cd* I lines originate from a level 2^1P near 4 e.v. The unblended line λ 4678.15 is present and unidentified in α Per and in the sun.

¶ All the rare-earth lines are strikingly weaker than in α Per. The weakening of many of the faint lines present in α Per is, in fact, good support for their identification by Dunham as rare-earth lines. They are also strong in γ Cyg, as shown by Adams and Joy (*Proc. Nat. Acad. Sci.*, **13**, 393, 1927).

plates or using both of the following techniques. Most lines were measured in the conventional manner, at every millimeter on the tracing; the equivalent widths were determined by summing. In the case of weak lines, or in regions of lower dispersion, a triangle was drawn with approximately the same area as the line, and only the apparent central intensity and the width of the line were recorded. The latter measures were calibrated and found to give results differing systematically by 5–10 per cent from the conventional method. The final values of $\log W/\lambda$ in Table 1 are all reduced to one scale. The mean error of an equivalent width ranges from ±4 to ±10 milliangstrom. The weakest lines measured, with W of the order of 10 mA, have a percentage error as large as 40 per cent;

the strongest lines (omitting hydrogen) have W of the order of 300 mA, and the percentage error is about 5 per cent. The systematic errors of the present scale of equivalent widths can be estimated only by comparison of the two overlapping plates. The total systematic difference produced in W by the change of dispersion, plate calibration-curve, and exposure between the two plates was found to be 7 per cent.

The sharpness of the lines in α Car results in the instrumental contour dominating in all but the strongest lines. Tracings of the comparison lines were measured to determine the instrumental contour. The apparent central intensities of all measured lines were available and will be discussed in a later section. The contours of the hydrogen lines were measured on Cd 132 and also on several Process plates taken with a dispersion of 50 A/mm.

TABLE 3

UNIDENTIFIED LINES, $I \geqslant 2$

α Car		α Per			Remarks
λ	I	λ	I	Ident.	
3938.37	8	3938.34	6r	⊙	
3945.19	10	3945.13	7	*Cr* II	Too strong
3987.59	6	3987.63	4	⊙	
4017.52	2	m	.....	*Ni* I, *Ti* I	
4090.99	2	m	.....	*Ce* II	Probably too strong
4159.20	2	m	.....	⊙	
4184.00	2	m	.....	⊙	
4371.35	3	4371.25	2n	⊙	
4500.34	2n	4500.40	3	*Cr* I	Much too strong
4518.35	4	4518.36	4w	⊙, *Ti* I	Much too strong
4646.21	2	4646.19	3	*Cr* I	Probably too strong
4744.36	2	4744.33	2	*Fe* I	Probably too strong
4748.11	3	4748.12	3	⊙	
4763.94	5	4763.89	5	*Ti* II	Probably too strong

THE CURVE OF GROWTH

The curves of growth of several typical stars are under investigation at the McDonald and Yerkes observatories. The conventional method of building up the curve from multiplets and supermultiplets might have been used here, except for the availability of tables of the observed central absorption coefficients of a large number of solar lines, as determined by Dr. Menzel and Dr. Goldberg at the Harvard College Observatory. Their kindness in permitting the use of these unpublished values is gratefully acknowledged. The tables permit the construction of curves of growth for stars of a wide range of spectral type, on a uniform scale of theoretical relative intensities, X_0 (or Nf); if revision is later desirable, a simple transformation should yield the corrected curves of growth.

Menzel and Goldberg prepared a solar curve of growth in the usual manner, using Allen's measured equivalent widths[3] and the intensity rules for LS coupling. From the mean solar curve, smoothed values of X_0 were read for a large number of lines, including many which could not be used in the preparation of the original curve. Deviations from the theoretical multiplet intensities are removed in part by this process. The definition[4] of X_0 is

$$X_0 = \frac{N_a}{b(T)}\, e^{-\chi_{j'}/\kappa T}\, \frac{1}{3\sqrt{\pi}\, R}\, \frac{\pi e^2}{mc}\, \varphi\, \frac{c}{v}\, S\, \frac{s}{\Sigma s}, \qquad (1)$$

[3] *Mem. Commonwealth Solar Obs.*, **1**, No. 5, 1934.

[4] *Ap. J.*, **87**, 81, 1938.

or[5]

$$X_0 = N_a \frac{g}{b(T)} e^{-\chi_j'/\kappa T} \frac{\pi e^2}{mc} f \frac{c}{\sqrt{\pi}\,\nu_0 v}, \tag{2}$$

where N_a is the number of atoms in the given state of ionization per cm². The value of X_0 is proportional to Nfc/v, where v is the most probable speed of the atoms involved, either thermal or turbulent in origin. A single curve of growth is obtained for given values of v and the damping constant by plotting log W/λ as a function of X_0.

The X_0's are proportional to the number of atoms of the element in the given lower level of excitation potential, χ_j'. For a star of different excitation temperature, T_{exc}, we have

$$\left.\begin{aligned} \frac{X_0}{X_0(\odot)} &\propto 10^{-\chi_j'(1/T_{exc}-1/T_\odot)5040^\circ} \\ \text{and} \\ \frac{X_0}{X_0(\odot)} &\propto 10^{-\chi_j'\Delta\theta_{exc}}. \end{aligned}\right\} \tag{3}$$

Since α Car is of considerably earlier spectral type than the sun, we might expect a large negative value of $\Delta\theta_{exc}$. In fact, the systematic deviations of lines of different excitation potentials from an approximate curve of growth, using uncorrected solar X_0's, were found to be surprisingly small. The excitation temperature is only slightly higher than that of the sun. A curve of growth for *Fe* I was prepared with lines arising from lower levels over a range of 3 e.v.; the systematic deviations gave $\Delta\theta = -0.12$. *Ti* II has fewer lines and a smaller range of excitation potential; at most, one can say that a similar value of $\Delta\theta$ is indicated. Menzel, Baker, and Goldberg[4] find T_{exc} for the sun to be 4400°; T_{exc} for α Car is then only 4900° or $\theta_{exc} = 1.03$.

The solar values of X_0 were derived from supermultiplet intensities, and we can also apply these theoretical intensities independently to determine θ_{exc} in α Car directly. The only suitable element is *Fe* I; two partial transition arrays—$3d^7 4s - 3d^7 4p$ (four multiplets, twelve lines) and $3d^6 4s 4p - 3d^6 4s 5s$ (two multiplets, eleven lines)—are available, with values of S and of $s/\Sigma s$ based on LS coupling. The range of χ is from 1.5 to 2.8 e.v.; θ_{exc} is found to be 1.1 ± 0.1. Another, and an independent, determination can be based on R. B. and A. S. King's laboratory measures[6] of relative f-values for *Fe* I. The quantity log W/λ^2 plotted against log gf will give partial curves of growth for two groups of lines. There are seven lines available in two multiplets at $\chi = 1.5$ e.v., $a^5D - z^7P^\circ$, z^7F°; there are eleven lines at $\chi = 0.0$ e.v., $a^3F - y^3F^\circ$, z^3G°, z^5G°, y^5F°. In Figure 1 these two curves of growth are plotted, together with sections of the final theoretical curves of growth. The shift of 1.22 between the two sections of the curve is caused by the Boltzmann factor in the population of a^5D_4, $\chi = 1.48$ e.v. The value of $\theta_{exc} = 0.83$, with an uncertainty of perhaps 0.15, depends on the temperature of the laboratory electric furnace and not at all on theoretical intensities. The determination of θ_{exc} in α Car is poor, however, because of the weakness of the neutral metals; ionized metals have a very small range of excitation potential. I have adopted θ_{exc} as 1.03; the ionization and effective temperatures are much higher, $\theta \approx 0.69$; and we shall see that a higher excitation temperature is required to explain the intensity of the hydrogen lines.

Curves of growth were obtained by using Menzel and Goldberg's solar values of $X_0 + 0.12\chi$, according to equation (3). Figure 2 gives the observed curve of growth for

[5] Menzel, *Ap. J.*, **84**, 462, 1936.

[6] *Ap. J.*, **87**, 24, 1938.

Fe I; it is apparent that no large error in the excitation temperature has been made, since lines from high and low levels fall together on the curve. The scatter on the lower portion of the curve is due to the large percentage error of W for weak lines. Figure 3 gives

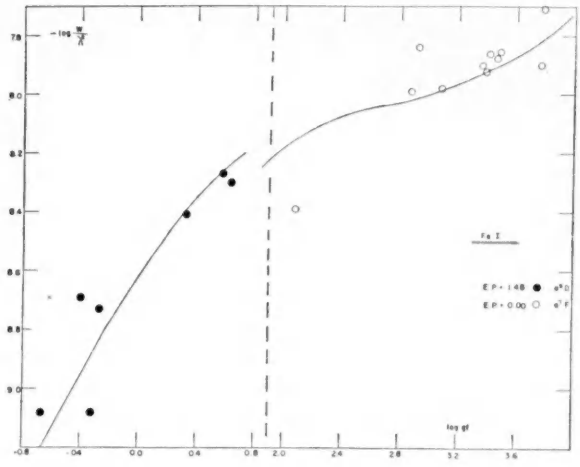

FIG. 1.—Partial curves of growth based on the laboratory gf values of *Fe* I. The shift between the two sections is a measure of the Boltzmann factor for a^5D_4.

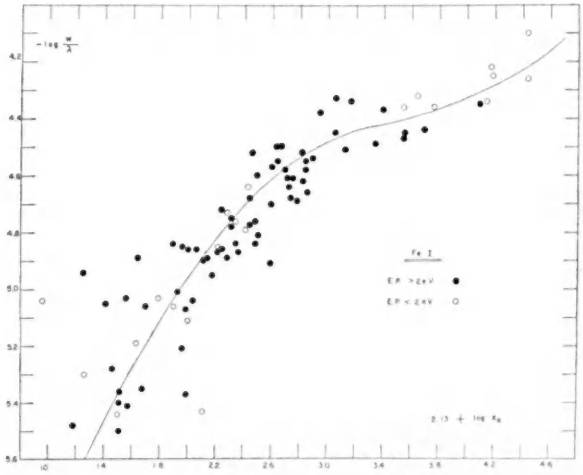

FIG. 2.—Final curve of growth for *Fe* I. The points represent the individual observed lines; the theoretical curve is the solid line. The abscissae are 2.13 + log X_0 and are equivalent to log Nf plus a constant. Note the absence of any systematic displacement between lines of high and low excitation potentials.

the composite observed curve of growth for *Ti* II, *Cr* II, *Fe* II, and *Zr* II. Arbitrary shifts on the log X_0 axis have been made to bring these metals into coincidence. *Cr* II shows a steeper gradient of line intensity with X_0 than the other elements. A single theoretical

curve of growth has been fitted to both these observed curves.[7] The parameters of the theoretical curve are found to be $\log v_0 = 5.55$ (3.5 km/sec) and $\log \Gamma = 9.18$. Note that the most probable speed, v_0, so determined, is considerably in excess of the thermal value; for $\theta = 0.69$, for *Fe* atoms, $v_0 = 1.8$ km/sec. The conventional explanation of such excess observed velocities is that there exists a turbulent velocity distribution in the star's atmosphere. Such turbulent velocities have been indicated by curves of growth determined by Struve and Elvey[8] for many supergiants. It is interesting to find that the turbulence in α Car is smaller than in α Per or ε Aur. The line profiles are obviously sharper in α Car, and the star is 2 or 3 mag. less luminous. The relation between turbulence and luminosity is apparently quite general; for example, among the A stars, coudé

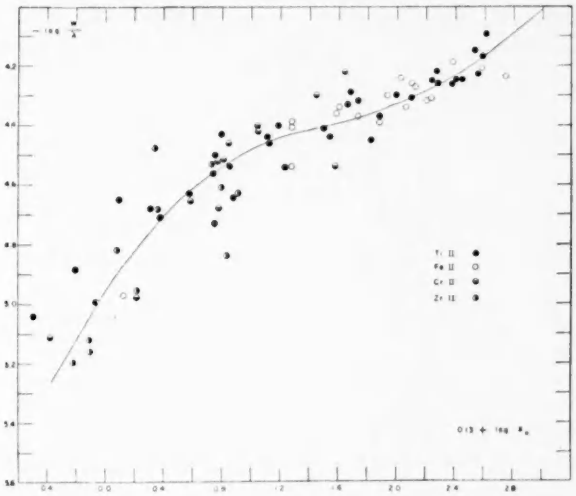

FIG. 3.—Combined curve of growth from four ionized metals. The abscissae are $0.13 + \log X_0$. The theoretical curve is the same as Fig. 2.

plates show that η Leo, a relatively faint supergiant, with Stark-effect wings easily visible, has much sharper lines than α Cyg. The damping constant, $\Gamma = 15 \times 10^8$, is fairly well determined in α Car. As has been noted by several other investigators, a mean damping constant about ten times the classical value (1.5×10^8) is required. In α Car, at least, collisional damping is probably negligible. Table 4 gives the co-ordinates of the curve of growth; it gives X_0, the optical depth at the center of the line, as a function of $-\log W/\lambda$.

THE HYDROGEN LINES

The most striking feature of the spectrum is the strength and width of the hydrogen lines. A good Cape trigonometric parallax gives the absolute magnitude of α Car as $-3^m8 \pm 0^m3$. The Henry Draper type is Fo—possibly A8 would be preferable; few comparable stars are known, since both α Lep and ε Aur are Fo supergiants of higher luminosity, with narrow hydrogen lines. The measured equivalent widths of $H\gamma$ and $H\delta$ are

[7] The theoretical curves of growth were computed by means of an approximation formula developed by J. G. Baker (*Ap. J.*, **84**, 474, 1936). The results are sufficiently accurate so long as the damping constant is of the order of 10^9; for smaller values Baker's formula distorts the flat portion of the curve of growth.

[8] *Ap. J.*, **79**, 409, 1934.

about 7.5 A on the coudé plate; on plates of shorter dispersion I find them near 8.5 A (including here some strong metallic lines). The final mean values are:

	$H\beta$	$H\gamma$	$H\delta$	$H+H\epsilon$	K
$-\log W/\lambda$.....	2.9 ::	2.7	2.7	2.7	2.9 :

The observed contour of $H\delta$ was derived on plate Cd 132. The mean values of R, the residual intensity in the line, were derived after reflecting the contour and are contained in Table 5. The instrumental correction will only slightly deepen the line; R_c is probably of the order of 0.15.

TABLE 4

CO-ORDINATES OF THE CURVE OF GROWTH

$-\log W/\lambda$	$\log X_\circ$	$-\log W/\lambda$	$\log X_\circ$
5.50.....	−0.76	4.75.....	+0.19
5.45.....	− .71	4.70.....	+0.28
5.40.....	− .66	4.65.....	+0.38
5.35.....	− .61	4.60.....	+0.50
5.30.....	− .55	4.55.....	+0.63
5.25.....	− .49	4.50.....	+0.80
5.20.....	− .43	4.45.....	+1.03
5.15.....	− .37	4.40.....	+1.45
5.10.....	− .31	4.35.....	+1.77
5.05.....	− .25	4.30.....	+2.00
5.00.....	− .18	4.25.....	+2.20
4.95.....	− .11	4.20.....	+2.36
4.90.....	− .04	4.15.....	+2.50
4.85.....	+ .03	4.10.....	+2.63
4.80.....	+0.11	4.05.....	+2.76

TABLE 5

MEAN CONTOUR OF Hδ*

$\delta\lambda$ in A	R	$\delta\lambda$ in A	R
0.0.....	0.20	8.0.....	0.84
0.5.....	.30	9.0.....	.87
1.0.....	.41	10.0.....	.89
1.5.....	.47	11.0.....	.92
2.0.....	.51	12.0.....	.94
3.0.....	.60	13.0.....	.95
4.0.....	.66	14.0.....	.96
5.0.....	.71	15.0.....	.97
6.0.....	.76	16.0.....	.98
7.0.....	0.80	17.0.....	0.99

* The contour is plotted in Fig. 4.

The surface gravity, g, must be estimated to discuss the Stark effect. The mass, from the mass-luminosity relation, is $9\odot$; the effective temperature, 7500°, is estimated from the spectral class and the ionization temperature (discussed in the final section). Then from equation (4) we find $\log g = 2.4$, about one-hundredth of the value in a main-sequence star:

$$\log \frac{g}{g\odot} = \log \frac{M}{M\odot} + 4 \log \frac{T_e}{T_e\odot} - \log \frac{L}{L\odot} . \qquad (4)$$

The theory of the Stark effect has been developed by Verweij,[9] who tabulates predicted contours[10] as a function of g and T_e. An inspection of the predicted values of R in his Table 11 shows that the observed contour of $H\delta$ can be represented when $\delta\lambda > 4$ A with $\log g = 3$, $\theta = 0.7$, $T = 7200°$. The representation of the core is extremely poor; the observed core is both narrower and less deep than the theoretical cores. No fit of the observed wings can be obtained with lower surface gravities; $\log g \geqslant 2$ gives no solution. A disturbing feature of the application of Verweij's theory is that the excitation temperature and the kinetic temperature have been assumed equal.

The shape of the extreme Stark wings can be used to estimate the number of absorbing atoms above an effective photosphere. I shall neglect stratification and assume that the hydrogen is the only source of opacity. I shall also assume that the thermal motion of the hydrogen atoms is given by the normal relation and that the turbulence does not appreciably affect this value. Then the absorption coefficient per atom in the second level, at distance $\delta\lambda$ from the center of the line, is

$$l(\delta\lambda) = C\,\frac{F_0^{3/2}}{\delta\lambda^{5/2}}, \tag{5}$$

where F_0, the normal field strength, is

$$F_0 = 47\left(\frac{2P_e}{T}\right)^{2/3}.$$

Finally, we obtain

$$l(\delta\lambda) = 2.0 \times 10^{-14} \cdot \frac{P_e}{T} \cdot \delta\lambda^{-5/2}. \tag{6}$$

The process of line formation in the wings follows the scheme of pure absorption. The line-absorption coefficient in the wings is less than the continuous absorption coefficient. Using formulae given by Unsöld,[11] the absorption A in the wing of a line is

$$A = 1 - R = \frac{l}{k} \cdot \left(\frac{1}{1 + \frac{\sqrt{3}}{\beta_0}}\right), \tag{7}$$

where β_0 is given in terms of the boundary temperature, T_0, as

$$\beta_0 = \frac{\frac{3}{8}u_0}{1 - e^{-u_0}}, \qquad u_0 = \frac{h\nu}{kT_0}.$$

The number of atoms above the effective photosphere, $N_2 h$, in the sense of the Schuster-Schwarzschild model, is measured by the optical depth in the line. With $\beta_0 = 2.0$, the photosphere is located at $\tau_0 = 0.54$. Then the optical depth in the line, $\tau(\delta\lambda)$, is

$$\tau(\delta\lambda) = A(\delta\lambda) \cdot \left(1 + \frac{\sqrt{3}}{\beta_0}\right) \cdot \tau_0. \tag{8}$$

[9] *Pub. Astr. Inst. Amsterdam*, No. 5, 1936.

[10] The abundance of hydrogen adopted by Verweij is one thousand times that of the metals. The opacity of the negative hydrogen ions has been neglected, but fortunately it does not play a role in α Car. The theory is not applicable to the cores of the lines.

[11] *Sternatmosphären*, Springer, 1938.

From equations (6) and (8) we derive

$$N_2 h = \frac{T}{P_e} \cdot A(\delta\lambda) \cdot \delta\lambda^{5/2} \cdot \left(1 + \frac{\sqrt{3}}{\beta_0}\right) \cdot \tau_0 \cdot 10^{13.7} . \tag{9}$$

The product $A(\delta\lambda)\delta\lambda^{5/2}$ should be constant in the wings and may be evaluated graphically from the observed contour; its mean value over the interval 6 A $< \delta\lambda <$ 15 A is found to be 30. The number of excited hydrogen atoms is found to be

$$N_2 h \approx \frac{T}{P_e} \cdot 10^{15.2} .$$

In a normal dwarf A star, T/P_e is of the order of 10; in a supergiant it may be a hundred times larger. If we adopt the values $T = 7300°$, $P_e \approx 10$ derived in α Car from ionization theory then we find $N_2 h \approx 10^{18.0}$. Such a large number of excited hydrogen atoms is unexpected and leads to the problem of the opacity of such a layer. In equation (7) we may write the mass-absorption coefficients in terms of the absorption coefficients per atom as

$$l = N_2 h \cdot l(\delta\lambda) ,$$

$$k = N_2 h \cdot K_2(T) ,$$

where $K_2(T)$ is the continuous absorption coefficient per atom of hydrogen in the second level. I have computed $K_2(T)$ for hydrogen at $\lambda = 4000$ A, with the results given in Table 6.

TABLE 6

CONTINUOUS ABSORPTION COEFFICIENT PER EXCITED HYDROGEN ATOM

T	θ	$\log K_2(T)$	$\log T \cdot K_2(T)$
10,000°	0.5	−17.75	−13.75
8,400	.6	−17.95	−14.03
7,200	.7	−18.17	−14.31
6,300	0.8	−18.38	−14.58

We can now evaluate the optical depth in the continuum, τ, corresponding to the observed intensity of the Balmer line; since $N_2 h \approx 10^{18.0}$, it is obvious that τ lies near unity. We can attempt to estimate P_e directly, since

$$A(\delta\lambda) = \frac{N_2 h \cdot l(\delta\lambda)}{N_2 h \cdot K_2(T)} \cdot \frac{1}{1 + \frac{\sqrt{3}}{\beta_0}} ,$$

$$P_e = T \cdot K_2(T) \cdot A(\delta\lambda) \cdot \delta\lambda^{5/2} \cdot \left(1 + \frac{\sqrt{3}}{\beta_0}\right) \cdot 10^{13.7} ,$$

$$P_e = T \cdot K_2(T) \cdot 10^{15.4} . \tag{10}$$

From equation (10) and Table 6 we see that for any probable temperature $6 < P_e < 25$ bar. The electron pressure we have determined is the value at the level where the hydro-

gen wings are formed. If the metallic absorption lines are produced in relatively extended higher layers of low excitation temperature and low opacity, we may picture the wings of the hydrogen lines as arising deeper in the atmosphere in layers where the continuous absorption is beginning to be appreciable. We should note that the excitation temperature derived for the metallic lines, $\theta_{exc} = 1.03$, is obviously impossible for hydrogen. The observed $N_2h = 10^{18.0}$ would then correspond to 10^{28} neutral hydrogen atoms, or more than 10^4 grams of hydrogen above the photosphere.

BLENDING EFFECTS

The strength of the wings of the hydrogen lines results in pronounced blending phenomena, in that lines of *Fe* I, *Fe* II, *Ti* II, *Cr* II, and *Zr* II near the hydrogen lines are

TABLE 7

THE WEAKENING OF LINES IN THE HYDROGEN WINGS

λ	Elem.	α Car log X_0	⊙ log X_0'	Δ log N_a	Remarks
3952.6	*Fe* I	+0.60:	+0.59	+0.01:	Plate weak
3953.2	*Fe* I	+0.05:	+0.33	−0.28:	Plate weak
3961.1	*Fe* I	−0.66::	−0.29	−0.37::	Blend, very weak
3966.1	*Fe* I	+0.01::	+0.76	−0.75::	Plate very weak
3974.1	*Fe* II	+0.50:	+1.14	−0.64:	Plate weak
3977.7	*Fe* I	+0.26:	+0.53	−0.27:	Plate weak
3986.2	*Fe* I	+0.14:	+0.18	−0.04:	Plate weak
4079.8	*Fe* I	−0.12	+0.01	−0.13	
4084.5	*Fe* I	+0.24	+0.52	−0.28	
4089.2	*Fe* I	−0.76	−0.63	−0.13	
4090.5	*Zr* II	+0.08	−0.12	+0.20	
4095.9	*Fe* I	0.00	+0.13	−0.13	Poor
4098.2	*Fe* I	−0.17	+0.21:	−0.38:	
4100.8	*Fe* I	−0.60	−0.08	−0.52	Poor
4106.5	*Fe* I	−0.65	−0.37	−0.28	
4107.5	*Fe* I	+0.21	+0.41	−0.20	
4109.1	*Fe* I	−0.37	−0.37	0.00	
4112.4	*Fe* I	−0.70	−0.67	+0.03	Poor
4114.5	*Fe* I	+0.01	+0.01	0.00	
4325.8	*Fe* I	+2.30:	+1.98	+0.32:	Line too strong*
4337.9	*Ti* II	+2.08:	+2.05	+0.03:	Line too strong*
4344.3	*Ti* II	+2.00:	.....	.....	Blended, too strong*
4350.8	*Ti* II	+0.89	+0.76	+0.13:	Line too strong*
4352.7	*Fe* I	+0.63	+0.18	+0.45	
4859.8	*Fe* I	−0.60::	+0.66	−1.26::	Plate weak
4864.4	*Cr* II	+0.28	+1.02	−0.74	
4865.6	*Ti* II	−0.06	+0.47	−0.53	
4874.0	*Ti* II	+0.14	+0.58	−0.44	

* Lines on the flat part of the curve of growth give values of X_0 subject to considerable uncertainty.

found to be weakened. The equivalent widths of such lines are measured with respect to the continuum defined by the hydrogen lines. By means of the curve of growth we then obtain the observed value of X_0, a measure of the number of atoms above the effective photosphere defined by the hydrogen atoms. The solar values of X_0 for the same lines are relatively unaffected by hydrogen-line absorption, since the Balmer lines are weaker in the sun. Consequently, we can determine the quantity $\Delta \log N_a$, the decrease in the number of atoms above the effective photosphere. For each element we must also know the difference in the mean number of atoms, as determined from unblended lines, between α Car and the sun. In Table 7 the lines used are tabulated with the value of X_0 de-

rived from the curve of growth. The next column contains the solar value of log X_0' as corrected for the difference of excitation temperatures and for the mean difference in the number of atoms of the element between star and sun. The last column, $\Delta \log N_a$, gives the reduction in the number of atoms produced by the blending effect. Note that the lines near $H + H\epsilon$ in the sun suffer from blending effects themselves and therefore deserve low weight. The data have been plotted in Figure 4.

The material is too scanty for a decisive test of possible stratification. I shall consider a model proposed by Unsöld.[11] Since we are working close to the core of the hydrogen line, the boundary value of the flux must be determined. Unsöld assumes that it is given by the central intensity of the Balmer lines. In a hydrogen line, $l_c \gg k$, and the contour of the hydrogen line is given by

$$R = R_c\left(1 + \frac{\frac{1}{4}u_0}{1 - e^{-u_0}} \cdot \frac{\bar{k}}{k_\nu + l_\nu}\right). \tag{11}$$

The optical depth of the effective photosphere, now produced by the hydrogen-line absorption, is τ_0,

$$\tau_0 = \frac{\bar{k}}{k_\nu + l_\nu}\left(1 + \frac{1 - e^{-u_0}}{\frac{1}{4}u_0} \cdot \frac{k_\nu + l_\nu}{\bar{k}}\right)^{-1}. \tag{12}$$

We evaluate the ratio of the absorption coefficients from equation (11) and find

$$\left.\begin{aligned} \tau_0 &= \frac{R - R_c}{R_c} \cdot \frac{1 - e^{-u_0}}{\frac{1}{4}u_0}\left(1 + \frac{R_c}{R - R_c}\right)^{-1}, \\ \tau_0 &= \frac{(R - R_c)^2}{R \cdot R_c} \cdot \frac{1 - e^{-u_0}}{\frac{1}{4}u_0}. \end{aligned}\right\} \tag{13}$$

If there were no hydrogen line present ($R = 1$) the metallic line would have been produced above optical depth $(\tau_0)_0$,

$$(\tau_0)_0 = \frac{(1 - R_c)^2}{R_c} \cdot \frac{1 - e^{-u_0}}{\frac{1}{4}u_0}. \tag{14}$$

Therefore, the reduction in the effective number of absorbing atoms is

$$\frac{N}{N_0} = \frac{\tau_0}{(\tau_0)_0} = \frac{1}{R}\left(\frac{R - R_c}{1 - R_c}\right)^2. \tag{15}$$

Physically, equation (15) takes account of both the raising of the photosphere and the reduction of the temperature gradient within the remaining atmosphere. The values of $\Delta \log N_a$, computed from equation (15) with $R_c = 0.2$, are plotted in Figure 4. The fit seems to be satisfactory. Thackeray[12] has obtained more complete observational material in the case of the sun and has made a more extensive theoretical discussion. The present material is sufficient only to establish the existence of the blending effect and to suggest that no very large stratification exists.

THE CENTRAL INTENSITIES

The microphotometer tracings yield the apparent central absorption of a line, $A_c' = 1 - R_c'$. The resolving-power of even the coudé dispersion is not sufficient to

[12] *Ap. J.*, **84**, 433, 1936.

make A_c' dependable for any but the strongest lines. A definitive evaluation of the true central intensities, such as Allen[13] has made for the sun, is hardly possible with the present resolving-power. For a preliminary discussion, fifty lines in the region λλ 4012–4177 were used to define the relation between equivalent width, W, and apparent central absorption, A_c', as given in Table 8. The data in Table 8 are uncertain at the lower end of the scale, and also at the upper, since very few strong lines can be found.

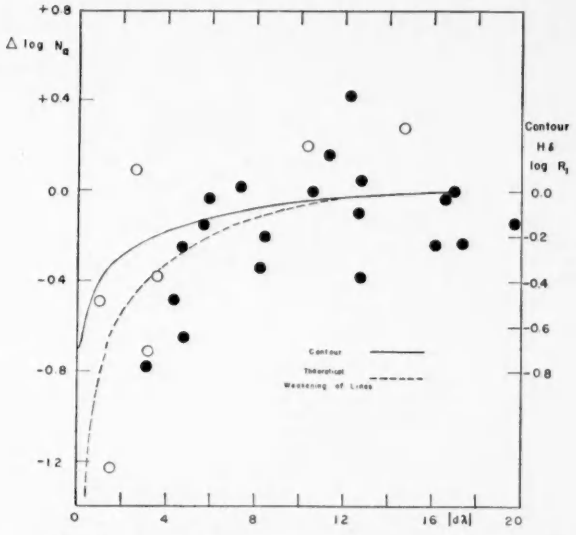

FIG. 4.—The contour of $H\delta$ in α Car is given by the solid line. The distance $\delta\lambda$ is measured in A from the center; R_I is the observed intensity in the line. The points represent the observed weakening of metallic lines in the wings of the hydrogen lines, as a function of $\delta\lambda$. The dotted line is the theoretically predicted weakening for an unstratified atmosphere. (Please note a small systematic error of approximately +0.03 in the plotting of $\Delta \log N_a$.)

TABLE 8

OBSERVED RELATION BETWEEN W AND A_c'

W in mA	A_c'	W in mA	A_c'
20	0.10:	150	0.51
30	.14	200	.60
50	.22	230	.66
80	.32	300	.69:
100	0.38	350	0.81::

The theoretical maximum resolving-power of the spectrograph is near 150,000; the finite slit width (≈ 0.04 mm) produces a large reduction of the expected resolving-power to 32,000. The Doppler width of the lines has negligible effect because of small turbulence. In the measuring engine several pairs of lines actually separated by 100 mA were clearly resolved, so that a resolving-power of 40,000 is possible. The slit width of the microphotometer was too small to diminish the resolving-power, but scattered light in the emulsion might possibly cut the effective resolving-power on the tracings. An experi-

[13] *Ap. J.*, **85**, 165, 1937.

mental evaluation of the resolving-power can be made from the iron comparison lines. Let us assume that the instrumental contour (assumed independent of wave length) can be expressed in linear measure as

$$K(x) = \frac{1}{b\sqrt{\pi}} \cdot e^{-(x/b)^2} . \tag{16}$$

Also assume that the true absorption-line contour is

$$A(x) = A_c \cdot e^{-(x/a)^2} . \tag{17}$$

The half half-width of the instrumental contour will be $0.83b$. The measured central absorption, A_c', is then

$$A_c' = A_c \left[1 + \left(\frac{b}{a}\right)^2 \right]^{-1/2} , \tag{18}$$

and the equivalent width is

$$W = \sqrt{\pi}\, a A_c .$$

We find that

$$\frac{1}{A_c^2} = \frac{1}{A_c'^2} - \frac{\pi b^2}{W^2} . \tag{19}$$

Equation (16) can be applied to the measures of the iron comparison lines if we assume that such lines are intrinsically infinitely narrow. Four lines whose maximum density was close to that in the stellar spectrum gave $b = 0.86$ mm on the tracings. Several extremely strong comparison lines gave about the same value of b for the center of the line but showed an increase of b to 1.47 mm for the wings. The strong comparison lines have contours which are approximately represented by

$$K(x) = K_0 \left(1 - \frac{x}{c} \right) .$$

Such an increase in b in the wings of an emission line is to be expected, since the error function is too strongly concentrated to represent the effects of photographic spreading and halation. The smaller value of b is to be used in the correction of the stellar absorption-line intensities, since the contrast in the stellar lines is seldom large enough to make the wings of the instrumental contour important. The dispersion on the tracings is 81 mA/mm; therefore $\beta = 70$ mA if we write equation (16) in terms of wave length. The resolving-power is then 35,000, in good agreement with the expected value. The corrected A_c, the central absorption, is given in Table 9 for a set of possible values of β. If $\beta = 110{,}120$ mA, the observed A_c' of weak lines correspond to imaginary values of A_c, i.e., to overcorrection. We have probably undercorrected the strong lines if we take $\beta = 70$ mA, and the results for $\beta = 120$ may be more nearly correct when $W > 200$ mA. The sixth column of the table contains Allen's accurate solar values of A_c as measured at λ 6300.

In spite of the uncertainty of the instrumental contour, it is probable that a weak line of given W has a lower central absorption (higher residual intensity) in α Car than in the sun; the effect is smaller for lines of moderate intensity. Some possible theoretical reasons for higher residual intensities may be mentioned here: (1) The higher temperature

in α Car results in higher central intensities. This effect has been partly removed by comparing results in the violet part of the spectrum with results in the red for the sun. (2) Possible stellar rotation or large-scale turbulence might artificially reduce A_c for weak lines. (3) The ratio of the absorption coefficient to the coefficient of absorption plus scattering, the parameter ϵ, might be larger in α Car than in the sun. (4) Small-scale turbulence, indicated by the curve of growth, results in larger values of W in α Car than in the sun for a given value of X_0, the optical depth at the center of the line.

The computation of a predicted relation between A_c and X_0 has been carried through for one model atmosphere. The relation between W and X_0, obtained through the curve of growth, is given in the seventh column of Table 9. We must know the boundary temperature, T_0, for which I adopt 6100°, and the continuous absorption coefficient, for

TABLE 9

CORRECTED CENTRAL ABSORPTIONS

W IN mA	α CAR, $A_C \times 10^2$, β IN mA				⊙ ALLEN	THEORETICAL, α CAR	
	70	90	110	120		X_0	$A_c \times 10^2$
20	12:	16:	>100:	>100:	32	0.3	15
30	17	21	48:	>100:	47	0.5	23
50	26	31	51	62:	53	0.9	30
80	37	41	56	61	77	1.9	43
100	43	47	60	65	80	3	50
150	56	60	71	74	84	20	75
200	64	68	76	77	84:	90	83
230	71	73	82:	83:	.....	160	84
300	72:	73:	78.	80:	87:	350	85
350	84::	86::	91::	92::	.....	500	85

which I adopt $k_\nu = \bar{k}$. The quantity, ϵ, was determined by assuming that for the strongest lines, with $X_0 \to \infty$, $A_c = 0.85$. The Milne-Eddington model atmosphere with constant η was used in Unsöld's formulation[11] (eqs. [65.4], [65.14], and [65.22]). Then ϵ is found to be 0.036. Finally, the last column of Table 9 gives the predicted value of A_c for the given X_0. A comparison of the observed and predicted A_c suggests that the agreement is sufficiently good for the present state of the observational material. Further studies of stellar spectra from this point of view are desirable, especially in cases of large turbulence. Then a direct determination of the Doppler width would be possible; in α Car the contours are too narrow to permit this valuable check on the curve of growth.

THE IONIZATION EQUILIBRIA

The exact analysis of the state of ionization and the abundances in a stellar atmosphere must wait for an extension of our knowledge of the absolute f-values of the metals. The most convenient parameters describing the level of ionization in α Car are the mean differences of log X_0 for a given element between the star and the sun. Let the state of ionization of the given element occur in the fraction ζ_i; let the total number of atoms of that element be ρ_a per gram, and let the abundances be the same in the star and in the sun. Let the Boltzmann factors be B; the opacity per gram, k; then

$$\frac{X_0}{X_0(\odot)} = \frac{\zeta_i \rho_a}{\zeta_i(\odot)\rho_a(\odot)} \cdot \frac{B}{B(\odot)} \cdot \frac{v(\odot)k(\odot)}{vk}, \qquad (20)$$

or

$$\log \frac{\zeta_i}{\zeta_i(\odot)} = \log \frac{vk}{v(\odot)k(\odot)} + \Delta\theta \cdot \bar{\chi} + \log \frac{X_o}{X_o(\odot)}, \qquad (20a)$$

or

$$\log \frac{\zeta_i}{\zeta_i(\odot)} = \log \frac{vk}{v(\odot)k(\odot)} + \log \frac{X_o'}{X_o(\odot)}. \qquad (20b)$$

The Boltzmann factor is replaced by a mean value for all lines used, since in general $\Delta\theta$ is small (≈ -0.12). The quantity X_o' is X_o corrected by the ratio of the Boltzmann

TABLE 10

STATE OF IONIZATION IN α CARINAE

Element	n	$\bar{\chi}$	$\Delta \log X_o$	$\log \zeta_i(\odot)$	$\log \zeta_i/k$ $\theta_{exc}=1.03$	$\log \zeta_i/k$ $\theta_{exc}=0.83$
Mg I	5	3.4	−2.36	−1.42	−3.02	−3.70
Mg II	1	8.8	+1.70:	−0.02	+1.79::	+0.03:
Al I	2	0.0	−2.37:	−1.86	−3.06:	−3.06:
Ca I	13	2.1	−2.00	−2.77	−3.85	−4.27
Sc II	7	0.6	−0.18	−0.01	+0.91	+0.79
Ti I	5	2.3	−1.83	−1.98	−2.92	−3.38
Ti II	36	1.4	−0.11	−0.01	+0.88	+0.60
V I	1	2.5	−2.60:	−1.64	−3.37:	−3.87:
V II	5	1.7	−0.23::	−0.01	+0.73::	+0.39::
Cr I	5	2.3	−1.82:	−1.86	−2.78:	−3.24:
Cr II	14	3.9	+0.32	−0.01	+0.89	+0.11
Mn I	6	2.2	−2.31	−1.37	−2.77	−3.21
Fe I	67	2.6	−1.86	−1.04	−2.04	−2.56
Fe II	20	2.7	+0.48	−0.04	+1.28	+0.74
Co I	3	3.0	−2.38	−0.87	−2.44	−3.04
Ni I	6	5.4	−1.50	−0.88	−1.86	−2.94
Sr II*	2	0.0	−0.67:	−0.00	+0.50:	+0.50:
Y II	6	0.6	−0.18	−0.04	+0.88	+0.76
Zr II	12	1.0	−0.05	−0.00	+1.00	+0.80
Ba II*	3	0.8	−0.63:	−0.02	+0.42:	+0.26:
La II	3	0.6	−0.48	−0.00	+0.62	+0.50

* *Ba* II and *Sr* II had no solar values of X_o; approximate values of the solar X_o were determined from Allen's equivalent widths.

factors in the star and the sun. The data for all elements for which Menzel and Goldberg have solar values of X_o are contained in Table 10. The number of lines is n; $\Delta \log X_o$ is positive if the lines are stronger in α Car than in the sun.

The data in Table 10 can be used in two ways. Independent of opacity or abundance, the ratio of ionized to neutral elements might be used to obtain the difference of the level of ionization in the two stars. Adopting a value of P_e and T for the sun, we obtain the ratio in α Car. Such a ratio defines a locus in the P_e, T plane for each element, which is determined by Saha's ionization equation. This method can be used for *Fe*, *Ti*, *V*, *Cr*, *Ca* (since we know f-values for λ 4227 and λ 3933), and *Mg* (poor, because of the high excitation potential of *Mg* II). Unfortunately, the ionization potentials are so closely the same that no reliable intersection of such loci are found. The material can be considerably extended if we know the sources of opacity in the star and the sun and apply equation (20*b*). The absolute intensities of both neutral and ionized metals should be pre-

dicted by one value of P_e, T, and k. Furthermore, the required value of the opacity defines a second locus in the P_e, T diagram, since the opacity is a known function of P_e and T. The intersections of this locus and the loci for the various elements computed from Saha's formula are well determined.

The physical parameters for the solar atmosphere were taken as $\log v(\odot) = 5.15$, $\log g = 4.44$, $\theta = 0.9$ ($T = 5600°$), and $\log P_e = 1.25$ for an effective photosphere at $\tau_0 = 0.65$. The opacity is the Rosseland-mean value computed for hydrogen and negative hydrogen ions, $\log k(\odot) = -0.77$; we shall neglect the wave-length dependence in both stars. The fifth column of Table 10 contains the fraction of the element $\zeta_i(\odot)$ in the given state of ionization in the sun; the sixth and seventh columns, the fraction ζ_i/k in α Car, as determined from

$$\log \frac{\zeta_i}{k} = \log \zeta_i(\odot) + 1.17 + \Delta \log X_0' . \qquad (21)$$

The sixth column has been computed with the previously adopted value of the excitation temperature, $\theta_{exc} = 1.03$; the seventh column, with the higher value $\theta_{exc} = 0.83$, suggested by the laboratory gf values for *Fe*.

The uncertainty of k still remains in the data of the sixth and seventh columns. One simple procedure is suggested by the fact that ζ_i is of the order of unity for the ionized iron-group elements and that in no case can it exceed unity. Then the largest entry will be roughly equal to $-\log k$. In the sixth column we should omit *Mg* II because of the large Boltzmann correction; then $\log k \leqslant -1.3$. In column 7 we find $\log k \leqslant -0.9$. The values of P_e, T for which the opacity of hydrogen and negative hydrogen ions is equal to either of the above values can be determined from computations by Wildt.[14] Another method is based on the relation between surface gravity and opacity; convenient tables of the relations between g, P_g, P_e, T, and k have been computed by Dr. P. C. Keenan, who has kindly permitted their use. The hydrogen abundance adopted was five thousand times that of the metals. The values of P_e, T, and k were determined for $\log g = 2.5$; it was apparent that these were such that k would be too high to account for the intensity of the ionized metals. A solution with $\log g = 1.5$ was carried through, and such a reduction of the effective surface gravity is not improbable. Investigations of turbulent atmospheres in late supergiants have suggested similar effects. If the atmospheric pressure gradient corresponds to the total atomic speed of the order of 3.5 km/sec, the effective value of g should be about 0.3 times the gravitational value valid for the thermal motions of 1.8 km/sec.

In Table 11 the estimated values of P_e and θ for each element are tabulated for the several methods of estimating the opacity. It should be noted that no solutions, or very indeterminate ones, exist for most of the ionized metals. If the opacity is high, no solutions are possible for any of the ionized metals. The uncertainty of the excitation temperature has a small effect on the final ionization temperatures; some of the individual determinations, such as *Mg* II, are very sensitive to excitation temperature. The agreement of the individual determinations is moderately good, although the maxima are very flat for the ionized metals, which yield poor determinations. No large range of ionization potentials exists, and no strong systematic effects are apparent. The ionized metals of low ionization potentials (both first and second ionizations are relevant), such as *Sr* II, *Ba* II, *La* II, *Sc* II, and especially *Y* II, indicate a lower ionization temperature than the rest of the metals. These lines are sensitive to absolute magnitude, and many details of the absolute-magnitude effects still await explanation. For the purposes of the other

[14] *Ap. J.*, **90**, 611, 1939.

computations of this investigation I shall adopt $\theta = 0.69$ and $\log P_e = 1$ as the ionization temperature and pressure.

Certain important lines of the lighter elements have been measured in α Car for which no solar values of X_0 are available. These can be useful only if the f-values are known. Table 12 contains the measured value of X_0 for such lines; the last column gives the estimated percentage of the element in the relevant stage of ionization.

TABLE 11

DETERMINATIONS OF θ AND P_e FROM IONIZATION EQUILIBRIA

Element	$\log k = -1.3$, $\theta_{exc} = 1.03$		$\log k = -0.9$, $\theta_{exc} = 0.83$		$\log g = 2.5$, $\theta_{exc} = 0.83$		$\log g = 1.5$, $\theta_{exc} = 1.03$	
	θ	$\log P_e$	θ	$\log P_e$	θ	$\log P_e$	θ	$\log P_e$
Mg I	0.75	−0.2	0.64	+0.5	0.64	+1.4	0.69	+0.9
Mg II	—	—	.60	−0.3*	.65	+1.4*	—	—
Al I	.75	− .1	.66	+0.9	.66	+1.4	.69	+ .9
Ca I	.75	+ .3	.69	+0.9	.68	+1.3	.70	+ .9
Sc II	.76	− .2	.69	+1.0	.72	+1.2*	.75	+ .9*
Ti I	.75	+ .2	.68	+0.8	.67	+1.3	.72	+ .7
Ti II	.74	− .2	.66	+0.7	—	—	.70	+ .9*
V I	.75	− .4	.64	+0.7	.64	+1.4	.67	+ .9
V II	.70	− .6	.64	+0.8*	—	—	—	—
Cr I	.75	+ .2	.67	+0.8	.68	+1.3	.73	+ .9
Cr II	.70	− .7	.61	−0.3*	—	—	—	—
Mn I	.76	+ .1	.66	+0.8	.65	+1.4	.69	+ .9
Fe I	.75	+ .2	.67	+0.9	.68	+1.4	.71	+ .9
Fe II	—	—	.64	+0.2*	.70	+1.3*	—	—
Co I	.75	− .1	.66	+0.7	.64	+1.4	.69	+ .9
Ni I	.75	+ .3	.69	+0.6	.64	+1.4	.73	+ .9
Sr II	.75	+ .2	.74	+1.1	.73	+1.2	.73	+ .9
Y II	.79	+ .5	.78	+1.5	.76	+1.2	.76	+ .8
Zr II	.70	− .1	.69	+0.9	.71	+1.2*	—	—
Ba II	.78	+ .4	.75	+1.4	.75	+1.1	.80	+ .5*
La II	0.75	+0.2	0.69	+1.1	0.70	+1.2	0.71	+0.9
Mean	0.75	0.0	0.67	+0.7	0.68	+1.3	0.71	+0.9

* The solution is nearly indeterminate; (−) the solution does not exist. The values of θ and $\log P_e$ were estimated from tables of the ionization equilibria. The uncertainty of such an estimate is about 0.02 in θ and 0.1 in $\log P_e$.

The resonance lines of *Ca* I and *Ca* II show an interesting discrepancy for which no obvious explanation is offered. From equation (2) we find in α Car that

$$\log Nf = \log X_0 + 11.77 - \log \frac{\lambda}{4000\,\text{A}} . \qquad (22)$$

Inserting the known f-values, we obtain

$$\log \frac{N(Ca\ \text{II})}{N(Ca\ \text{I})} = 3.5 ,$$

a value which is too low for the level of ionization determined by the other metals or from the body of excited *Ca* I lines. The ionization equation for $\theta = 0.69$ and $\log P_e = 1.0$ predicts that the above ratio should be 4.6. The K line is, of course, too strong for satis-

factory use of the curve of growth to measure X_0. The damping constant may also be quite different from that of the subordinate metallic lines which define the curve of growth; other forms of damping may possibly be of importance. An alternative explanation is that the resonance line of *Ca* I is produced in a higher layer of the star's atmosphere. Such an explanation would be of great significance for an interpretation of the entire spectrum. The anomalously great strength of the wings of the hydrogen lines sug-

TABLE 12

X_0 OBSERVED IN α CAR; NO SOLAR VALUE AVAILABLE

Element	λ	χ	log X_0	log ξ_i
C I	4770.00	7.5	+0.05	−0.7
	4771.72		+0.53	
	4775.89		+0.19	
N I	4151.46	10.3	−0.49	−0.1
Si II	4128.05	9.8	+1.71::	0.0
	4130.88		+0.69:	
S I	4694.18	6.5	−0.28	−1.1
	4695.51		−0.34:	
Ca I	4226.74	0.0	+2.04	−5.0
Ca II	3933.68	0.0	+5.2:	−0.4
Eu II	4129.73	0.0	−0.08:	−0.5:

TABLE 13

ESTIMATED RELATIVE ABUNDANCES

ELEMENT	log $\rho_a/\rho_{\text{Carbon}}$				ADOPTED
	$\bar{\chi}$	$\theta_{\text{exc}}=1.03$	$\theta_{\text{exc}}=0.83$	$\theta_{\text{exc}}=0.69$	
H	10.2	+7.6	+7.0	+6.6	+4.1
N	10.3	+0.4	−0.1	−0.6	+0.5
Si	9.8	+1.3	+0.8	+0.5	−0.3
C	7.5	0.0	0.0	0.0	0.0
S	6.5	−1.3	−1.1	−1.0	−1.1
Ca	0.0	−3.9	−2.4	−1.3	−1.7

gests that they are produced at an optical depth where the pressure is moderately high and where the excitation temperature is probably close to $\theta_{\text{exc}} = 0.69$, i.e., to the ionization (and effective) temperatures. There is little possibility of so high an effective temperature for the region in which the metallic lines are produced. The value of P_e determined from the ionization equilibria of the metals is low; and, consequently, the abundance of hydrogen predicted from the strength of the Stark wings is very high; i.e., log $N_2 h \approx 18$. We shall see that the abundances are reasonable for all elements but hydrogen—either the electron pressure or the excitation temperature is high, or both are high, in the region where the hydrogen wings are produced.

The logarithm of the relative abundances, log $\rho_a/\rho_{\text{Carbon}}$, has been computed in Table 13, for the possible range of excitation temperatures. Equation (22) gives log Nf; the sum rule gives the sum of the f-values when all transitions to the given level are considered. The data are incomplete, in that a small region of the spectrum is covered by the present investigation. The arbitrary assumption has been made that the sum of the f-values for all the actually observed lines of each atom is equal to unity. For comparison a set of adopted abundances derived from an unpublished investigation of τ Sco by Unsöld, and for *Ca* from the sun by B. Strömgren,[15] is given in the last column. The relative abundances of all elements but hydrogen seem satisfactory, especially if we adopt $\theta_{\text{exc}} = 0.83$. The abundances of the other metals are all probably close to their solar values, since the discussion of the ionization equilibria and opacity left no large discrepancies between the predicted and the observed intensities of the metallic lines.

McDonald Observatory
and
Yerkes Observatory
October 1941

[15] *Festschrift Elis Strömgren*, p. 256, Copenhagen, 1940.

THE NEAREST STARS*

GERARD P. KUIPER

ABSTRACT

In Table 1 a list is given of the known stars with $p \geq 0''.095$; its chief purpose is to show which data are still lacking. The data at hand define the distribution of $M(v)$ and Sp shown in Figure 1. Figure 2 shows the incompleteness of our knowledge of the nearest stars fainter than $M = 11$; but rapid progress may be made by continuing the spectrographic survey which has already added about 25 per cent to the number previously known. Some results are derived from the nearest binaries and multiple stars; but larger numbers are required for a proper statistical treatment. It is found that of the masses exceeding that of the sun, at least two-thirds have divided into stable binary or multiple systems.

1. It is of interest to summarize from time to time the observational data collected for the nearest stars. These stars make up the best sample available for the study of all but the rarer subdivisions; they provide data on the luminosity function; the distribution of stars in the Hertzsprung-Russell diagram (including such problems as the width of the main sequence); the empirical mass-luminosity relation; the total amount of stellar matter per unit volume and hence the amount of interstellar matter (the sum being known); and finally, the velocity distribution of the dwarfs and binary-star statistics.

The chief purpose of this article is to present a list of the known stars nearer than 10.5 parsecs (parallaxes $0''.095$ and larger); this list is found in Table 1. We hope that it will stimulate observations of the quantities still lacking. In addition, some of the problems mentioned above are briefly reviewed.

2. *Table 1.*—The following explanations may suffice. Components of visual binaries are listed separately because their magnitudes, and usually other quantities, may be determined. Proper-motion and parallax data are listed only once for each system, the weighted mean having been used in each case. But magnitude, spectral, and radial-velocity data (spectroscopic binaries!) are given for each component.

The magnitude measures were reduced to the IPv system; half-weight was given to the reduction based on Mrs. Gaposchkin's compilation[1] and half-weight to that based on the Potsdam catalogue.[2] For three stars (Nos. 148, 149, 225) the unchanged HD magnitudes were used. Some measures were taken from the *General Catalogue* without change. For fainter stars data by Willis[3] and by Seyfert[4] could be used, while much unpublished material by the writer was incorporated. Photographic magnitudes, by Luyten,[5] are in italics.

The spectral types are the writer's, with the following exceptions: the Sirius companion, No. 36, and the stars south of $-50°$; for the latter the Harvard types were used when available. Miss Hoffleit has revised some of the Harvard types[6] and has very kindly supplied revisions for a few additional stars. All her revised types are designated by an asterisk in Table 1. The unchanged HD types are italicized. For a few stars Luyten's color class[5] is given.

* *Contributions from the McDonald Observatory, University of Texas*, No. 44.

[1] *Harvard Obs. Mimeograms*, Ser. III, Nos. 1 and 2, 1938.

[2] *Pub. Astr. Obs. Potsdam*, **17**, 1907.

[3] *Ap. J.*, **80**, 319, 1934.

[4] *Ap. J.*, **91**, 117, 1940.

[5] *Pub. Obs. Minnesota*, **3**, No. 1, 1941.

[6] *Harvard Ann.*, **105**, 45, 1937.

TABLE 1

No.	Name	α (1900) δ	$m(v)$	Sp	μ	θ	$p(t)$	$p(Sp)$	V_r	$M(v)$
1	+43°44 A	$0^h12^m.7$ +43° 27′	8.1	M2	2″.90	82°	284±5	250	+ 8±2	10.4
2	..... B	.....	10.9	M5+	.....	.....	.....	.....	.....	13.2
3	ζ Tuc	0 14.9 −65 28	4.38	Go*	2.07	56	138±7	.....	+ 9±0	5.1
4	β Hyi	0 20.5 −77 49	2.93	G1*	2.25	82	143±6	.....	+ 23±0	3.7
5	+66°34 A	0 26.3 +66 42	10.38	M2+	1.76	96	103±7	96	− 4±6†	10.4
6	..... B	.....	12.3	M4+	.....	.....	.....	.....	.....	12.4
7	54 Psc	0 34.2 +20 43	5.97	K1	0.59	232	104±6	110	− 34±1	6.1
8	η Cas A	0 43.0 +57 17	3.60	Go	1.22	115	182±5	143	+ 9±0	4.9
9	η Cas B	.....	7.34	K6	.....	.....	.....	.....	+ 13±2	8.6
10	HR 222	0 43.1 + 4 46	5.86	K2	1.37	147	148±6	134	− 13±1	6.7
11	vMaanen 2	0 43.9 + 4 55	12.4	wG	3.00	155	243±6	.....	(+238)	14.3
12	−31°325	0 48.1 −30 54	7.17	K3	0.62	86	107±9	84	.....	7.3
13	+70°68b	0 55.1 +71 09	9.9	M3	1.78	102	109±5	140	0±5†	10.1
14	+61°195	0 56.3 +61 48	9.5	M1+	0.74	82	.....	120	− 6±4†	*9.9*
15	Wolf 47	0 57.0 +61 50	13.7	M7	0.82	80	.....	140	.....	*14.4*
16	μ Cas	1 01.6 +54 26	5.19	G5	3.77	115	133±5	105	− 97±0	5.8
17	−68°41	1 06.7 −68 00	*11.4*	k	0.71	33	111±10	.....	.....	(11.6)
18	p Eri A	1 36.0 −56 42	6.03	K2*	0.27	85	150±5	.....	.....	6.9
19	p Eri B	.....	6.07	K2*	.....	.....	.....	.....	.....	7.0
20	107 Psc	1 37.1 +19 47	5.37	Ko	0.73	204	132±6	130	− 33±0	6.0
21	τ Cet	1 39.4 −16 28	3.66	G5	1.92	297	298±6	210	− 16±0	6.0
22	HR 511	1 40.5 +63 22	5.66	K1	0.64	113	111+5	130	+ 2±1	5.9
23	Ross 555	1 46.8 −11 17	11.2	M4	0.80	135	.....	110	.....	*11.4*
24	Ross 15	1 52.5 +58 14	12.1	M5	0.39	130	.....	110	.....	*12.3*
25	+2°348	2 07.4 + 3 10	10.3:	M2	2.58	223	95±7	95	.....	10.2
26	HR 753 A	2 30.6 + 6 25	6.00	K3	2.32	51	144±5	150	+ 23±0	6.8
27	..... B	.....	11.5	M6	.....	.....	.....	.....	.....	12.3
28	Ross 556	2 38.4 +25 06	10.5	M4	0.90	112	.....	150	.....	*11.4*
29	HR 857	2 47.7 −13 11	6.10	K2:	0.43	113	134±10	120:	+ 28±3†	6.7
30	κ Cet	3 14.1 + 3 00	5.07	G4	0.28	70	106±5	100	+ 19±0	5.2
31	ξ² Ret	3 16.0 −62 53	5.19	G3*	1.48	64	105±8	.....	+ 12±0	5.3
32	ξ¹ Ret	.....	5.51	G4*	.....	.....	.....	.....	+ 12±1	5.6
33	82 Eri	3 15.9 −43 27	4.29	G5	3.15	76	159±7	160	+ 87±0	5.3
34	ε Eri	3 28.2 − 9 48	3.75	K2	0.98	271	303±6	350	+ 15±0	6.2
35	−45°1184	3 29.6 −45 03	11.0:	M4	0.35	294	83±11	120:	.....	10.6:
36	−48°1011	3 31.9 −48 46	9.3	*K5*	0.50	51	107±12	.....	.....	9.4
37	δ Eri	3 38.5 −10 06	3.63	Ko	0.75	353	110±4	.....	− 6±0	3.8
38	−1°565 A	3 52.4 − 1 27	8.6	K4	0.24	229	101±10	58	.....	8.6
39	..... B	.....	12.0	M3+	.....	.....	.....	.....	.....	12.0
40	Wolf 1322	3 53.8 +25 49	12.2	M5	0.80	94	.....	95	.....	*12.1*
41	40 Eri A	4 10.7 − 7 49	4.52	K1	4.08	213	202±3	220	− 42±0	6.0
42	..... B	.....	9.62	wA	.....	.....	.....	.....	.....	11.1
43	 C	.....	11.1	M6	.....	.....	.....	.....	.....	12.6
44	Ross 594	4 23.6 +39 39	13.7	M6	0.53	180	.....	100	.....	*13.7*
45	+18°683	4 37.0 +18 47	9.8	M2+	1.25	149	104±6	130	.....	9.9
46	π^3 Ori	4 44.4 + 6 47	3.32	F6	0.47	88	128±5	130	+ 25±0	3.9
47	Wolf 1539	4 46.7 + 6 19	11.8	M5	0.32	152	.....	115	.....	*12.1*
48	HR 1614	4 55.9 − 5 52	6.38	K4	1.22	153	107±4	*140*	+ 24±1	6.5
49	−45°1841	5 07.7 −44 59	8.8	Mo	8.72	131	262±6	.....	+242±1	10.9
50	Ross 41	5 22.6 + 9 35	12.5	M5	0.89	192	108±5	91	.....	12.7
51	−3°1123	5 26.4 − 3 42	8.1	M1	2.24	160	166±4	200	+ 11±1	9.2
52	Ross 42	5 26.7 + 9 45	11.4	M6	0.30	243	.....	250	.....	13.4
53	HR 1925 A	5 33.2 +53 26	6.30	K2	0.52	179	97±5	100	+ 1±1	6.2
54	..... B	.....	9.8	M1	.....	.....	.....	.....	.....	9.7
55	Ross 47	5 36.4 +12 29	11.7	M5+	2.54	127	166±8	170	.....	12.8
56	Wolf 237	5 39.5 +44 06	12.4	M5	0.67	235	.....	100	.....	12.5
57	γ Lep A	5 40.3 −22 29	3.83	F6	0.47	219	122±4	115	− 10±0	4.3
58	γ Lep B	.....	6.30	K3	.....	.....	.....	.....	− 10±1	6.7
59	χ^1 Ori	5 48.5 +20 15	4.52	Go	0.20	245	104±6	100	− 14±0	4.6

TABLE 1—*Continued*

No.	Name	α (1900) δ	$m(v)$	Sp	μ	θ	$p(t)$	$p(Sp)$	V_r	$M(v)$
60...	AC 82°1111	5^h49^m1 +82°08′	10.1	M2+	1″.30	5°	108±8	115	− 21±2†	10.3
61...	Ross 79	6 05.4 +10 21	10.4	M3+	0.93	174	.....	130	.....	*11.0*
62...	−21°1377	6 06.4 −21 49	8.2	Mo	0.72	191	183±6	150	.....	9.5
63...	α Men	6 13.2 −74 43	5.12	G9*	0.25	151	118±10	....	+ 35±0	5.3
64...	Ross 417	6 14.5 − 6 36	12.8	M5+	0.67	187	.....	100	.....	*12.8*
65...	Ross 64	6 18.6 +23 30	13.6	M6	0.49	128	117±8	110	.....	13.9
66...	Ross 614	6 24.3 − 2 44	11.3	M6+	1.01	135	260±5	*360*	.....	13.4
67...	+17°1320	6 31.5 +17 38	9.5	Mo	0.86	293	100±5	83	− 59±2	9.5
68...	α CMa A	6 40.7 −16 35	− 1.52	A1	1.32	204	376±3	360:	− 8±0	1.4
69...	..... B	....	8.54	wA5	.....	.....	.....	....	(+12)	11.4
70...	−5°1844	6 47.4 − 5 03	6.60	K3	0.54	270	95±7	110	− 10±2	6.5
71...	Wolf 294	6 48.4 +33 24	9.9	M3	0.86	240	161±9	140	.....	10.9
72...	−44°3045	6 54.9 −44 09	10.8	M5	1.13	264	.....	*170*	.....	*12.3*
73...	Ross 986	7 03.3 +38 43	12.0	M5	1.12	208	.....	130	.....	*12.5*
74...	+5°1668	7 22.0 + 5 32	10.0	M4+	3.75	171	262±6	240	+ 22±2†	12.1
75...	+36°1638	7 25.4 +36 26	10.8	M4	0.41	224	.....	130	.....	*11.4*
76...	Ross 989	....	12.2	M5+	.....	.....	.....	....	.....	*12.8*
77...	α CMi A	7 34.1 + 5 29	0.53	F4	1.25	214	291±4	400	− 3±0	2.8
78...	..... B	....	10.8	.....	.....	.....	.....	....	.....	13.1
79...	L 745–46	7 35.8 −17 10	13.1	wF	1.29	117	177±14	....	.....	14.3
80...	β Gem	7 39.2 +28 16	1.34	G8	0.62	265	100±10	....	+ 3±0	1.3
81...	Ross 882	7 39.4 + 3 48	11.6	M6	0.64	218	.....	230	.....	*13.4*
82...	L 97–12	7 52.6 −67 30	14.5	f–g	2.05	135	170±30	....	.....	15.6
83...	Ross 619	8 06.5 + 9 11	12.5	M6	5.40	167	154±7	140	.....	13.4
84...	L 829–19 A	8 49.2 −12 45	12.4	M6	0.62	144	.....	130	.....	*12.9*
85...	..... B	....	12.7	.....	.....	.....	.....	....	.....	*13.2*
86...	Ross 686	8 55.6 + 5 38	12.1	M5	0.47	221	.....	100	.....	*12.1*
87...	Ross 687	....	12.5	M5	.....	.....	.....	....	.....	*12.5*
88...	+53°1320	9 07.6 +53 07	7.90	K7	1.68	248	162±3	130	+ 10±1	8.9
89...	+53°1321	....	8.01	K9	.....	.....	.....	....	+ 11±1	9.0
90...	−59°1362	9 19.2 −59 52	10.0	*Mo*	0.87	282	120±11	....	.....	10.4
91...	Ross 439	9 24.0 − 6.55	11.6	M4+	0.71	191	.....	115	.....	*11.9*
92...	−12°2918	9 26.5 −13 03	10.2	M4	0.75	92	79±12	170	.....	*11.*
93...	11 LMi A	9 29.7 +36 16	5.48	G8	0.75	250	95±5	91	+ 13±0	5.4
94...	..... B	....	13.0	.....	.....	.....	.....	....	.....	12.9
95...	−45°5378	9 40.7 −45 17	10.6	M4	0.75	218	103±11	140	.....	10.7
96...	−45°5627S	9 54.6 −45 57	11.6:	M4+	0.69	135	.....	115:	.....	*11.9*
97...	+50°1725	10 05.3 +49 58	6.54	K8	1.45	249	220±8	260	− 27±1	8.2
98...	+20°2465	10 14.2 +20 22	9.46	M5	0.49	265	193±8	330	+ 9±2	10.9
99...	+1°2447	10 23.9 + 1 21	9.6	M2	0.98	219	130±7	130	− 3±5†	10.2
100...	L 1113–55	10 30.9 + 5 38	12.2	M6	0.68	280	.....	170	.....	*13.4*
101...	Wolf 358	10 45.8 + 7 22	11.5	M5	1.21	224	136±7	150	.....	12.2
102...	Wolf 359	10 51.6 + 7 36	13.5	M8	4.76	234	403±10	360:	− 90	16.5
103...	Ross 104	10 54.8 +23 22	10.3	M3	0.45	238	.....	120	.....	*10.7*
104...	+36°2147	10 57.9 +36 38	7.47	M2+	4.78	187	388±6	380	− 87±2	10.4
105...	+44°2051 A	11 00.5 +44 02	8.7	Mo+	4.53	282	174±8	140	+ 64±4	9.9
106...	..... B	....	14.8	M8	.....	.....	.....	....	.....	16.0
107...	ξ UMa A	11 12.9 +32 06	4.41	F9	0.73	216	138±6	90	− 16±0	5.1
108...	..... B	....	4.87	Go	.....	.....	.....	....	− 16±0	5.6
109...	+66°717	11 14.8 +66 23	9.3	M1	2.95	273	120±5	115	+ 47±2	9.7
110...	61 UMa	11 35.8 +34 46	5.34	G4	0.39	182	109±9	90	− 5±0	5.5
111...	L 1405–28	11 36.9 +27 17	10.9	M3	1.06	138	.....	95	.....	*10.8*
112...	I(UC37)	11 40.5 −64 17	*12.5*	b	2.68	97	193	....	.....	(13.9)
113...	AC 79°3888	11 41.3 +79 14	11.0	M4+	0.87	57	201±10	150	.....	12.5
114...	Ross 128	11 42.6 + 1 23	11.0	M5+	1.40	151	.....	230	.....	*12.8*
115...	β Vir	11 45.5 + 2 20	3.73	F8	0.79	110	101±7	120	+ 5±0	3.8
116...	HR 4550	11 47.2 +38 26	6.42	G6	7.04	145	108±4	....	− 98±1	6.6
117...	L 901–10	11 48.2 − 6 49	11.9	M4+	0.54	196	.....	100	.....	*11.9*
118...	−26°8883	11 53.0 −27 08	7.00	K4	1.25	240	98±11	110	.....	7.0

TABLE 1—*Continued*

No.	Name	α (1900) δ	$m(v)$	Sp	μ	θ	$p(t)$	$p(Sp)$	V_r	$M(v)$
119	Ross 689	12^h00^m6 +70°06′	13.1	M6	0″.59	258°	.....	110	.....	*13.3*
120	Ross 690	12 18.4 +64 35	11.2	M4	0.73	305	.....	110	.....	*11.4*
121	Ross 695	12 19.6 −17 38	11.7	M4+	2.53	154	.....	110	.....	*11.9*
122	L 68–28	12 22.8 −70 56	*15.7*	.....	1.17	339	152±47	....	.....	(16.6)
123	L 68–29	....	*17.7*	.....	.....	.....	.....	....	.....	(18.6)
124	Wolf 414	12 23.9 + 8 59	11.8	M5	0.70	232	.....	115	.....	*12.1*
125	Wolf 424 A	12 28.4 + 9 34	12.7	M7	1.84	278	225±7	250:	.....	14.5
126	B	....	12.7		.....	.....	.....	....	.....	14.5
127	β CVn	12 29.0 +41 54	4.32	Go	0.76	292	108±6	110	+ 7±0	4.5
128	Wolf 427	12 30.0 +10 23	11.1	M4	0.56	236	.....	115	.....	*11.4*
129	−51°6859	12 32.5 −51 27	*11.2*	.....	1.02	271	117±11	....	.....	(11.5)
130	Wolf 437	12 43.0 +10 18	11.13	M4	1.06	243	106±8	130	.....	1.3
131	AC 66°3955	12 45.1 +66 40	10.5	M3	0.44	259	117±9	110	−18±4†	10.8
132	+0°2989	12 45.6 − 0 13	8.50	K8	0.40	186	98±7	105	.....	8.5
133	Wolf 461	12 55.6 + 6 13	13.2	M6	1.01	290	.....	120	.....	*13.6*
134	+13°2618	12 55.9 +12 54	9.9	M1	0.70	268	.....	95	.....	*9.8*
135	β Com	13 07.2 +28 23	4.30	Go	1.19	318	121±6	110	+ 6±0	4.7
136	61 Vir	13 13.2 −17 45	4.83	G5	1.52	225	116±6	125	− 8±0	5.2
137	Ross 486 A	13 23.2 − 1 50	11.4	M4+	0.51	160	.....	100:	.....	*11.4*
138	B	....	14.2	M6:	.....	.....	.....	....	.....	*14.2*
139	+11°2576	13 24.9 +10 55	9.2	M1	1.51	137	123±10	115	+ 12±2†	9.6
140	Wolf 489	13 31.8 + 4 13	14.5	Con	3.94	252	130±9	....	.....	15.1
141	+15°2620	13 40.7 +15 26	8.58	M1+	2.30	129	191±8	180	+ 15±1	10.0
142	η Boo	13 49.9 +18 54	2.85	F9	0.37	190	116±11	....	0±0	3.2
143	Ross 845	14 07.8 −11 33	13.5	M6	0.79	236	.....	95	.....	*13.4*
144	−58°5467	14 12.0 −58 54	6.7	*Ko*	0.96	209	114±9	....	.....	7.0
145	Ross 848	14 14.8 − 9 09	12.7	M5+	1.13	213	.....	105	.....	*12.8*
146	Prox. Cen	14 22.8 −62 15	11.3	m	3.85	282	762±5	....	.....	15.7
147	−11°3759	14 28.9 −12 06	11.4	M4	0.69	334	.....	100	.....	*11.4*
148	α Cen A	14 32.8 −60 25	0.33	G4*	3.67	281	756±7	....	−22 ±0	4.7
149	B	....	1.70	K1*	.....	.....	.....	....	.....	6.1
150	ξ Boo A	14 46.8 +19 31	4.81	G6	0.17	129	147±6	150	+ 4±0	5.7
151	B	....	6.77	K6	.....	.....	.....	....	+ 6±2	7.6
152	HR 5568 A	14 51.6 −20 58	5.90	K4	1.99	149	172±4	180	+ 20±0	7.1
153	B	....	8.08	Mo+	.....	.....	.....	....	+ 25±4	9.2
154	−7°4003	15 14.2 − 7 21	10.6	M4	1.25	266	151±5	140	− 30±2	11.5
155	−40°9712	15 25.7 −40 54	10.2	M4:	1.57	229	166±5	170:	.....	11.3
156	λ Ser	15 41.6 + 7 40	4.45	G1	0.24	252	95±5	110	− 66±0	4.3
157	Gron. 20	16 21.1 +48 36	10.3	M2+	1.23	111	132±14	105	.....	10.9
158	−12°4523	16 24.7 −12 25	9.8	M4	1.17	186	255±5	210	.....	11.8
159	ζ Her A	16 37.5 +31 47	3.06	Go	0.61	309	113±5	....	− 71±0	3.3
160	B	....	5.86	.....	.....	.....	.....	....	.....	6.1
161	+33°2777	16 41.4 +33 41	8.21	K6	0.37	352	113±6	91	− 31±2	8.5
162	−8°4352 A	16 50.1 − 8 09	9.90	M3+	1.19	222	148±4	150	+ 11±2	10.8
163	B	....	10.00		.....	.....	.....	....	.....	10.8
164	C	....	11.5	M5+	.....	.....	.....	....	.....	12.4
165	+45°2505 A	17 09.2 +45 50	10.04	M3+	1.59	171	143±6	140	− 19±3	10.8
166	B	....	10.34		.....	.....	.....	....	.....	11.1
167	36 Oph A	17 09.2 −26 27	5.17	K2	1.24	203	179±5	180	− 1±0	6.4
168	B	....	5.20	K1	.....	.....	.....	....	− 1±0	6.5
169	C	....	6.53	K6	.....	.....	.....	....	− 10±1	7.8
170	HR 6416 A	17 11.5 −46 32	5.62	Ko	1.00	78	132±6	120	+ 19	6.2
171	B	....	8.8	Mo+	.....	.....	.....	....	.....	9.4
172	HR 6426 A	17 12.1 −34 53	6.28	K3	1.18	99	147±6	120	0±1	7.1
173	B	....	7.0	K4	.....	.....	.....	....	.....	7.8
174	C	....	10.16	M2+	.....	.....	.....	....	.....	11.0
175	Ross 868	17 16.0 +26 42	11.2	M5	0.47	342	.....	130	.....	*11.8*
176	Ross 867	....	13.4	M6	.....	.....	.....	....	.....	*14.0*
177	+2°3312	17 20.8 + 2 14	7.53	K7	1.33	206	124±5	140	− 29±1	8.0

TABLE 1—*Continued*

No.	Name	α (1900) δ	$m(v)$	Sp	μ	θ	$p(t)$	$p(Sp)$	V_r	$M(v)$
178	−46°11540	17^h21^m1 −46°47′	9.7	M3+	1″.07	148°	225±6	180	.....	11.5
179	−44°11909	17 29.8 −44 14	10.9	M5	1.15	217	208±6	190	.....	12.5
180	Slocum An.	17 33.4 +18 37	9.8	Mo+	1.39	43	113±9	83	− 10±1	10.1
181	+68°946	17 37.0 +68 26	9.13	M3+	1.31	196	213±5	240	− 17±3	10.8
182	I(UC 48)	17 38.2 −57 14	*12.7*	.....	1.72	219	158±7	....	.....	(13.7)
183	+43°2796	17 40.9 +43 26	10.41	M2	0.61	181	102±7	91	.....	10.4
184	μ Her A	17 42.5 +27 47	3.47	G7	0.81	203	109±6	....	− 16±0	3.7
185	..... B	....	10.36	M4	.....	.....	.....	150	.....	10.6
186	 C	....	10.66		.....	.....	.....	.....	.....	10.8
187	+4°3561	17 52.9 + 4 25	9.46	M5+	10.25	356	543±3	440	−110±4	13.1
188	−3°4233	17 59.8 − 3 02	9.2	M1	0.62	112	131±9	120	.....	9.8
189	70 Oph A	18 00.4 + 2 31	4.19	K1	1.13	167	196±4	230	− 7±0	5.7
190	..... B	....	5.87	K5	.....	.....	.....	.....	− 7±0	7.3
191	HR 6806	18 06.3 +38 27	6.39	K2	0.57	213	98±7	105	− 18±2	6.4
192	L 1064–75	18 11.3 + 1 29	12.4	M5	0.73	213	.....	95	.....	*12.3*
193	χ Dra	18 22.9 +72 41	3.62	F8	0.63	125	122±7	120	+ 33±0	4.3
194	α Lyr	18 33.6 +38 41	0.17	Ao	0.34	35	121±4	140:	− 14±0	0.6
195	+59°1915 A	18 41.7 +59 29	8.92	M3+	2.28	324	282±4	240	0±2	11.2
196	..... B	....	9.73	M4	.....	.....	.....	.....	+ 7±3	12.0
197	Ross 154	18 43.6 −23 56	10.5	M5+	0.67	106	350±6	290	.....	13.2
198	Ross 730	19 02.9 +20 44	10.7	M1+	0.57	234	115±8	66	.....	11.0
199	Ross 731	....	10.7	M1+	.....	.....	.....	.....	.....	11.0
200	17 Lyrae C	19 03.8 +32 21	11.77	M5	1.66	49	127±4	120	.....	12.3
201	..... D	....	12.07		.....	.....	.....	.....	.....	12.6
202	Wolf 1062	19 07.0 + 2 44	11.3	M4	1.95	103	105±7	105	.....	11.4
203	+4°4048	19 12.1 + 5 02	9.2	M3	1.46	204	170±4	200	.....	10.4
204	L 347–14	19 13.4 −45 42	*13.4*	m	2.94	168	182±9	....	.....	(14.7)
205	σ Dra	19 32.6 +69 29	4.73	G9	1.84	162	181±4	170	+ 27±0	6.0
206	Ross 165 A	19 41.7 +26 55	12.7	M5+	1.34	183	116±11	110	.....	13.0
207	..... B	....	13.7	.....	.....	.....	.....	.....	.....	14.0
208	α Aql	19 45.9 + 8 36	0.91	A5	0.66	54	208±5	170	− 26±2	2.5
209	δ Pav	19 58.9 −66 26	3.67	G7*	1.65	134	174±8	....	− 22±0	4.9
210	HR 7703 A	20 04.6 −36 21	5.24	K2	1.63	164	177±9	170	−131±0	6.5
211	..... B	....	11.5	M5	.....	.....	.....	.....	.....	12.7
212	−45°13677	20 06.7 −45 28	8.4	Mo	0.80	102	145±9	140	.....	9.2
213	HR 7722	20 09.1 −27 20	5.56	K1	1.25	98	110±6	130	− 56±1	5.8
214	AC 65°6955	20 29.1 +65 05	10.56	M3+	0.53	58	136±8	120	.....	11.2
215	−32°16135 A	20 35.6 −32 47	10.9	M5	0.45	140	.....	200	+ 5	*12.4*
216	..... B	....	11.1	M5+	.....	.....	.....	.....	.....	*12.6*
217	−31°17815	20 39.0 −31 42	8.7	M1+	0.45	140	.....	170	+ 10.	*9.9*
218	Wolf 1084	20 40.5 +54 57	15.3	M7+	1.87	21	.....	110:	.....	*15.5*
219	Furuhj. 53	20 41.5 +44 08	10.6	M3	0.50	58	.....	105	.....	*10.7*
220	+61°2068	20 51.3 +61 48	8.7	Mo+	0.77	180	138±5	140	− 9±2	9.4
221	Furuhj. 54 A	20 56.2 +39 41	10.26	M2	0.67	113	97±8	95	− 57±3	10.2
222	..... B	....	12.3	.....	.....	.....	.....	.....	.....	12.2
223	61 Cyg A	21 02.4 +38 15	5.35	K3	5.20	52	296±3	200	− 65±0	7.7
224	..... B	....	6.05	K5	.....	.....	.....	....	− 63±1	8.4
225	−39°14192	21 11.4 −39 15	6.65	Mo	3.47	251	257±7	310	+ 22±2	8.7
226	γ Pav	21 18.2 −65 49	4.35	F8*	0.80	6	124±9	....	− 30±0	4.8
227	Ross 775	21 24.8 +17 12	10.4	M4+	1.10	69	150±10	200	.....	11.3
228	Wolf 922	21 25.8 −10 14	11.5	M4+:	1.19	93	161±10	120:	.....	12.5
229	−49°13515	21 26.9 −49 26	8.9	M3	0.82	185	207±10	230	.....	10.5
230	−60°7528	21 52.3 −60 13	*11.4*	*K:*	0.87	96	97±9	....	.....	(11.3)
231	ε Ind	21 55.8 −57 12	4.70	K5*	4.69	123	288±6	....	− 40±0	7.0
232	Ross 265	21 57.0 +16 07	10.7	M3	0.36	67	.....	100	.....	*10.7*
233	+0°4810	21 57.1 + 0 56	9.24	Mo+	0.55	248	.....	110	+ 20±6†	*9.6*
234	−5°5715	22 04.4 − 5 08	10.2	M4	1.03	91	.....	170	.....	*11.4*
235	Wolf 1561 A	22 12.1 − 9 18	13.5	M6	0.55	240	.....	100	.....	*13.5*
236	..... B	....	14.5	M7	.....	.....	.....	.....	.....	*14.5*

TABLE 1—*Continued*

No.	Name	α (1900) δ	$m(v)$	Sp	μ	θ	$p(t)$	$p(Sp)$	V_r	$M(v)$
237	+56°2783 A	22^h24^m4 +57°12′	9.87	M4	0″.90	245°	256±4	220	− 24±2	11.9
238	B	....	11.3	M6	.....	.....	.....	.....	.....	13.3
239	I(UC 53)	22 31.5 −65 54	*12.8*	.....	0.82	102	96±10	....	.....	(12.7)
240	L 789–6	22 33.0 −15 52	12.3	M6+:	3.27	46	328±11	230:	.....	14.9
241	+43°4305	22 42.5 +43 49	10.25	M5	0.85	237	207±7	250	+ 2±2	11.8
242	−15°6290	22 47.9 −14 47	10.27	M5	1.11	123	220±11	250	.....	12.0
243	HR 8721	22 50.8 −32 06	6.33	K3	0.36	117	121±10	135	.....	6.7
244	+15°4733	22 51.8 +16 02	8.6	M2	1.10	255	161±7	210	− 19±1†	9.6
245	α PsA	22 52.1 −30 09	1.37	A3	0.37	117	135±8	120	+ 6±0	2.0
246	−23°17699	22 55.0 −23 04	8.11	K0	0.92	274	125±7	140	+ 16±2	8.6
247	−36°15693	22 59.4 −36 26	7.23	M0+	6.90	79	278±6	270	+ 10±1	9.4
248	HR 8832	23 08.5 +56 37	5.55	K3	2.09	82	146±6	180	− 20±1	6.4
249	−73°2209	23 33.7 −73 15	7.36	*K0*	0.74	170	135±10	....	.....	8.0
250	Ross 248	23 37.0 +43 39	12.2	M6+	1.82	176	314±7	240:	.....	14.7
251	+1°4774	23 44.0 + 1 52	9.10	M2	1.37	134	167±6	170	− 64±3	10.2
252	85 Peg A	23 56.9 +26 33	5.91	G5	1.30	140	95±5	76	− 36±1	5.8
253	B	....	8.7	.....	.....	.....	.....	.....	.....	8.6
254	−37°15492	23 59.5 −37 51	8.57	M3	6.11	112	222±7	260	+ 24±2	10.3

NOTES TO TABLE 1

Double-star notes refer to the discoverer of the companion, to ADS or SDS, the distance and the position angle, or the orbital elements if the latter are known.

1, 2. OΣ, no number = ADS 246; A = Groombridge 34; 38″, 53°–58°.

5, 6. Vyssotsky; ADS 440 = ADS 433; 3″.0, 98°–122°.

8, 9. Σ60 = ADS 671; $P = 526^a$, $a = 12''.53$, $e = 0.53$; masses 0.72 and 0.46.

13. Found to have common proper motion with the binary 5, 6, at Greenwich (*Astr. Cat.*, **5**, 146, 1929) in spite of large angular distance (5°.1 = 18500″); the near-equality of the p values, as well as Popper's V_r values, enhances the probability of nearly parallel space motions. But, since the velocity of escape is only 0.1 km/sec, the physical connection is still uncertain, and the star has not been included in the counts. $D = 0.84$ parsecs; $\log D = 5.24$ (in astronomical units).

14, 15. Probably common proper motion; $d = 294''$.

18, 19. Dunlop 5, SDS; orbit indeterminate (Finsen, *Union Circ.*, No. 100).

26, 27. Van Maanen; 164″, 109°.

31, 32. Meridian catalogues; $d = 309''.8$ (G.C.).

38, 39. β 543 = ADS 2894; 11′, 32°–26°; p (*dyn.*) = 0″.095 (Russell and Moore).

41, 42. Σ 518 AB = ADS 3093; 83″, 105°.

42, 43. Σ 518 BC; $P = 248^a$, $a = 6''.89$, $e = 0.40$; masses 0.45 and 0.20.

48. Probably spectroscopic binary (*Lick Obs. Pub.*, Vol. 18); confirmed by high value of $p(Sp)$.

49. Kapteyn's star; nearest subdwarf.

53, 54. Burnham (βPM); 97″, 70°.

57, 58. S 498 = ADS 4334; 95″, 350°.

66. Reuyl found this star to have a "dark" companion.

68, 69. A. C. Clark 1 = ADS 5423; $P = 49.94^a$, $a = 7''.62$, $e = 0.59$; masses 2.35 and 0.98. Reality of duplicity of B still doubtful; cf. *Observatory*, **52**, 22–25, 1929.

72. Double ($d = 1''.5$) according to Luyten (*Pub. Obs. Minnesota*, **3**, 1941).

75, 76. Ross; 38″.6, 354°.

77, 78. Schaeberle 1 = ADS 6251; $P = 40.23^a$, $a = 4''.26$, $e = 0.31$; masses 1.48 and 0.46.

82. Parallax and color class by Luyten (*Harvard Anno. Card*, No. 602, 1941).

84, 85. Stearns 9 (*A.J.*, No. 1101; cf. also Luyten, *Harvard Bull.*, No. 906); $d = 2''$.

86, 87. Ross; 29″.2, 115°.

88, 89. Σ1321 = ADS 7251; 19″, 48°–75°.

92. Poor agreement between $p(Sp)$ and $p(t)$; close binary?

93, 94. Hu 1128 = ADS 7441; 6″–2″, 35°–26°.

103. Possibly close binary.

105, 106. Van Maanen; 28″.1, 134°. B variable (van Maanen, *Ap. J.*, **91**, 505, 1940).

107, 108. Σ1523 = ADS 8119; $P = 59.86^a$, $a = 2''.536$, $e = 0.41$; combined mass 1.7 (presumably A = 1.0 and B = 0.7, roughly). A was found to be a spectroscopic binary by W. H. Wright; $P = 669^d$. Van

den Bos found $a_1 = 0''.051$, $e = 0.53$. *B* is also a spectroscopic binary (Lick); $P = 3^d.98$. The mass function of *Bb* is excessively small, giving for *b*'s mass 0.03 as lower limit.

112. Color class by Luyten (*Harvard Ann. Card*, No. 602, 1941), who also quotes a parallax derived at the Cape.

122, 123. Luyten, $d = 15''$; rough parallax by Luyten (*Harvard Bull.*, No. 910).

125, 126. Reuyl, $d = 1''$; rapid motion. Unpublished Yerkes parallax incorporated by courtesy of Dr. Titus.

137, 138. Kuiper; $d = 10''$.

140. Color class about g8.

142. Spectroscopic binary (J. H. Moore); $P = 492^d$, $e = 0.23$. Orbit should be measurable photographically ($a_1 \geqslant 0''.04$).

146, 148. Innes; $d = 2^\circ.2 = 7849''$.

148, 149. Richaud, SDS; $P = 80.09^a$, $a = 17''.665$, $e = 0.52$; masses 1.10 and 0.89.

150, 151. Σ1888 = ADS 9413; $P = 150^a$, $a = 4''.88$, $e = 0.51$; masses 0.88 and 0.75.

152, 153. Herschel; ADS 9446; 10″–20″, 251°–300°.

159, 160. Σ2084 = ADS 10157; $P = 34.42^a$, $a = 1''.35$, $e = 0.46$; masses 0.89 and 0.55.

162, 163. Kuiper; $P = 1.72^a$, $a = 0''.19$, $e = 0.04$; average mass 0.36. The most rapid visual binary known.

162, 164. Wolf; $d = 72''$.

165, 166. Kuiper; unpublished orbit by Van Biesbroeck: $P = 13.37^a$, $a = 0''.74$, $e = 0.75$; average mass 0.39.

167, 168. Sh 243 = ADS 10417; 4″, 227°–178°. Remarkably small $p(dyn.)$, $0''.045$, indicating high orbital inclination.

167, 169. Meridian catalogues; $732''.1$, $74^\circ.2$. Difference in V_r unexplained.

170, 171. Brs 13, SDS; orbit indeterminate (Finsen).

172, 173. Mlb. 4, SDS; $P = 42.2^a$, $a = 1''.83$, $e = 0.55$. Total mass 1.1.

172, 174. h 4935, SDS; 31″, 134°.

175, 176. Ross; $15''.9$, 268°.

184, 185. Σ2220 = ADS 10786; 30″–33″, 241°–246°.

185, 186. A. C. 7 = ADS 10786; $P = 43.02^a$, $a = 1''.287$, $e = 0.18$; average mass 0.44.

187. Barnard's star; largest proper motion known.

189, 190. Σ2272 = ADS 11046; $P = 87.85^a$, $a = 4''.56$, $e = 0.50$; masses 0.90 and 0.73.

193. Spectroscopic binary (W. H. Wright); $P = 281^d$, $e = 0.42$. Alden found $a_1 = 0''.056$.

195, 196. Σ2398 = ADS 11632; 12″–17″, 134°–157°.

198, 199. Ross; $114''.7$, 111°. Either $p(t)$ is too large, or stars are below main sequence.

200, 201. Kuiper; $d < 1/3''$, rapid motion; unpublished Yerkes parallax included, courtesy of Dr. Titus.

206, 207. Duplicity suspected by van Maanen, confirmed by Kuiper (*Ap. J.*, **84**, 360, 1936); $0''.5$–$0''.6$, 145°–191° (seven-year interval).

210, 211. h 5173, SDS; $d = 8''$.

215, 216. Duplicity found by Adams, Humason, and Joy (*Pub. A.S.P.*, **39**, 367, 1927); 3″, 240°.

215, 217. Luyten found common proper motion, in spite of large distance ($1^\circ.3 = 4700''$). Confirmed by Mount Wilson radial velocities and spectroscopic parallaxes; again confirmed here. All three components have strong emission lines, and p may be somewhat less than found here (cf. text, sec. 3).

221, 222. Kuiper; 1″, 82°–112° (seven years).

223, 224. Σ2758 = ADS 14636; 15″–26″, 90°–138°.

235, 236. Kuiper (*Ap. J.*, **92**, 126, 1940); $d = 8''$.

237, 238. Burnham discovered this important pair but called it Krüger 60 AB after a wide, faint optical pair without further interest. $P = 44.52^a$, $a = 2''.36$, $e = 0.41$; masses 0.25 and 0.14.

243, 245. Luyten (*A.J.*, **47**, 115, 1938) pointed out that these stars have nearly common motion and parallax; $d = 1^\circ.96 = 7060''$. But measured radial velocities differ somewhat (Popper, unpublished).

252, 253. β 733 = ADS 17175; $P = 26.46^a$, $a = 0''.82$, $e = 0.41$. Included because of $p(t)$, though resulting masses indicate that p is probably well below $0''.095$. Abnormal mass ratio, $A/B = 1$, indicating that *B* may be double.

We have used all ten subdivisions of type K in order to avoid the need of half-tenths; but in class M the accuracy of the classification warrants the use of half-tenths. The M stars were classified by the strength of the red *TiO* band, which gives accurate results (cf. Fig. 1) and makes stars as faint as 18 mag. photographic easily accessible with the 82-inch telescope.

The proper motions are from the *General Catalogue* or, if not included therein, are based on all other published data. For several stars only the original "blink" results

were available; measurement of μ_δ as well as of μ_α in parallax determinations would supply the needed information.

The parallaxes are expressed in units of $0''.001$. The trigonometric results include two unpublished values kindly supplied by Dr. Titus. The spectral parallaxes were computed by supposing the star to be central on the main sequence; their usefulness is apparent from Table 1 (in the computation an extra decimal in the type was carried, the value being usually the mean of two or more independent determinations). However, in case of unresolved binaries they will, of course, be too large.

The radial velocities are mostly those in Moore's catalogue.[7] Dr. Popper has generously made available several unpublished results, usually based on two plates per star; they are designated by a dagger. The dispersion used was 76 A/mm at Hγ. Much valuable work remains to be done in this field. The last column gives the absolute visual magnitude, computed from m and $p(t)$; if p has not yet been measured $p(Sp)$ was used, i.e., it was assumed that the star lies on the main sequence. In the case of binaries the weighted mean of $p(Sp)$ was used, and the components may then deviate somewhat from the main sequence, in the opposite sense. Values of M based on $p(Sp)$ are printed in italics. Parentheses indicate photographic M values.

Many additional details, especially with regard to duplicity, are found in the footnotes to the table.

3. *The Hertzsprung-Russell diagram.*—Figure 1 is based on the columns $M(v)$ and Sp. All spectral types except those printed in italics were used. White dwarfs have been plotted according to their color indices. The open circles correspond to italicized M values and should therefore be disregarded in the study of the scatter across the main sequence. The sun is added at 4.73 G2.[8]

Figure 1 shows one giant (No. 80), two subgiants (Nos. 37 and 184), and two or three "bright dwarfs" (Nos. 159, 142, and 77). (The run of the upper part of the main sequence was determined from a much larger number of stars than are shown in Fig. 1). Below the main sequence we find, first, seven white dwarfs and, further, two or more subdwarfs (Nos. 49, 116, and possibly 198 and 199), none of which is very extreme.

The vertical width of the main sequence is not much over 1 mag., so that the central line represents M with a p.e. not over ± 0.3 mag. The true width must be even less; but it is not zero, because some of the best-determined stars are definitely either somewhat below the central line (Nos. 21, 107, 108, 223, 224) or somewhat above (e.g., No. 98). In this connection it is of interest to mention the following preliminary result: There appears to be a correlation, for a fixed spectral type, between the strength of the emission lines and the deviation from the main sequence, in the sense that stars with stronger emission lines lie higher. In addition, there is an increase of the average strength of the emission lines with advancing type; types later than M6 seem all to have emission. Barnard's star is one of the latest types without pronounced emission. While this correlation rests only on a few dozen stars and needs further study, it seems to show that the emission is caused by certain astrophysical conditions smoothly varying over the Hertzsprung-Russell diagram and not by *mechanical* conditions (such as duplicity), which would inevitably entail an additional parameter (separation), which presumably would be independent of M and Sp. The astrophysical parameters might include, in addition to T and g, the hydrogen content, which, on the basis of evidence supplied by clusters, would be higher for the stars showing emission. A fuller discussion of this problem will be given in another paper.

4. *The luminosity function for the main sequence.*—Figure 2 shows three curves: the full-drawn curve a shows the numbers of main-sequence stars within 10.5 parsecs with $p(t)$ known (components of visual binaries are counted separately); b shows all the main-sequence stars known in that volume, the difference $b-a$ being the numbers added

[7] *Pub. Lick Obs.*, **18**, 1932.

[8] *Ap. J.*, **88**, 438, 1938.

spectroscopically in the writer's survey; while *c* (dashed line) gives a preliminary determination of the luminosity function of main-sequence stars, valid for the same volume of space. Curve *c* is based on a discussion, soon to be published of all data now available for the stars of large proper motion, including *m* and *Sp* observations of about 2000 stars by the writer. The difference *c*−*b* shows how much remains to be discovered even for the nearest stars.

5. *Binary stars.*—While the sample of Table 1 is too small for a detailed study of the frequency of binary stars, some approximate results may nevertheless be obtained. First,

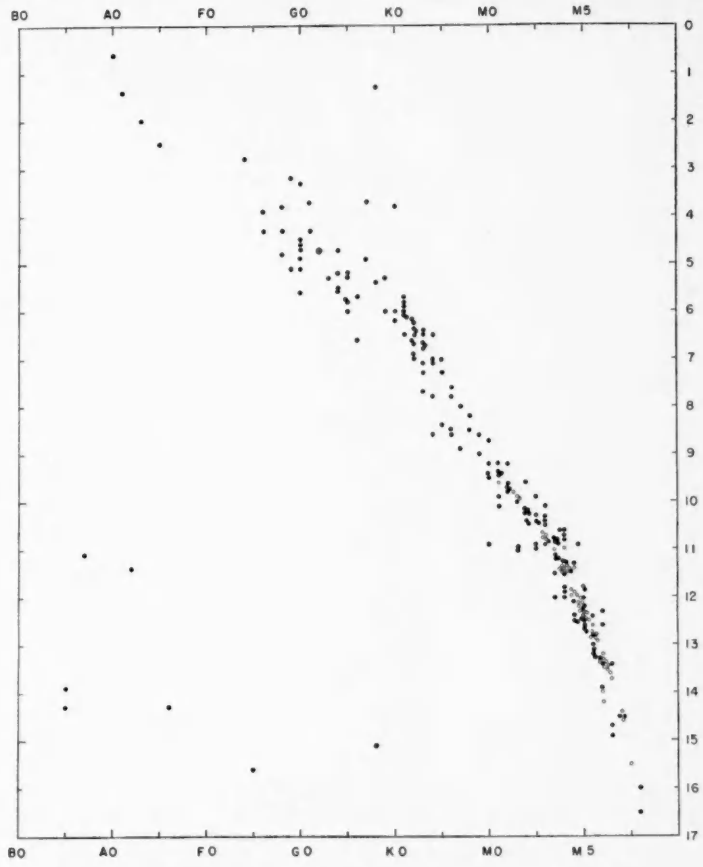

FIG. 1.—Hertzsprung-Russell diagram for the nearest stars

we subdivide the systems by spectral type; in case of duplicity or multiplicity the type of the primary is used. The counted numbers are in Table 2, the sun has been included. The 73 systems of types A–K have 36 known companions (109 components), or 50 per cent known doubles (in this way of counting, a triple counts as two doubles, a quadruple as three). This value is still well below the 80 per cent found several years ago,[9] in a study which took account of the observational-selection factors; the amount of the difference seems not unreasonable.

Whether the M dwarfs have actually a smaller fraction of double stars, as Table 2

[9] *Pub. A.S.P.*, **47**, 139, 1935.

would indicate, or whether the result is wholly due to the faintness of these objects remains as yet an open question.

More significant than a subdivision by spectral type is a subdivision by total mass. For instance, if a binary with two dMo components were replaced by a single star having the combined mass, it would be a star closely resembling the sun. In order to be able to perform a count between limits of total mass we need to know the mass-luminosity relation expressed in terms of $M(v)$. Table 3 gives the relation for the main sequence, based on data compiled earlier.[10]

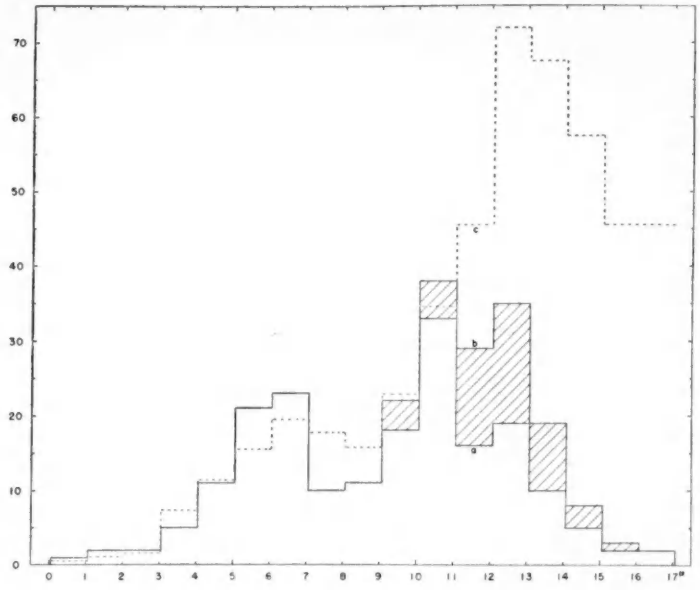

FIG. 2.—Luminosity function for the main sequence

TABLE 2

Type	A, F, G	K	A–K	M	WD	Type	A, F, G	K	A–K	M	WD
Single	24	20	44	99	5	Triple	2	3	5	2	0
Double	12	11	23	22	0	Quadruple	1	0	1	0	0

Table 4 gives the numbers between limits of total mass. The sun is included, but the five white dwarfs of Table 2 are omitted. It now appears that *of the masses larger than the sun more than two-thirds (0.68) are known to have divided up into two or more parts;* for the intervals 1.0–0.5–0.25–0.10 the fractions are, respectively, 0.3, 0.15, and 0.08. The true values must be higher than the minimum values found here, at least if we ignore the white dwarfs. While the latter are not very frequent if we classify stars by $M(v)$, as they account for only 3 per cent of the known near-by stars, they become of considerable prominence if stars are classified by mass; in fact, they are about as frequent as F dwarfs, and their masses are not very different. More data on the trigonometric parallaxes of the known white dwarfs[11] are urgently needed.

[10] *Ap. J.*, **88**, 484, 1938.

[11] Cf. *Pub. A.S.P.*, **53**, 249, 1941.

In addition to the frequency of binaries, their distribution over the various possible separations is of interest. Since these separations vary through a range of 10^7, we shall plot them on a logarithmic scale. If the orbit is known, log a may be derived; because for a visual binary $a = a''/p''$, while in a spectroscopic binary Kepler's third law may be used, together with a sufficiently accurate estimate of the combined mass. But for wide binaries only the apparent separation, d'', taken for a certain standard epoch, and the parallax are known. If $D = d''/p''$, we may ask what correction should be made to

TABLE 3

$M(v)$	Mass	$M(v)$	Mass	$M(v)$	Mass
1.0	2.8	5.0	0.97	11.0	0.33
1.5	2.3	6.0	0.83	12.0	0.25
2.0	1.9	7.0	0.71	13.0	0.17
2.5	1.6	8.0	0.60	14.0	0.12:
3.0	1.4	9.0	0.51	15.0	0.09:
4.0	1.15	10.0	0.42		

TABLE 4

Mass	1.0	0.5	0.25	0.10		Mass	1.0	0.5	0.25	0.10	
Single	12	33	61	33	4	Triple	5	2	0	0	0
Double	20	11	11	3	0	Quadruple	1	0	0	0	0

log D in order that a correct average value of log a may be found. We shall use an earlier result,[12]

$$\log a = \log D + 0.11 \pm 0.14 \text{ (p.e.)}.$$

Because the individual values of log a, or log $D + 0.11$, are of interest, they are listed in Table 5. The standard epoch was taken to be 1940. Three possible binaries (Nos. 48, 92, and 103) were counted somewhat arbitrarily as two binaries with log $a = +\frac{1}{2}$ and $-\frac{1}{2}$. They were included in Figure 3 together with the data of Table 5.

The broken curves of Figure 3 show the counted numbers grouped in two different ways; the smooth curve (open circles) gives the best representation. The curve is roughly Gaussian with a maximum near log $a = 1.7$. In an earlier investigation,[13] which took account of observational selection, a similar result was found, except that the maximum was at log $a = 1.3$. The two results would seem to be quite consistent, in view of the fact that the higher value found here is distorted because of very incomplete discoveries of spectroscopic and close visual binaries. A larger volume of space than that considered here would be required for a proper statistical treatment, eliminating selection factors; even then only rough results could be expected, pending the completion of surveys now in progress.

[12] *Pub. A.S.P.*, **47**, 127, 1935. In the text of this article the words "harmonic mean" should be replaced by "geometric mean."

[13] *Ibid.*, pp. 128 and 138.

Finally, the seven triples and the one quadruple, giving effectively nine triples, may be used to determine a rough value of the geometric-mean ratio of the separations in the wide pair and the close pair. From the data in Table 5 we find

$$\overline{\Delta \log a} = 2.07 \pm 0.21 \text{ (p.e.)},$$

in which the p.e. refers to the mean itself, not to individual deviations. The geometric-mean ratio is therefore roughly 100; it may be slightly affected by the selection, which distorted certain results found earlier.

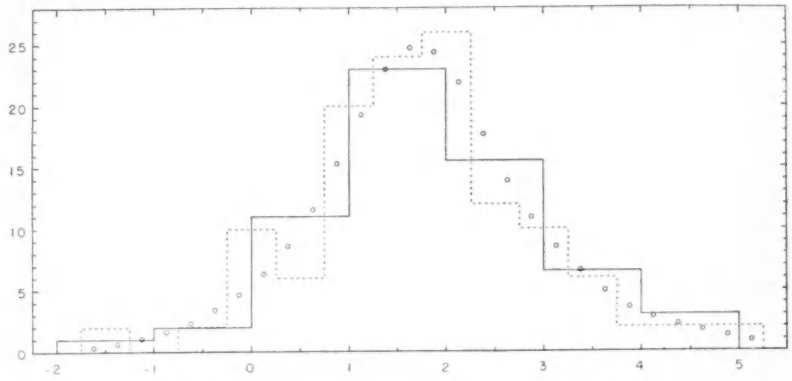

FIG. 3.—Numbers of observed binaries for unit interval of log a

TABLE 5

Pair	log a*	Pair	log a	Pair	log a	Pair	log a
1, 2	*2.23*	75, 76	*2.58*	148, 149	1.37	189, 190	1.37
5, 6	*1.57*	77, 78	1.17	150, 151	1.52	193	−0.03
8, 9	1.84	84, 85	*1.37*	152, 153	*2.19*	195, 196	*1.88*
14, 15	*3.46*	86, 87	*2.58*	159, 160	1.08	198, 199	*3.11*
18, 19	*1.89*	88, 89	*2.17*	162, 163	0.11	200, 201	*0.2*
26, 27	*3.17*	93, 94	*1.53*	162, 164	*2.80*	206, 207	*0.84*
31, 32	*3.58*	105, 106	*2.32*	165, 166	0.71	210, 211	*1.78*
38, 39	*2.14*	107, 108	1.26	167, 168	*1.50*	215, 216	*1.31*
41, 42	*2.72*	107	0.18	167, 169	*3.72*	215, 217	*4.52*
42, 43	1.53	108	−1.36	170, 171	1.52	221, 222	*1.07*
53, 54	*3.11*	122, 123	*2.10*	172, 173	1.10	223, 224	*2.05*
57, 58	*3.00*	125, 126	*0.80*	172, 174	*2.44*	235, 236	*1.99*
66	0.4	137, 138	*2.11*	175, 176	*2.20*	237, 238	0.97
68, 69	1.31	142	0.12	184, 185	*2.59*	243, 245	*4.84*
72	*1.06*	146, 148	*4.12*	185, 186	1.07	252, 253	0.94

* Figures in italics indicate that log D +0.11 was used.

It is clear that for some of the problems discussed the volume considered here is really too small. Double the radius (i.e., $p \geqslant 0''.05$), or eight times the volume, would appear adequate. Fortunately, trigonometric parallaxes of some accuracy may be determined up to just that limit.

YERKES OBSERVATORY
November 19, 1941

THE SPECTRA OF α CYGNI AND α LYRAE IN THE REGION λλ 3000–3300*

J. H. Rush

ABSTRACT

The wave lengths of absorption lines in α Cygni and in α Lyrae are listed between λ 3040 and λ 3298.

In 1939 O. Struve[1] published the results of an investigation of the spectra of several A-type stars, based upon plates taken with the Cassegrain spectrograph of the McDonald Observatory, using quartz prisms and UV-glass collimating and camera lenses. After quartz lenses were installed in 1940, the present study was undertaken to utilize the extended range of the instrument in supplementing Struve's tabulation. Duplicate plates, using different exposures, were obtained for α Cygni and α Lyrae with the 500-mm camera on Eastman Process film; each plate was measured independently, and the mean was recorded for those wave lengths which appeared on both plates of a pair. The residual correction for radial velocity was determined by fitting the present tabulation to the overlapping portion of the earlier measurements.

As might be expected, the spectrum in this region is due almost entirely to *Fe* II, *Ti* II, *Cr* II, and *V* II; one occurrence of *Mg* II, two of *Ni* II, and three of *Ca* II are noted. Comparison with the earlier compilation by Wyse[2] of the spectrum of α Cygni reveals twenty-four new lines in the present list, while three lines given by Wyse were not observed here; in addition, eight blends listed by Wyse are resolved in this study.

The accuracy of the observed wave lengths varies widely, ranging from the order of ±0.05 A, for the sharpest lines of moderate intensity, to ±0.3 A, in the case of faint, diffuse lines near the low wave-length limit of the plate. Diffuse or nebulous lines are denoted *n*.

The observed intensities were estimated on a scale of 0–10, 0 denoting a line so faint that its existence was questioned until verified by comparison with the duplicate plate or by its consistency with laboratory wave lengths. In the case of α Cygni, the laboratory intensities corresponding approximately to unit observed intensity are: *Fe* II, 4; *Cr* II, 25; *Ti* II, 20; *V* II, 375.

Unless otherwise noted, laboratory wave lengths for *Fe* II are from Dobbie's *The Spectrum of Fe II; V* II from Meggers and Moore's *Description and Analysis of the Second Spectrum of Vanadium; Ti* II from the *M.I.T. Wavelength Tables; Cr* II and others from Miss Moore's *A Multiplet Table of Astrophysical Interest* and unpublished material.

Grateful acknowledgment is due Dr. O. Struve and Dr. P. Swings, for the use of the plates and other material, and Dr. Paul Rudnick, for his personal assistance in connection with the work.

* *Contributions from the McDonald Observatory, University of Texas*, No. 45.

[1] *Ap. J.*, **90**, 699, 1939. [2] *Lick Obs. Bull.*, No. 492, 1938.

TABLE 1

ABSORPTION SPECTRA OF α CYGNI AND α LYRAE IN THE REGION λλ 3000–3300

α Cygni		α Lyrae		Identification			α Cygni		α Lyrae		Identification		
λ	*I*	λ	*I*	Element	λ	*I*	λ	*I*	λ	*I*	Element	λ	*I*
3040.98	0	1.14	0	*Fe* II	0.83	0	3073.02	4	2.92	1	*Ti* II	2.98	40
				Fe II	1.16	0					*Fe* II	3.24	2
				Cr II	0.92	70					*Cr* II	3.25	15
3042.04	0	.....	...	*Cr* II	1.74	50	3075.32	5	5.21	1	*Fe* II	5.23	4
											Ti II	5.24	40
3044.89	1	.....	...	*Fe* II	4.84	5							
							3076.55	0	.....	...	*Fe* II	6.46	6
3047.81	2n	.....	...	*Cr* II	7.63	20							
				Cr II	7.76	25	3077.25	5n	7.05	1	*Fe* II	7.17	10
				V II	8.21	200					*Cr* II	7.24	18
											Cr II	7.79	25
3049.16	0	.....	...	*Ti* II	8.79	6							
				Fe II	9.01	5	3078.64	6n	8.51	3n	*Ti* II	8.66	50
											Fe II	8.70	8
3050.16	2	0.24	0	*Cr* II	0.14	100					*Cr* II	9.34	15
3053.59	0n	.....	...	*V* II	3.39	200	3083.14	0	.....	...	*Fe* II	3.02	3
				Cr II	3.65	10							
				V II	3.89	80	3084.50	0	.....	...	*Cr* II	4.46	15
3055.63	0n	.....	...	*Fe* II	5.37	4	3087.18	0	6.86	0	*Ni* II	7.08	20
				Cr II	5.44	12							
							3088.09	7	7.92	4	*Cr* II	7.90	20
3056.98	1	.....	...	*Fe* II	6.80	5					*Ti* II	8.04	75
3058.24	0	.....	...	*Cr* II	7.86	12	3089.48	3	.....	...	*Fe* II	9.39	4
				Ti II	8.08	50					*Ti* II	9.40	15
				Cr II	8.38	12							
							3093.21	6n	2.94	5n	*V* II	3.11	2500
3059.47	3n	.....	...	*Cr* II	9.41	10							
				Cr II	9.52	25	3094.18	0	3.98	0	*Cr* II	3.48	40
											Cr II	3.97	15
3062.16	6n	.....	...	*Cr* II	1.59	8					*V* II	4.20	200
				Fe II	2.23	9							
							3094.97	0	.....	...	*Cr* II	4.94	10
.....	.....	63.20	0	*V* II	3.25	200							
							3096.20	2	.....	...	*Cr* II	6.11	35
3065.44	2	.....	...	*Fe* II	5.32	6					*Fe* II	6.30	5
3066.41	3	6.17	2	*Ti* II	6.23	30	3097.29	2	6.87	2n	*Ti* II	7.18	25
				Ti II	6.37	20					*Fe* II	7.42	2
3067.32	2	7.21	1	*V* II	7.10	200	3100.90	0	.....	...	*V* II	0.94	100
				Cr II	7.18	20							
							3102.21	5	2.17	1	*V* II	2.30	2000
3068.79	0n	.....	...	*Fe* II	8.76	2							
							3103.58	2	.....	...	*Cr* II	3.48	30
3070.84	2n	.....	...	*Fe* II	0.69	4					*Ti* II	3.82	50
				Fe II	1.14	4							
				Ti II	1.25	15	.....	.....	4.66	1	*Mg* II	{4.72 4.78}	30
				Fe II	1.27	2							
3072.20	3n	1.96	0	*Fe* II	1.65	2							
				Ti II	2.12	30							
				Cr II	2.47	8							

TABLE 1—*Continued*

α Cygni		α Lyrae		Identification		
λ	*I*	λ	*I*	Element	λ	*I*
3105.06..	2n	6.08	1	*Ti* II	5.10	20
				Fe II	5.17	5
				Fe II	5.55	5
3106.33..	4n			*Ti* II	6.24	35
				Fe II	6.56	4
3107.53..	2	.....	...	*Cr* II	7.58	50
3108.70..	0	.....	...	*Cr* II	8.66	10
3110.68..	5n	0.61	1	*Ti* II	0.70	20
				V II	0.71	1500
3111.82..	1n	1.92	0	*Cr* II	1.95	15
3112.31..	1n	.....	...	*Ti* II	2.08	10
3114.38..	4n	4.31	1	*Fe* II	4.30	7
				Fe II	4.68	4
3115.50..	0	.....	...	*Cr* II	5.28	12
				Fe II	5.35	2
				Fe II	5.49	1
				Cr II	5.65	20
3116.58..	3	6.45	0	*Fe* II	6.59	6
				Cr II	6.76	20
3117.63..	1	.....	...	*Ti* II	7.66	20
3118.55..	9n	8.47	3	*Cr* II	8.14	10
				V II	8.38	1000
				Cr II	8.65	60
3120.24..	9	0.29	3	*Cr* II	0.37	75
3122.66..	3n	.....	...	*Cr* II	2.60	30
				V II	2.89	100
3125.05..	10	5.05	6	*Cr* II	4.98	100
				Cr II	5.02	15
				V II	5.28	600
3126.20..	0n	.....	...	*V* II	6.22	150
				Cr II	5.79	5
3128.71..	6	8.63	2	*Ti* II	8.64	8
				Cr II	8.70	40
3130.26..	2	0.27	0	*V* II	0.26	100
3130.76..	1	.....	...	*Fe* II	0.56	2
				Ti II	0.80	15
3132.00..	9	1.96	3	*Fe* II	1.72	4
				Cr II	2.06	125
3133.17..	2	.....	...	*Fe* II	4.05	4
				V II	4.33	150
3134.30..	0	.....	...	*Cr* II	4.33	25
3135.40..	4	.....	...	*Cr* II	5.35	20
				Fe II	5.36	9
				Cr II	5.74	30
3136.66..	4	6.49	2	*V* II	6.50	160
				Cr II	6.68	40
3140.11..	3n	9.74	0	*V* II	9.73	160
				Cr II	9.91	8
				Cr II	0.21	25
3142.38..	0	.....	...	*Fe* II	2.22	0
				V II	2.48	150
3143.81..	2	3.59	0	*Cr* II	3.68	7
				Ti II	3.76	10
				Cr II	3.91	7
3144.90..	3	.....	...	*Fe* II	4.75	5
				Cr II	5.10	10
3147.13..	4	7.17	1n	*Fe* II	6.75	2
				Cr II	7.23	50
3148.11..	1n	7.88	1n	*Ti* II	8.04	12
3149.86..	3	.....	...	*Cr* II	9.83	20
				Fe II	9.85	0
				Cr II	0.11	20
3152.24..	3	2.15	0	*Cr* II	2.21	40
				Ti II	2.26	15
3153.21..	1	.....	...	*Fe* II	3.06	2
				Cr II	3.35	20
3154.12..	6	4.19	3	*Cr* II	4.04	5
				Cr II	4.10	2
				Ti II	4.20	12
				Fe II	4.20	12
3155.64..	3	5.60	1	*Ti* II	5.66	12
				Fe II	5.95	2
3157.58..	0	.....	...	*Ti* II	7.41	2
				Cr II	8.03	20
3158.86..	4	8.82	4	*Ca* II	8.89	9
				Cr II	9.10	5

TABLE 1—*Continued*

α Cygni		α Lyrae		Identification			α Cygni		α Lyrae		Identification		
λ	*I*	λ	*I*	Element	λ	*I*	λ	*I*	λ	*I*	Element	λ	*I*
3160.16..	0	.....	...	*Cr* II	0.11	3	3196.02..	3	5.97	1	*Fe* II	6.07	10
				Cr II	9.86	5							
3161.12..	1			*Ti* II	1.20	25	3197.10..	4	6.94	1	*Cr* II	6.96	20
		1.52	1n	*Ti* II	1.78	30					*Cr* II	7.12	75
3161.90..	3			*Fe* II	1.94	5	3202.49..	2	2.47	1	*Cr* II	2.52	15
											Ti II	2.54	40
3162.76..	5n	2.55	1n	*Cr* II	2.46	10							
				Ti II	2.57	35	3203.47..	1	.....	...	*Fe* II	3.51	1
				Fe II	2.80	8					*Cr* II	3.53	15
				Fe II	3.09	5							
							3205.11..	2	.....	...	*Cr* II	5.11	25
3166.66..	2n	.....	...	*Fe* II	6.67	4							
							3209.00..	5n	9.01	1	*Cr* II	8.62	20
3167.91..	3			*Fe* II	7.85	11					*Cr* II	9.21	50
		8.24	1										
3168.57..	1			*Ti* II	8.53	40	3210.46..	7	0.39	2	*Fe* II	0.45	10
											Cr II	0.53	20
3170.32..	4	0.39	0	*Fe* II	0.34	6							
							3213.29..	8	3.21	2	*Fe* II	3.31	13
3172.04..	2	.....	...	*Cr* II	2.08	40							
							3214.91..	2	4.92	0	*V* II	4.75	120
3175.03..	0	.....	...	*Fe* II	5.08	4					*Ti* II	4.78	4
3177.51..	5	7.44	2	*Fe* II	7.53	10	3217.12..	5	7.04	3	*Cr* II	6.55	20
											Ti II	7.07	30
3179.42..	4	9.31	5	*Ca* II	9.34	10					*V* II	7.12	400
				Cr II	9.45	8		0			*Cr* II	7.44	50
				Fe II	9.50	8							
							3218.09..		.....	...	*Ti* II	8.25	25
3180.72..	4			*Cr* II	0.73	75		3				8.28	
		1.02	3n	*Ca* II	1.28	6							
3181.40..	2			*Cr* II	1.43	20	3222.78..	2	2.80	1	*Ti* II	2.86	35
3183.14..	5	3.02	2	*Fe* II	3.12	8	3224.32..	0	4.15	0	*Ti* II	4.25	4
				Cr II	3.32	40							
							3225.80..		.....	...	*Cr* II	5.39	12
3185.23..	3	5.00	0	*Fe* II	5.10	1					*Cr* II	5.44	8
				Fe II	5.32	5					*Fe* II	6.38	2
3186.98..	6n	6.64	2n	*Fe* II	6.74	11	3227.73..	5n	7.71	2	*Fe* II	7.73	13
				Cr II	6.75	18							
				Fe II	7.29	8	3229.23..	4	9.20	2	*Ti* II	9.21	40
											Cr II	9.38	8
3188.52..	1	.....	...	*V* II	8.52	300					*Ti* II	9.43	35
3190.78..	3n	0.74	3n	*V* II	0.69	500							
				Ti II	0.85	30	3231.56..	2n	2.37	0	*Cr* II	1.64	8
				Fe II	0.84	pr					*Fe* II	1.70	5
							3232.71..	4n			*Ti* II	2.29	30
3192.00..	0	.....	...	*Fe* II	2.06	3					*Fe* II	2.79	7
3192.83..	3n	.....	...	*Fe* II	2.92	9	3234.45..	8	4.38	4	*Cr* II	4.06	50
											Ti II	4.52	75
3193.83..	4n	3.69	2n	*Fe* II	3.81	11							

TABLE 1—*Continued*

α Cygni		α Lyrae		Identification			α Cygni		α Lyrae		Identification		
λ	*I*	λ	*I*	Element	λ	*I*	λ	*I*	λ	*I*	Element	λ	*I*
3236.45	5	6.39	3	*Ti* II	6.14	20	3266.87	1			*Fe* II	6.94	4
				Ti II	6.59	70	3267.26	1			*Fe* II	7.04	3
3237.75	2			*Fe* II	7.82	8							
				V II	7.88	350	3267.69	1			*V* II	7.71	1000
3239.12	5	9.02	3	*Cr* II	8.77	50	3269.94	1n			*Fe* II	9.77	2
				Ti II	9.05	60					*Cr* II	9.77	15
											Cr II	0.14	40
3241.96	4	1.90	3	*Fe* II	1.68	2							
				Ti II	2.01	60	3271.19	2			*V* I	1.12	1200
3243.75	3			*Fe* II	3.72	8	3271.66	2	1.66	2	*Ti* II	1.67	25
3247.26	4	7.27	0	*Fe* II	7.17	9			72.00	0	*Ti* II	2.10	25
				Cr II	7.33	8							
				Fe I	7.39	3	3273.51	0			*Fe* II	3.50	3
3248.62	1	8.54	2	*Ti* II	8.61	50	3274.70	1			*Ni* II	4.91	3
3249.73	1n			*Fe* II	9.66	4	3276.22	2n			*V* II	6.12	1500
				Fe II	9.91	1					*Cr* II	5.92	10
3251.90	1	1.82	0	*V* II	1.87	200	3277.24	4n	7.26	0	*Fe* II	7.35	9
				Ti II	1.86	30	3281.27	2			*Fe* II	1.29	7
					1.94								
3253.00	2	2.87	0	*Ti* II	2.85	40	3282.42	1n			*Ti* II	2.34	25
					2.89						*V* II	2.53	150
3254.25	2	4.17	1	*Ti* II	4.26	30	3285.40	1n			*Fe* II	5.42	3
3255.89	4	5.78	0	*Fe* II	5.88	8	3287.70	2	7.90	2	*Ti* II	7.67	40
											Cr II	8.04	15
3258.95	7	8.94	1	*Cr* II	8.77	30							
				Fe II	8.77	10	3289.36	2			*Fe* II	9.35	7
				Fe II	9.05	10							
							3291.76	1n			*Cr* II	1.75	40
3261.62	4	1.57	2	*Fe* II	1.51	1							
				Ti II	1.58	60	3295.59	6	5.45	1	*Fe* II	5.24	4
											Cr II	5.43	50
3264.48	2n	4.12	0	*Cr* II	4.26	35					*Fe* II	5.81	6
				Fe II	4.76	pr							
							3297.97	1			*Fe* II	7.89	5

Physics Department
Texas Technological College
Lubbock, Texas
October 1941

NOTES

REMARKS ON THE SPECTRA OF COMETS 1941*c* (PARASKEVOPOULOS–DE KOCK) AND 1941*d* (VAN GENT)*

The relative intensities of the C_2 and *CH* bands compared to *CN* are definitely lower in Comet 1941*c* (Paraskevopoulos–de Kock) than in Comet 1940*c* (Cunningham) for similar heliocentric distances, thus suggesting differences in chemical constitution of the heads of these two comets. Such differences have been mentioned for other comets, especially by F. Baldet.[1] Our spectrograms of Comet 1941*c* show *NH* bands having the same structure as in Comet 1940*c*; their intensity relative to *CN* is also similar in these two objects. A spectrogram of 1941*c* taken with a dispersion of 44.5 A/mm at λ 3870 and with an effective slit width of 0.8 A shows interesting features in the structure of

TABLE 1

OH LINES IN THE SPECTRUM OF COMET 1941*d* (VAN GENT)

COMET		LABORATORY		
λ	Intensity	λ	Notation	K'
3079.0	1–0	3078.43	$Q_1(1\frac{1}{2})$	1
3081.7	3	3081.64	$P_1(1\frac{1}{2})$	0
3090.2	1	3090.46	$Q_2(\frac{1}{2})$	1
3093.6	2	3093.72	$P_2(1\frac{1}{2})$	1

the $\Delta v = 0$ sequence of *CN*. The strong *P* branch has two maxima at λλ 3880.3 and 3881.7; the first one corresponds to $P(11)$, the emission extending from $P(8)$ to $P(13)$, and the latter to $P(15)$, the emission extending from $P(13)$ to $P(19)$. Emission is observed in the entire spectral interval from λ 3862.2 to λ 3870.5, with three maxima at λλ 3863.8 (intensity 1), 3866.6 (intensity 1), and 3869.6 (intensity 3). This emission belongs to the *R* branch of the (0, 0) band. Between the strong *P* and *R* branches the lines which had been observed as single and sharp with lower dispersion in Comet 1940*c*[2] show now a definite width corresponding, respectively, to $P(2) + P(3) + P(4)$ and $R(1) + R(2) + R(3)$. The effective slit width being 0.8 A, the three components obviously cannot be separated, although there appears some kind of structure in the lines.

The spectrum of Comet 1941*d* (van Gent) between June 21 and July 25, 1941 (*r* from 1.51 to 1.25), was characterized by the strength of the *OH* bands compared with the *NH* bands, whereas in Comet 1940*c* the *OH* lines were always weak with respect to the *NH* lines. Differential extinction would tend to give this effect since the comets were observed at different zenith distance; however, the magnitude of the effect is so large that the major portion of it is real. That the heliocentric distance *r* plays an important role

* *Contributions from the McDonald Observatory, University of Texas*, No. 46.

[1] *Ann. Obs. Astr. Phys. de Paris*, **7**, 1926.

[2] *Ap. J.*, **94**, 320, 1941.

in the relative intensities of the *OH* and *NH* bands appears clearly from a comparison of the spectrograms taken on June 21, 22, and 23 (r approximately 1.50) with those taken on July 13, 14, and 15, 1941 (r approximately 1.25). This comparison reveals an appreciable increase in intensity of *NH* relative to *OH* as the heliocentric distance decreases; however, further study is required to ascertain the relative effects of the heliocentric distance and of the differences in chemical constitution on the intensity ratio of the *NH* and *OH* bands. The intensities of the C_2 and *CH* bands relative to the *CN* band are also smaller than in Comet 1940*c*.

The structure of the *OH* bands in Comet 1941*d* is very different from that of Comet 1940*c*. The *OH* lines observed in Comet 1941*d* are listed in Table 1, which shows that only the strongest lines arising from the excited levels $K' = 0$ and 1 are observed in Comet 1941*d*. Compared to the P branches, the Q_2 line is very much weaker than in Comet 1940*c;* the reason is that, in the latter case, the feature observed at λ 3090 was a blend of $Q_2(\frac{1}{2})$, $Q_2(1\frac{1}{2})$ and $Q_2(2\frac{1}{2})$, whereas the line measured in Comet 1941*d* is probably only $Q_2(\frac{1}{2})$.

C. T. Elvey
P. Swings
H. W. Babcock

McDonald Observatory
July 1941

NOTICE

A committee, consisting of Professors W. L. Hart (Minnesota), W. M. Whyburn (California at Los Angeles), and C. C. Wylie (Iowa), is now engaged in preparing an outline of a college course to serve as preparation for the Army Air Corps training course. This is being done under the auspices of the American Association for the Advancement of Science. The objective of the committee is to have such an outline, with references to books in which the material can be obtained, ready for use during the second semester, which will begin in most colleges and universities about February 1.

Dr. F. R. Moulton, permanent secretary of the American Association for the Advancement of Science, has asked me to make this known to all astronomers. He states: "The courses to be given are in the fields of elementary mathematics and astronomy, so far as the latter pertains to air navigation. As I see it, the mathematicians and astronomers of the country will have to carry these courses at least initially."

As I interpret his communication, an important feature is that these courses to be given in colleges and universities should be of such a nature as to *prepare* men for the army course without *unnecessary duplication* of material contained in the latter. To that end, since the army course is already established and functioning, the college courses should be revised to conform with the outline so far as practicable. Needless to say, the nature and extent of such revision will not be known until the outline prepared by the committee is distributed.

I have been asked by Dr. Moulton to furnish a list of all institutions in which I think there is a possibility of such a course being given in the coming second semester. The time is very short, and in my ignorance of the curricula of most institutions I am appealing for information to all astronomers.

Please let me know at once whether you are equipped to conduct courses in celestial navigation, more particularly aerial navigation. If you yourself would not be able to carry on such work, is there any member of the faculty of your institution who could do so?

Dean B. McLaughlin, *Secretary*
American Astronomical Society

Observatory, Ann Arbor, Michigan
January 15, 1942

REVIEWS

The Milky Way. By BART J. BOK and PRISCILLA F. BOK. Philadelphia: Blakiston Co., 1941. Pp. v+204. Figs. 93. $2.50.

The subject matter and the results of modern astronomical research, grandiose and exciting, hold much fascination for the intelligent layman, amateur astronomer, and student. Yet a wide gap has existed between the elementary astronomical text or work of popularization, both devoted largely to the classical physical description of the solar system, and the papers and monographs of the astronomer. Specialization has resulted in some overemphasis of small problems; the inability to close the gap has resulted in a considerable lag of college astronomy behind such fields as physics. *The Milky Way*, one of the new "Harvard Books on Astronomy," is a successful attempt to outline for an intelligent reader with some knowledge of elementary astronomy the problems of stellar motions, the structure of the Galaxy, and the physics of interstellar space. The field is complex and less linked with physics and everyday life than most of modern astronomy. The discovery of graphic illustrations, of lucid analogies, which will illuminate the dimness of the readers' minds with that physical intuition required for understanding, is more difficult than usual. It is interesting to see how much of modern research in their field the Boks have been able to clarify and to illuminate for the thinking reader.

After a description of the "working model" of the Milky Way come the technical definitions and methods involved in spectral types, magnitudes, proper motions, and parallaxes. Some tables illustrating the physical data concerning the stars are given, and the methods for exploring the Russell-Hertzsprung diagram are outlined. Then follow the newer methods for extending distances beyond the realm of direct parallax determinations, e.g., the discovery of the galactic center from the distribution of the globular clusters. The sections on stellar motions, star streaming, asymmetry, and galactic rotation give a particularly lucid presentation of subjects which are intrinsically difficult to popularize. After some introduction to atomic theory the physical nature of gaseous nebulae and interstellar matter are discussed. The problems of the absorbing clouds and the coloring effects of interstellar dust lead to methods for the estimation of absorption. A chapter, "Men at Work," discusses the unfinished business and the still fragmentary results of the attempt to describe our Galaxy in detail. A grander and clearer view is taken, however, of our Galaxy as seen from the outside, together with comparisons with external galaxies. The age of the Milky Way is discussed in a new approach, with some unfamiliar arguments ranging from those on the age of the earth to problems of stellar energy generation.

The book has ninety-three illustrations and portraits, many of them new. There are some minor misprints, but few errors of fact. Among omissions, there is little or no discussion of double stars, Oort's limit, the ratio of absorption to reddening, or methods of estimating the mass of our Galaxy. The book can be recommended for any intelligent reader. It would serve as an excellent text for an advanced descriptive course, although it omits all mathematical analysis; it can be further recommended for any astronomical specialist who wants a clear, accurate, and well-rounded survey of one active phase of modern astronomy.

JESSE L. GREENSTEIN

Yerkes Observatory

The "Photismi de Lumine" of Maurolycus. By FRANCESCO MAUROLICO. Translated by HENRY CREW. New York: Macmillan Co., 1940. Pp. 134. $3.00.

The system of nomenclature of features of the moon's surface initiated by Langrenus and re-established by Riccioli, in which mountains and craters bear names of astronomers, philosophers, etc., provides a veritable "Who's Who" of early science. My first introduction to Maurolycus was in seeing his name attached to one of the great walled plains. Since, in general, important lunar features bear names prominent in the history

of science, one must infer that Maurolycus was highly regarded. Through the medium of Professor Crew's translation of the *Photismi de Lumine* of Maurolycus, I am happy to renew and extend the acquaintance.

Professor Crew has recognized the shift of emphasis in linguistic studies—from Greek and Latin to the modern languages—also that modern physicists are not universally equipped to wrestle successfully and joyously with Latin; and therefore he has deemed it worth while to offer this early treatise on optics "in English dress, as a slight contribution to the history of science." But one may note also his curiosity "to learn just how a well-trained mind looked upon the subject of optics in an age when almost nothing was known about the nature of light; neither its speed nor its law of refraction, much less anything about its oscillatory and corpuscular nature, its diffraction or its polarization." Maurolycus (1494–1575) chronologically fits in between Copernicus (1473–1543) and Tycho (1546–1601). His life antedated the invention of the calculus.

In our day geometrical concepts and relationships are constantly in our minds, but geometry is taught more as an exercise in precise logical thought than to serve as a tool. It was otherwise with Maurolycus, and one may share with Professor Crew the interest in the solution by geometrical means of problems which in many cases yield their solutions more easily by use of the calculus.

Maurolycus, one of the first in the revival of letters "to distinguish himself as a mathematician and philosopher" and "whom Chasles calls 'le plus savant geomètre de son temps,' " follows the method of Euclid. He states his theorem, passes through the steps of the proof to the conclusion. On page xvii, Professor Crew has written: "The author repeatedly checks his experiments by observation; seldom by experiment." This seems rather paradoxical. The word "experiments" should be changed to "conclusions." The statement would then more closely represent the practice. Maurolycus was, however, not averse to citing experiment. In his Theorem XXXV, "By convergence of rays it is possible to kindle a fire," he states: "The Theorem is therefore established by reason and by experience"; and again at the end of p. 47: "All these matters are easily shown and established by experiment."

Euclid begins with certain definitions and axioms. In similar fashion, on pages 5 and 6 Maurolycus sets down his definitions and postulates. I fail to see the distinction between Postulate 2, "The denser the rays, the more intense the illumination; equal densities yield equal illuminations," and Postulate 5, "The greater the number of rays, the more intense the illumination; equal numbers of rays produce equal illuminations." We associate intensity with illumination on unit area. A distinction appears if for the words "more intense" are substituted the words "greater the total."

That, having stated the postulates, he leans heavily on them is illustrated in many instances. To cite one example, in Theorem XXVI (pp. 32 and 33): "A ray of light falling perpendicularly upon a mirror is reflected back upon itself"; on discussing other paths he writes: ". . . . a conclusion which by our *third postulate* is absurd." In later days school children test the theorem by experiment.

Some theorems are so stated that their import is not at once apparent. Theorem XXIV, "Rays passing through a dark region are more clearly evident," is equivalent to generalizing on the fact that a candle light can be seen farther at night than in sunlight.

The proofs are, in some cases, very roundabout, needlessly involved (sometimes ending by essentially affirming a postulate)—Theorems XXIX and XXX, for example. Some conclusions are not general, applying only to special cases. Theorem VI, under "Refraction," applies only for minimum deviation. The inadequacy or inaccuracy of statements which sometime appear does not escape the translator (p. 53 n.).

Maurolycus touches many points of astronomical significance other than those of optics. He recognized (p. 22) that the full moon illuminates less than half of the earth. He notes (p. 8) that "regions to which the sun's rays are equally inclined receive equal amounts of heat, those areas to which the rays are more steeply inclined receive more

heat, and those upon which the rays fall perpendicularly receive most heat of all. This is because heat always accompanies the light of the sun, increasing and decreasing with this light." This thought is repeated on page 45: " . . . . heat accompanies the light; being radiated and reflected with it."

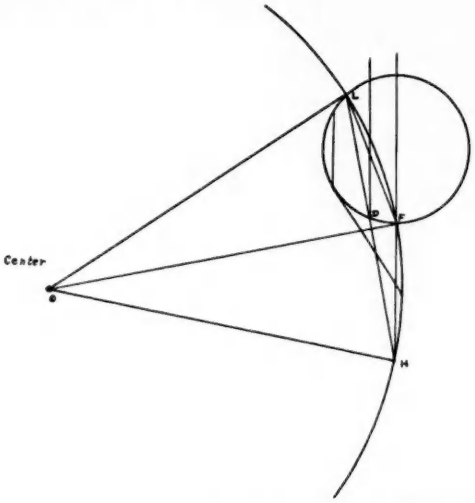

Following through the various proofs provides an excellent review of geometry. In a footnote on page 66 Professor Crew notes that he has been unable to locate the cited twelfth lemma of Ptolemy but finds in Manitius' translation of the Almagest a theorem which apparently is the equivalent: "If in any circle two chords are drawn, the ratio of the greater chord to the smaller is less than the ratio of the arc of the greater chord to the arc of the smaller chord." (The sine of an angle increases less rapidly than the arc.) Utilizing Figure 57 of Maurolycus and his lettering and the theorem just cited, the proof that $HD/DL >$ angle DLF/angle FHD, which involves the lemma just mentioned, follows:

In the circle passing through H, F, and L, with center at O,

$$\frac{\frac{1}{2}\text{ arc } FH}{\frac{1}{2}\text{ arc } FL} = \frac{\angle\, DLF}{\angle\, FHD},$$

$$\frac{\text{arc } FH}{\text{arc } FL} < \frac{FH}{FL},$$

$$\frac{\angle\, DLF}{\angle\, FHD} < \frac{FH}{FL},$$

but

$$HD > FH,$$

$$FL > DL,$$

$$HD \times FL > FH \times DL,$$

$$\frac{HD}{DL} > \frac{FH}{FL},$$

$$\frac{HD}{DL} > \frac{\angle\, DLF}{\angle\, FHD}.$$

There is pleasure in seeing the scholarly approach to the presentation of this translation; the portrait frontispiece taken from Father Scina's, *Elogio de Francesco Maurolico* (Palermo, 1808); the scholarly searching of various editions of the *Photismi* (*1611 Corrigende* by Clavius, [?] Naples, the 1613 Lyons edition; the first edition, Venice, 1575, was not available); the mention that almost thirty years were devoted to the preparation of the original volume; the reading of other works of Maurolycus. Knowing Professor

Crew, when he mentioned the publication of the three dialogues, the *Cosmographia* (Venice, 1543), one was assured that he would refer to "two great books, one by Copernicus, the other by Vesalius, which have made the date unforgettable." Nor would one have expected him to omit mention that the 1611 edition of *Photismi* appeared in the same year as the King James version of the Bible, nor did he. In like vein, in recounting the incident of the prediction of weather during the period of the expedition of Don John of Austria to the Levant, Professor Crew writes: "Maurolycus would doubtless have preferred a chat with the youthful Miguel de Cervantes who was at the moment a member of that fleet."

It is cheering and challenging to note that this translation, with its keen freshness and deep appreciation, is by a scholar who has advanced beyond his eighty-first anniversary.

PHILIP FOX
Colonel Infantry

316 Federal Building
Mobile, Alabama

Doctor Wood: Modern Wizard of the Laboratory. By WILLIAM SEABROOK. New York: Harcourt, Brace & Co., 1941. Pp. xiv+335. $3.75.

This popular biography of one of the greatest living physicists will be appreciated by scientists as well as by laymen. There is a bibliography of the scientific publications of Professor R. W. Wood.

The Story of Variable Stars. By LEON CAMPBELL and LUIGI JACCHIA. Philadelphia: Blakiston Co., 1941. Pp. v+226. $2.50.

This member of the "Harvard Books on Astronomy" will be particularly welcomed for it satisfies a need which has existed for a long time. Of the other two books on this subject which have appeared in recent years, one is devoted more especially to the long-period variables, and the other is a technical monograph rather than a survey of the field for the general reader. *The Story of Variable Stars* plays no favorites and does not attempt to include all the technical details of the subject. Its style and language are of the "popular" type, and the book is distinctly "alive."

There are eight chapters, besides an Epilogue, Addenda, and Appendix. The order of treatment appears to be the most logical one of the many possibilities. This will be evident from a listing of the chapter headings: (1) "How Variables Are Found"; (2) "Observing the Variables"; (3) "Using the Observations"; (4) "Pulsating Stars"; (5) "The Red Variables"; (6) "Explosive Stars"; (7) "Erratic Stars"; and (8) "Stellar Eclipses."

Methods of discovery and observation are treated concisely but with sufficient completeness to present a well-balanced picture of the techniques. The third chapter gives a very readable account of the determination of light-curves and of the calculations involved; but, in the attempt to simplify the subject, some lack of rigor has been introduced. In the reviewer's experience the concept of approximate calculations is actually more difficult of comprehension by the person untrained in mathematics than is the rigorous procedure. To such a person, approximations seem to be in direct contradition to the scientist's avowed purpose of discovering truth. For this reason the use of phases only to the nearest ten days (p. 46) is likely to defeat its purpose.

The authors are at their best in the chapters on the several classes of intrinsically variable stars. There seems to be no case of disproportionate emphasis of any topic or of omission of anything of fundamental importance. But one could wish for another page or so of more detailed explanation of the pulsation theory in its most modern dress. There are a number of excellent examples of typical light-curves for all classes of variables; these are sufficiently numerous to cover all the main types without wearying the reader with duplications. The series of light-curves of Cepheids and of novae are particularly commendable. The authors have given all kinds of variables their just due, including Z Andromedae and the Z Camelopardalis stars. It is gratifying to note that the authors have not hesitated to indicate clearly that they have not "swallowed hook, line and sinker" the absurdities of the collapse hypothesis of common novae.

The account of the methods of determining dimensions, masses, and other characteristics of eclipsing binaries is handled very well, and without mathematics; the presentation is clearer than in most texts.

The Addenda consist of brief accounts of the Draper classes of stellar spectra, the Doppler effect, and absolute magnitude. The Appendix contains tables of constellation abbreviations, decimals of a day, Julian days, and short lists of interesting variables and novae.

There are a few places in which the manner of presentation or the language may convey an erroneous impression to the reader who has little previous astronomical background, and a few attempts at conciseness have resulted in the use of words in connotations not in accord with general practice. On page 19 the general reader may be confused by a diagram in which magnitude increases with light-intensity. On page 57 the use of the expression "axis of the orbit," to mean a line perpendicular to its plane, must be deplored. And on pages 195 and 196, in connection with ζ Aurigae and VV Cephei, the general reader could easily conclude that the smaller stars in those systems pass *through*, instead of *behind*, the atmospheres of the larger components.

There are also what appear to be a few errors and one or two omissions. Thus, the statement on page 135 that the nebular lines in novae are sometimes "already visible at maximum" is certainly incorrect. It may possibly refer to the early appearance of [*O* I] emission, but even that is not seen *at* maximum, and the statement would be better omitted. That [*O* I], and not [*O* III], is meant seems to be indicated by the closely following statement that the lines have been produced in the laboratory. On page 182 the outmoded belief that limb darkening is due to absorption in the stellar atmosphere is perpetuated. In connection with changes of period in eclipsing systems (pp. 192–93) the possibility of equation of light or of Doppler effect due to a third body is mentioned, and reference is made to *suspected* cases; yet the best-known and most conclusively demonstrated example of this sort—Algol itself—is not pointed out, though unexplained changes of its period are mentioned in the same paragraph. In the description of the Draper spectral classes (pp. 207–8) only bright-line objects are mentioned in class O.

Against such minor faults we can set the conspicuous merit of the book in giving a well-balanced view of the whole field. It packs between its covers a great deal of authoritative information which is conveyed to the reader in lucid and nontechnical language. A happy choice of expressions helps, as in the statement of the relation of U Geminorum stars to novae (p. 149), where these variables are compared to geysers and volcanoes, respectively. It is quite surprising to see how well the authors have succeeded in presenting topics, which could be quite technical, without either mathematical expressions or involvement in long discussions in which the general reader would bog down.

Both because of, and in spite of, its "popular" style *The Story of Variable Stars* will serve as a most useful source of information for the general reader with limited astronomical background, the student, the amateur, the teacher, and even the professional astronomer.

DEAN B. MCLAUGHLIN

The Observatory of the
University of Michigan